Crafting pore architecture of water-stable microporous MOFs for selective CO$_2$ capture

A Thesis
Submitted in Fulfilment of the Requirements
for the Degree of

Doctor of Philosophy

by

Rahul Maity
ID: 20153366

Department of Chemistry

Indian Institute of Science Education and Research (IISER), Pune

2021

Dedicated to

My parents and Ganesh Dada

Certificate

This is to certify that the work incorporated in this thesis entitled "**Crafting pore architecture of water-stable microporous MOFs for selective CO_2 capture**" submitted by Rahul Maity carried out by the candidate at the Indian Institute of Science Education and Research (IISER), Pune, under my supervision. He has fulfilled all the requirements for the Doctor of Philosophy (Ph.D.). He has been duly registered, and the thesis presented here is worthy of being considered for the award of the Ph.D. degree. This is further certified that the work embodied here or any part of it has not been included in any other thesis submitted previously to award any degree or diploma from any other University or Institution.

Date- 28-Jan-2021

Dr. Ramanathan Vaidhyanathan

(Doctoral Thesis Supervisor)
C-217, Advanced Porous Materials Lab
Department of Chemistry, IISER Pune,
Pune, Maharashtra, India
E-mail: vaidhya@iiserpune.ac

Declaration

I hereby declare that the thesis entitled "**Crafting pore architecture of water-stable microporous MOFs for selective CO₂ capture**" submitted for the degree of Doctor of Philosophy in Chemistry at Indian Institute of Science Education and Research (IISER), Pune, India, has not been submitted by me to any other university or Institution. This work was carried out at the Indian Institute of Science Education and Research (IISER), Pune, India, under the supervision of Dr. R. Vaidhyanathan. The information derived from the literature has been duly acknowledged in the text and the list of references provided in the thesis.

Date-

Rahul Maity

29.01.2021

Rahul Maity
ID: 20153366

Acknowledgments

At the very beginning, I would like to express my sincere thanks and deepest gratitude to my research supervisor Dr. Ramanathan Vaidhyanathan for his continuous support and encouragement throughout my Ph.D. tenure. His inspiring guidance has helped me independently design and execute different research projects, successfully addressing various current research problems. He also guided me in learning the structure solution of various small molecules, supramolecular complex, Metal-Organic framework, perovskites, and many more via the Single Crystal X-ray Crystallographic Technique. Under his supervision, one of the most significant achievements that I have accomplished is bringing textbook-based elegant ideas into Materials Chemistry and executing the research projects through in-depth studies.

I would like to express my sincere gratitude to the former director of the Indian Institute of Science Education and Research (IISER) Pune, Prof. K. N. Ganesh, and the current director Prof. J. B. Udgaonkar, for providing state-of-art research facilities, funding, and an excellent vibrant research environment. I am also grateful to former chair Prof. M. Jayakannan, current chair Prof. H. N. Gopi, and all other faculty members of the chemistry department to be approachable for any help and maintain such a research-friendly environment at the department.

I am also extremely thankful to my research advisory committee (RAC) members, Prof. Vinod C. Prabhakaran (NCL, Pune) and Prof. R. Boomishankar (IISER, Pune), for their valuable scientific suggestions and support to shape my projects during the RAC meetings for the annual evaluation of my doctoral research. I am also thankful to Prof. Guillaume Maurin (Université Montpellier, Frans) and Dr. Vinod C. Prabhakaran (NCL Pune) for their Collaborative research inputs.

I would like to thank my lab seniors: Shyamapada, Shalini, Dinesh, Aparna, and lab mates: Debanjan, Sattwick, Rinku, Himan, Pragalbh, and Deepak, for their help and support during my doctoral study. I would like to give special thanks to MS student Ankit Kumar Yadav for assisting me in most of my research projects. I would also like to express my greetings to the summer project students: Suchit (NIT Rourkela), Dhrubangshu (IISER Pune), Aiswarya (IISER Thiruvananthapuram), and other MS Students: Deep (IISER Pune), Chandana (IISER Pune). I am also thankful to the students of our collaborator Dr. Rajnith (Université Montpellier, Frans) and Sergio (Université Montpellier, Frans).

I would like to express my sincere regards to all of my teachers for making my Today's happened. I would like to acknowledge especially my B.Sc. Inorganic Chemistry teacher Sujoy Roy Choudhuri (SRC), Organic Chemistry teacher Amrit Mitra, and Physical Chemistry teacher Suman Dey for teaching me Basic

Rahul Maity

Table of contents

Table of contents

Abstract

The sky-rocketing rise of global CO_2 concentration is one of the major environmental concerns today because of its detrimental effects on climate change, species extinction, and plant nutrition. Therefore, cutting CO_2 emissions is among the prime targets of the coming decades. CO_2 is mainly emitted from the combustion of fossil fuels by industries and transport systems. Our daily lifestyles are almost entirely dependent on the power generated from fossil fuels and will also be so for the up-coming few decades. Consequently, the only technique to allow continued use of fossil fuels while minimizing CO_2 footprint is Carbon Capture/separation and Storage (CCS technology). As CCS technology, solid-sorbents get priority over the industrially accessible liquid amine sorbents because of their lower regeneration costs and environment and plant affability. Apart from the engineering modifications, the performance of the CCS technology relies to a large extent on the sorbent capacity. Hence, finding suitable cheap designer crystalline porous material is highly needful for carbon capture technology.

Metal-Organic Frameworks (MOFs) form a class of crystalline porous material made of metal nodes connected via organic linkers and have tuneable architectures and fuctionalizable pores. MOF can display excellent low-energy physisorption based gas capture capabilities. Most industrial and power plant flue gas emissions contain substantial humidity. Pre-drying such streams for capture itself incurs sizeable cost shying industries away from investing into these capture technologies. Hence being able to capture CO_2 directly from the humid flue gas is desirable. For humid CO_2 capture, producing humidity/water stable porous materials is still challenging. This thesis's primary goal is to bring water stability into the framework of MOFs, simultaneously increasing the number of CO_2-interacting sites into the pore-architecture. This thesis proposes two strategies using the concept of "*Werner's theory of coordination complexes*." First, choosing high charge density metal ions (hard metals) combined with O-donor ligands (hard ligand). Second, choosing low charge density metal ions (soft metals) in conjunction with azolate (adeninate) ligands. In the first strategy, the choice is tri-positive lanthanide (Ln^{3+}) ions with polytopic carboxylic acid linkers taking advantage of the hard-acid (high charged metal)-hard acid (O-donor ligands) bonding favourability. The second strategy describes the synthesis of water-stable MOFs using adeninate as an azolate ligand combined with other dicarboxylic acid ligands and comparatively softer transition metal ions. Adeninate is chosen because, in the ligand field strength of azolate is more than the water. So, water is unable to destroy the framework, giving a water-stable MOF. Besides, adeninate MOFs consist of multiple N-centres and can polarise CO_2 for better physisorptive selectivity. This facilitates the easy regeneration of CO_2 from the framework. Moreover, being a short and inexpensive linker adeninate can generate cost-effective ultra-microporous MOFs, which are the most useful for CO_2 capture/separation applications. The MOFs described in this thesis are water/humid stable and have moderate to good CO_2 uptakes under ambient conditions with optimum HOA for facile regeneration of CO_2 and good CO_2-selectivity over other gases.

Abbreviations

Å	Angstrom	min	Minutes
Ad	Adenine	ml	Millilitre
OAc	Acetate	µl	Micro litter
BDC	Benzene Di-Carboxylate	mmol	Milli moles
BET	Brunauer-Emmett-Teller	MOF	Metal Organic Framework
BPDC	4,4′-biphenyldicarboxylate	NLDFT	Non-local Density Functional Theory
CCDC	Cambridge Crystallographic Data Centre	OMS	Open Metal Site
CCS	Carbon Capture and Storage	PSA	Pressure Swing Adsorption
CMS	Carbon Molecular Sieve	PXRD	Powder X-Ray Diffraction
COF	Covalent Organic Framework	ROA	Rate of Adsorption
3D	Three Dimensional	RT	Room temperature
2D	Two Dimensional	S	Selectivity
D_c	Diffusion Coefficient	SCXRD	Single Crystal X-ray Diffraction
DCM	Dichloromethane	SSL	Single Site Langmuir
DFT	Density Functional Theory	EDXA	Energy Dispersive X-Ray Analysis
DMA	Dimethylacetamide	TGA	Thermo Gravimetric Analysis
DMF	Dimethylformamide	THF	Tetrahydrofuran
DOBDC	2,5-dihydroxybenzene-1,4-dicarboxylate	Um-MOF	Ultra-microporous MOF
DSC	Differential Scanning Calorimetry	ZIF	Zeolitic Imidazolate Framework
DSL	Dual Site Langmuir	µl	Micro litter
EtOH	Ethanol	mmol	Milli moles
g	Gram	MOF	Metal Organic Framework
GCMC	Grand Canonical Monte Carlo	NLDFT	Non-local Density Functional Theory
HCl	Hydrochloric Acid	OMS	Open Metal Site
HOA	Heat of Adsorption	PCP	Porous Coordination Polymer
HOF	Hydrogen-bonded Organic Framework	PSA	Pressure Swing Adsorption
IAST	Ideal Adsorption Solution Theory	PXRD	Powder X-Ray Diffraction
IMDA	Imino Diacetate	Q_{st}	Isosteric Heat of Adsorption
INA	Iso-nicotinic acid	RH	Relative Humidity
MeOH	Methanol	RT	Room temperature
mg	Milligram	Temp.	Temperature
M-L bond	Metal-ligand bond		

Publications

Included in Thesis:

1. **Rahul Maity**, Debanjan Chakraborty, Shyamapada Nandi, Kushwaha Rinku and Ramanathan Vaidhyanathan, Microporous mixed-metal mixed-ligand metal organic framework for selective CO_2 capture, *CrystEngComm*, 20, 6088–6093, (**2018**).

2. **Rahul Maity**, Himan D. Singh, Ankit K. Yadav, Debanjan Chakraborty and Ramanathan Vaidhyanathan, Water-stable Adenine-based MOFs with Polar Pores for Selective CO_2 Capture, *Chem. Asian J.*, 14, 3736 – 3741, (**2019**).

3. **Rahul Maity**, Shyamapada Nandi, Sergio R. T. Filho, Renjith S. Pillai, Guillaume Maurin, and Ramanathan Vaidhyanathan, Investigating the Presence and Absence of CO_2 Interactions in MOFs with Comparable Pores having Divergent Environments, (2021) submitted.

Not included in thesis:

4. **Rahul Maity**, Debanjan Chakraborty, Shyamapada Nandi, Ankit K. Yadav, Dinesh Mullangi, C. P. Vinod, and Ramanathan Vaidhyanathan, Aqueous-Phase Differentiation and Speciation of Fe^{3+} and Fe^{2+} Using Water-Stable Photoluminescent Lanthanide-Based Metal-Organic Framework, *ACS Appl. Nano Mater*., 2, 5169–5178, (**2019**).

5. Debanjan Chakraborty, Shyamapada Nandi, **Rahul Maity**, Radha K. Motkuri, Kee Sung Han, Sean Collins, Paul Humble, James C. Hayes, Tom K. Woo, Ramanathan Vaidhyanathan, Praveen K. Thallapally, An Ultra-microporous Metal Organic Framework with Exceptional Xe Capacity, *Chem. Eur.J.*, 26, 12544 –12548, (**2020**).

6. Shyamapada Nandi, Phil De Luna, **Rahul Maity**, Debanjan Chakraborty, Thomas Daff, Thomas Burns, Tom K. Woo and Ramanathan Vaidhyanathan, Imparting Gas Selective and Pressure Dependent Porosity into a Non-Porous Solid via Coordination Flexibility, *Mater. Horiz*., 6, 1883—1891 (**2019**).

7. Debanjan Chakraborty, Shyamapada Nandi, Rajith Illathvalappil, Dinesh Mullangi, **Rahul Maity**, Santosh K. Singh, Sattwick Haldar, Chathakudath P. Vinod, Sreekumar Kurungot, and Ramanathan Vaidhyanathan, Carbon Derived from Soft Pyrolysis of a Covalent Organic Framework as a Support for Small-Sized RuO2 Showing Exceptionally Low Overpotential for Oxygen Evolution Reaction. *ACS Omega*, 4, 13465–13473, (**2019**).

8. Sattwick Haldar, Rinku Kushwaha, **Rahul Maity**, and Ramanathan Vaidhyanathan, Pyridine-rich Covalent Organic Frameworks as High-performance Solid State Supercapacitors. *ACS Materials Lett*., 1, 490−497, (**2019**).

9. Shyamapada Nandi, **Rahul Maity**, Debanjan Chakraborty, Hemkalyan Ballav, and Ramanathan Vaidhyanathan, Preferential Adsorption of CO_2 in an Ultramicroporous MOF with Cavities Lined by Basic

Groups and Open-Metal Sites. *Inorg. Chem.*, 57, 5267−5272, (**2018**).

10. Sorout Shalini, Shyamapada Nandi, Anita Justin, **Rahul Maity** and Ramanathan Vaidhyanathan, Potential of ultramicroporous metal-organic frameworks in CO_2 clean-up. *Chem. Commun.*, 54, 13472-13490, (**2018**).

11. Shyamapada Nandi, Jens Rother, Debanjan Chakraborty, **Rahul Maity**, Ulrike Werner-Zwanzigerd and Ramanathan Vaidhyanathan, Exceptionally stable Bakelite-type polymers for efficient pre-combustion CO_2 capture and H2 purification, *J. Mater. Chem. A*, 5, 8431–8439, (**2017**).

12. Shyamapada Nandi, Debanjan Chakraborty, **Rahul Maity**, Ramanathan Vaidhyanathan, Selective CO_2 capture in ultra-microporous MOFs simultaneously functionalized with bare metal site and amine group (**2020**) submitted.

13. Mahendra Wagh, **Rahul Maity**, Rohit Bhosale, Divyam Semwal, Ramanathan Vaidhyanathan, Gangadhar Sanjayan, Three in one: Triple G-C-T base coded nucleobase amino acid: Synthesis, peptide formation and structural features. (**2020**) submitted

Chapter 1

Introduction to adsorbents for selective CO₂ capture to curb carbon emission

Source: https://esgclarity.com/global-warming-set-to-wipe-at-least-10-from-gdp/

1.1 Introduction:

The sky-rocketing rise of global CO_2 concentration is one of the major environmental concerns today because of its detrimental effects on temperature rises, climate change, insufficiency in supply of water, drought, weed and pest invasions, wildfire threats, extreme storm damage, and coastal-land salinity, just to name a few (Figure 1.1). According to the report (June 4, 2019) of the National Oceanic and Atmospheric Administration (NOAA),[1] 2019 is the second hottest year on the record, trailing only 2016. NOAA has reported that the highest value of CO_2 concentration in May 2019 was 3.5 ppm more than the 411.2 ppm was observed in May 2018, and it was the second-highest annual jump in the CO_2 concentration data set. The entire world is not on the appropriate track to meet its agreed goal of the limiting warming to 2°C. Under current policies and regulations, the expected warming will be in the range 3.1-3.7 °C.[2] Therefore, cutting CO_2 emissions is among the prime targets
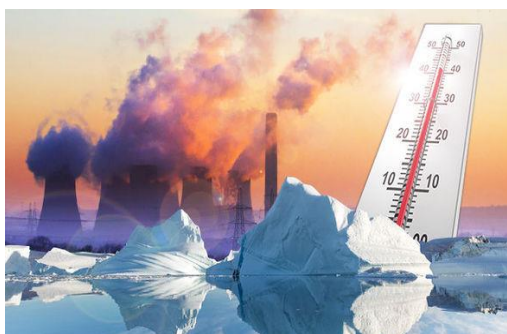
Figure 1.1. World-wide temperature jumps and global warming[1a]

of the coming decades. CO_2 is mainly ejected from the burning of fossil fuels by industries and transport systems. Although it is world-wide efforts to look for alternate energy sources, our comfortable daily lifestyles are still now almost fully dependent on the power generated from the fossil fuels and will be so for the up-coming few decades. Consequently, as of now, the only and immediate technique to continue using fossil fuel while cutting CO_2 footprint is Carbon Capture and Storage (abbreviated to CCS technology).

1.2 What is the state of CCS?

Carbon capture and storage (CCS) is a kind of technology that can reduce about 90% of the total CO_2 emission[3] for the ignition of fossil-fuels in the power-plants, human made industries, and transportation systems, etc avoiding the release of CO_2 into the atmosphere. CCS involves following three counter process.[3]

1. *Capturing the CO_2 from industrial waste gas,*

2. *Transporting the CO_2, and*

3. *Securely, storing the CO_2 via underground it in the consumption of gas and oil fields, enhanced oil recovery (EOR) or deep saline aquifer formation.*

CO_2 capture technology describes the capture and separation of CO_2 from other gasses. CO_2 can be separated in three ways - pre-combustion capture, post-combustion capture, and air-capture. CO_2 is then transported by pipelines, road tanker, or ships for safe storage. CO_2 is then stored for selected geological rock formation in the underground, several kilometres below the earth surface.

1.3. Process of capturing the CO_2 from industrial waste gas under CCS technology:

1.3.1. Pre-combustion capture:

Pre-combustion capture describes mainly the capture and separation of CO_2 from the H_2 (Figure 1.2).[4] In the pre-combustion process, the aim is to remove the carbon from the coal fuel before its combustion. As for example in the gasification processes a feedstock such as coal is generally partially oxidised in the steam and O_2/air using high temperature and pressure to from synthesis gas (Syn gas: mixture of H_2 and CO), CO_2 and small amount of other gaseous components like CH_4. The Syn gas is allowed to undergo water gas shift reaction (CO + $H_2O \rightleftharpoons CO_2 + H_2$) to form ultimately CO_2 and H_2 gas mixture. Generally, CO_2 present in 15-50 % in the final gas mixture and the CO_2 is then captured, separated and the H_2-rich fuel is used for combustion. It is worth to mention that H_2 can be separated and either burned directly as fuel or compressed to store for using it in the fuel-cell cars. Commercially available pre-combustion technologies use physical and chemical adsorption processes. And the adsorption process will cost about 60 USD/tonne of CO_2 to capture CO_2 generated from the power plant by the integrated gasification combined cycle (IGCC) process. But target of the DOE is to reduce this cost to 30 USD/tonne of CO_2.[5] Pre-combustion capture process involves three key separation processes viz. advanced solvents, sorbents, and membranes which should be the topic of research to achieve the DOE's limiting target.
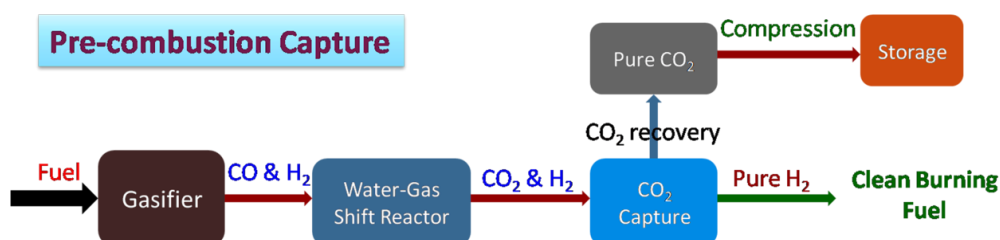
Figure 1.2. Schematic representation of the pre-combustion CO_2 capture unit.

In this regard, ultra-microporous metal-organic frameworks (UMMOFs) with pore size less than 6 Å built from short-rigid linkers are well-suited materials for excellent molecular sieving of CO_2 over H_2 for selective CO_2 capture/separation. In this context, Nandi et al.[6] reported ultra-microporous nickel isonicotinate MOF with pore sizes of 3.5 and 4.8 Å. It has large CO_2-working capacities (3.95 mmol g^{-1}) and exceptional CO_2/H_2 separation capability for pre-combustion CO_2 capture and hydrogen purifications. Computational analysis indicated a high number density of CO_2-loving sites which allow $CO_2\cdots CO_2$ and cooperative interactions. In addition, the ultra-micropores generated by a short and rigid isonicotinate offers mechanical, hydrolytic, and hydrostatic stabilities of isonicotinate-framework toward humid gas mixture. Similarly, Eddaoudi and co-workers[7] reported ultra-microporous fluorinated MOFs: SIFSIX-3-M (M = Cu and Zn) having a pore width of 3.5 and 3.84 Å in Cu and Zn analogues respectively. SIFSIX-3-Cu showed an excellent volumetric high CO_2 capacity of 82.6 cm^3 cm^{-3} (3.7 mmol g^{-1}) whereas SIFSIX-3-Zn uptakes 55 cm^3 cm^{-3} (2.5 mmol g^{-1}) at 10 mbar (1% CO_2) and 298 K. Moreover, both the SIFSIX MOFs were able to capture CO_2 from extremely low concentration (400 ppm) and proven to be applicable for direct CO_2 capture. However, the thesis, is more pertinent to post-combustion CO_2 capture and the ultra-micropores could be equally effective for CO_2/N_2 separation.

1.3.2. Post-combustion CO₂ capture process:

The post-combustion capture process refers to the capture of diluted CO_2 (5-15 %) from the flue gas containing huge amount of N_2 while combustion of fossil fuel in the air (containing a major portion of N_2, Figure 1.3).[8] First, the widely used capture methods involves passing the lean CO_2-laden flue gas through a solvent in adsorption-based column followed by desorption or striping the column by heating or dropping the pressure to release the CO_2. The second method involves calcium cycle capture process where lime is used for capturing CO_2 to chemically produce limestone. Then the produced limestone is heated to desorb the already chemically adsorbed CO_2. Comparably, the post-combustion technology, removes only 5-10 % of CO_2 as the gas stream contains very low partial pressures of CO_2) than pre-combustion technology which separates higher percentage of CO_2 (as gas
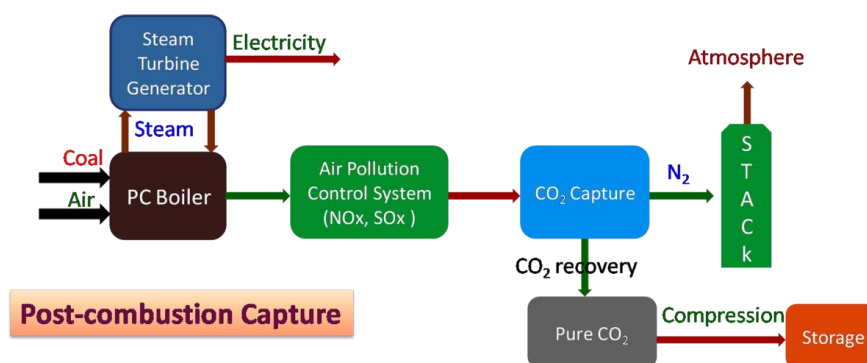
Figure 1.3. Schematic representation of the post-combustion CO_2 capture unit.

stream contains 15-50 % CO_2). Both these processes require and input of large energy penalty to remove the CO_2 from the liquid solvents or solid sorbents which use chemi-sorption process.

1.4. Solid porous physi-sorbents for selective CO_2 capture:

CO_2 from the flue gas mixture could be removed using a range of solid porous-physi-sorbents, and the mechanism of physisorption, for CO_2 capture could be shown as,

$$CO_2 + surface = (CO_2) \bullet (surface)$$
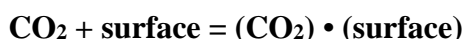
Here, the selective CO_2-sorption, is dependent on the strength of van der Walls force of attraction between the CO_2 and sorbent pore-surface and on the ion-pole and pole-pole interactions between the quadruple of carbon di-oxide and the ionic or polar binding sites of the solid surface of the sorbent.[9] However, over time people came up with various porous solid physisorbents (Figure 1.4), such as porous carbonaceous
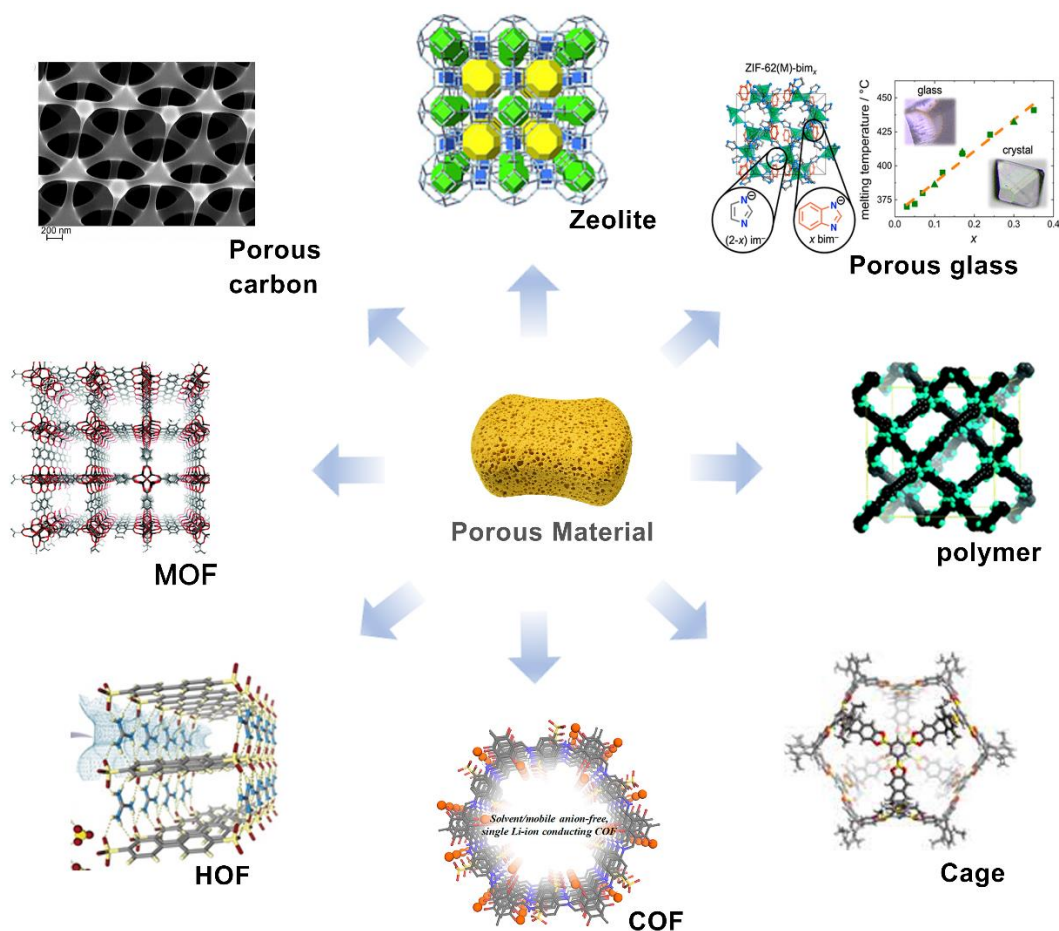
Figure 1.4. Schematic shows various types of solid-porous adsorbents for CO_2 capture. Image are reprinted (adapted) with permission from reference 10.

materials, zeolites, porous polymer, porous cages, covalent-organic framework, H-bonded-organic framework, and metal-organic frameworks (MOFs) etc. But, out of the mentioned porous solid sorbents, many suffer from poor stability in moisture or humid environments posed by flue gas and rest of the materials have problem of poor CO_2 selectivity over other gasses. However, Metal Organic Framework, abbreviated to MOF, attracts much more attention in the field of CO_2 capture and separation technology.

1.5. Description of Metal-Organic Frameworks:

Before coming to metal-organic framework one should know about the porous co-ordination polymers (PCPs). PCPs are a class of coordination compounds composed of metal ions or cluster as a connecting node, polymerised through the rigid organic ligands to build 1D, 2D, and 3D-porous structures. These metals offer coordination environment with a range of structural geometries like tetrahedral, pyramidal octahedral and trigonal square bipyramidal. Generally, metal complexes are labile during synthesis and this liability of complexes, which helps in the reversible formation and destruction of coordination bonds between the inorganic metal ions/cluster and the organic linkers. This reversible property facilates the rearrangement of metal ions and organic linkers during the polymerization-process to generate the highly ordered coordination framework (Figure 1.5).[11] In the words of Prof. Omar M. Yaghi, that MOF is porous crystal or porous sponges having very high porosity and enormous internal surface area. So, there is a difference between PCPs and MOF.[12]
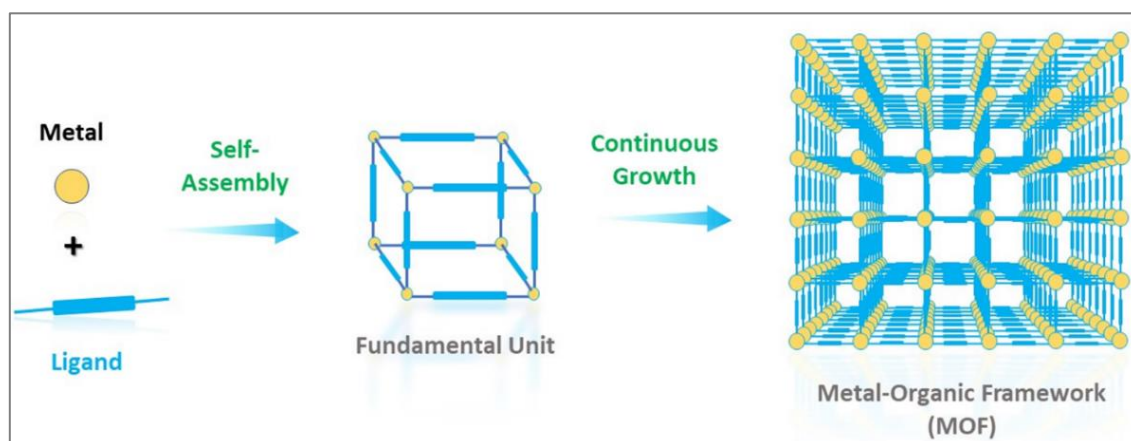
Figure 1.5. Schematic for the construction of metal-organic framework (MOF).

Later on, IUPAC gave the definition for both MOF and PCP.[13] According to the IUPAC, "*Metal-Organic Framework, abbreviated to* MOF, is a Coordination Polymer with an open 3D framework containing potential voids*" So, the MOFs are special case of PCPs (Figure 1.6).
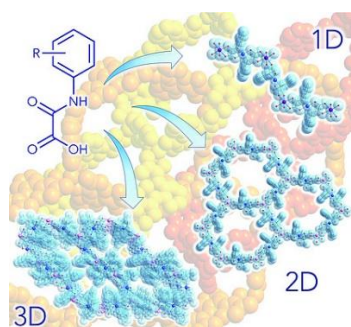
Figure 1.6. 1D, 2D and 3D coordination polymers (PCPs) using oxamate and oxamidate ligands. *Figure is reprinted (adapted) from reference 14 with permission from John Wiley and Sons.*

There are various synthetic routes for the preparation of different MOFs reported till to date. MOFs may be prepared using slow diffusion,[15] hydrothermal (solvothermal),[16] electro-chemical,[17] mechanochemical,[18] etc. Due to the scope of manipulating or substituting the metal and ligands, there are limitless possible number to design and synthesis of a library of porous MOFs. MOFs are unique compare to other aforementioned traditional sorbents owing to their tuneable pore sizes ranging from
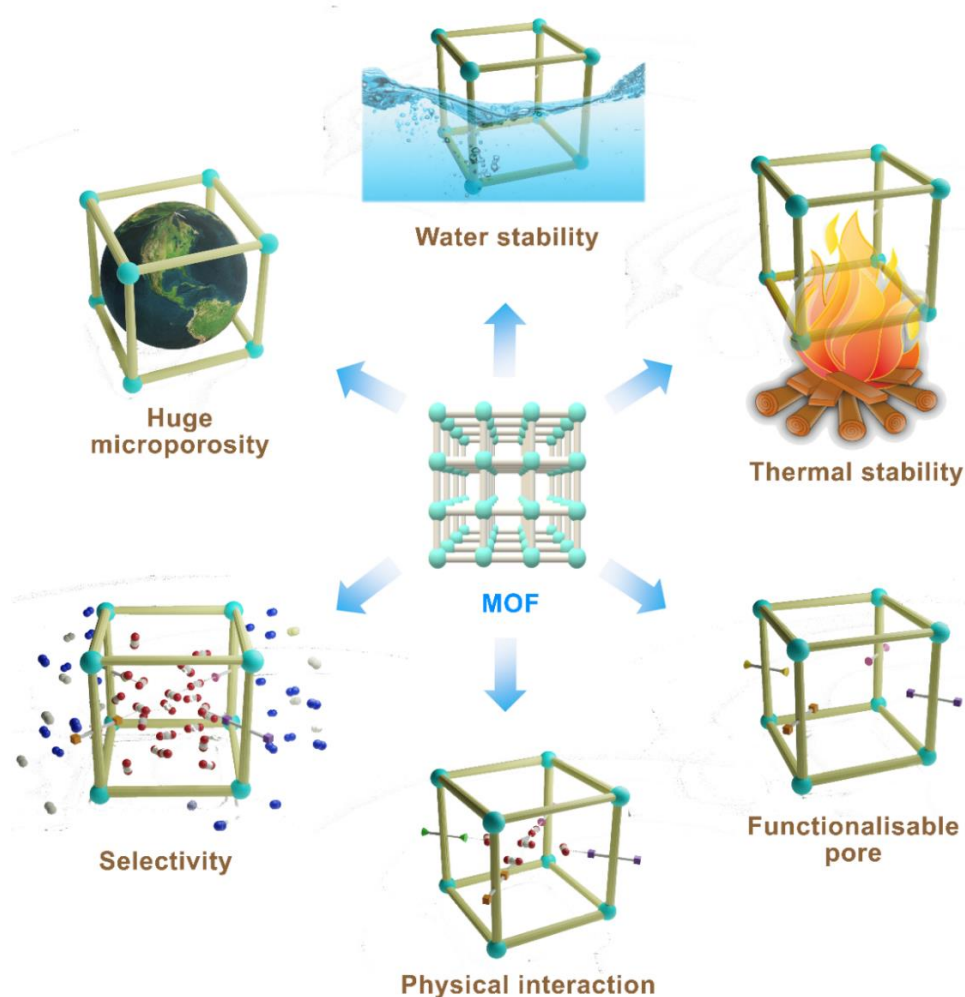
Figure 1.7. Schematic overview of the potential properties of MOF for gas capture application under the CCS technology.

microporous to the mesoporous region (Ultra-microporous: pore size < 6 Å; Microporous: pore size 6-20 Å; Mesoporous: pore size > 20 Å), high volume capacities, large surface areas, fuctionalizable pore, water and thermal stability, desirable electrochemical characteristics, electronic transduction, optical and multiple affinity (including hydrophobicity and hydrophilicity)[19] (Figure 1.7). MOFs with highly functionalized pores allow adsorption-desorption aided host−guest chemistry. These properties combined with the thermal and chemical stability make MOFs find applications in different types of captures and separations including gasses,[20] gas storage,[21] different types of catalysis such as organic catalysis, chiral catalysis, photocatalysis, and electrocatalysis etc.,[22] sensing of environmental pollutants,[23] temperature,[24] and humidity,[25] and clean energy applications like fuel cell,[26] charge storage like batteries and super capacitors,[27] magnetism,[28] and solar cell,[29] etc (Figure 1.8). But here in this thesis, we focus only on the CO_2 capture and its separation from other gasses using MOF based sorbents. MOF can display excellent low-energy physisorption based gas capture capabilities. Most industrial and power plant flue gas emissions contain substantial humidity. Pre-drying such streams for capture itself incurs sizeable cost shying industries away from investing into these capture technologies. Hence being able to capture CO_2 directly from the humid flue gas is desirable. For humid CO_2 capture, producing humidity/water stable porous materials simultaneously a good amount uptake is still challenging. This thesis's primary goal is to bring water stability into the framework of MOFs, simultaneously increasing the number of CO_2-interacting sites in the interior of the micropore of the MOF architecture.
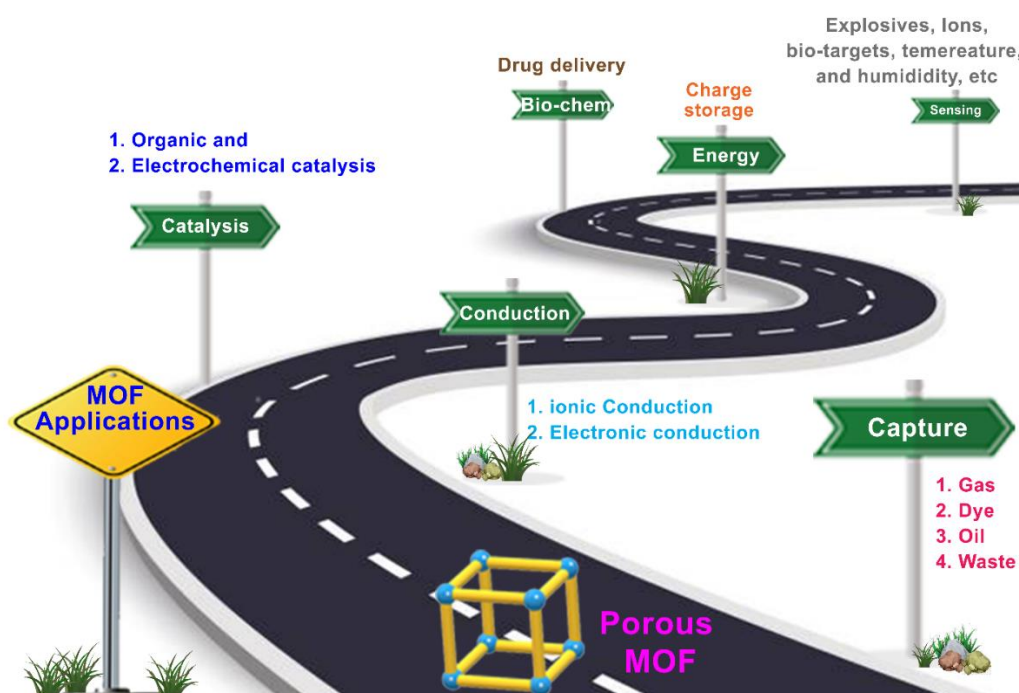
Figure 1.8. Different types of application of porous MOFs.

1.6. Water-Stable Microporous MOFs for CO_2 Capture: A Brief Discussion:

Microporous Metal–organic frameworks (MOFs) with pore size of less than 10 Å, are one of the most noticeable designer materials for selective CO_2 capture due to their tuneable micropore and pore-functionality. However, an emerging technology for CO_2 capture is the construction of water/humidity stable sorbent MOFs specially using azolate, pyridyl based linkers along with other ligands, these functional groups can provide the sufficient basicity required for the capture of the acidic CO_2. The optimisation of the physio–chemical interactions between CO_2 and MOFs via introducing the favourable binding sites in the pore-surface either in ligand backbone or as extra-framework guests to further amplifying capture ability. In the last decade, several water-stable microporous MOFs have been widely explored for CO_2 capture application. Some of the best performing water-stable microporous MOFs are discussed below.

1.6.1. Metal-adeninate based bio-MOFs for selective CO_2 capture:

Rosi and co-workers reported a series of cobalt-based adeninate MOFs (bio-MOFs-11–14). All bio-MOFs were crystallized in the I4$_1$/a space group and consisted of cobalt–adeninate–acetate 'paddle-wheel' counterparts. The unidirectional pore of bio-MOFs-11–14 is decorated with acetate (CH_3COO^-), propionate ($C_2H_5COO^-$), butyrate ($C_3H_7COO^-$), and valerate ($C_4H_9COO^-$), respectively (Figure 1.9). The channels of bio-MOF-11 are heavily functionalized with Lewis-basic amine groups are lined with -CH_3 groups from the acetates, propionate, butyrate, and valerate of the building blocks. The permanent micro-porosity of bio-MOFs-11–13 was checked from 77 K N_2 adsorption isotherm. Each MOF displayed a Type-I adsorption isotherm featuring a microporous nature of the material.[30] It is noteworthy that with the increase of lengths of the aliphatic chains, the pore size and the BET surface area decreased from 1148 $m^2 g^{-1}$ in bio-MOF-11 to 17 $m^2 g^{-1}$ in bio-MOF-14, respectively. Due to the same reason CO_2:N_2 selectivity was increased, with more molecular sieving effect, which was also supported by the increase of heat of adsorption value (HOA; *see* Table 1.6). IAST selectivity was calculated at 298 K up to 1 bar pressure using a 10:90 mixture of CO_2 and N_2, respectively (Table 1.1). It had been noted that as the chain length of the aliphatic acid moieties increases, the water/humidity-stability of azolate functionalized bio-MOFs-11–14 was enhanced. Bio-MOF-14 was able to retain its porosity and crystallinity even after one month of soaking it into the water.[30]

The study showed that the adeninate containing bio-MOFs are potential materials to defy the water-vapor present in the flue gas. Although the uptake of bio-MOFs is decent, the isosteric heat adsorptions are quite high, CO_2:N_2 selectivity is quite low, which could increase the parasitic

energy30 cost of instalment of CO_2 capture technology using MOFs in industries. So, there is a still room for exploring the new metal-adeninate frameworks for selective capture and separation of CO_2.

Table 1.1. Chemical formula, CO_2 uptake, isoteric heats of adsorption, and $CO_2:N_2$ selectivity of bio-MOFs.

Sorbent	Chemical formula	CO_2 Uptake (mmol g^{-1}) at 298 K	Q_{st} (kJ mol^{-1}) (loading, cm^3 g^{-1})	*IAST* Selectivity[a]
Bio-MOF-11	$Co_2(Ad)_2(CH_3CO_2)_2$	4.69	33.1(2.18)	43
Bio-MOF-12	$Co_2(Ad)_2(C_2H_5CO_2)_2$	3.17	38.4(2.91)	52
Bio-MOF-13	$Co_2(Ad)_2(C_3H_7CO_2)_2$	2.01	40.5(3.01)	40
Bio-MOF-14	$Co_2(Ad)_2(C_4H_9CO_2)_2$	1.39	-	-
[a] Selectivity was calculated at 1 bar and 298 K $CO_2:N_2$ (10:90 mixture)				
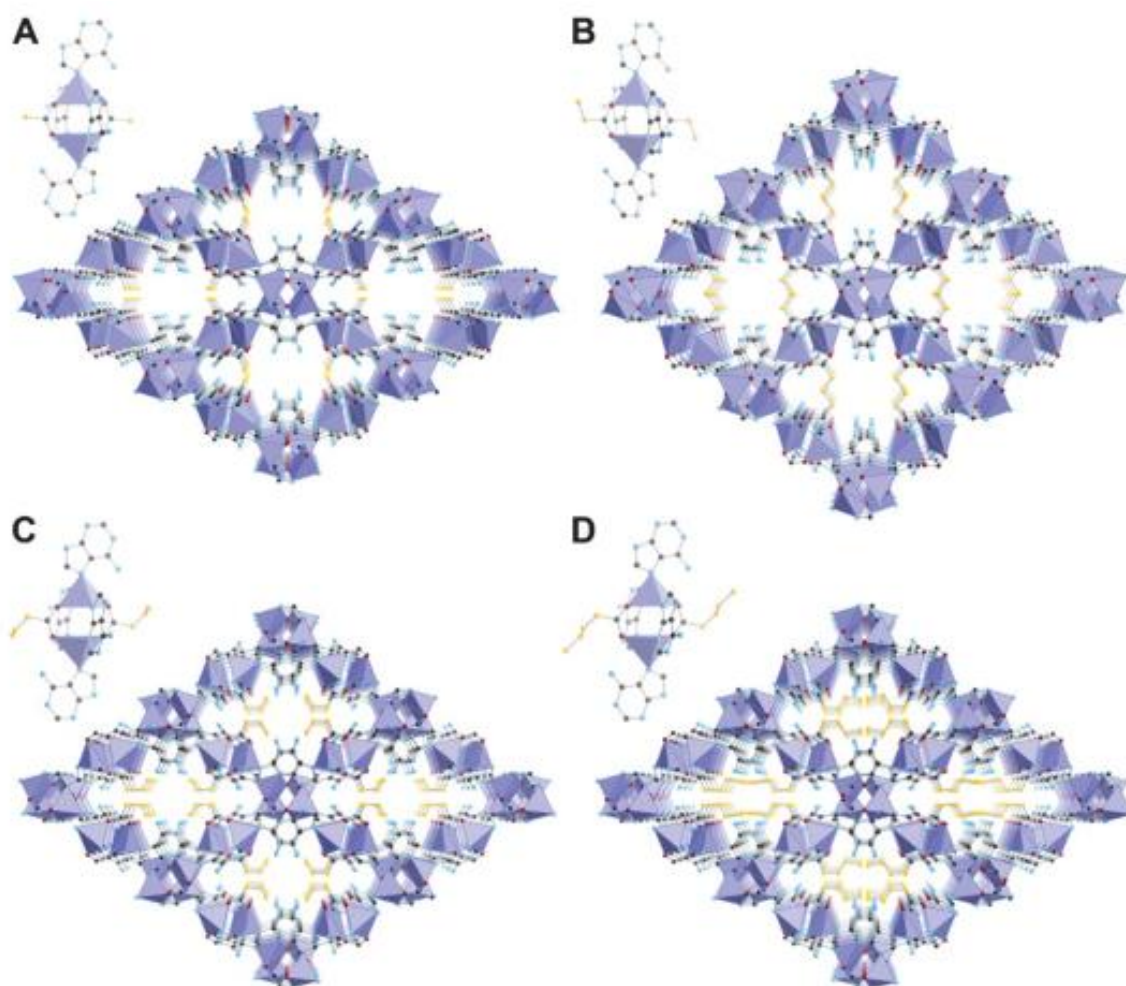
Figure 1.9. X-ray crystallographic structures of bio-MOF-11, 12, 13, and 14 (A, B, C, and D, respectively). Upper left inset shows secondary building units (SBUs). aliphatic C, orange spheres; aromatic C, gray spheres; O, deep red spheres; N, pale blue spheres; Co^{2+}, pale purple polyhedra. H are removed for clarity. (Adopted from ref. 30 from the Royal Society of Chemistry with permission)

1.6.2. Water stable Mg-CUK-1 MOF for selective CO₂ capture:

Humphrey and co-workers reported CO_2 adsorption studies on a pyridine dicarboxylate based porous 3D Mg-coordination polymer (Mg-CUK-1) containing 1D channels with square pore windows (Figure 1.11A).[31] The MOF is highly robust and has excellent moisture-stability and thermal stability up to 500 °C. The existence of the infinite 1D metal hydroxide (M-OH) chains in Mg-CUK-1 provides rigidity and strength to the corrugated framework. Generally, transition-metal MOF undergoes slow hydrolytic decomposition over time, but due to the higher hardness of Mg^{2+}, and presence of pyridyl functionality, the desolvated or activated Mg-CUK-1 is very stable to water when suspended in fresh H_2O. The water stability of the Mg-CUK-1 was confirmed from the PXRD. Mg^{2+} metal ions in the as made MOF have octahedral coordination environment. These Mg^{2+} ions strongly bridge into the infinite chains of Mg_3OH triangles. CO_2 uptakes were found to be 3.2 mmol g^{-1} and 3.5 mmol g^{-1} at 303 K for the desolvated MOF (black squares) and in the presence of 18 % relative humidity (RH) (blue circles), respectively (Figure 1.11B). Kinetic CO_2 uptake experiments revealed a 1.8-fold enhancement (from 4.6 wt% to 8.5 wt%) in the CO_2 uptake for the water-
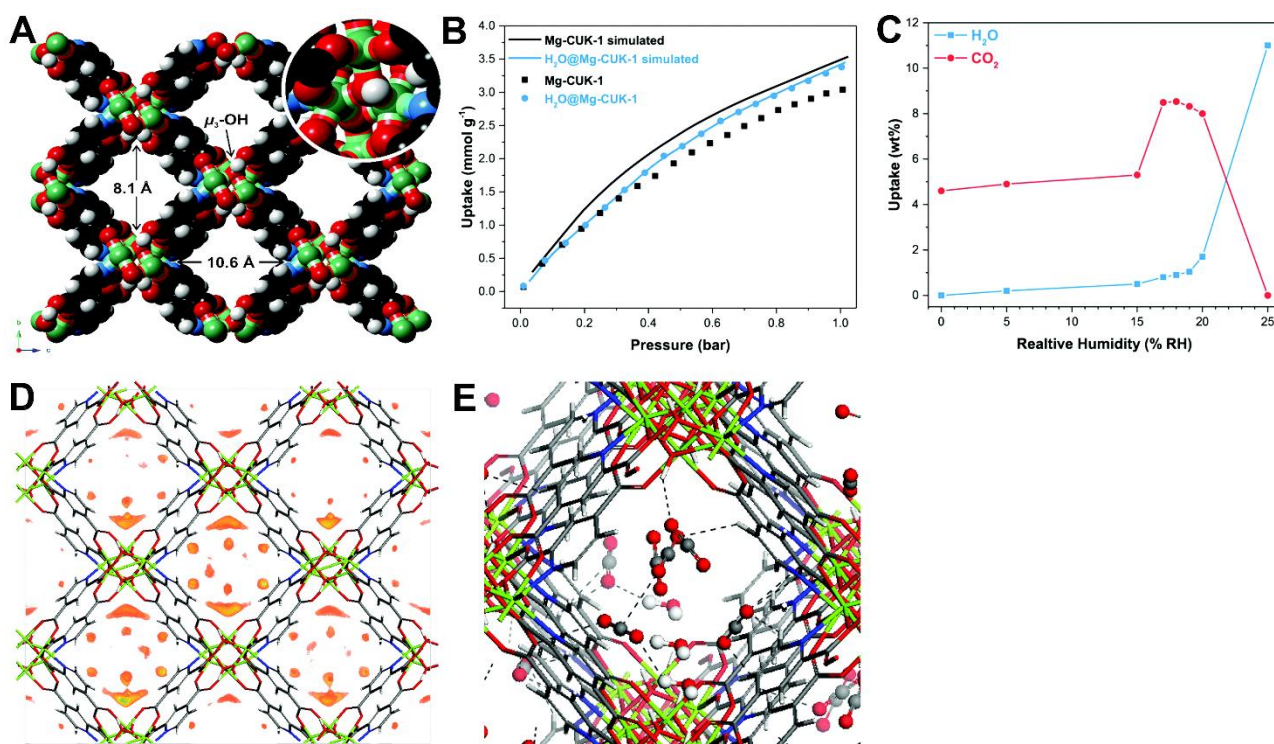
Figure 1.11. (A) Single crystallographic 3D structure of Mg-CUK-1 (along a-axis), showing hydroxyl group lined 1D channels along the b-axis. (B) CO_2 gas adsorption isotherm of activated Mg-CUK-1 without humidity (black squares) and in the presence of 18% relative humidity (blue circles) at 303 K and 1 bar pressure. The simulated sorption isotherms are represented as solid lines. (C) CO_2 uptake of H_2O presorbed-sample and Mg-CUK-1 at various %RH and 303 K (obtained from the kinetic adsorption experiments). (D) Position of mass distribution of H_2O in Mg-CUK-1 obtained from GCMC calculation assuming one H_2O/unit cell at 303 K. (E) Diagram shows the CO_2-framework, CO_2-water interactions at the distances between CO_2 and other surrounding atoms less than 3 Å. *(Adopted from ref. 31 with permission from Royal Society of Chemistry).*

tolerant Mg-CUK-1 under 18 % RH (Figure 1.11C). Grand Canonical Monte Carlo simulations were employed to visualize the molecular level insights into the adsorption mechanism for the observed increment in CO_2 sorption capacity. The high HOA value (36.5 kJ mol^{-1}) of CO_2 in the presence of H_2O, is caused by the favourable intermolecular adsorbate-adsorbate interactions between CO_2 and H_2O trapped inside the micropores of the MOF and that was also validated from the molecular simulations study. Simulation showed the CO_2-framework and CO_2-H_2O interaction (Figure 1.11D and E) within the pocket of Mg-CUK-1.

1.6.3. Moisture stable MW- Co-PL-1 MOF for CO$_2$ capture:

Lin and co-workers have been described CO_2 adsorption studies of a layer-pillared MW-Co-PL-1 MOF (Figure 1.12A).[32] The moisture stable MW- Co-PL-1 was synthesized from 4,5-imidazole dicarboxylate, and 4,4′-bipyridyl ligands via micro-wave assisted synthesis pathway only in 30 min at 180 ºC. The MOF has surface area of 345 m^2 g^{-1} calculated from the 77 K N_2 sorption isotherm (Figure 1.12B). MW-Co-PL-1 showed decent CO_2 uptake (89 mg g^{-1} or 2.0 mmol g^{-1}; Figure 1.12C) at 298 K and 1 bar partial pressure of CO_2, and also at very low pressure (53 mg g^{-1} at 298 K, 0.15 bar), but with very high zero loading HOA value (55 kJ mol^{-1}; Figure 1.12D) and very low IAST CO_2/N_2 selectivity (19.8 at 1 bar and 44 at 0.15 bar) at 298 K using 15CO_2:85N_2. The MOF showed reversible CO_2 uptake over several adsorption-desorption cycles at 25 °C and desorption was done at relatively higher temperature i.e., 65 °C suggesting a very strong framework-CO_2 interaction that is also reflected by the high HOA value.
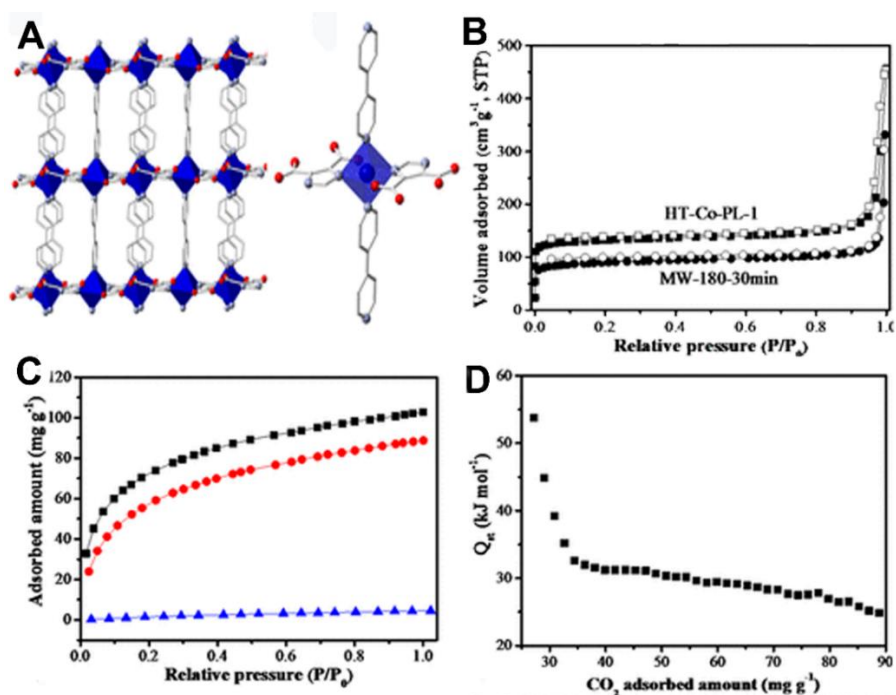
Figure 1.12. (A) Crystal structure view of the Co-PL-1 and its secondary building unit (SBU). (B) N_2 gas-sorption isotherms of Co-PL-1 MOFs at 77 K up to 1 bar pressure. (C) CO_2 gas-sorption isotherm at 5 °C (black square) and 25 °C (red ball), and N_2 gas-sorption isotherm (blue triangle) at 25 °C. (D) The heat of sorption of CO_2 on MW-180-30 min sample *(Adopted from ref. 32 with permission from American Chemical Society).*

1.6.4. Water Stable PCN-200 MOF for Selective CO_2 Capture:

Zhou and co-workers synthesized a Cu-based MOF (named as PCN-100), from the tetrazolate-5-carboxylate (tzc) and the 1,3-di(4-pyridyl)propane) (dpp) ligands (Figure 1.13A).[33] The choice of ligands was to make an ultra-microporous MOF that can only fit one CO_2 in the small-size cavity of MOF to get very strong
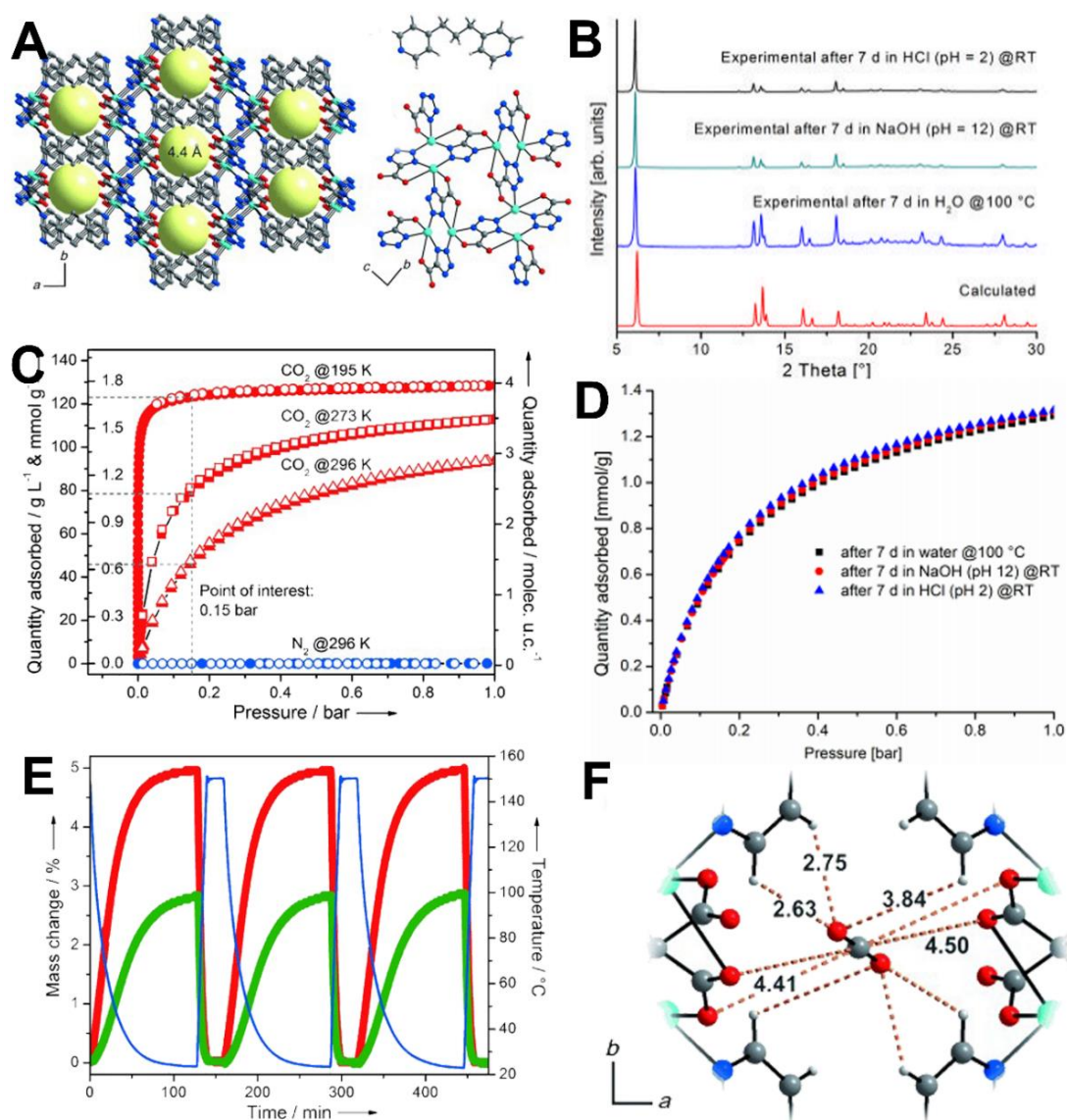
Figure 1.13. (A) Single crystal structure view of activated PCN-200 along c axis. Inset shows the linker: 1,3-di(4- pyridyl)propane and a [Cu(tzc)]$_n$ layer along a axis. (B) Powder XRD patterns shows water and chemical stability of PCN-200. (C) The graphic shows gas sorption isotherms for CO_2 and N_2 of PCN-200 at different temeratures. (D) CO_2 adsorption isotherm at 296 K shows retention of porosity even after treatment with water, NaOH and HCl. (E) The graph shows gravimetric sorption studies on activated PCN-200 using Thermo-Gravimetric Analysis. Percent of Mass changes with respect to temperature are plotted for pure CO_2 as red circles and for CO_2/N_2 (15:85) mixture as green circles. The gas flow rates are maintained at 40 mL min^{-1} and temperatures of sample are plotted with blue lines. (F) Crystallographic view of multiple binding sites for CO_2 in the pore of PCN-200, obtained by in situ synchrotron-based powder diffraction. Distances are given in Å. *(Adopted from ref. 33 with permission from American Chemical Society).*

framework-CO_2 interactions. PCN-200 is able to hold its framework integrity up to 218 °C. The MOF has stability even after stirring in aqueous HCl solution of pH = 2 and aqueous NaOH solution of pH = 12. It can also hold its framework integrity and porosity after boiling in water for 7 days as confirmed from PXRD patterns and CO_2 sorption data (Figure 1.13B and D). This ultra-chemical and thermal stability of the MOF was supported by the significantly strong intersheet stability obtained due to having the stronger N-Cu bonds in the framework-backbone. The MOF has very low uptake (about 1.25 mmol g^{-1}) at 296 K and 1 bar pressure (Figure 1.13C). The solved crystal structure (from in situ synchrotron-based powder diffraction data followed refinement it by the Rietveld method) of the PCN-200-CO_2 after CO_2 loading, suggested about the CO_2 trapping mechanism inside the activated PCN-200. Due to presence of propylene chain in bpp ligand, upon activation PCN-200 gets shrinked (volume of unit-cell was reduced from 2489 to 2226 Å^3) and create an ultra-microporous channel of pore-size of 4.4 Å suitable for high CO_2 selectivity. Its strong CO_2-framework interaction reflected in high zero-coverage HOA value: 38 kJ mol^{-1} and 49 kJ mol^{-1}, respectively, obtained from the virial and Langmuir model fits. The CO_2/N_2 selectivity values were found to be 260 and 205 using 50:50 and 15:85 compositions for CO_2/N_2 at 296 K and up to 1 bar pressure according to the GCMC simulations protocol. Good CO_2/N_2 selectivity and dynamic cycling behaviour of activated PCN-200 were confirmed from the variable-temperature gravimetric-adsorption of activated PCN-200 MOF using the TGA (Figure 1.13E). The crystallographic positions of CO_2 at the center of the cavity was determined by annealing simulations technique and DFT methods, showing multiple CO_2 binding sites which was responsible for high CO_2/N_2 selectivity (Figure 1.13F). Overall, MOF has excellent chemical stability but has very poor uptake.

1.6.5. Water Stable Surface Hydrophobic MOFs for Retaining the Porosity and CO$_2$ Uptake:

Zhu and co-workers have developed a facile solution-immersion process as a proof of concept to get water stable MOF just by depositing a hydrophobic coat on the external surface of as made MOF particles (As MOF) or crystallites without blocking their intrinsic pores.[34] This surface hydrophobic (SH) coating enhances MOFs' water stability as well as resist from the attack of water and helps in retaining the morphology, crystallinity, surface area and amount of CO_2 uptake. To generalize the strategy, entire gas adsorption studies were done by three MOFs using NH_2-MIL-121 (Ti), ZIF-67, and HKUST-1 (Figure 1.14A, B, and C). The water-based contact angle was calculated to be ~146° revealing the surface hydrophobicity (SH) of the MOFs (Figure 1.14D). After exposure to water, the CO_2 uptake of three "AS MOFs" become remarkably lower, which is very similar to that of reported surface areas for same as made MOFs while "SH MOFs" showed no significant loss in CO_2 uptake (Figure 1.14E, Fand G) and surface areas. Table 1.2 shows the surface areas before and after water treatments for both As- and SH-MOFs.
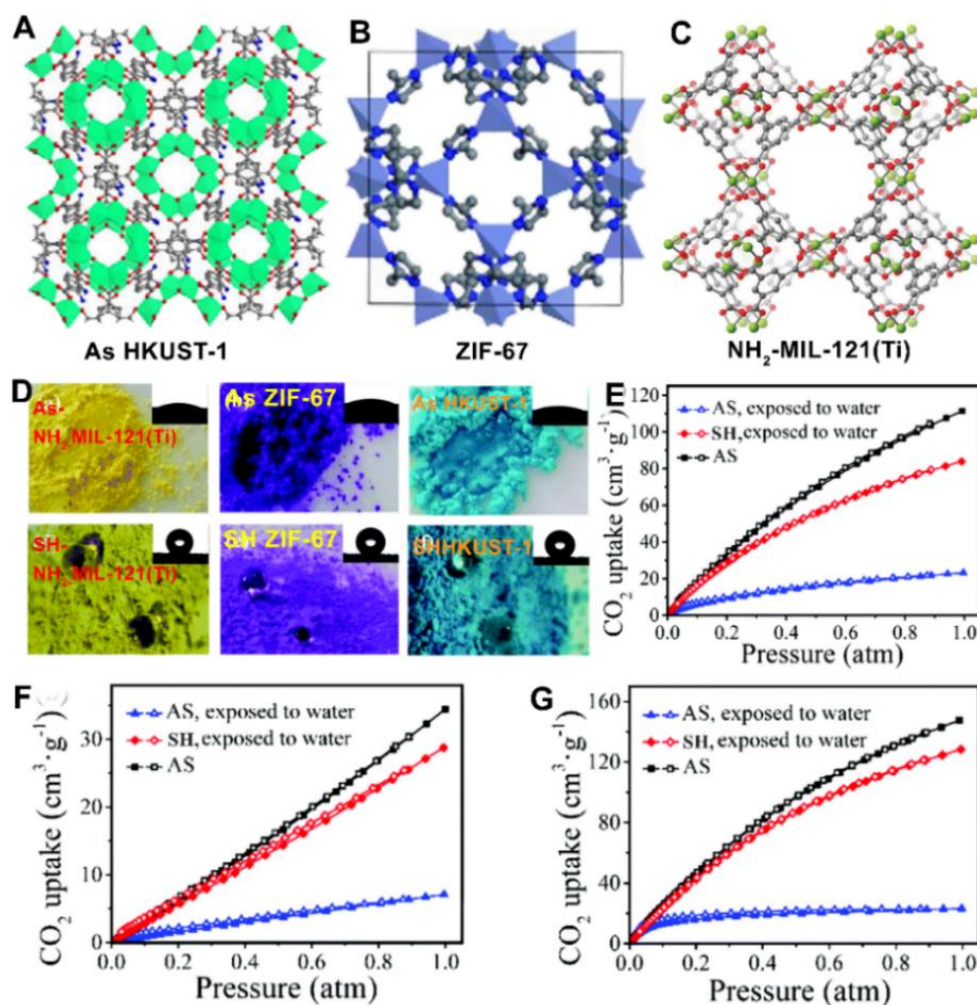
Figure 1.14. View of X-ray diffracted single crystal structures of (A) AS HKUST-1, (B) AS ZIF-67, and (C) AS NH_2-MIL-121 (Ti). (D) Optical microscopic photographs of the AS NH_2-MIL-125(Ti), AS ZIF-67, and AS HKUST-1, and SH NH_2-MIL-125(Ti), SH ZIF-67, and SH HKUST-1. Inset shows the contact angle image. CO_2 sorption isotherms 298 K up to 1 bar pressure for (E) NH_2-MIL-125(Ti), (F) ZIF-67 and (G) HKUST-1 after soaking in water for 5 days. *(Adopted from ref. 34 with permission from Royal Society of Chemistry).*

Table 1.2. List of surface areas before and after water treatments and CO_2 uptakes of different MOFs.

Material	BET Surface area ($m^2 g^{-1}$)		CO_2 uptake ($Cm^3 g^{-1}$)	
	Before water treatment	After water treatment	Before water treatment	After water treatment
As NH_2-MIL-121 (Ti)	1134	225	111	23.3
As ZIF-67	1587	67	34	6.8
As and HKUST-1	1386	39.6	149	23.84
SH NH_2-MIL-121 (Ti)	-	968	-	84.36
SH ZIF-67	-	1321	-	28.22
SH HKUST-1	-	1206	-	128.14

1.6.6. Zinc-Adenine-Isonicotinate MOF:

Zeolite Imidazolium Frameworks (ZIFs) which mimics the structure of zeolites is one of the most investigated MOFs for different purposes. ZIFs are structurally constructed by tetrahedrally coordinated di-valent metal ions and imidazolate linkers. However, the choice of frameworks with just imidazolate linker is limited. To expand the library, attempts have been made to replace imidazolate ligand with mono-negatively charged ligands. For example, adenine, which offers similar coordination atmosphere, is one of the potential candidates.
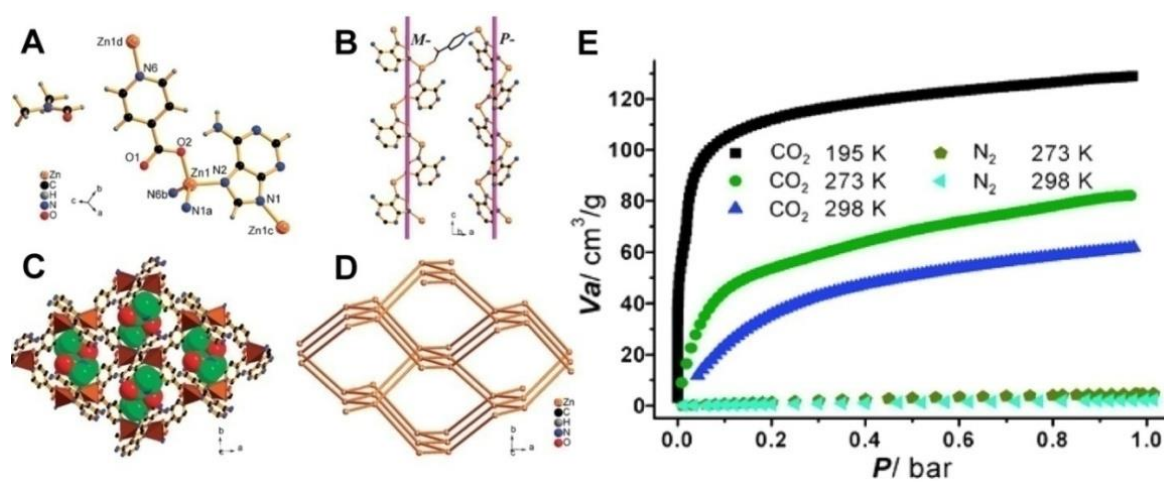
Figure 1.15. (A) The fundamental unit shows the coordination environment around $Zn^{(II)}$ (B) The zigzag Zn-adenine helices (C) 3D structure with guest DMF molecules in the pore (D) dmp topology present in the as made MOF. (E) Gas adsorption isotherms at various temperatures *(Adopted from ref. 35 with permission from Royal Society of Chemistry)*.

Wang *et al.*[35] prepared adeninate and isonicotinate based mixed ligand MOF, TIF-A1 with a molecular formula [Zn(ad)(int)](DMF) and studied its CO_2 adsorption behaviour. Similar to ZIFs, in this MOF, $Zn^{(II)}$ is tetrahedrally coordinated to two adeninate ligands and two isonicotinate ligands (Figure 1.15A). Nitrogen from two five membered rings bridge between two $Zn^{(II)}$ resulting in infinite 2_1 helices along c- axis (Figure 1.15B). Both the type of helices (right- and left-handed) together present in the crystal structure. These helices are now connected via isonicotinate to generate the 3D framework which possesses large rhombic channels with aperture size of 8.0 x 7.0 $Å^2$ along the c-axis as displayed in figure 1.15C and 1.15D. The CO_2 adsorption isotherms at different temperatures revealed high capacity of 82.2 cc g^{-1} (3.67 mmol g^{-1}) at and 61.7 cc g^{-1} (2.75 mmol g^{-1}) at 273 K and 298 K, respectively (Figure 1.15E). In comparison, ZIF-69 possesses the maximum capacity of CO_2 of 70 cc g^{-1} at 1 bar at 273 K.[146] The authors attributed the high CO_2 uptake mainly to three factors, (1) Isonicotinate as a rigid aromatic molecule provides stable and permanent porous framework, (2) Adenine can provide imidazolate coordination environment as ZIFs, (3) Uncoordinated amino and pyrimidine groups provide Lewis basic sites for adenine-guest interactions. These observations have provided some key insights for the design and synthesis of newer MOFs with varied compositions.
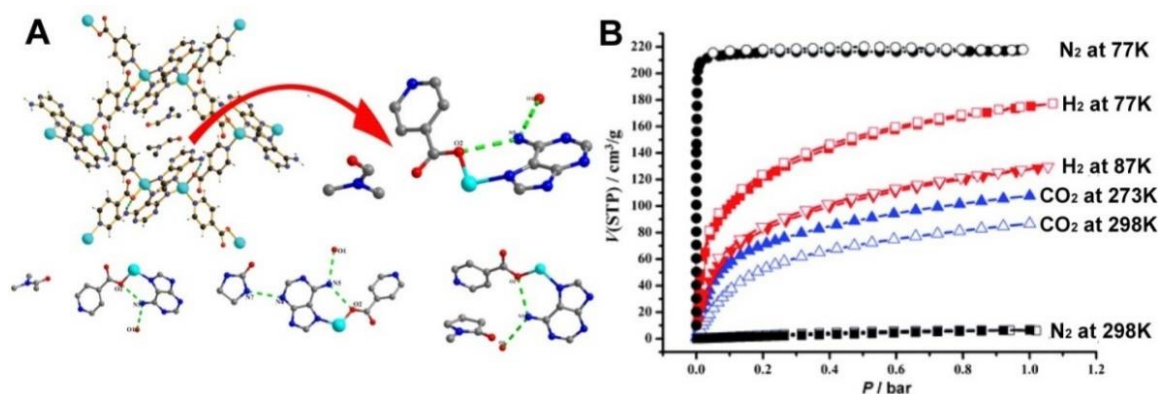
Figure 1.16. (A) Crystal stucture of the MOF showing H-bonding interaction between the guest molecules and the framework. (B) The different gas adsorption and desortion isotherms at different temperatures *(Adopted from ref. 36 with permission from Royal Society of Chemistry).*

Wang *et al.*[36] reported guest selectivity during the crystallization of the Zn-adenine-isonicotinate MOF. The order of the guest selctivity is DMF > e-urea > NMP > DMA. The guest is hydrogen bonded with the uncoordinated amine group of the adenine moiety as shown in figure 1.16A. The guests seem to play both structure directing as well as templating role. However, the guest could be post-synthetically exchanged with low boiling solvents such as methanol, DCM etc. The methanol exchanged phase exhibited high H_2 and CO_2 sorption-capacity (4.81 mmol g^{-1} at 273 K and 3.87 mmol g^{-1} at 298 K) and amazing selectivity towards CO_2 over N_2 as observed from figure 1.16B. Isosteric HOA value for CO_2 obtained for the methanol exchanged phase was 31.0 kJ mol^{-1} which is slightly high for facile regeneration. The high CO_2/N_2 selectivity (90 obtained from *IAST* model) makes this material a potential solid sorbent for post-combustion CO_2 capture.

1.6.7. Water Stable Acylamide functionalized MOF for Selective CO_2 Adsorption:

Bai and co-workers[37] reported a humid-stable porous MOF ({[Cu_2(TCMBT)(bpp)(μ^3-OH)]·$6H_2O$}$_n$), synthesized from bpp: 1,3-bis(4-pyridyl)propane) and TCMBT: N,N′,N″-tris(carboxymethyl)-1,3,5-benzenetricarboxamide. The structure of MOF was composed of the 2-D hybrid sheets which were pillared by bpp units. There are two kinds of open channels of 6.0×3.4 $Å^2$ and 4.6×3.0 $Å^2$ dimensions along the a and b crystallographic axes, respectively (Figure 1.17A) between each two layers. The very good stability of as made MOF in water for 2 months, was confirmed from the PXRDs (Figure 1.17B). This interesting pillar-layered MOF possesses a BET surface area of 808.5 m^2 g^{-1} calculated from the N_2 gas sorption at 77 K. N_2 isotherm at 77 K exhibits a typical type I curve (Figure 1.17C), indicating the sustainable constant microporosity of the activated or desolvated MOF. MOF exhibited higher CO_2 uptake than N_2 at 298 K (Figure 1.17D) that was also reflected in reasonable selectivities such as CO_2/N_2 selectivity = 20.1:1 and CO_2/CH_4 selectivity = 4:1, which are very similar to those of some of the ZIF series MOFs.
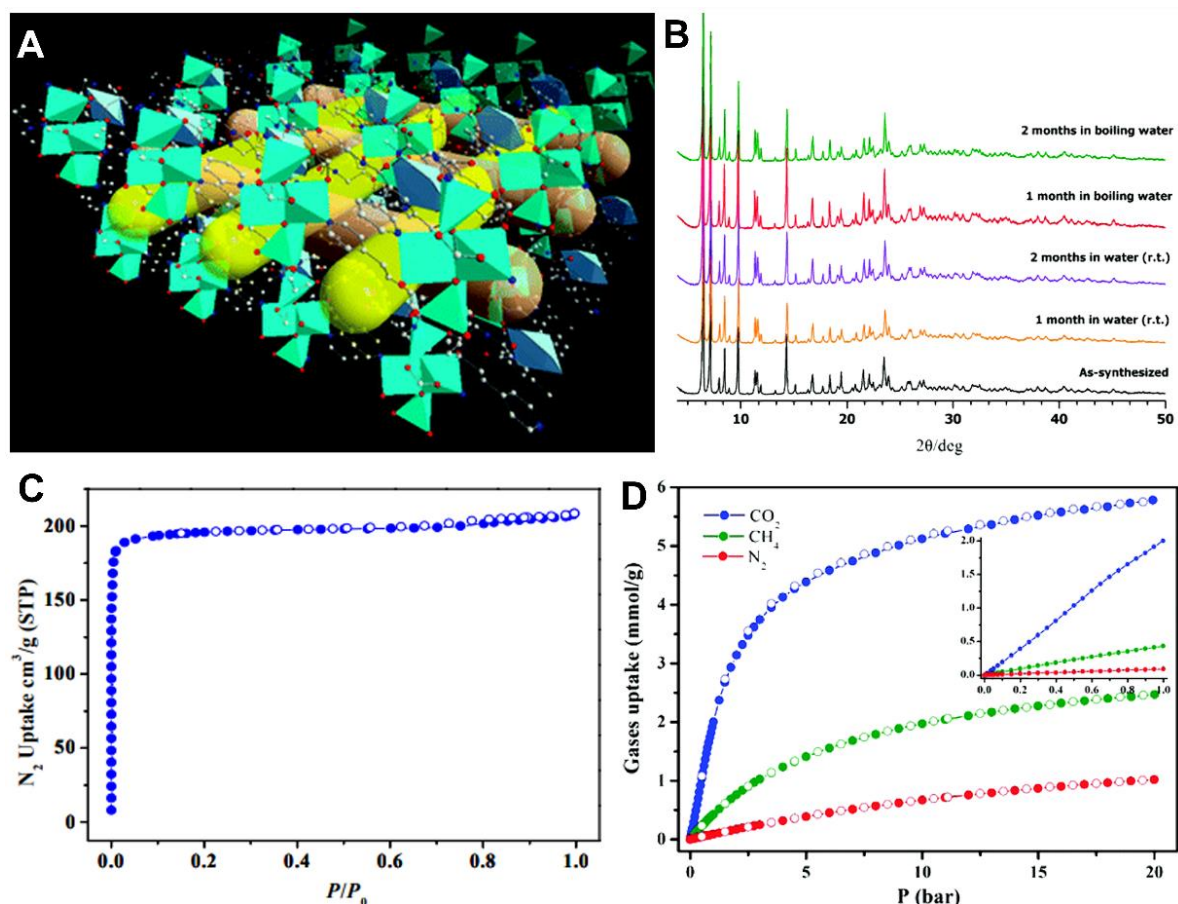
Figure 1.17. (A) The crystallographic structure of as made MOF with two types of channels between the adjacent layers: Yellow (along b-axis) and pale orange (along a-axis) columns. (B) Powder XRD patterns are showing retention of crystallinity of MOF even after water and boiling water treatment for various time intervals at ambient temperature. (C) N_2 gas-sorption isotherm at 77 K up to 1 bar pressure. Adsorption -filled circles, and desorption-open circles. (D) Gas sorption isotherms of activated MOF at 298 K up to 1 bar pressure. CO_2 (blue) CH_4 (green), and N_2 (red). *(Adopted from ref. 37 with permission from American Chemical Society).*

1.6.8. The Water-Stable Interpenetrated Co-MOF for Selective CO₂ Capture:

A interpenitrated robust MOF ($\{[Co_2(4,4'\text{-bpy})(L)]\cdot H_2O\cdot 0.5(DMF)\}_n$), was synthesized from the cobalt(II) nitrate hexahydrate, rigid tetra-carboxylate: 4,4′,4″,4‴-silanetetrayltetrabenzoate (L) and a rigid bidentate linker: 4'4'-bipyridine (4,4'-bpy) using the solvothermal reaction method.[38] Single crystal X-Ray diffracted structure of as made MOF consists of a Co(II)-paddle wheel based SBU, which was propogated to form a two-fold interpenetrated 3D network. There are rhombic (9.6 × 11.0 (5.4 × 7.0) Å^2) and trigonal (5.5 × 6.2 (1.7 × 2.5) Å^2) open channels in this framework along all three axes (Figure 1.18A). It has bulk phase purity and water stability confirmed from the intact PXRD profile (Figure 1.18B). The as made MOF was thermally stable up to 350 ºC without any crystallinity loss as confirmed from TGA and powder XRD (Figure 1.18C). The BET surface area and the Langmuir surface area were fall in the microporous range (224 m^2 g^{-1} and 343 m^2 g^{-1}
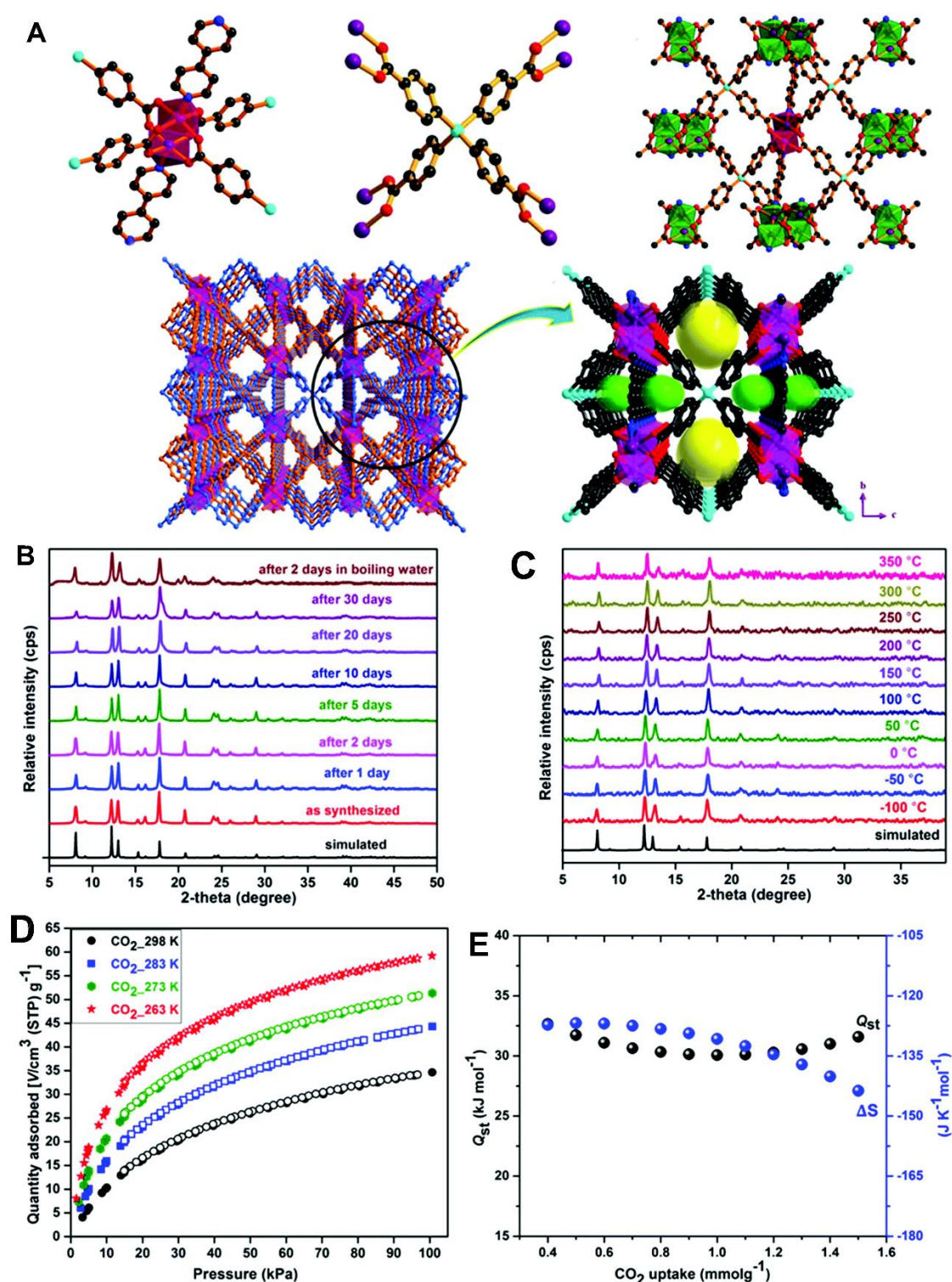
Figure 1.18. (A) View of X-ray single crystal structure of as made MOF. (B) Powder XRD patterns of MOF after soaking in water for several days to a month at room temperature and in boiling water for 2 days. Powder XRD shows the excellent water stability of MOF. (C) Variable temperature powder XRD profiles of as made MOF is showing thermal stability of as made MOF. (D) CO_2 sorption isotherms at various temperatures. Filled circles and open circles represent adsorption and desorption isotherms at 1 bar pressure. (E) ΔS and Heat of adsorption (Q_{st}) for CO_2, over loading 0-1 mmol g^{-1} using the van't Hoff isochore for isotherms in the range of 263–298 K. *(Adopted from ref. 38 with permission from American Chemical Society).*

respectively) for the solvent free MOF. The desolvated MOF exhibited decent uptake of CO_2 such as 53.8 and 36.4 cm^3 g^{-1} at 0 °C and 25 °C respectively at 1 bar pressure (Figure 1.18D), MOF showed very high zero loading HOA value of 29–3 kJ mol^{-1} (Figure 1.18E). But, MOF has moderate selectivities for CO_2/N_2 = 194.7 and 70.5 respectively, at 298 and 273 K under 1 bar partial pressure of CO_2 whereas CO_2/CH_4 selectivities were found to be 19.3 and 9.9 respectively at 0 °C and 25 °C under 1 bar partial pressure of CO_2.[38]

1.6.9. A Water-Stable IITKGP-6 MOF for Selective CO₂ Adsorption:

The 2-fold interpenetrated IITKGP-6 ({[Co₂(SDB)₂(L)]·(H₂O)₄·(DMF)}ₙ), framework (Figure 1.19A and B) was reported by Das and co-workers.[39] IITKGP-6 was built from 4,4′-sulfonyldibenzoic acid (H₂SDB) and 1,4-bis(4-pyridyl)-2,3-diaza1,3-butadiene (L) with Co(NO₃)₂·6H₂O. The MOF has microporous nature as confirmed from the N₂ adsorption isotherm at 77K and a solvent-accessible void volume was found to be of 25.5% of total unit cell volume. It has a 1D channels along [110] plane with channel width of ∼3.4 × 5.0 Å². This MOF revealed high stability toward humidity. The solvent free framework showed moderate CO₂ capacity (50.6 and 37.4 cm^3 g^{-1} at 273 and 295 K under 1 bar partial pressure of CO₂, respectively (Figure 1.19C and D). The N₂ sorption isotherms of activated and water-soaked samples displayed the uptake of 83.4 cm^3 g^{-1} and
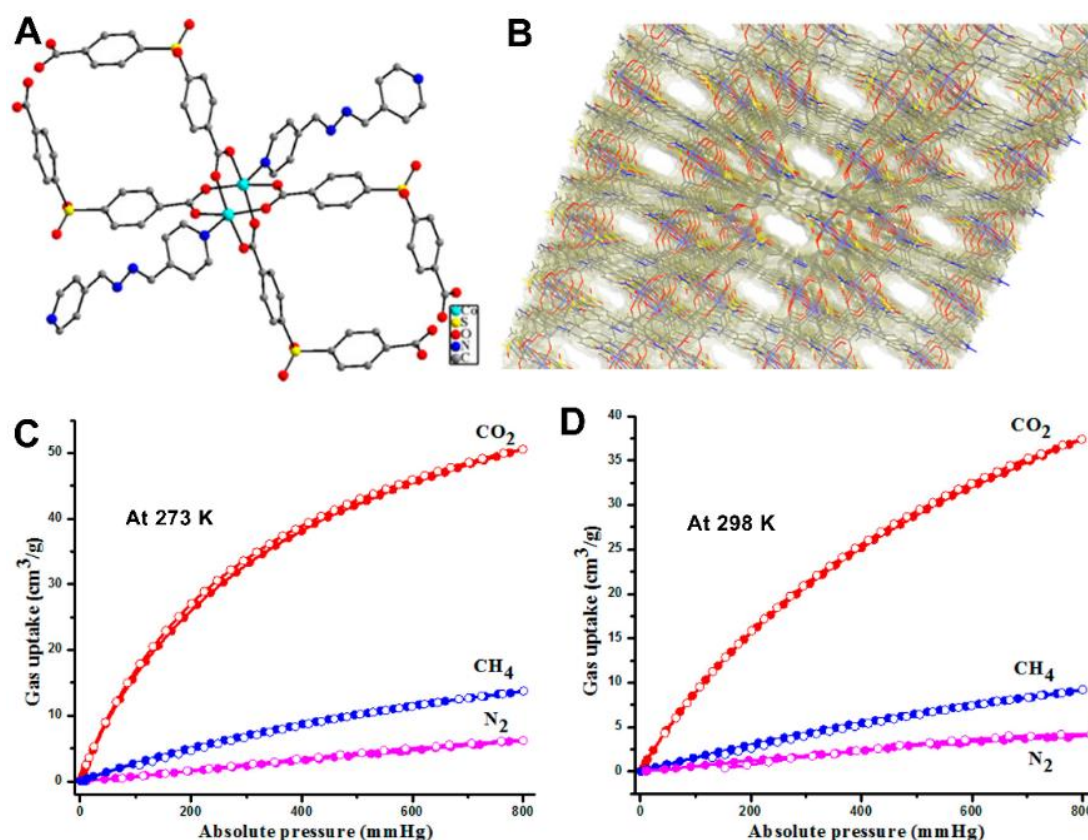
Figure 1.19. (A) A view of coordination environment with Co^{2+}-paddle-wheel unit present in IITKGP-6. (B) 3D framework showing 1D pore along [110] plane. Gas adsorption isotherms for activated IITKGP-6 (C) at 273 K and (D) at 295 K (CO₂: deep red, CH₄: dark blue, N₂: light magenta) *(Adopted from ref. 39 with permission from American Chemical Society).*

76 cm^3 g^{-1} respectively at 1 bar pressure suggesting minor drop in surface area relative to the pristine desolvated MOF (BET surface areas are 254 m^2 g^{-1} and 279 m^2 g^{-1} in water-soaked and pristine MOF). This suggests IITKGP-6 has water or moisture stability. The MOF has high *IAST* selectivity for CO_2/N_2 (51.3 and 42.8 at 273 and 295 K respectively) and CO_2/CH_4 (36 and 5.1 at 273 K and 295 K respectively) using 15:85 CO_2/N_2 and 50:50 CO_2/CH_4 compositions under 100 kPa (Figure 1.20).
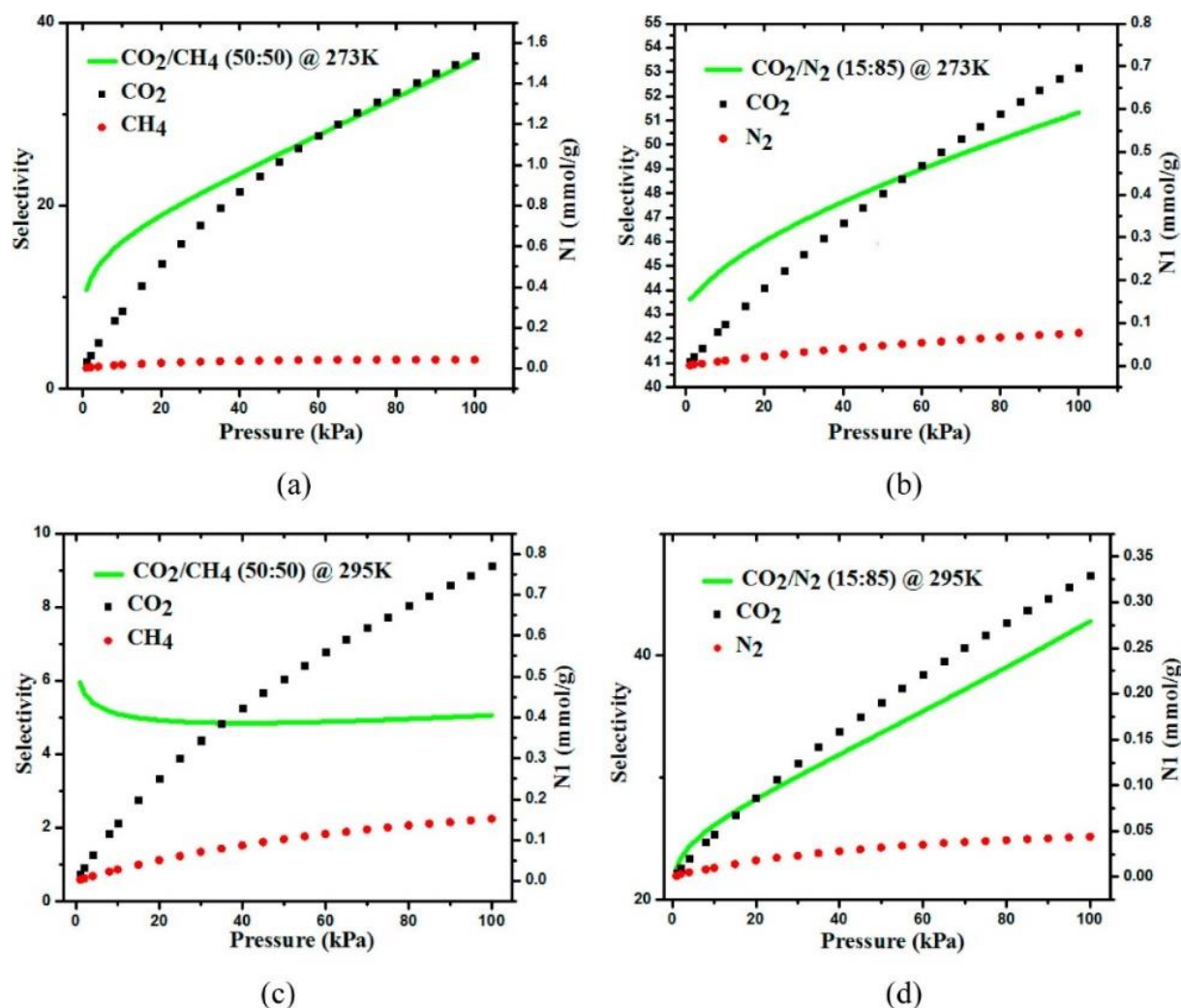
Figure 1.20. *IAST* selectivities at 273 K (A, B) and 295 K (C, D) for CO_2/CH_4 (50:50) and CO_2/N_2 (15:85). *(Adopted from ref. 39 with permission from American Chemical Society).*

1.6.10. CO$_2$ capture and direct observation of amine-CO$_2$ interactions sites inside ZnAtzOx:

Incorporation of CO_2 interaction sites in the MOF pore enhances the selectivity for CO_2 over other gases. Shimizu and co-workers synthesized an amine functionalised ultra-microporous MOF from Zn^{2+}, oxalic acid and amino triazole linkers.[40] This layer-pillared MOF consisted of Zn-ATZ layers which were pillared by oxalate units (Figure 1.21A and B). CO_2 loving free amine groups of triazolate are oriented towards the pore of MOF backbone. During CO_2 adsorption, the free amine

groups site-specifically interact with the CO_2 which is reflected in the sharp CO_2 uptake at very low CO_2-partial pressures with high capacity (3.8 mmol g^{-1}) at 298 K and 1 bar (Figure 1.21C). However, the MOF didn't show any affinity for other gases like Ar, N_2, and H_2 etc. The heat of adsorption (HOA) value was obtained using the Virial method and it was calculated to be 40 kJ mol^{-1}. Such a high HOA gave information of very strong CO_2-framework interaction (CO_2-amine and CO_2-oxalate). However, there was an unusual trend in the profile of HOA plot, a constant value over a wide CO_2 loading range, which was attributed to CO_2-NH_2 interactions and the cooperative CO_2-CO_2 interactions (solid-state crystalline CO_2 resembling T-shaped interactions) of comparable strength (Figure 1.21D). Further, the interactions were directly observed by locating the CO_2 binding sites within a single crystal of the MOF and that was also supported by theoretical study.[40]
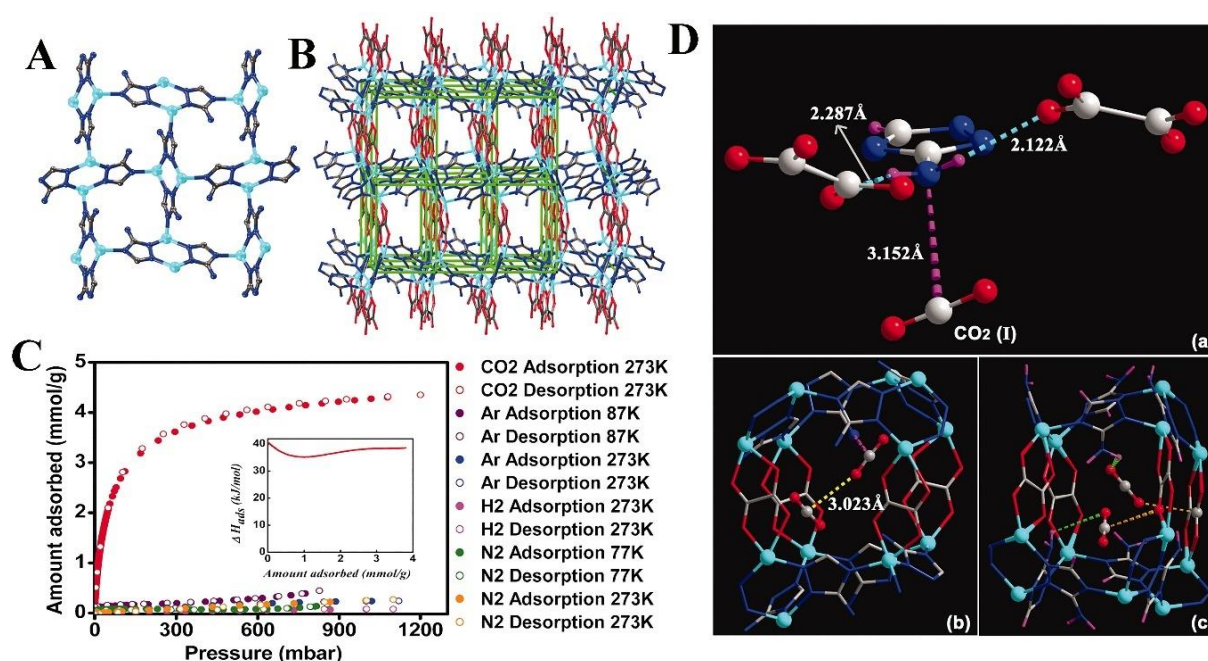
Figure 1.21. (A) Structure of Zn Amino triazole layer. (B) Three-dimensional structure of the MOF, Zn-ATZ layers pillared by oxalate linkers. (C) Different gas adsorption isotherms of the MOF at 273K. Inset shows the Heat of Adsorption curve obtained from Virial method. (D) X-ray crystallographic structure of the CO_2 loaded MOF showing the CO_2 binding sites and CO_2…CO_2 cooperative interaction. *(Adopted from ref. 40 from the American Association for the Advancement of Science with permission.).*

However, most of the transition metal-based MOFs lose their crystallinity and porosity after prolonged exposure to moisture due to the hydrolysis of their M-L coordination bonds (M = transition metal ions). On the other hand, the reported water-stable MOFs are having either very poor uptake/low selectivity or high heat of adsorption. So, through the studies of the different examples (Section 1.6 and Table 1.3) of water stable microporous MOFs for selective CO_2 capture, it is understood that still there is a room for designing and synthesis of excellent water-stable MOFs with

high CO_2 uptake, very good CO_2 selectivity, and simultaneously possessing the optimal HOA value (18-25 kJ mol^{-1}). Herein, the thesis's primary goal is to bring water stability into the framework of MOFs, simultaneously optimising the number of CO_2-interacting sites in the interior of the micropore of MOF architecture to get good uptake, selectivity and optimal HOA.

Table 1.3. Data showing the CO_2 and N_2 uptakes of different ultra-microporous MOFs at pressures relevant to vacuum swing adsorption-based CO_2/N_2 separation from flue gas (85N_2:15CO_2) compositions.

Materials	CO_2 uptake (mmol g^{-1}) at 298 K and 1 bar	Heat of adsorption (kJ mol^{-1})	CO_2/N_2 Selectivity	Ref.
Zn-FMA (IRMOF-1)	1.44	16 (at high loading)	6[a]	41
Zr-FMA (MOF-801)	2.22	29	78[a]	41
Zr-Tp (UiO-66)	1.8	25	27[a]	41
UiO-66-NH$_2$	2.97	~ 28	58[a]	41
ZnMOF-74	1.67	~ 27	87.7[b]	42
MgMOF-74	6.20	35	182.1[b]	42
UTSA-16	2.37		314.7[b]	42
NaX zeolite	2.72		145.9[b]	42
Cu-SSZ13	1.78	32.3	67.4[b]	42
H-SSZ13	1.74	33.6	71.3[b]	42
JBW	1.42		524.4[b]	42
mmenCuBTTri	2.22		329.0[b]	42
Cu-TDPAT	1.82		57.8[b]	42
ZIF-78	0.76		41.4[b]	42
MFI	0.26		11.2[b]	42
MOF-177	0.16		3.6[b]	42
MAF-66	4.41	26	185[a]	43
Mg-dobdc	5.0	47-52	-	44
SIFSIX-3-Zn		45	1818[a]	44
SIFSIX-2-Cu	1.84	22	13.7[a]	44
SIFSIX-2-Cu-i	5.41	39	140[a]	44
IISERP-MOF2	~5.25	~33	1853[a]	45

Note. [a]Measured at 298 K and 1 bar pressure, [b]Measured at 296 K and 100 kPa.

1.7. The Designing Principle of Thesis Work:

These selected MOFs, presented above, strongly describes the potential of MOF to act as porous sorbent for selective CO_2 capture. The existing library of functionalised MOFs nano-structures and the optimized synthesis routes are now helpful to explore a new generation of microporous MOFs with improved CO_2 uptakes, optimal HOAs for facile regeneration of CO_2 from the framework, water stability, huge number of amine/base functionalities, from cheap and readily available ligands. To bring the water stability in the framework, we propose two strategies using the textbook concept of Werner's theory of coordination complex:

i) **Approach-1:** *choosing the high charge metal ions (hard and oxophilic metal center) in combination with O-donor ligand (hard ligand).*

ii) **Approach-2**: *choosing the low valent transition metal ions (soft metal center) in conjunction with the strong field azolate ligands.*
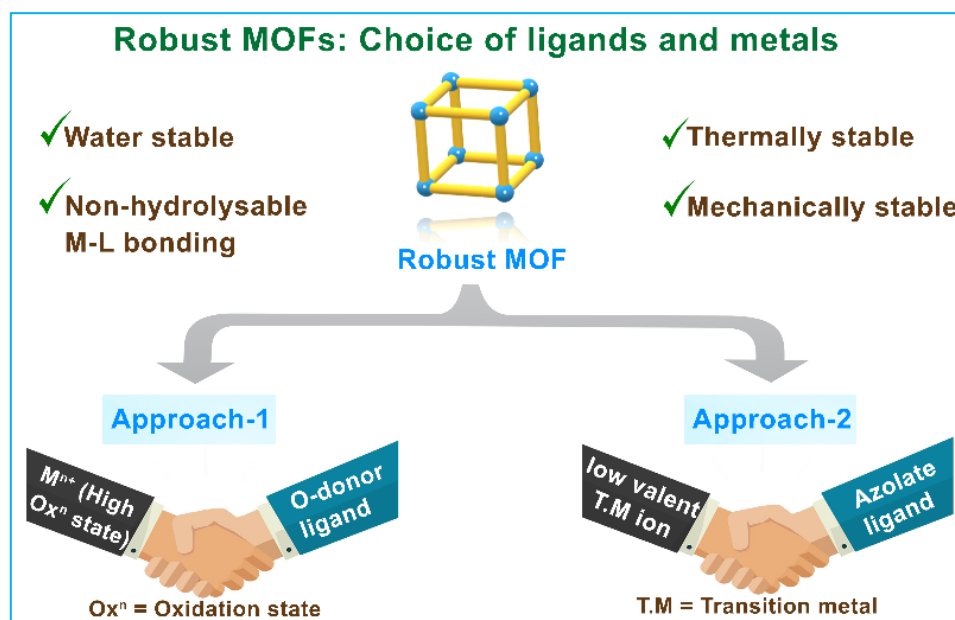
Scheme 1.1. Schematic diagram shows two different approaches to the synthesis of water-stable MOFs.

1.7.1. Approach-1:

Generally, high charge metal ions have strong oxophilicity. If one can prepare a MOF of high charge density metal ions in combination with O-donor ligands (Scheme-1, left), it will have non-hydrolysable metal-oxygen bonds, which will provide water stability. Here, the choice is of lanthanide metal ions of +3 charge (Ln^{3+}) with polytopic carboxylic acids as linkers. The thesis will focus on high-valent metal ion Ce^{3+} because the chemical bonding in MOFs based on these metals is accepted to remain unaffected by water due to the Lanthanide Contraction, and hence MOF is water-stable (*see* Scheme-1.1, left).
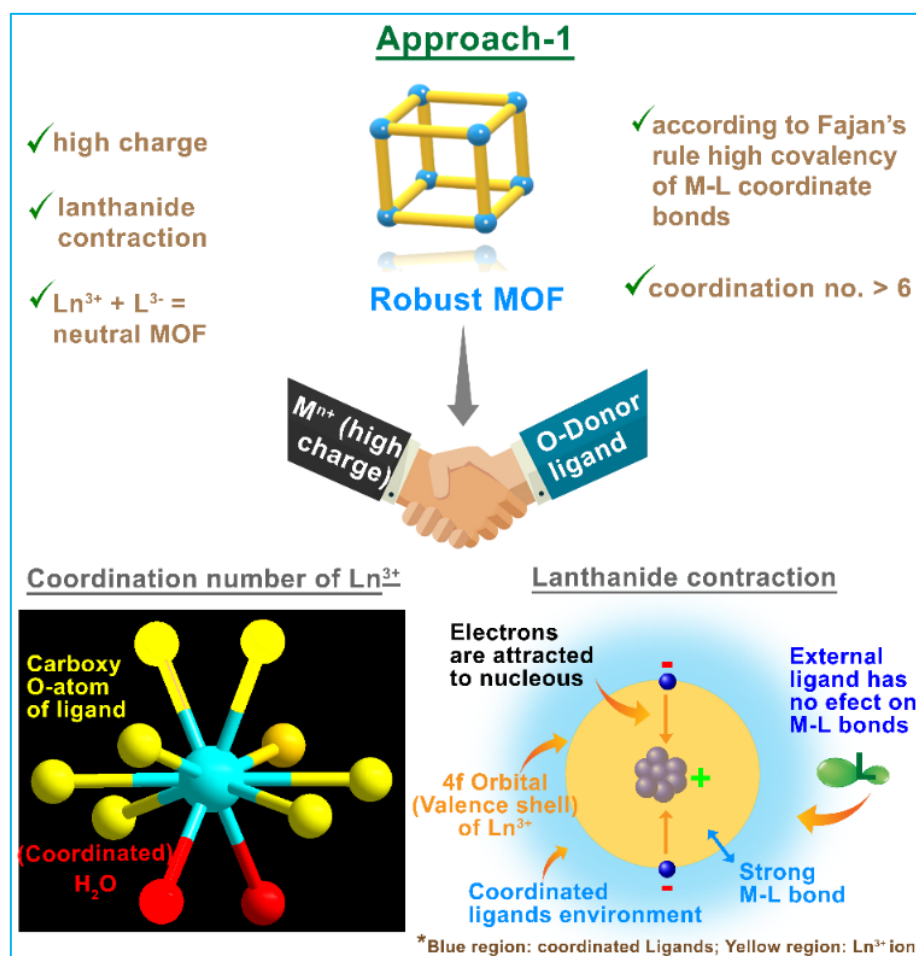
Scheme 1.2. Schematic diagram shows two different approaches to the synthesis of water-stable MOFs.

1.7.2. Approach-2

This describes the synthesis of water-stable MOFs using an azolate ligand in combination with other dicarboxylic acid ligands and comparatively softer transition metal ions (Scheme-1, right). Here, we choose adeninate as an azolate building block for the following reasons.

1) In the spectrochemical series, pyridyl and azolate sit above water. So, ligand field strength of azolate is more than the water and that is reason why water is unable to destroy the framework, giving a water-stable MOF. Here, adeninate has imidazolate as well as pyridyl functionality which make strong co-ordination bond between adeninate and transition metal cations.

2) Adeninate contains both charged and neutral N-centres so it can satisfy both the primary and secondary valency which generates neutral and saturated co-ordination sites of the metal ions in the framework. This give means better metal encapsulation and offers water stability to the framework.

3) Adeninate containing MOFs consist of multiple N-centres, and can polarise CO_2 via physisorption (without formally bonding to it like liquid amine does) for better selectivity. This facilitates the regeneration of CO_2 from the framework.
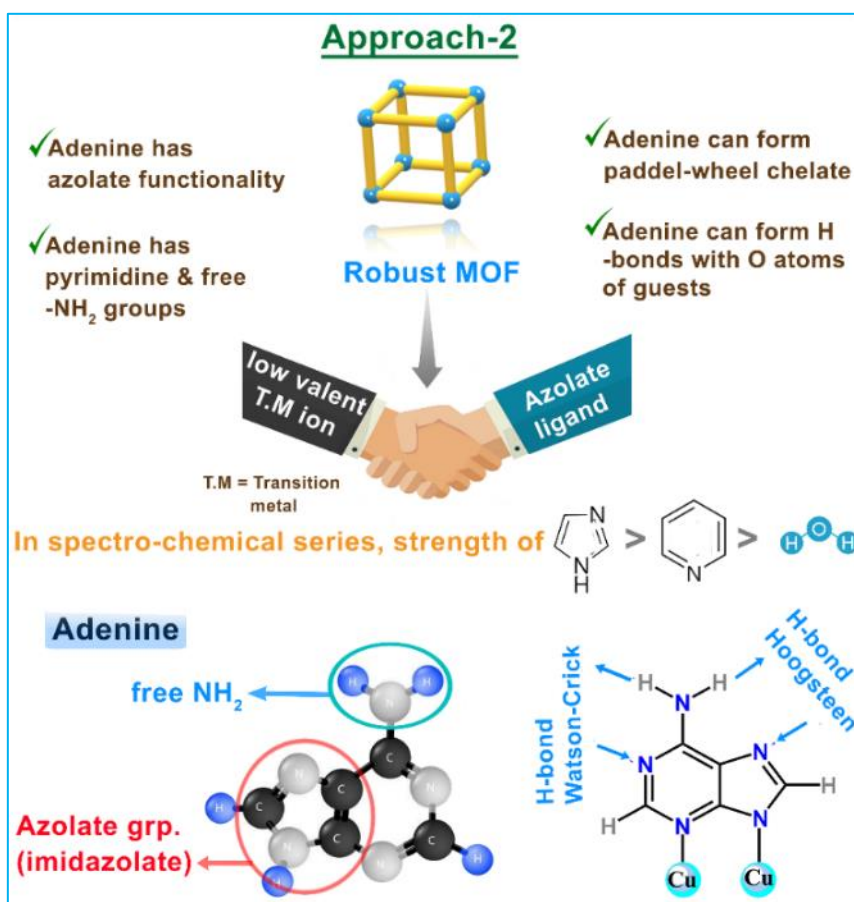
Scheme 1.3. Schematic diagram shows two different approaches to the synthesis of water-stable MOFs. And adenine's ability to form H-bonding.

4) Adenine is an inexpensive, readily available linker precursor which makes MOF synthesis a cost-effective synthesis.

5) Being a short linker adeninate can help to generate ultra-microporous MOFs, which are the most useful for CO_2 capture/separation applications because of their molecular sieving properties and co-operative interaction between the adsorbed CO_2 molecules (a bottleneck concept).

6) As a nucleobase adenine is able to form a hydrogen bond (Scheme 1.3) between the hydrogen atoms of amino group of adeninate and O atom of CO_2 leads to the stronger CO_2-framework interaction.

Overall, we propose the idea of introducing adeninate into the framework to synthesize water-stable, ultra-microporous MOFs, simultaneously introducing as many as possible CO_2 interaction sites to enable the efficiency of the selective CO_2 capture and separation. In addition, being a short-linker and providing strong metal-azolate bonds, adeninate framework also provides enough rigidity and microporosity to the MOF to maintain framework integrity under high temperature and extremely low pressure.

1.8. References

1. (a) https://www.express.co.uk/news/science/845901/climate-change-natural-global-warming-evidence-jennifer-marohasy; (b) https://earthsky.org/earth/atmospheric-co2-record-high-may-2019.

2. https://ourworldindata.org/co2-and-other-greenhouse-gas-emissions

3. https://19january2017snapshot.epa.gov/climatechange/carbon-dioxide-capture-and-sequestration-overview_.html

4. https://usea.org/sites/default/files/122011_Precombustion%20capture%20of%20CO2%20in%20IGCC%20plants_ccc191.pdf

5. D. Y. C. Leung, G. Caramanna, M. M. Maroto-Valer, *Renewable and Sustainable Energy Reviews* **2014**, *39*, 426-443.

6. S. Nandi, P. De Luna, T. D. Daff, J. Rother, M. Liu, W. Buchanan, A. I. Hawari, T. K. Woo, R. Vaidhyanathan, *Sci. adv.* **2015**, *1*, e1500421.

7. O. Shekhah, Y. Belmabkhout, Z. Chen, V. Guillerm, A. Cairns, K. Adil, M. Eddaoudi, *Nat. Commun.* **2014**, *5*, 1-7.

8. J. Oexmann, A. Kather, *Energy Procedia* **2009**, *1*, 799-806.

9. D. M. Ruthven, *Principles of adsorption and adsorption processes*, John Wiley & Sons, **1984**.

10. (a) M. Mastalerz, *Acc. Chem. Res.* **2018**, *51*, 2411–2422; (b) K. Jeong, S. Park, G. Y. Jung, S. H. Kim, Y.-H. Lee, S. K. Kwak, S.-Y. Lee, *J. Am. Chem. Soc.* **2019**, *141*, 5880–5885; (c) A. Karmakar, R. Illathvalappil, B. Anothumakkool, A. Sen, P. Samanta, A. V. Desai, S. Kurungot, S. K. Ghosh, *Angew. Chem. Int. Ed.* **2016**, *55*, 10667 –10671; (d) K. Sillar, A. Hofmann, J. Sauer, *J. Am. Chem. Soc.* **2009**, *131*, 4143–4150; (e) D. B. Burckel, C. M. Washburn, A. K. Raub, S. R. J. Brueck, D. R. Wheeler, S. M. Brozik, R. Polsky, *small* **2009**, *5*, 2792–2796; (f) L. F.-Beyme, M. Kloß, P. Kolodzeiski, R. Pallach, S. Henke, *J. Am. Chem. Soc.* **2019**, *141*, 12362−12371; (g) W. Lu, D. Yuan, D. Zhao, C. I. Schilling, O. Plietzsch, T. Muller, S. Br€ase, J. Guenther, J. Blumel, R. Krishna, Z. Li, H.-C. Zhou, *Chem. Mater.* **2010**, *22*, 5964–5972. (h) https://asdn.net/asdn/chemistry/zeolites.php.

11. https://www.nanoshel.com/metal-organic-frameworks.

12. J. L. Rowsell, O. M. Yaghi, *Microporous Mesoporous Mater.* **2004**, *73*, 3-14.

13. S. R. Batten, N. R. Champness, X.-M. Chen, J. Garcia-Martinez, S. Kitagawa, L. Öhrström, M. O'Keeffe, M. P. Suh, J. Reedijk, *CrystEngComm* **2012**, *14*, 3001-3004.

14. Y. Journaux, J. Ferrando-Soria, E. Pardo, R. Ruiz-Garcia, M. Julve, F. Lloret, J. Cano, Y. Li, L. Lisnard, P. Yu, H. Stumpf, C. L. M. Pereira, *Eur. J. Inorg. Chem.* **2018**, 228–247.

15. J.-Y. Wu, T.-C. Chao, M.-S. Zhong, Cryst. Growth & Des. **2013**, 13, 2953.

16. Y. Zhang, X. Bo, A. Nsabimana, C. Han, M. Li, L. Guo, *J. Mater. Chem. A* **2015**, *3*, 732-738.

17. N. A. Khan, S. H. Jhung, *Coord. Chem. Rev.* **2015**, *285*, 11-23.

18. M. Y. Masoomi, A. Morsali, P. C. Junk, *CrystEngComm* **2015**, *17*, 686-692.

19. (a) https://mat.sabanciuniv.edu/tr/arastirma-alanlari/carbon-based-materials; (b) M. Bilal, M. Adeel, T. Rasheed, H. M. Iqbal, *J. Mater. Res. Technol.* **2019**, *8*, 2359-2371; (c) J. Wang, *Chem. Rev.* **2008**, *108*, 814-825; (d) H. Furukawa, K. E. Cordova, M. O'Keeffe, O. M. Yaghi, *Science* **2013**, *341*; (e) K.-Y. A. Lin, H.-A. Chang, R.-C. Chen, *Chemosphere* **2015**, *130*, 66-72; (f) Q. Wang, X. Zhang, L. Huang, Z. Zhang, S. Dong, *Angew. Chem.* **2017**, *129*, 16298-16301; (g) Q. Wang, X. Lian, Y. Fang, H.-C. Zhou, *Catalysts* **2018**, *8*, 166.

20. (a) J.-R. Li, R. J. Kuppler, H.-C. Zhou, *Chem. Soc. Rev.* **2009**, *38*, 1477-1504; (b) I. Akpinar, R. J. Drout, T. Islamoglu, S. Kato, J. Lyu, O. K. Farha, *ACS Appl. Mater. Interfaces* **2019**, *11*, 6097-6103; (c) B. Chen, C. Liang, J. Yang, D. S. Contreras, Y. L. Clancy, E. B. Lobkovsky, O. M. Yaghi, S. Dai, *Angew. Chem. Int. Ed.* **2006**, *45*, 1390-1393; (d) S. Qiu, M. Xue, G. Zhu, *Chem. Soc. Rev.* **2014**, *43*, 6116-6140; (e) Y. Liu, W. Xuan, Y. Cui, *Adv. Mater.* **2010**, *22*, 4112-4135; (6) J.-R. Li, J. Sculley, H.-C. Zhou, *Chem. Rev.* **2012**, *112*, 869-932.

21. (a) Y. Lin, C. Kong, Q. Zhang, L. Chen, *Adv. Energy Mater.* **2017**, *7*, 1601296; (b) M. P. Suh, H. J. Park, T. K. Prasad, D.-W. Lim, *Chem. Rev.* **2012**, *112*, 782-835; (c) Y. Peng, V. Krungleviciute, I. Eryazici, J. T. Hupp, O. K. Farha, T. Yildirim, *J. Am. Chem. Soc.* **2013**, *135*, 11887-11894.

22. (a) Y.-B. Huang, J. Liang, X.-S. Wang, R. Cao, *Chem. Soc. Rev.* **2017**, *46*, 126-157; (b) L. Zhu, X.-Q. Liu, H.-L. Jiang, L.-B. Sun, *Chem. Rev.* **2017**, *117*, 8129-8176; (c) D. Samanta, P. Verma, S. Roy, T. K. Maji, *ACS Appl. Mater. Interfaces* **2018**, *10*, 23140-23146; (d) T. Prakasam, A. Devaraj, R. Saha, M. Lusi, J. Brandel, D. Esteban-Gómez, C. Platas-Iglesias, M. A. Olson, P. S. Mukherjee, A. Trabolsi, *ACS Catal.* **2019**, *9*, 1907-1914; (e) C. Zhu, Q. Xia, X. Chen, Y. Liu, X. Du, Y. Cui, *ACS Catal.* **2016**, *6*, 7590-7596.; (f) J.-H. Li, Y.-S. Wang, Y.-C. Chen, C.-W. Kung, *Appl. Sci.* **2019**, *9*, 2427.

23. (a) S. Pramanik, C. Zheng, X. Zhang, T. J. Emge, J. Li, *J. Am. Chem. Soc.* **2011**, *133*, 4153-4155; (b) Z. Hu, B. J. Deibert, J. Li, *Chem. Soc. Rev.* **2014**, *43*, 5815-5840.; (c) T. K. Kim, J. H. Lee, D. Moon, H. R. Moon, *Inorg. Chem.* **2013**, *52*, 589-595.

24. L. Zhang, Y. Xie, T. Xia, Y. Cui, Y. Yang, G. Qian, *Journal of Rare Earths* **2018**, *36*, 561-566.

25. Y. Gao, P. Jing, N. Yan, M. Hilbers, H. Zhang, G. Rothenberg, S. Tanase, *Chem. Commun.* **2017**, *53*, 4465-4468.

26. H. W. Langmi, J. Ren, N. M. Musyoka, in *Nanomaterials for Fuel Cell Catalysis*, Springer, **2016**, pp. 367-407.

27. (a) Z. Wang, B. Wang, Y. Yang, Y. Cui, Z. Wang, B. Chen, G. Qian, *ACS Appl. Mater. Interfaces* **2015**, *7*, 20999-21004; (b) S. J. Yang, S. Nam, T. Kim, J. H. Im, H. Jung, J. H. Kang, S. Wi, B. Park, C. R. Park, *J. Am. Chem. Soc.* **2013**, *135*, 7394-7397.

28. (a) M. Kurmoo, *Chem. Soc. Rev.* **2009**, *38*, 1353-1379; (b) G. M. Espallargas, E. Coronado, *Chem. Soc. Rev.* **2018**, *47*, 533-557.

29. (a) C.-C. Chueh, C.-I. Chen, Y.-A. Su, H. Konnerth, Y.-J. Gu, C.-W. Kung, K. C.-W. Wu, *J. Mater. Chem. A* **2019**, *7*, 17079-17095; (b) S. Goswami, L. Ma, A. B. Martinson, M. R. Wasielewski, O. K. Farha, J. T.

Hupp, *ACS Appl. Mater. Interfaces* **2016**, *8*, 30863-30870; (c) D. Y. Lee, C. Y. Shin, S. J. Yoon, H. Y. Lee, W. Lee, N. K. Shrestha, J. K. Lee, S.-H. Han, *Sci. Rep.* **2014**, *4*, 3930.

30. T. Li, D.-L. Chen, J. E. Sullivan, M. T. Kozlowski, J. K. Johnson, N. L. Rosi, *Chem. Sci.* **2013**, *4*, 1746-1755.

31. M. Sagastuy-Breña, P. G. Mileo, E. Sánchez-González, J. E. Reynolds, T. Jurado-Vázquez, J. Balmaseda, E. González-Zamora, S. Devautour-Vinot, S. M. Humphrey, G. Maurin, *Dalton Trans.* **2018**, *47*, 15827-15834.

32. C. Chen, Q. Jiang, H. Xu, Z. Lin, *Ind. Eng. Chem. Res.* **2019**, *58*, 1773-1777.

33. M. Wriedt, J. P. Sculley, A. A. Yakovenko, Y. Ma, G. J. Halder, P. B. Balbuena, H. C. Zhou, *Angew. Chem.* **2012**, *124*, 9942-9946.

34. X. Qian, F. Sun, J. Sun, H. Wu, F. Xiao, X. Wu, G. Zhu, *Nanoscale* **2017**, *9*, 2003-2008.

35. F. Wang, Y.-X. Tan, H. Yang, H.-X. Zhang, Y. Kang, J. Zhang, *Chem. Commun.* **2011**, *47*, 5828-5830.

36. F. Wang, H. Yang, Y. Kang, J. Zhang, *J. Mater. Chem.* **2012**, *22*, 19732-19737.

37. Z. Lu, H. Xing, R. Sun, J. Bai, B. Zheng, Y. Li, *Cryst. Growth & Des.* **2012**, *12*, 1081-1084.

38. V. Gupta, S. K. Mandal, *Dalton Trans.* **2019**, *48*, 415-425.

39. A. Pal, S. Chand, M. C. Das, *Inorg. Chem.* **2017**, *56*, 13991-13997.

40. R. Vaidhyanathan, S. S. Iremonger, G. K. Shimizu, P. G. Boyd, S. Alavi, T. K. Woo, *Science* **2010**, *330*, 650-653.

41. S. Shalini, S. Nandi, A. Justin, R. Maity, R. Vaidhyanathan, *Chem. Commun.* **2018**, *54*, 13472-13490.

42. S. Xiang, Y. He, Z. Zhang, H. Wu, W. Zhou, R. Krishna, B. Chen, *Nat. Commun.* **2012**, *3*, 1-9.

43. R.-B. Lin, D. Chen, Y.-Y. Lin, J.-P. Zhang, X.-M. Chen, *Inorg. Chem.* **2012**, *51*, 9950-9955.

44. P. Nugent, Y. Belmabkhout, S. D. Burd, A. J. Cairns, R. Luebke, K. Forrest, T. Pham, S. Ma, B. Space, L. Wojtas, *Nature* **2013**, *495*, 80-84.

45. S. Nandi, S. Collins, D. Chakraborty, D. Banerjee, P. K. Thallapally, T. K. Woo, R. Vaidhyanathan, *J. Am. Chem. Soc.* **2017**, *139*, 1734-1737.

Chapter 2A

Water-stable Lanthanide Metal-organic Framework Proposed for Selective CO$_2$ Capture
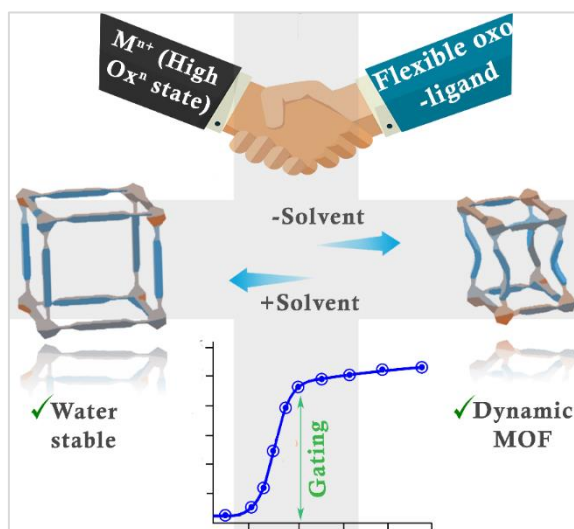
2A.1 Introduction:

Metal−organic frameworks (MOFs) built from the polytopic organic ligands furnish tuneable framework motifs and variety of functionalities. These combined with their mechanical, thermal and chemical robustness make them find their applications in gas,[1−3] and charge storage,[4,5] photo-chemical properties,[6−10] magnetism,[11,12] capture/separation,[13−18,] and various kind of catalysis.[19−22] However, archetypically, MOF is pronounced for its use in adsorption-based gas capture techniques. The purification of natural gas/bio gas and treatment of effluent gases are essential to improve fuel efficiency and address environmental challenges.[23] While capturing CO_2 from natural or flue gas, the stability of the framework towards humidity is always a concern.[24] Compared to available transition metal ions, Ln^{3+} ions when combined with oxo-ligands can feature non-hydrolyzable M-L bonds, and hence it can provide water stability to the framework. Due to having a large ionic radius and high charge, Ln^{3+} ions can be readily ligated by more atoms, hence coordination numbers greater than six are common. This, in principle, can generate highly crosslinked three-dimensional framework comprising of substantially strong M-O bonds. Also, there is a provision for solvent (e.g., water) for forming bonds to the metal centers while construction of framework and is replaceable upon activation creating unsaturated open metal sites (OMS). So, when exposed to humid environments, water can further coordinate to the OMS of the activated MOF instead of replacing the existing ligands via hydrolysis. Due to the
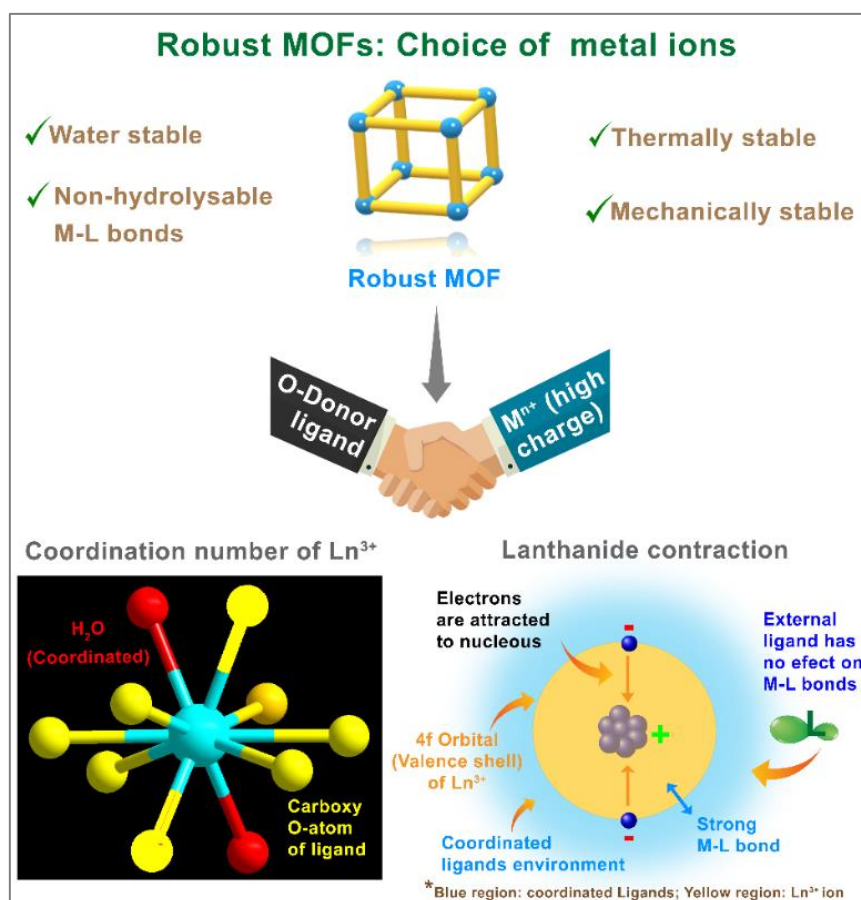
Scheme 2A.1. The figure shows an approach to the synthesis of water-stable and rigid MOFs.

"Lanthanide-Contraction" and high charge, lanthanide ions become very hard and according to Fajan's rule, leading to high degree of covalency in their M-O bonds (Scheme 2A.1). Hence, water cannot hydrolyze the M-L bonds under normal conditions. Ln^{3+} ion, in combination with the ligand of -3 charge, can produce thermally and mechanically stable neutral MOF as the neutral species is always more stable than the charged one. Herein, using the first approach and exploiting all the above advantages of a lanthanide, we have chosen Ce^{3+} as high charge metal ions and 2,2′-((4-carboxyphenyl)azanediyl)diacetic acid (H_3CPADA) as a precursor for O-donor ligand in the synthesis of a new water-stable Ce-MOF.

2A.2. Materials and Methods:

2A.2.1. Synthesis of 2,2'-((4-carboxyphenyl)azanediyl)diacetic acid (H_3CPADA):

The Ligand H_3CPADA was synthesized according to the procedure reported in literatures[25]. An aqueous KOH solution was prepared by dissolving KOH (33.6 g, 0.6 mol) in 100 mL water. In round bottom flask aqueous solution of chloroacetic acid (28.4 g, 0.3 mol in 100 mL) was prepared. Then the freshly prepared KOH solution was added dropwise to the round bottom flask containing chloroacetic acid solution. Afterward, p-aminobenzoic acid (13.7 g, 0.1 mol) was added pinch-wise to the resulting alkaline mixture in round bottom flask. The entire reaction mixture was then refluxed at 90 °C for 48 h. Then the whole reaction mixture was slowly cooled down to room temperature, and after adjusting the pH of the solution to 2.5 with 3 M aqueous HCl, the desired acid was precipitated as a white solid. The white precipitate was then collected by filtration, cleaned with copious amounts of water (yield: 32 %) and then dried in oven. Final product is obtained as a yellowish white coloured powder.

2A.2.2. Synthesis of Ce-MOF ([$Ce_2(CPADA)_2$•($H_2O)_4$](DMF)($H_2O)_4$):

The Ce-MOF was synthesized via the solvothermal method. In a synthesis protocol, $Ce(NO_3)_3 \cdot 6H_2O$ 43.4 mg (0.1 mmol) and 25.32 mg (0.1 mmol) H_3CPADA ligand were taken successively in an 8 ml Pyrex vial, and then a mixture of 3 ml DMF and 1ml H_2O was added to completely dissolve the ligand and metal salt. 20 μL of concentrated HCl was slowly added dropwise to the vial, and the vial was then kept in a 120 °C programming oven for 3 days. On slow cooling to room temperature over 12 hrs, plate-shaped colorless crystals suitable for X-ray diffraction (the average size of the crystal is 100 μm) were formed. Then, the Ce-MOF crystals were collected by filtration followed by washing 3-4 times with fresh DMF and methanol. Then the product was dried in an oven (yield, 80 %; Scheme 2A.2). Although there are two types of crystals (pallets and a few needle-like crystals), they correspond to the same phase. Moreover, we did not get any additional peaks due to Needle shape crystals other than the simulated peaks (obtained from the SCXRD analysis) in the PXRD profile of the Ce-MOF. The different shapes of crystals could be explained by the insufficient growth of a few crystals.
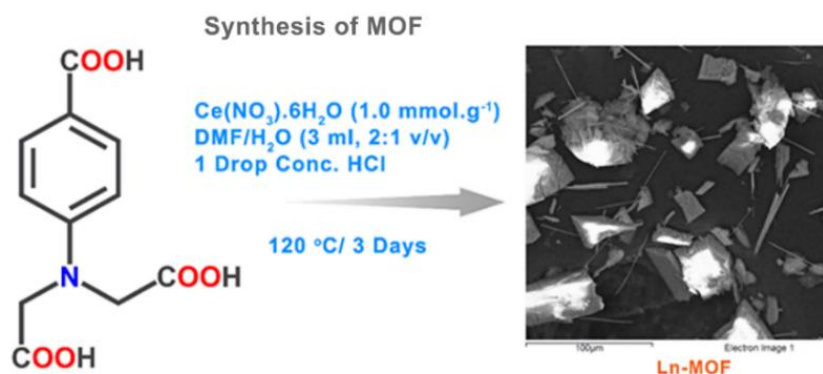
Scheme 2A.2. Reaction scheme of solvothermal synthesis of Ce-MOF.

2A.2.3. Analytical Characterisations:

All solvents and chemicals were procured from the commercial source and utilized for the synthesis without any further purification.

Single Crystal X-ray diffraction and Structures determinations:

Single-crystal X-ray diffraction was done on a Bruker SMART APEX four-circle diffractometer coupled with a CMOS photon 100 detector and Microfocus (IμS) using Cu-Kα radiation. The Ce-MOF crystal was mounted on the nylon Cryo loops using Paraffin oil. Diffraction data were collected at temperature of 100 K. Total data were integrated using Bruker SAINT Software and it was corrected for absorption using SADABS. The structure solution was done using the Intrinsic Phasing routine and was refined using the SHELXTL 6.3.1 (2004) software suite. All the non-H atoms were located from an iterative examination of difference F-maps, following which the structure was refined using a least-squares method. H atoms were fixed geometrically in a riding model.

Powder X-ray Diffraction:

Powder XRDs data collections were done using a Rigaku Miniflex-600 instrument and data were processed using PDXL software. The Variable temperature PXRDs (VT-PXRD) were recorded out on a full-fledge Bruker instrument using the in-built furnace and in air.

Scanning Electron Microscopy:

Field Emission Scanning Electron Microscopic (FESEM) study was done using the Ultra Plus Field Emission Scanning Electron Microscope combined with integral charge compensator and coupled EsB and AsB detectors.

Thermogravimetric Analysis:

Thermogravimetry analysis (TGA) of as-made MOF was performed using the NETSZCH TGA-DSC instrument. The TGAs were done under N_2 flow (flow rate = 20 ml min^{-1}) in a purge-protective mode and samples were heated in the temperature range of 25 to 550 °C with a constant heating rate of 5 °K min^{-1}

Infrared (IR) spectroscopy:

The infrared (IR) spectrum of the sample was recorded utilizing the Nicolet FT-170SX instrument using KBr pellet in the range of 400−4000 cm^{-1}.

Water Adsorption Analysis:

Water sorption isotherm was measured on a Micrometrics ASAP 2020 instrument using distilled water. Materials were introduced to an analysis glass-tube/cell, with one step activation: about 100 mg of the methanol-exchanged MOF was introduced to the analysis cell and evacuated at 120 °C on the outside degas port 12 hrs (under pressure of 10^{-4} mbar).
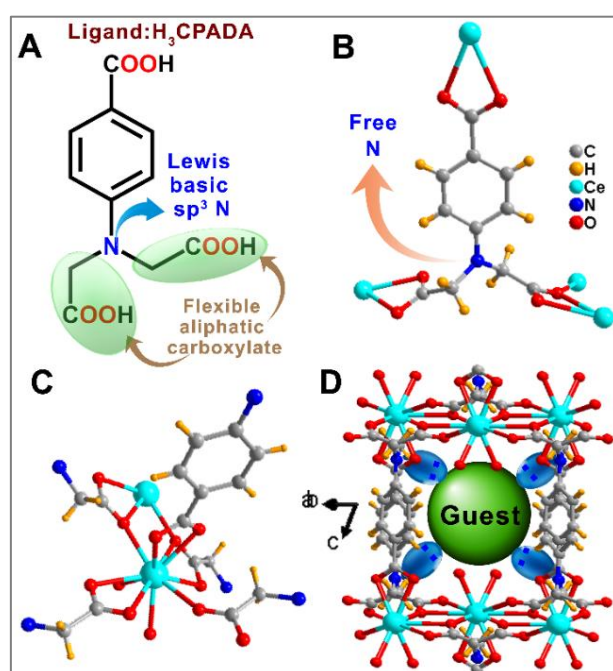
Figure 2A.1. (A) The structure of the ligand shows its unique functionalities. (B) Coordination mode of the CPADA^{3-} Ligand. (C) Coordination environments of Ce^{3+}. (D) The graphic obtained from the crystal structure of Ce-MOF, displaying the nitrogen rich pocket apt for interactions with guests. The trap-guest (green ball) inside the cavity is the representative of single or multiple guests of the same type, e.g., CO$_2$ molecules.

2A.3. Results and Discussion:

The structural analysis of crystal X-ray diffracted single crystal, shows that Ce-MOF crystallizes in the triclinic system and space group P-1 with the following unit cell parameters: a(Å) = 8.9262(23), b(Å) =9.88, c(Å) = 11.54, α = 64.7°, β = 79.7°, γ = 65.1°, V(Å) = 835.69 Å^3; Z = 2; Molecular mass: 997.66 g mol^{-1}. Molecular formula: [Ce(CPADA)·(H$_2$O)$_2$]$_2$·(DMF)(H$_2$O)$_4$ (Figure 2A.A1 and Tables 2.A1-A3). As made, Ce-MOF contains deprotonated CPADA^{3-} and only one crystallographically unique Ce^{3+} metal ion (Figure 2.1A1A-C). Two of the Ce^{3+} ions are coordinated to the flexible aliphatic-carboxylate part of the CPADA^{3-}. The third Ce^{3+} is coordinatively bonded to the relatively rigid phenyl carboxylate unit of CPADA^{3-}. There are two metal (Ce^{3+})-coordinated water molecules (Figures 2.A1 C-D, and Figure 2A.A1-A2) in the

structure of Ce MOF. The tricarboxylate ligand is fully deprotonated to counter-balance 3+ charge on lanthanide centers, and as a result, overall MOF has a neutral framework. These metal-carboxylate linkages forms an inorganic Ce-CPADA layer, that is pillared by the phenyl unit resulting in a 3D framework. The Ce-MOF contains 1D square channels of width: 11.14 Å × 6.24 Å (including Vander Waal radii) (Figures 2.A1D and Figure 2A.A1 and 2A.A2). Importantly, the channel is highly polar because, as expected, the free sp^3 nitrogen atoms of the CPADA^{3-} are periodically lined up along the 1D channels (Figure 2A.1D and Figure 2A.A2F). These nitrogen centers now can offer their lone pair to the incoming CO_2 molecules enabling the strong CO_2-framework interaction. Furthermore, the coordinated water molecules upon activation leave the metal centers creating the Lewis acidic OMS, which can interact with the oxygen end of CO_2 molecules. Due to the presence of strongly polar channels in the Ce-MOF, it should possess high CO_2 uptake. The activated/desolvated phase was obtained when methanol-exchange Ce-MOF was subjected to evacuation at 120 °C under vacuum for 12 hours.
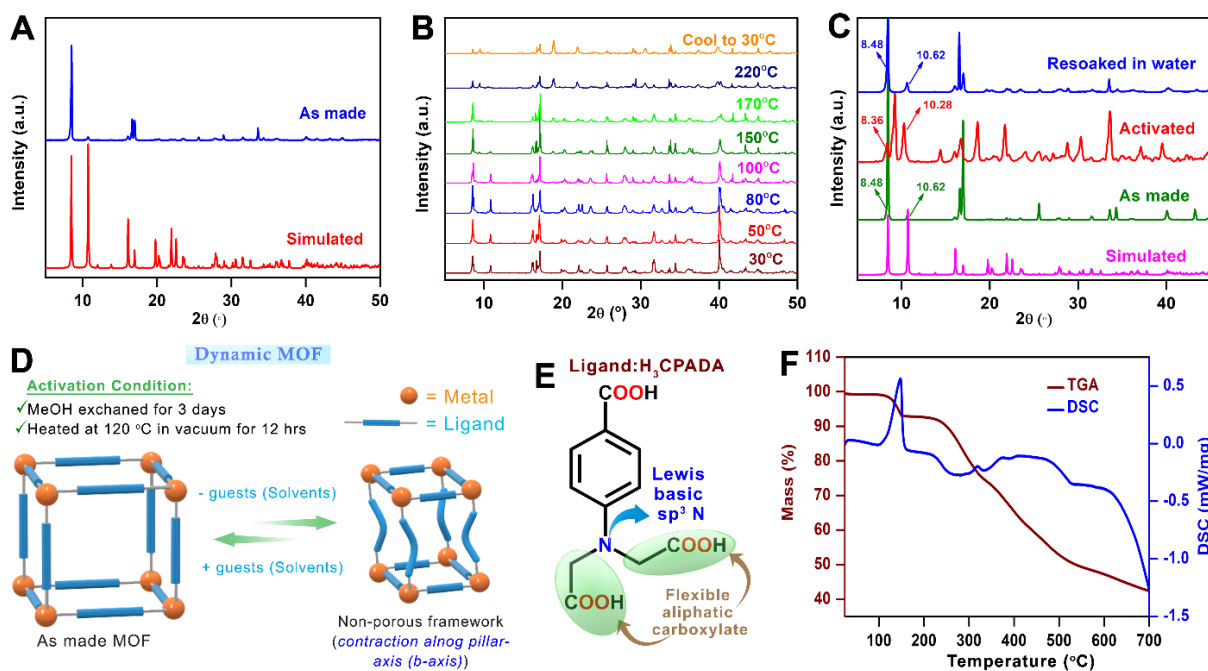
Figure 2A.2. (A) The PXRD pattern of as-made Ce-MOF, experimental (blue) and simulated (red) from the single crystal XRD. (B) Variable temperature PXRDs of Ce-MOF. (C) The PXRD pattern of Desolavted/activated Ce-MOF (red) and the role of water on the PXRD pattern of the desolvated Ce-MOF (blue). The activated sample was obtained by frequently exchanging the pore DMF and water molecules with comparatively low boiling methanol for three days followed by heating at 120 °C under vacuum. (D) The schematic diagram shows the dynamic behavior of Ce-MOF. (E) The pictorial diagram shows the flexible aliphatic and rigid phenyl backbones in the ligand structure. (F) TGA and DSC profiles of as made Ce-MOF.

The MOF is crystallized in the pure phase as confirmed by powder XRD (Figures 2A.2A). The variable temperature PXRDs (Figure 2A.2B) shows a phase change at 150 °C and above. This reveals that the framework goes through the phase change upon solvent loss and another stable crystalline lattice, which is closely related. We impute this to a solvent-loss assisted phase change phenomenon. A similar kind of phase-

change behavior was also observed in the La-based MOF (IISERP-MOF25).[25] Importantly, as the temperature rises, at 150 °C, a new peak appears at 2θ = ~9.2° and ~18.2° and at the same time, 150 °C onwards, most of the reflections shift to the higher angles revealing a framework shrinkage, which we attribute to a solvent-loss assisted lattice contraction. The PXRD pattern of the 220 °C phase remains the same upon cooling to 30 °C that suggested the contracted phase obtained by heating to 220 °C was not reversible to the cooling to 30 °C (Figure 2A.2B; orange line vs wine line). Interestingly, after soaking the 220 °C phase in methanol or water, the as-made MOF was recovered in its solvated form. However, upon pore solvent (DMF and water) exchanging with methanol for three days followed by heating the MOF at 120 °C for 12 hours yielded a contracted phase similar to that of 220 °C phase that can again retain the original as made phase just upon resoaking in either water or methanol (Figure 2A.2C). This flexible behavior of MOF is a ligand-based flexibility (Figure 2A.2D). Two flexible carboxylic acid moieties in the ligand backbone attached to the phenyl ring formed the layer (Figure 2A.2E), which imposed sufficient flexibility into the framework so that upon solvent removal due to surface tension framework got completely squeezed, retaining the overall bonding connectivity of the MOF. Upon resolution, it again opened its squeezed pore. So, Ce-MOF had a stable dynamic framework, and this dynamic character arises from the same flexible ligand unit which forms both the layering and pillaring units of the framework.

Despite this dynamic behavior, the MOF showed excellent water and aqueous acid-base stability, confirmed from the retained PXRD profile of water/boiling water-soaked MOF (Figure 2A.A3). The MOF had excellent thermal stability, which was investigated from the thermo-gravimetry analysis (TGA) carried out from 25 °C to 800 °C (Figure 2A.2F). There were two steps of mass loss: the first mass loss was due to the removal of pore water and the second mass loss corresponds to the removal of pore DMF. The MOF was stable up to 220 °C as confirmed from PXRD and TGA (Figure 2A.2B, Figures 2A.A4, and 2A.A5). However, the temperature/solvent-loss assisted phase change was further supported by the exothermic peak in the DSC profile (Figure 2A.2F and Figure 2A.A4) of the as-made sample at 130 °C, upon removal of water molecules
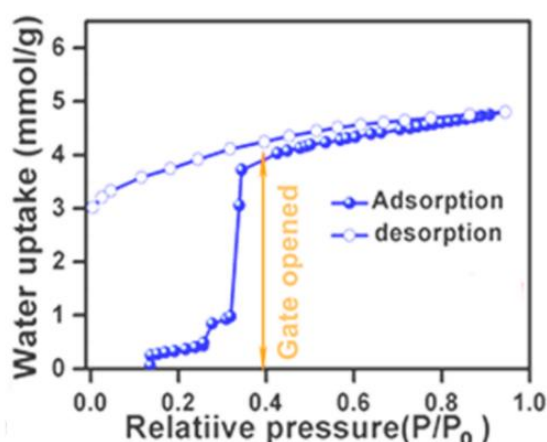
Figure 2A.3. Water adsorption (close blue sphere) and desorption (open blue sphere) isotherms for desolvated Ce-MOF. Gating around P/P_0 = 0.34 suggests the water-assisted opening of the contracted pore of the desolvated Ce-MOF.

(Figure 2A.2F and Figure 2A.A4). IR spectrum showed the typical peaks due to the COO^-, $C-H$ stretching, and bending bands (Figure 2A.A6). The strong and broad absorption bands in the $3200-3600$ cm^{-1} indicate -OH stretching vibration frequencies corresponding to the coordinated water molecules.

Activated Ce-MOF showed water uptake with a certain gating (Figure 2A.3), which suggested opening the squeezed pore via solvent assisted gating. The gating is due to the contraction of pore volume upon removal of pore DMFs and water molecules, and when resolvated, the solvent molecules again enter into the cavity of Ce-MOF and fill-up similar positions of the framework voids and metal coordination sites. The water adsorption profile showed that the adsorption of water started at a relatively higher pressure that suggested a certain amount of high-water vapor pressure was needed to open the squeezed pore. There was a hysteresis in the water adsorption profile for Ce-MOF, which strongly suggested that after entering the MOF channel, water molecules coordinated to the unsaturated open Ce sites (having a high oxophilicity) (Figure 2A.1D) as well as fill the MOF cavity, interacting strongly with the framework. However, due to the same structural flexibility and pore contraction, Ce-MOF did not show any gas-dependent porosity.

A look into the literature and CCDC reveals that the H3CPADA ligand forms the coordination polymers with the bivalent group-II metal ions and bivalent transition metal ions (Table 2A.1), wherein sp^3 N centers coordinate to the metal centers, resulting in either 2D layer or discrete complex. There are also a few 3D networks with this ligand, but those are dense interpenetrated and non-porous in nature. Few of the 3D frameworks are formed via supramolecular H-bonds, possessing crystallographic pores. These make the frameworks weaker with a chance of disintegration of these supramolecular frameworks in presence of water or moisture. Moreover, these MOFs are made of low valent transition or alkaline earth metal ions, which are prone to hydrolysis by water at their M-L sites. However, judicial choice of high-valent lanthanide metal ions in combination with this and tuning the reaction conditions, this Ce-MOF was obtained as a water-stable dynamic framework with water accessible pores. It has Lewis-basic sp^3 nitrogen and metal-coordinated water (that produces open-metal sites upon removal) lined highly polar-pore. It shows gating in the water adsorption isotherm at very low partial pressure of water vapour, making it an ideal candidate for water harvesting application. Notably, only one report of a lanthanide MOFs with this ligand exists and it does not investigate for porosity or gas separation, but is more focused on photoluminescent properties.[31]

Table 2A.1. List of reported coordination polymers based on N-(4-carboxyphenyl) iminodiacetic acid.

MOFs	Nature of framework	Property and application	Ref.
[Ni(HCPADA)(H2O)3] (**1**) [Ni2(HCPADA)2(bpy)(H2O)4](H2O)2 (**2**) *H3CPADA: N-(4-carboxyphenyl) iminodiacetic acid, and bpy: 4,4'-bipyridine*	**1** exhibits a 3D-supramolecular framework with 1D channels, formed by H- bonding interactions.	N/A	26

	2 has a 2D ladder shaped network built via H-bonding and pi–pi staking.		
[Zn₂(p-CPADA)(OH)]ₙ (**1**) [Zn₂(pHCPADA)₂(bipy)(H₂O)₄]·2H₂O (**2**) *H₃CPADA: N-(4-carboxyphenyl) iminodiacetic acid, ibpy: 4,4'-bipyridine*	**1** have 3D network while **2** has supramolecular 3D framework obtained via aggregation of the 2D layered structure by H-bonding	Both the compounds are fluorescent.	27
{[Pb₃(CPADA)₂(H₂O)₃] H₂O}ₙ (**1**), {[Cd₃(CPADA)₂(H₂O)₄] 5H₂O}ₙ (**2**), [Cd(HCPADA)(bpy)(H₂O)]ₙ (**3**) {[Co₃(CPADA)₂(bpy)₃(H₂O)₄]2H₂O}ₙ (**4**) *H₃CPADA: N-(4-carboxyphenyl) iminodiacetic acid, and bpy: 4,4'-bipyridine*	**1** has 3D porous framework, whereas **2** has 3D supramolecular framework, stacked via H- bonding interactions. **3** has a 2D layer-sheet structure. **4** has dense supramolecular 3D-framework.	All four coordination polymers are luminescent	*28*
[Ln(CPADA)(H₂O)]ₙ Ln=La (**1**), Ce (**2**), Pr (**3**) and Nd (**4**)} {[Ln(CPADA)(H₂O)]·2H₂O}ₙ Ln=Sm (5), Eu (6), Gd (7), Tb (8), Dy (9), Ho (10), Er (11) and Yb (12)}. *CPADA: N-(4-carboxyphenyl) iminodiacetate*	Layer-pillared structure	All the MOFs are photoluminescent. The magnetic property analysis was done for **7** and **9**	29
[(DMA⁺)][Zn₃Na₂(CPIDA)₃]•2.5DMF (DMF = N,N-dimethylformamide). *CPADA: N-(4-carboxyphenyl) iminodiacetate, DMA⁺ = dimethyl ammonium cation*	Anionic Layer-pillared structure with counter dimethyl ammonium cations (DMA⁺) in the pore of MOF.	MOF is used for proton conduction and the selective sensing of acetone and Cu²⁺ ions.	30
[Cu₃(CPADA)₂(H₂O)₄]ₙ·4nH₂O (**1**) and [Zn(HCPADA)]ₙ·nH₂O (**2**) *CPADA: N-(4-carboxyphenyl) iminodiacetate*	**1** possess 2D layer-structure via parallel AA stacking whereas **2** has 2D framework structure.	1 is fragile upon guest removal while activated 2 shows photoluminescent behaviour.	31

The next target was to get the porosity out of this material, and we took the help of a retrosynthetic approach. In this Ce-MOF, since the layering and pillaring units are part of the same flexible system, contraction of the framework is arising from a single unit. Though the dynamic framework in a MOF brings advantages, for many gas separation applications, the MOF needs to be rigid. Now, in this Ce-MOF, if we separate the flexible aliphatic part and the rigid aromatic carboxylate unit, then it might provide rigid and porous MOF (Scheme 2A.3). Thus, when this CPADA unit is broken to two synthons, one synthon is a 4,4-biphenyl dicarboxylic acid, and another is iminodiacetic acid. So, we anticipated that if iminodiacetate acts as

layering unit, the layers formed by them can be pillared by BPDC units to get the same kind of layered-pillared MOF, but with improved rigidity (see the Chapter-2B).
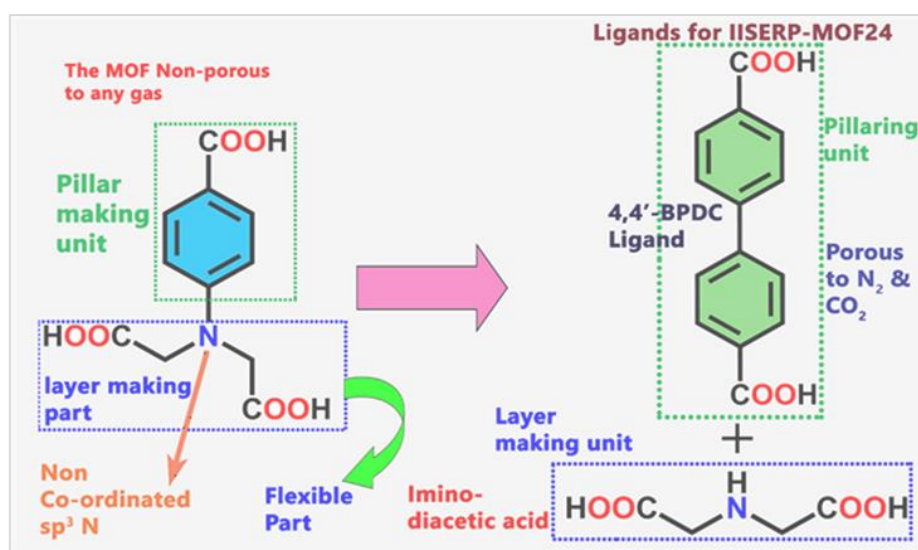
Scheme 2A.3. Retrosynthetic analysis of H₃CPADA showing two different synthons: 4,4-biphenyl dicarboxylic acid and iminodiacetic acid.

2A.4. References:

1. Y. Lin, C. Kong, Q. Zhang, L. Chen, *Adv. Energy Mater.* **2017**, *7*, 1601296.

2. M. P Suh, H. K. Park, T. K. Prasad, D. -W. Lim, *Chem. Rev.* **2012**, *112*, 782− 835.

3. Y. Peng, V. Krungleviciute, I. Eryazici, J. T. Hupp, O. K. Farha, T. Yildirim, *J. Am. Chem. Soc.* **2013**, *135*, 11887−11894.

4. Z. Wang, B. Wang, Y. Yang, Y. Cui, Z. Wang, B. Chen, G. Qian, *ACS Appl. Mater. Interfaces* **2015**, *7*, 20999−21004.

5. S. J. Yang, S. Nam, T. Kim, J. H. Im, H. Jung, J. H. Kang, S. Wi, B. Park, C. R. Park, *J. Am. Chem. Soc.* **2013**, *135*, 7394−7397.

6. T. W. Duan, B. Yan, *J. Mater. Chem. C* **2015**, *3*, 2823−2830.

7. L. Shen, L. Yang, Y. Fan, L. Wang, J. Xu, *CrystEngComm* **2015**, *17*, 9363−9369.

8. S. Samanta, U. Manna, T. Ray, G. Das, *Dalton Trans* **2015**, *44*, 18902−18910.

9. M. A. M. Lucena, M. F. L. Oliveira, A. M. Arouca, M. Talhavini, E. A. Ferreira, S. J. Alves, F. H. Veiga-Souza, I. T. Weber, *ACS Appl. Mater. Interfaces* **2017**, *9*, 4684−4691.

10. A. Mukhopadhyay, V. K. Maka, G. Savitha, J. N. Moorthy, *Chem.* **2018**, *4*, 1059−1079.

11. M. Kurmoo, *Chem. Soc. Rev.* **2009**, *38*, 1353−1379.

12. G. Minguez Espallargas, E. Coronado, *Chem. Soc. Rev.* **2018**, *47*, 533−557.

13. J.-R. Li, R. J. Kuppler, H. C. Zhou, *Chem. Soc. Rev.* **2009**, *38*, 1477−1504.

14. L. Akpinar, R. J. Drout, T. Islamoglu, S. Kato, J. Lyu, O. K. Farha, *ACS Appl. Mater. Interfaces* **2019**, *11*, 6097−6103.

15. C. Chen, C. Liang, J. Yang, D. S. Contreras, Y. L. Clancy, E. B. Lobkovsky, O. M. Yaghi, S. A. Dai, *Angew. Chem*. **2006**, *118*, 1418−1421.

16. S. Qiu, M. Xue, G. Zhu, *Chem. Soc. Rev*. **2014**, *43*, 6116−6140.

17. B. Y. Liu, W. Xuan, Y. Cui, *Adv. Mater*. **2010**, *22*, 4112−4135.

18. J.-R. Li, J. Sculley, H.-C. Zhou, *Chem. Rev*. **2012**, *112*, 869−932.

19. Y.-B. Huang, J. Liang, X.-S. Wang, R. Cao, *Chem. Soc. Rev*. **2017**, *46*, 126−157.

20. L. Zhu, X.-Q. Liu, H. L. Jiang, L.-B. Sun, *Chem. Rev*. **2017**, *117*, 8129−8176.

21. D. Samanta, P. Verma, S. Roy, T. K. Maji, *ACS Appl. Mater. Interfaces* **2018**, *10*, 23140−23146.

22. T. Prakasam, A. Devaraj, R. Saha, M. Lusi, J. Brandel, D. esteban-Gomez, C. Platas-Iglesias, M. A. Olson, P. S. Mukherjee, A. Trabolsi, *ACS Catal*. **2019**, *9*, 1907−1914.

23. A. Rehman, S. Farrukh, A. Hussain and E. Pervaiz, *Energy & Environment*, **2020**, *31*, 367–388.

24. (a) K. Zhang, X.-J. Xie, H.-Y.Li, J.-X. Gao, L. Nie, Y. Pan, J. Xie, D. Tian, W.-L.Liu, Q.-L. Fan, H.-Q. Su, L. Huang,W.Huang, Adv.Mater. 2017, 29,1701804. (b) T. -Y.Luo, C. Liu, S. V. Eliseeva, P. F. Muldoon, S. Petoud and N. L. Rosi, J. Am.Chem. Soc. 2017, 139,9333–9340. (c) G.-X. Wen, Y. -P.Wu, W.-W.Dong, J. Zhao, D.-S. Li, J. Zhang, *Inorg. Chem*., **2016**, *55*, 10114–10117.

25. R. Maity, D. Chakraborty, S. Nandi, A. K. Yadav, D. Mullangi, C. P. Vinod, and R. Vaidhyanathan, *ACS Appl. Nano Mater*. **2019**, *2*, 5169−5178.

26. G. Yonga, Z. Wanga, J. Chen, *J. Mol. Struct*. **2004** *707*, 223–229.

27. S. Kisslinger, H. Kelm, S. Zheng, A. Beitat, C. Würtele, R. Wortmann, S. Bonnet, S. H.-Pawlis, H.-J. Krüger, S. Schindler, *Z. Anorg. Allg. Chem*. **2012**, *638*, 641−647.

28. X. Chai, H. Zhang, S. Zhang, Y. Cao, Y. Chen, *J. Solid State Chem*. **2009**, *182*, 1889−1898.

29. C.-H. Gao, G.-F. Hou, D.-F. Zuo, W.-H. Jiang, Y.-H. Yu, D.-S. Ma, P.-F. Yan, ChemistrySelect **2017**, *2*, 1111 – 1116.

30. X. Meng, X.-Z. Song, S.-Y. Song, G.-C. Yang, M. Zhu, Z.-M. Hao, S.-N. Zhao, H.-J. Zhang, *Chem. Commun*. **2013**, *49*, 8483--8485.

31. G.-P. Yong, Z.-Y. Wang, Y. Cui, *Eur. J. Inorg. Chem*. **2004**, 4317-4323.

2A.A. Appendix:

2A.A.1. X-ray Crystallographic structure determination:

2A.A.1.1. Number of Solvent molecules determination:

Solvent composition of Ce-MOF using *PLATON-SQUEEZE* data:

Total Potential Solvent Accessible Void Vol (SOLV-Map Value) = 244 $Å^3$

Unit cell volume, V = 835.0 $Å^3$

and void volume = ~ 29.2 %

Asymmetric unit present in Ce-MOF is $Ce(CPADA)(H_2O)_2•(DMF)x(H_2O)y$

Again, Z for Ce-MOF is 2.

So, 2 units of asymmetric unit: $Ce(CPADA)(H_2O)_2•(DMF)_x(H_2O)_y$ is present in the unit Cell. where x, y = integer numbers.

Hence, unit cell formula is $Ce_2(CPADA)_2(H_2O)_4•(DMF)_{2x}(H_2O)_{2y}$.

Again, squeeze results suggest that 83 electrons are present from solvent molecules in the unit cell. So, per asymmetric unit $83/2 = 41.5$ electrons are present.

Considering 40 electrons for DMF and 10 for water, the best possible solvents combination and their electrons counts are given in table 2.A1.

Table 2A.A1. solvent composition analysis for Ce-MOF.

No. of DMF	No. of water	Total number of electrons from DMF	Total number of electrons from H_2O	Electron counts
1	4	(1 X 40) = 40	(4 X 10) = 40	40 + 40 = 80

So, 2x = 1 and 2y = 4

So, actually from *PLATON-SQUEEZE* analysis it is understandable that 1 DMF and 4 water molecules present in the unit cell.

So, the unit cell formula is $Ce_2(CPADA)_2(H_2O)_4•(DMF)_1(H_2O)_4$.

Molecular mass of unit cell with solvent $Ce_2(CPADA)_2(H_2O)_4•(DMF)_1(H_2O)_4$ or

$(C_{11}H_8CeNO_6)_2(C_3H_7NO)(H_2O)_8$ or $C_{25}H_{39}Ce_2N_3O_{21}$ is = 997.66 g mol^{-1}.

% mass of DMF = (73/997.66) X 100 = 7.3

% mass of water = (8x18/997.66) X 100 = 14.4

Total calculated % mass loss = (7.3 + 14.4) = 21.7 %

TGA analysis:

For TGA plot see Figure 2A.3F and Figure 2A.A4. Now, from TGA curve mass loss due to water at around 130 °C is 8.5 % and mass loss due to DMF at around 220 °C is 9.8 %.

Total calculated % mass loss = (8.5 + 9.8) = 18.3 %

So, the calculated and observe mass loss approximately matches with each other.

Table 2A.A2. CHN analysis of as made Ce-MOF

Solvent combination	8 H_2O + 1 DMF
Unit cell formula with solvent	$Ce_2(C_{11}H_8NO_6)_2(H_2O)_4\bullet(C_3H_7NO)(H_2O)_4$ or $Ce_2(CPADA)_2(H_2O)_4\bullet(DMF)(H_2O)_4$
Calc. CHN analysis	C = 30.09 H = 3.94 N = 4.21
Obsd. CHN analysis	C = 31.50, H = 3.81 and N = 4.21

The formula of the unit cell of Ce-MOF is $Ce_2(C_{11}H_8NO_6)_2(H_2O)_4\bullet(C_3H_7NO)(H_2O)_4$ or $Ce_2(CPADA)_2(H_2O)_4\bullet(DMF)(H_2O)_4$.

Table 2A.A3. Crystal structure information for the solvated and squeezed structure of Ce-MOF obtained from SCXRD and PLATON analysis.

Crystal Parameters	Non-squeezed Ce-MOF	Squeezed Ce-MOF
Chemical formula	$Ce_2(CPADA)_2(H_2O)_4\bullet(DMF)(H_2O)_4$	$Ce_2(CPADA)_2(H_2O)_4$
Formula weight	852.66	997.66
Crystal system	Triclinic	Triclinic
Space group	P-1	P-1
Unit-cell parameter	a(Å) =8.9262(23), b(Å) =9.8826(22), c(Å) =11.5446(25), α = 64.708(9) °, β = 79.761(13) °, γ = 65.175(13) °, V(Å) = 835.69(68)	a(Å) =12.8523(4), b(Å) =12.8523(4), c(Å) =45.7558(17), α = β = 90°, γ = 120°, V(Å) = 835.69(68)
Crystal color	Colorless platy crystal	Colorless platy crystal
Temperature	100(2)	100(2)
No. of formula units in unit cell (Z)	2	2

Density (g cm^{-1})	2.91	2.91
Abs. Coeff. (mm^{-1})	82.583	82.583
F(000)	640	640
Reflection Data		
No. of reflections meas.	10969	10969
No. of uniq. reflections	2816	2816
No. of obs. reflections	2179	2179
λ (Å)	1.54178	1.54178
R_{merge}	0.078	0.078
Av. I/sig(l)	13.66	13.66
θ_{max}	78.5	78.5
θ_{min}	4.2	4.2
Refinement Data		
R_{all}	0.179	0.130
R_{obs}	0.139	0.098
$wR_{2(all)}$	0.357	0.278
$wR_{2(obs)}$	0.334	0.244
Goodness-of-fit (GOOF)	2.509	1.053
Largest diff. peak and hole: Delta-rho (eÅ^3)$_{max}$	7.171	4.545
Largest diff. peak and hole: Delta-rho (eÅ^3)$_{min}$	-2.267	-2.053

*Note. PLATON analysis suggests the presence of a significant amount of solvent accessible voids in the structure of Ce-MOF (Ce$_2$(CPADA)$_2$(H$_2$O)$_4$•(DMF)$_{2x}$(H$_2$O)$_{2y}$). The solvents could not be modeled satisfactorily. From the SQUEEZE analysis was done to evaluate the number of DMF & H$_2$O molecules. From squeezed electron counts and utilizing the feasible analytical method like thermogravimetric analysis (TGA), the solvent content in the framework was estimated. It was found that 1 DMF and 8 water molecules present in each unit cell of Ce-MOF. So, the actual formula of Ce-MOF is Ce$_2$(CPADA)$_2$(H$_2$O)$_4$•(DMF)(H$_2$O)$_4$.

The structure of Ce-MOF:
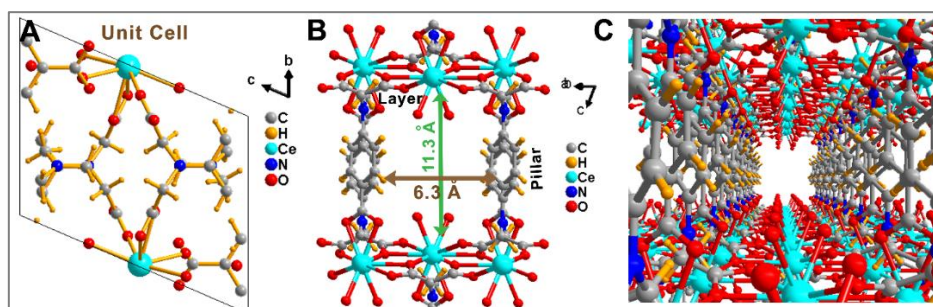
Figure 2A.A1. (A) Unit cell of the Ce-MOF. (B) The 3D layered-pillared topology of as made Ce-MOF showing the 1D channel of dimension 6.3 Å x 12.3 Å. As made MOF has Ce-coordinated water molecules. (C) Persective view of single channel shows Lewis basic nitrogens are decorated along the channel pointing their lone pairs towards the centre of the channel.
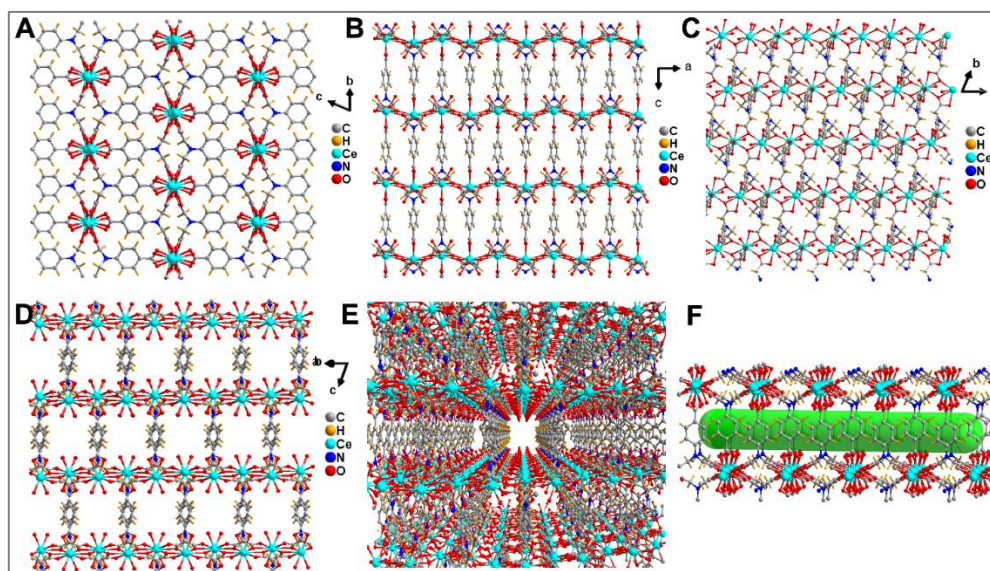
Figure 2A.A2. (A) View along a-axis, (B) View along b-axis (a layered pillared structure), (C) View along c-axis, (D) Layered-pillared framework with 1D Pore view (without pore DMF molecules), (E) Perspective view of the channels, (F) The yellow balls represent the solvent-spaces in the channel of the MOF.

2A.A.2. Analytical characterizations:
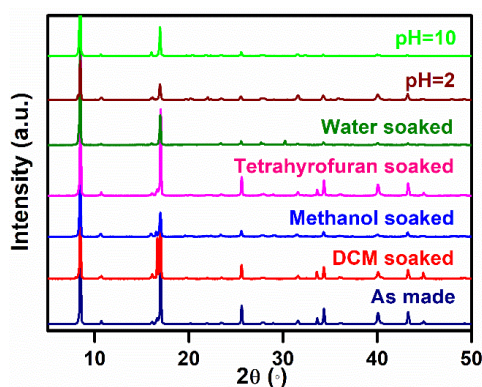
Figure 2A.A3. PXRDs of as made Ce-MOF subjected to different solvents and aqueous acid-base solution treatments.
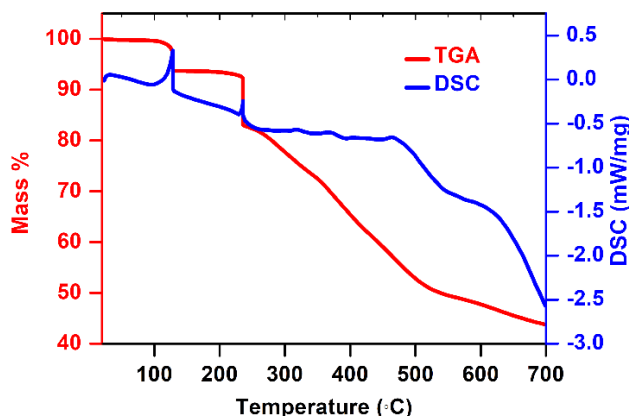
Figure 2A.A4. Isothermal TGA was carried out on the as made Ce-MOF via holding the heating at 130 and 220 °C. In the TGA profile as made Ln-MOF has clear plateau up to 220 °C after first mass loss, suggesting MOF is stable up to 220 °C. Two clear exothermic peaks at 130 and 220 °C in DSC profile suggests two types of mass loss due to the pore water and DMF molecules.
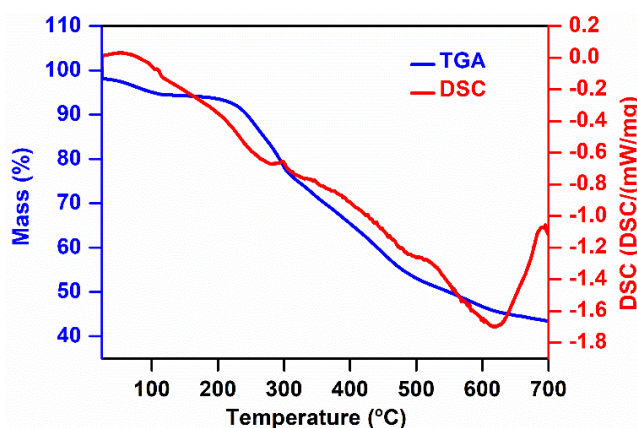
Figure 2A.A5. TGA carried out under N_2 on the pre-activated Ce-MOF via heating the MOF externally at 220 °C.
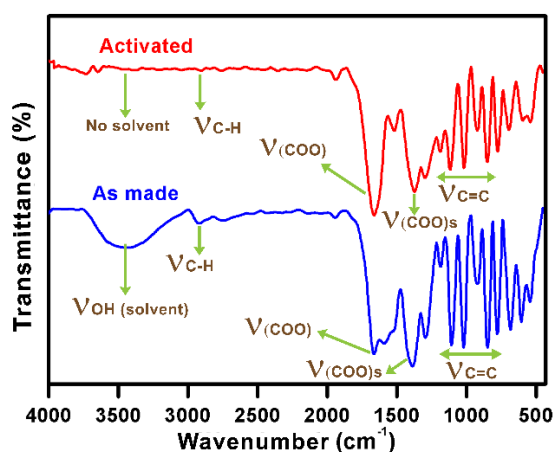
Figure 2A.A6. Infrared spectra (IR) of as made (blue) and activated (red) Ce-MOF exhibits different bending and stretching vibrational modes in Ce-MOF. Characteristics peaks: IR: v(C=C): 1189 to 780 vs; v(COO)s 1298s, 1395s; v(COO): 1665s and 1594s; v(N-H): 2751; v(C-H): 2925; v(O-H) solvent: 3456s. (*Source: Infrared and Raman Spectra of Inorganic and Coordination Compounds, Part B, Applications in Coordination, Organometallic, and Bioinorganic Chemistry, 6th Edition, Kazuo Nakamoto*).

Chapter 2B

Microporous mixed-metal mixed-ligand metal-organic framework for selective CO₂ capture
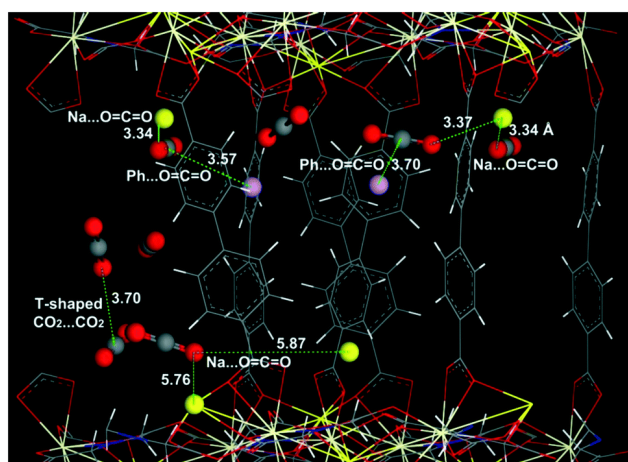
2B.1 Introduction:

Buoyant economic growth severely impacts global climate changes,[1] to which anthropogenic CO_2 emissions are a major contributor. Selective removal of this greenhouse gas will aid its mitigation.[2] There are many different CO_2 capture approaches, including biogas upgrading,[3] flue gas separation,[4] trace CO_2 removal utilizing confined space,[5] and direct air capture.[6] Designable adsorbents that show controlled sorption behavior can contribute immensely to CO_2 capture technology. Solid sorbents are attractive for energy-efficient cyclable CO_2 capture because capture occurs via a low-energy physisorptive process. Some key features, such as adsorption capacity, kinetics, selectivity, and ease of regeneration, are largely decided by the pore-size, shape, and the nature of the adsorption sites.[7] Therefore, several types of fascinating porous materials, including porous organic polymers,[8] metal organic frameworks,[9] ZIFs,[10] porous organic cages,[11] and more traditional adsorbents, such as activated carbons, zeolites, and organosilicas,[12] with diverse interaction sites have been developed and studied extensively in selective gas separations. Among them, MOFs are being considered as promising next generation materials for efficient and cost-effective gas separation due to their uniform pore structure, high porosity, designable structures, and tunable pore size.[9a,c,13–15] Furthermore, due to their crystalline nature, an accurate molecular-level understanding of MOF adsorption sites is viable and enables adsorption site modeling.[8,9,15,16] Several strategies, such as introducing an amine group into the ligand structure,[9b,c] creating open metal sites, grafting pendent amine groups to open metal sites for further capacity enhancement, and inserting charged guests inside the pore of cationic/anionic frameworks, have been used to enhance capture performance.[17] Rosi and coworkers have shown how tuning the pore confinement effect in bio-MOF-1 via organic guest cation exchange helps to improve the CO_2 adsorption capacity.[18] In another report, Ahn and coworkers described the effect of the size and electronic effect of the exchanged extra-framework metal cations on MOF CO_2 uptake.[19] Among these approaches, using mixed ligands to prepare MOFs is an effective way to expand the library of porous MOFs with divergent pore environments.[20] Fully understanding the adsorption sites within such mixed-ligand materials using experimental or modelling studies is extremely important to developing superior sorbents.

Herein, we report the synthesis, structural analysis, and gas separation properties of a novel layer-pillar MOF, $Ce_3Na_3(BPDC)_3(IMDA)_3 \cdot (DMF)_2(H_2O)_9$ (IISERP-MOF24). This MOF shows moderate CO_2 uptake and CO_2/N_2 selectivity at room temperature, smooth CO_2 diffusion kinetics, and an optimal heat of adsorption (HOA) for the facile regeneration of adsorbed CO_2. Furthermore, using simulation methods, we have modelled the CO_2 adsorption sites within these heterogeneously functionalized pores.

2B.2. Materials and Methods:

2B.2.1. Synthesis of $Ce_3Na_3(BPDC)_3(IMDA)_3 \cdot (DMF)_2(H_2O)_9$, IISERPMOF24:

A mixture of $Ce(NO_3)_3 \cdot 6H_2O$ (95.0 mg, 0.219 mmol), iminodiacetic acid (H₃IMDA, 69.0 mg, 0.519 mmol), and 4,4'-biphenyldicarboxylic acid (H₂BPDC, 65 mg, 0.269 mmol) was dissolved into a mixed solvent

of N,N′- dimethyl formamide (DMF) and H_2O (9 mL; v/v = 8:1) in a screw-capped vial (20 mL), to which 50 µL of 10 M NaOH was added. The vial was capped and heated in an oven at 90 °C for 5 days. Colourless prismatic crystals were obtained by filtration and washed several times with DMF to afford IISERP-MOF24 in 75 % yield based on metal salt. The experimental powder X-ray diffraction (XRD) profile of IISERP-MOF24 matches well with the simulated one based on the single-crystal X-ray data, indicating that the sample forms as a pure phase. (CHN: Calc. C- 37.70; H- 3.74; N- 3.66: Obsd. 37.79; 3.64, 5.35) calculated using the formula: $Ce_3Na_3(C_{14}H_8O_4)_3(C_4H_5NO_4)_3.(C_3H_7NO)_2(H_2O)_9$. The discrepancies in the observed values could be attributed to the partial loss of the solvent molecules when exposed to air.
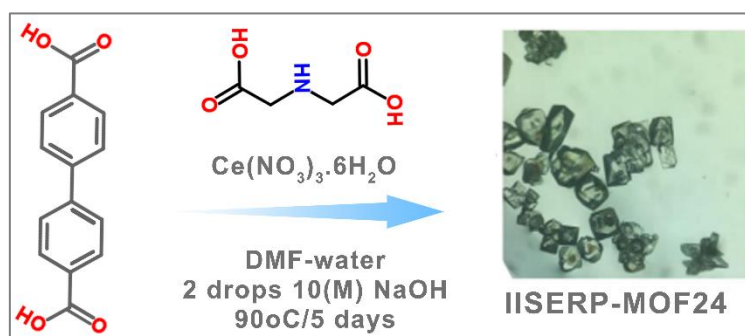
Scheme 2B.1. Schematic representation of the synthesis of IISERP-MOF24.

2B.2.2. Analytical Characterisations:

All reagents and solvents were purchased from a commercial source and used without further purification.

2B.2.2.1. Single Crystal X-ray diffraction and Structures determinations:

Single-crystal X-ray diffraction was done on a Bruker SMART APEX four-circle diffractometer equipped with a CMOS photon 100 detector and Micro focus (IµS) using Cu-Kα radiation. The crystal of IISERP-MOF24 mounted on nylon Cryo loops using Paratone-N oil. Data were collected at 100 K. Total data were integrated using Bruker SAINT Software and using SADABS it was corrected for absorption. The structure was solved using Intrinsic Phasing routine and was refined using the SHELXTL 6.3.1 (2004) software suite. All the non-hydrogen atoms were located from iterative examination of difference F-maps following which the structure was refined using least-squares method. Hydrogen atoms were fixed geometrically in a riding model. CCDC: 1841713 contain the supplementary crystallographic data for this paper. These data are provided free of charge by The Cambridge Crystallographic Data Centre.

2B.2.2.2. Powder X-ray Diffraction:

Powder XRDs were done using a Rigaku Miniflex-600 instrument and processed using PDXL software. The Variable temperature powder X-ray diffraction (VT-PXRD) was carried out on a full fledge Bruker instrument using the in-built furnace and in air.

2B.2.2.3. Infrared (IR) spectroscopy:

The infrared (IR) spectrum was recorded on a Nicolet FT-170SX instrument using KBr discs in the $400-4000$ cm^{-1} region.

2B.2.2.4. Scanning Electron Microscopy:

Field Emission Scanning Electron Microscopic (FESEM) study was done using the Ultra Plus Field Emission Scanning Electron Microscope with integral charge compensator and embedded EsB and AsB detectors.

2B.2.2.5. Thermogravimetric Analysis:

Thermogravimetry analysis (TGA) of as made MOF was performed on NETSZCH TGA-DSC instrument. The routine TGAs were done under N_2 gas flow (20 ml min^{-1}) (purge + protective) and samples were heated in the temperature range of 25 to 550 °C with a heating rate of 5 °K min^{-1}.

2B.2.3 Adsorption Analysis

All the gas adsorption analysis was carried out using ~100 mg of IISERP-MOF24. The sample was directly activated by evacuation at 150 °C for 24 hrs (10^{-6} mbar) till an outgassing rate was $\leq$ 2 µbar min^{-1} was achieved. Then the activated MOF was transferred to the analysis port of Micromeritics ASAP 2020HD or 3-FLEX instrument for the gas sorption analysis. Gas analyses were carried out with ultrahigh purity gases ($\geq$4.8 grade).

2B.2.3.1. Langmuir Fits:

In all cases the isotherms were fit to the Single-Site Langmuir (SSL) equation. The isotherms were fit by solving the Langmuir isotherm equation using the solver function in Microsoft Excel following a similar protocol to Keller et al. [2.A1] Utilizing this routine circumvents some of the problems associated with favouring either high- or low-pressure regions when linearizing the Langmuir equation 2.A2 and offers a balanced approach.

Single-Site Langmuir (SSL): $\quad q_i = q_m \dfrac{k_i}{1 + k_i P} P$

Dual-Site Langmuir (DSL): $\quad q_i = q_{m,1} \dfrac{K_1}{1 + K_1 P} P + q_{m,2} \dfrac{K_2}{1 + K_2 P} P$

2B.2.3.2. Ideal Adsorbed Solution Theory (IAST):

IAST calculations were undertaken as described by Prausnitz et al 2.A3. The selectivity equation involved in calculation is provided below.

Selectivity: $\quad S_{1,2} = \dfrac{q_1/q_2}{p_1/p_2}$

2B.2.3.3. CO₂ cycling Experiment Procedure:

Isotherm cycling experiments were done using ASAP 2020HD instrument associated with Iso-Cycling software. About 100 mg of samples were loaded in the sample cell and activated until the outgassing rate was ≤ 2 µbar min^{-1}. The iso-cycling program was created with 15 cycles, each cycle having 14 to 15 data points (equilibration time 100 sec) in between 0.015 bar to 1.2 bar. After each cycle, the material was maintained under vacuum for 10 mins before continuing the subsequent cycles.

2B.2.3.4. Rate of Adsorption (ROA) measurements:

Rate of adsorption (ROA) experiments were carried out on the Micromeritics ASAP2020HD instrument equipped with a ROA software capability. An extremely high-resolution isotherm measurement was carried out using the ASAP2020HD instrument at 273 K in the pressure range of 0-1 bar. The diffusion coefficient was calculated as a function of CO_2 loading. For this purpose, 8 different loading points were used and each of the ROA data was fitted to a spherical pore model[2,A4] F = fractional uptake; τ = non-dimensional time given by $\tau = Dt/R_2$, where R= particle size; t= time (secs); D = apparent diffusivity. The single-component diffusion coefficient was estimated to be 8.1932×10^{-9} m^2 s^{-1} for IISERP-MOF24 taking the average of these eight points. Note: the kinetics of the low loadings (< 1 mmol g^{-1}) were extremely hard to model.

$$F = 1 - \frac{6}{\pi^2} \sum_{n=1}^{\infty} \frac{1}{n^2} Exp(-n^2\pi^2\tau)$$

2B.3. Results and discussion:

Single-crystal diffraction analysis showed that IISERP-MOF24 crystallized in a trigonal crystal system (space group, R32, Table 2.1). Two different metal ions (Ce^{3+} and Na^+) were present in the crystal structure of IISERP-MOF24. One crystallographically unique Ce^{3+} centre was present, which was nine coordinated in a bicapped pentagonal-bipyramid geometry (Figure 2B.A1A top). Two BPDC ligands were coordinated to each Ce^{3+} metal center in a bidentate chelating fashion (Figure 2B.1A and B). Therefore, among nine coordination sites, four were occupied by O atoms from BPDC, one was occupied by the sp^3 N-atom of the IMDA ligand, and the remaining four were occupied by O atoms from iminodiacetate binding in a monodentate fashion. There were two crystallographically unique Na^+ centers, Na(1) and Na(2). Na(1) was in the plane of the inorganic layer formed by coordination with the carboxylate moieties. Na(1) occupied a special position and was fully occupied (Figure 2B.1C). Na(2) also resided in a special position, but was only 50% occupied (Figure 2B.A1). Furthermore, the N-atom of iminodiacetic acid occupied a special position with full occupancy. Therefore, the three-dimensional structure was made up of a Ce–Na– carboxylate inorganic layer pillared by the BPDC units. The distance between two adjacent Ce metal centers was ~6.43 Å, while that

Table 2B.1. Crystal structure information.

Crystal parameter	Parameter value
Chemical formula	With solvent: $Ce_3Na_3(BPDC)_3(IMDA)_3 \cdot (DMF)_2(H_2O)_9$ Without solvent: $Ce_3Na_3(BPDC)_3(IMDA)_3$
Formula weight	With solvent: 1911.5 g mol^{-1} without solvent: 1603.19 g mol^{-1}
Crystal system	Trigonal
Space group	R32
Crystal color	Colorless prismatic crystal
Unit-cell parameter	a(Å)=12.8523(4), b(Å)=12.8523(4), c(Å)= 45.7558(17), $\alpha = \beta = 90°$, $\gamma = 120°$, V (Å) = 6545.43(4)
Temperature	100 (2)
No. of formula units in unit cell (Z)	3
Density (g cm^{-1})	1.22
Abs. coeff. (mm^{-1})	12.522
F(000)	2340
Flack	−0.087(7)
Reflection data	
No. of reflections meas	5365
No. of uniq. reflections	2862
No. of obs. reflections	2821
λ (Å)	1.54178
R_{merge}	0.027
Av. I/sig(l)	24.88
θ_{max}	72.3
θ_{min}	4.4
Refinement data	
R_{all}	0.028
R_{obs}	0.027
$wR_{2(all)}$	0.080
$wR_{2(obs)}$	0.080
Ext. coeff.	0.0003
Goodness-of-fit (GOOF)	1.132
Largest diff. peak and hole: delta-rho (e Å^{-3})$_{max}$	1.044
Largest diff. peak and hole: delta-rho (e Å^{-3})$_{min}$	−0.623

Figure 2B.1. (A) and (B) Show the connectivity among the building units present in the inorganic layers of IISERP-MOF24. (C) The Connolly representation showing the channels along the a-axis with dumb-bell shaped openings.

between adjacent Ce and Na ions in the same layer was ~3.84 Å (Figure 2B.A1). A Connolly pore surface generated with a probe radius of 1.4 Å showed the presence of dumb-bell shaped pores with dimensions of approx. 8×7 Å. These ran along both the a- and b-axes (Figure 2B.1C). Alternatively, the structure can be seen as anionic framework, $[Ce_3Na_2(BPDC)_3(IMDA)_3]^{1-}$, with pores accommodating the charge-balancing Na^+ cations. A MOF formed by combining an aromatic dicarboxylate with iminodiacetate has not been reported previously, but a closely related MOF has been prepared using oxy-diacetate.[21] Surprisingly, no MOF combining IMDA with even the most common terephthalate ligand has been reported. A dense Cu–iminodiacetate MOF with interwoven 2-D honeycomb layers has been reported, but with 4,4′- bipyridyl used instead of BPDC.[22]

The phase purity of the MOF was confirmed by powder X-ray diffraction (XRD) (Figure 2B.2A). PLATON analysis suggested a solvent-accessible void volume of 40.0 %. The electron counts obtained from the SQUEEZE routine[23] can be assigned to nine water and two DMF molecules. This agreed well with those calculated by TGA. The thermal stability of IISERP-MOF24 was examined using TGA from room temperature to 550 °C (Figure 2B.2B). There was a two-step gradual weight loss up to 210 °C, which could be assigned to solvent losses (see Appendix). When these high boiling solvents were exchanged with THF, the MOF was stable up to 330 °C (Figure 2B.2B and 2B.A3). IR spectra showed characteristic peaks due to carboxylates, and N–H and C–H stretching and bending bands (Figure 2B.A4). Elemental mapping using energy dispersive X-ray analysis (EDXA) showed a homogenous distribution of Ce and Na across the entire sample (Figure

2B.A5). A Ce:Na ratio of 1:1 was expected from the formula of IISERP-MOF24, and was confirmed by SEM-EDX analysis (Table 2B.A2).

Gas sorption properties of IISERP-MOF24:

The permanent porosity of IISERP-MOF24 was established from N_2 sorption analysis at 77 K, which displayed a typical type-I isotherm with ~8.7 mmol g^{-1} uptake, as expected from its microporous structure (Figure 2B.2C). Brunauer–Emmett–Teller (BET) and Langmuir surface areas were calculated as 771 and 851 $m^2 g^{-1}$, respectively (Figure 2B.A6 and A7). An NLDFT fit (slit pore, carbon, 77 K N_2) to the adsorption branch of the 77 K N_2 isotherm yielded two major pore sizes (6.79 and 8.04 Å, Figure 2B.2C). This agreed well with the dimensions of the micropores present in the crystal structure (Figure 2B.2C and 2B.1D). The permanent porosity, potentially polarizing inorganic layers, and Na^+ ions in the MOF inspired us to investigate the CO_2 adsorption characteristics of this material. CO_2 adsorption isotherms were collected at 248, 273, and 298 K up to 1 bar (Figure 2B.2D). All gas adsorption isotherms were completely reversible without any appreciable hysteresis. The CO_2 uptakes at 298, 248, and 273 K were ~2, ~3, and 4.8 mmol g^{-1}, respectively (Figure B2.2D). Although IISERP-MOF24 showed moderate CO_2 uptake at 298 K, the N_2 uptake at 298 K was negligible (Figure 2B.A9). This motivated us to evaluate the CO_2/N_2 selectivity at 273 K and 298 K using the IAST model and employing a typical composition of $15CO_2:85N_2$, which is industrially relevant for flue gas separation. The selectivities were found to be 100 and 68 at 273 and 298 K, respectively (Figure 2B.3A). To establish the interaction strength between CO_2 and the framework, we calculated the HOA using the virial method, employing CO_2 isotherms collected at 248, 273, and 298 K. The zero loading HOA was found to be 23 kJ mol^{-1} and did not show any significant variation across the entire loading (Figure 2B.3B). Considering potentially restricted CO_2 diffusion within the Na^+-ion occupied pores of the IISERP-MOF24, the CO_2 self-diffusion coefficient (D_c) was calculated from rate of adsorption (ROA) measurements at 273 K. The average CO_2 self-diffusion coefficient was found to be in the range of 0.42×10^{-9} to 15.4×10^{-9} $m^2 s^{-1}$ (Figure 2B.3C). This is comparable to some other well-known MOFs, such as MOF-5 (1.17×10^{-9} $m^2 s^{-1}$) or MOF-177 (2.3×10^{-9} $m^2 s^{-1}$).[24] Notably, despite the presence of Na^+ ions in the channels, CO_2 diffused easily. The moderate HOA and favorable diffusion values were reflected in smooth CO_2 cycling at 298 K (Figure 2B.3D). Importantly, the CO_2 uptake remained unaltered over several cycles.

In our experience with MOFs, obtaining the same capacity across multiple syntheses can be difficult and the uptake capacities can fall with repeated adsorption cycles. However, IISERP-MOF24 showed excellent homogeneity across different synthesis batches and also good CO_2 uptake repeatability. PXRD studies indicated the complete retention of crystallinity after multiple adsorption–desorption cycles (Figure 2B.A13). To establish the hydrolytic stability of IISERP-MOF24, the sample was exposed to a humid stream of N_2 (75 % RH) for about 12 h. A PXRD pattern of this steam-treated sample confirmed the complete retention of crystallinity (Figure 2B.A13). Furthermore, the MOF exhibited good solvent stability, as confirmed by the PXRD
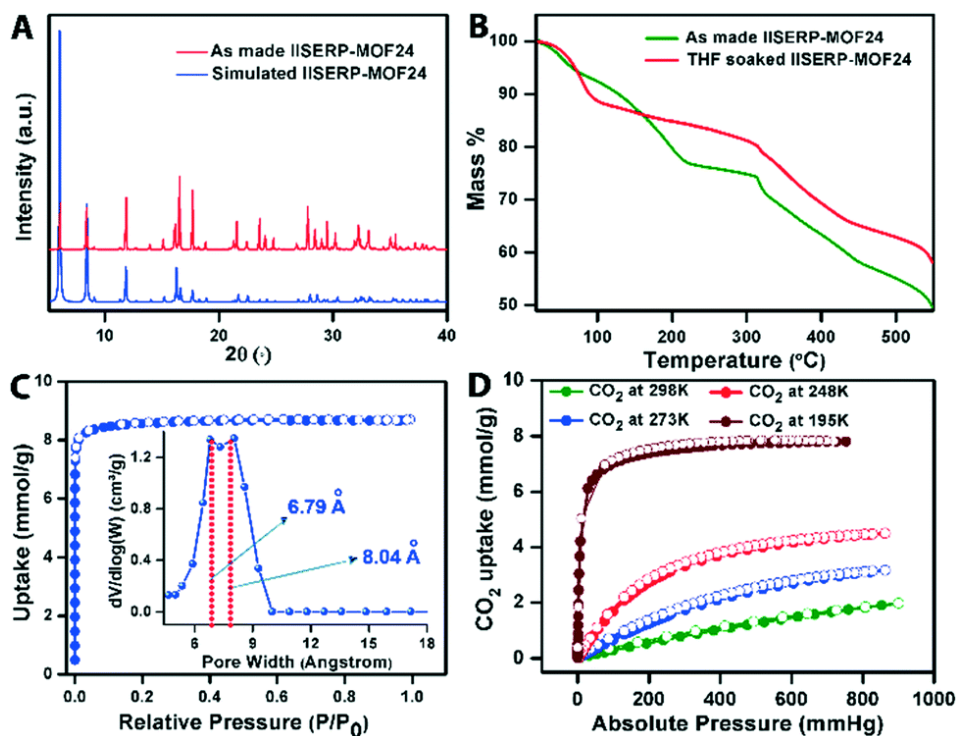
Figure 2B.2. (A) Comparison of PXRD patterns of as-synthesized IISERPMOF24 with the simulated pattern. (B) TGA curves of the as-made and THF-soaked IISERP-MOF24. (C) N_2 isotherm of IISERP-MOF24 measured at 77 K. Inset shows the pore size distribution (NLDFT, slit-pore carbon, and N_2 77 K). (D) CO_2 isotherms of IISERP-MOF24 at 195, 248, 273, and 298 K.
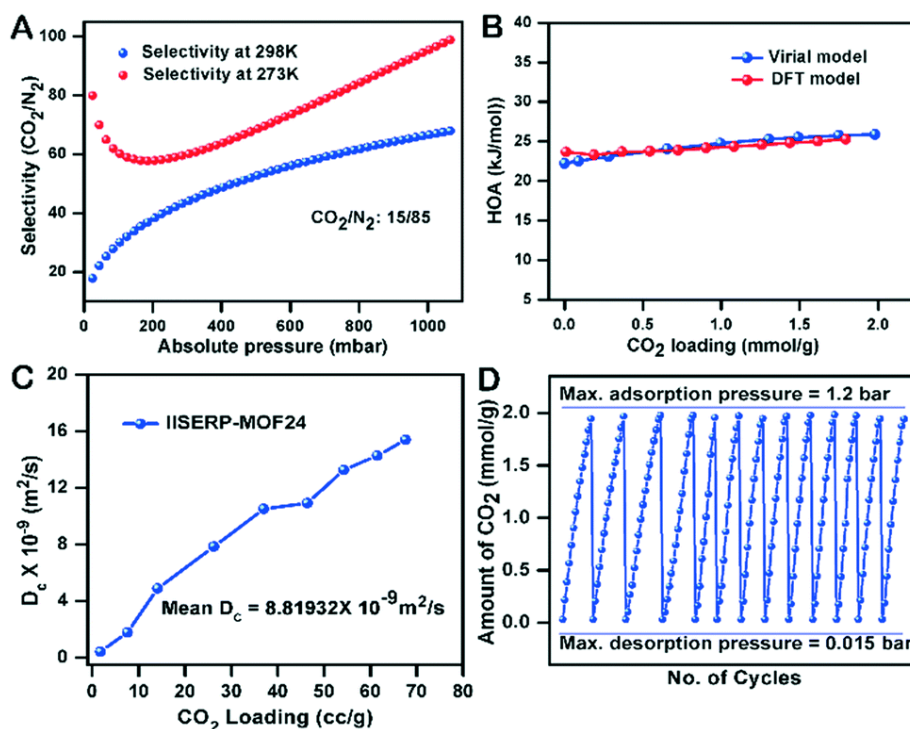
Figure 2B.3. (A) CO_2/N_2 selectivity of IISERP-MOF24 calculated at 298 and 273 K (composition: $15CO_2:85N_2$) using the IAST method and without considering competitive binding. (B) HOA for CO_2 in IISERP-MOF24. (C) CO_2 self-diffusion coefficient in IISERP-MOF24. (D) CO_2 adsorption cycles at 25 °C. Note the uptake remains nearly the same in all cycles.

patterns of the solvent-treated samples (Figure 2B.A14). Notably, the morphology and texture of even the crystals remained visibly intact following solvent treatment and repeated adsorption–desorption cycles (Figure 2B.A15). The flexible iminodiacetate ligand and the long BPDC pillars in the structure can give rise to solvent-loss-assisted or temperature assisted structural changes. To verify this, we conducted variable temperature PXRD runs. The results confirmed that there were no phase changes, even at up to 200 °C (Figure 2B.A16).

A major advantage of crystalline sorbents, such as zeolites and MOFs, is that highly accurate structural details can be obtained.[16,25] Importantly, this facilitates adsorption site modelling. Woo and coworkers[9c] have developed a systematic computational protocol for modelling and analyzing adsorption sites in MOFs and quantifying the gas–framework interactions. Herein, we employed a similar strategy to understand the adsorption sites of this MOF. There is significant interest in understanding adsorption sites of many solid sorbents using such modelling and spectroscopic studies.[9,15,16] We simulated the 298 K CO_2 adsorption isotherm using GCMC methods embedded in Materials Studio V.6.0 software. In the pressure range 0–1 bar, the simulated isotherm showed an adsorption profile that matched well with the experimental isotherm (Figure 2B.A17). However, the uptakes were slightly overestimated throughout the calculated pressure range.
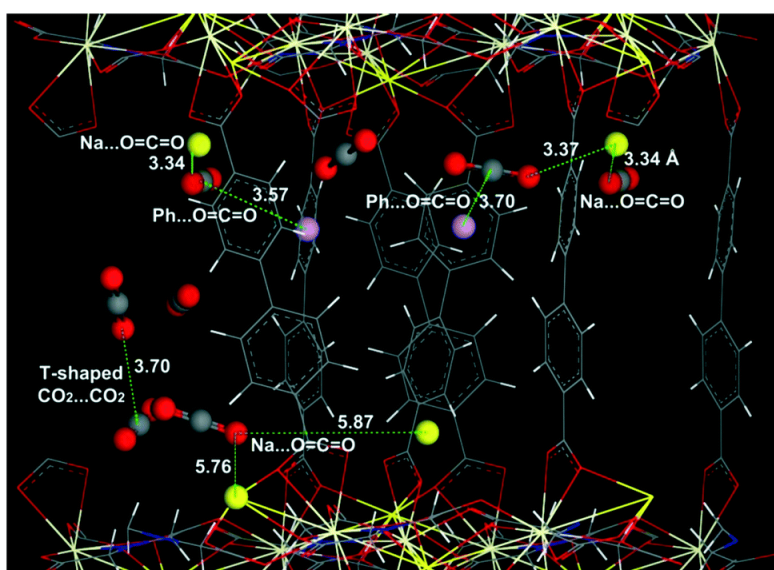
Figure 2B.4. GCMC-simulated structure showing the lowest energy sites for CO_2 and different CO_2–framework, CO_2–Na^+, and CO_2–CO_2 interactions. Color code: Na, yellow; Ce, pale greenish-yellow; centroid of phenyl rings, magenta; C, grey; O, red; and N, blue. Interactions are shown as green dotted lines.

Next, we extracted the CO_2 positions in the MOF by employing a saturation amount of CO_2 derived from the experimental uptakes (13CO_2/unit cell). During this routine, the framework was frozen and the CO_2 molecules were allowed to diffuse freely (see Appendix). The CO_2 positions observed in the simulations showed that the sodium ions in the channels served as favorable adsorption sites, with the oxygen atoms of CO_2 pointing towards the Na^+ ions (O=C=O···Na^+ = 3.34– 5.87 Å), while some of the CO_2 sat flat on the

phenyl rings of the BPDC at a distance of $CO_2 \cdots Ph(centroid) = 3.6–3.7$ Å (Figure 2B.4). Furthermore, some CO_2 molecules occupied the center of the slit pore and were stabilized by $CO_2 \cdots CO_2$ interactions between CO_2 molecules oriented in a T-shaped fashion, resembling those in solid crystalline phases of CO_2. 16e However, the experimentally determined moderate and nearly unchanged HOAs (over the entire loading) suggested that these sites had similar interactions with CO_2 molecules. This contrasted with the recently reported sodium copper silicate compound (HOA ≥ 45 kJ mol^{-1}), in which the observed interactions were much weaker despite having free sodium cations.[25]

2B.4. Conclusions

We have successfully synthesized a 3-D layered-pillared MOF by combining readily available iminodiacetic and 4,4′-biphenyl-dicarboxylic acid with a trivalent metal for the first time. The resulting MOF is permanently porous, with a moderate CO_2 uptake and CO_2/N_2 selectivity. Other attributes include humid stability, an optimal HOA, a favorable CO_2 diffusion kinetics, and smooth cycling. The porous anionic framework formed by this specific mixed-metal mixed-ligand system suggested that different cations can be accommodated in this composition without losing its gas-accessible porosity. So, in conclusion, we can say following the Approach-1 we have successfully designed and synthesized humidity stable mixed-metals (Ce and Na) based micro-porous MOF applicable to CO_2 capture. Our modelling also suggested the role of extra-framework ions on the adsorption within a single MOF using this approach.

2B.5. References:

1. https://en.wikipedia.org/wiki/Carbon_capture_and_ storage; (b) Inventory of U.S. Greenhouse Gas Emissions and Sinks: 1990–2016.

2. (a) D. W. Keith, *Science* **2009**, *325*, 1654-1655; (b) G. T. Rochelle, *Science* **2009**, *325*, 1652-1654.

3. K. Zhou, S. Chaemchuen, F. Verpoort, *Renew. Sust. Energ. Rev.* **2017**, *79*, 1414-1441.

4. (a) J. Mustafa, M. Farhan, M. Hussain, *J. Membra. Sci. Technol.* **2016**, 6, 153; (b) D. Aaron, C. Tsouris, *Sep. Sci. Technol.* **2005**, *40*, 321-348.

5. Q. Ke, T. Sun, X. Wei, Y. Guo, S. Wang, *ChemSusChem* **2017**, *10*, 4207-4214.

6. (a) M. Ranjan, H. J. Herzog, *Energy Procedia* **2011**, *4*, 2869-2876; (b) M. Mazzotti, R. Baiocchi, M. J. Desmond, R. H. Socolow, *Climatic change* **2013**, *118*, 119-135; (c) https:// www.aps.org/policy/reports/assessments/upload/dac2011.pdf; (d) https://www.ipcc.ch/pdf/special-reports/srccs/srccs_ wholereport.pdf.

7. (a) J. P. Sculley, W. M. Verdegaal, W. Lu, M. Wriedt, H. C. Zhou, *Adv. Mater.* **2013**, *25*, 3957-3961; (b) A. D. Wiersum, J.-S. Chang, C. Serre, P. L. Llewellyn, *Langmuir* **2013**, *29*, 3301-3309; (c) Z. Zhang, Z.-Z. Yao, S. Xiang, B. Chen, *Energy Environ. Sci.* **2014**, *7*, 2868-2899; (d) J. M. Huck, L.-C. Lin, A. H. Berger, M. N. Shahrak, R. L. Martin, A. S. Bhown, M. Haranczyk, K. Reuter, B. Smit, *Energy Environ. Sci.* **2014**, *7*, 4132-4146.

8.   (a) S. Nandi, J. Rother, D. Chakraborty, R. Maity, U. Werner-Zwanziger, R. Vaidhyanathan, *J. Mater. Chem. A* **2017**, *5*, 8431-8439.; (b) S. Nandi, U. Werner-Zwanziger, R. Vaidhyanathan, *J. Mater. Chem. A* **2015**, *3*, 21116-21122.

9.   (a) S. Nandi, S. Collins, D. Chakraborty, D. Banerjee, P. K. Thallapally, T. K. Woo, R. Vaidhyanathan, *J. Am. Chem. Soc.* **2017**, *139*, 1734-1737; (b) A. Banerjee, S. Nandi, P. Nasa, R. Vaidhyanathan, *Chem. Commun.* **2016**, *52*, 1851-1854; (c) R. Vaidhyanathan, S. S. Iremonger, G. K. Shimizu, P. G. Boyd, S. Alavi, T. K. Woo, *Science* **2010**, *330*, 650-653; (d) R. Vaidhyanathan, S. S. Iremonger, K. W. Dawson, G. K. Shimizu, *Chem. Commun.* **2009**, 5230-5232; (e) K. Sumida, D. L. Rogow, J. A. Mason, T. M. McDonald, E. D. Bloch, Z. R. Herm, T.-H. Bae, J. R. Long, *Chem. Rev.* **2012**, *112*, 724-781.

10. (a) R. Banerjee, A. Phan, B. Wang, C. Knobler, H. Furukawa, M. O'Keeffe, O. M. Yaghi, *Science* **2008**, *319*, 939-943; (b) A. Phan, C. J. Doonan, F. J. U. Romo, C. B. Knobler, M. O'Keeffe and O. M. Yaghi, *Acc. Chem. Res.* **2010**, *43*, 58-67.

11. J. R. Holst, A. Trewin, A. I. Cooper, *Nature Chem.* **2010**, *2*, 915-920.

12. (a) J. C. Hicks, J. H. Drese, D. J. Fauth, M. L. Gray, G. Qi, C. W. Jones, *J. Am. Chem. Soc.* **2008**, *130*, 2902-2903; (b) A. Sayari, Y. Belmabkhout, R. Serna-Guerrero, *Chem. Eng. J.* **2011**, *171*, 760-774; (c) A. Thomas, *Angew. Chem. Int. Ed.* **2010**, *49*, 8328-8344; (d) R. V. Siriwardane, M.-S. Shen, E. P. Fisher, J. A. Poston, *Energy & Fuels* **2001**, *15*, 279-284.

13. (a) P. Nugent, Y. Belmabkhout, S. D. Burd, A. J. Cairns, R. Luebke, K. Forrest, T. Pham, S. Ma, B. Space, L. Wojtas, *Nature* **2013**, *495*, 80-84; (b) X. Kong, E. Scott, W. Ding, J. A. Mason, J. R. Long, J. A. Reimer, *J. Am. Chem. Soc.* **2012**, *134*, 14341-14344.

14. (a) D. Wu, Q. Xu, D. Liu and C. Zhong, J. Phys. Chem. C, 2010, 114, 16611; (b) D.-S. Zhang, Z. Chang, Y.-F. Li, Z.-Y. Jiang, Z.-H. Xuan, Y.-H. Zhang, J.-R. Li, Q. Chen, T.-L. Hu, X.-H. Bu, *Sci. Rep.* **2013**, *3*, 3312; (c) H. Jasuja, Y.-g. Huang, K. S. Walton, *Langmuir* **2012**, *28*, 16874-16880; (d) H. Jasuja, Y.-g. Huang, K. S. Walton, *Langmuir* **2012**, *28*, 16874-16880; (e) T. Wu, L. Shen, M. Luebbers, C. Hu, Q. Chen, Z. Ni, R. I. Masel, *Chem. Commun.* **2010**, *46*, 6120-6122; (f) R. Feng, Y.-Y. Jia, Z.-Y. Li, Z. Chang, X.-H. Bu, *Chem. Sci.* **2018**, *9*, 950-955.

15. (a) E. J. Carrington, I. J. Vitórica-Yrezábal, L. Brammer, *Acta Crystallogr., Sect. B: Struct. Sci., Cryst. Eng. Mater.* **2014**, *70*, 404–422; (b) P. G. Boyd, T. K. Woo, *CrystEngComm* **2016**, *18*, 3777-3792; (c) S. P. Collins, T. D. Daff, S. S. Piotrkowski, T. K. Woo, *Sci. Adv.* **2016**, *2*, e1600954; (d) H. Wu, J. M. Simmons, G. Srinivas, W. Zhou, T. Yildirim, *J. Phys. Chem. Lett.* **2010**, *1*, 1946-1951; (e) Y. Jiao, Z. Li, Y. Ma, G. Zhou, S. Wang, G. Lu, *AIP Adv.* **2017**, *7*, 085009; (f) Z. Lu, H. G. W. Godfrey, I. da Silva, Y. Cheng, M. Savage, F. Tuna, E. J. L. McInnes, S. J. Teat, K. J. Gagnon, M. D. Frogley, P. Manuel, S. Rudić, A. J. Ramirez-Cuesta, T. L. Easun, S. Yang, M. Schröder, *Nat. Commun.* **2017**, *8*, 1-10.

16. (a) N. A. Ramsahye, G. Maurin, S. Bourrelly, P. L. Llewellyn, T. Devic, C. Serre, T. Loiseau, G. Ferey, *Adsorption* **2007**, *13*, 461-467; (b) S. Xiang, Y. He, Z. Zhang, H. Wu, W. Zhou, R. Krishna, B. Chen, *Nat. Commun.* **2012**, *3*, 1-9; (c) F. Luo, C. Yan, L. Dang, R. Krishna, W. Zhou, H. Wu, X. Dong, Y. Han, T.-L. Hu, M. O'Keeffe, *J. Am. Chem. Soc.* **2016**, *138*, 5678-5684; (d) T. Pham, K. A. Forrest, D. M. Franz, Z. Guo, B. Chen, B. Space, *Phys. Chem. Chem. Phys.* **2017**, *19*, 18587-18602.; (e) S. Nandi, R. Maity, D. Chakraborty, H. Ballav, R. Vaidhyanathan, *Inorg. Chem.* **2018**, *57*, 5267-5272; (f) Z. Wang, S. M. Cohen, *Chem. Soc. Rev.* **2009**, *38*, 1315-1329; (g) K. K. Tanabe, S. M. Cohen, *Chem. Soc. Rev.* **2011**, *40*, 498-519; (h) S. Nandi, P. De Luna, T. D. Daff, J. Rother, M. Liu, W. Buchanan, A. I. Hawari, T. K. Woo, R. Vaidhyanathan, *Sci. Adv.* **2015**, *1*, e1500421.

17. (a) Y. Lin, C. Kong, Q. Zhang, L. Chen, *Adv. Energy Mater.* **2017**, *7*, 1601296; (b) D. Britt, H. Furukawa, B. Wang, T. G. Glover, O. M. Yaghi, *Proc. Natl. Acad. Sci.* **2009**, *106*, 20637-20640; (c) J. Qian, Q. Li, L. Liang, T.-T. Li, Y. Hu, S. Huang, *Dalton Trans.* **2017**, *46*, 14102-14106; (d) J. Park, H. Kim, S. S. Han, Y. Jung, *J. Phys. Chem. Lett.* **2012**, *3*, 826-829; (e) Z. Qiao, N. Wang, J. Jiang, J. Zhou, *Chem. Commun.* **2016**, *52*, 974-977; (f) R. W. Flaig, T. M. Osborn Popp, A. M. Fracaroli, E. A. Kapustin, M. J. Kalmutzki, R. M. Altamimi, F. Fathieh, J. A. Reimer, O. M. Yaghi, *J. Am. Chem. Soc.* **2017**, *139*, 12125-12128; (g) N. Al-Janabi, H. Deng, J. Borges, X. Liu, A. Garforth, F. R. Siperstein, X. Fan, *Ind. Eng. Chem. Res.* **2016**, *55*, 7941-7949; (h) S. Couck, J. F. Denayer, G. V. Baron, T. Rémy, J. Gascon, F. Kapteijn, *J. Am. Chem. Soc.* **2009**, *131*, 6326-6327; (i) A. Demessence, D. M. D'Alessandro, M. L. Foo, J. R. Long, *J. Am. Chem. Soc.* **2009**, *131*, 8784-8786.; (j) M. Kim, J. F. Cahill, H. Fei, K. A. Prather, S. M. Cohen, *J. Am. Chem. Soc.* **2012**, *134*, 18082-18088.

18. J. An, N. L. Rosi, *J. Am. Chem. Soc.* **2010**, *132*, 5578-5579.

19. (a) C. Chen, J. Kim, D.-A. Yang, W.-S. Ahn, *Chem. Eng. J.* **2011**, *168*, 1134-1139; (b) Y. Noori, K. Akhbari, *RSC advances* **2017**, *7*, 1782-1808.

20. (a) Q. Huang, J. Ding, X. Huang, X. Wei, W. Wang, *Energy Procedia* **2017**, *105*, 4395-4401; (b) D.-M. Chen, N. Xu, X.-H. Qiu, P. Cheng, *Cryst. Growth & Des.* **2015**, *15*, 961-965; (c) B. Liu, H.-F. Zhou, L. Hou, Y.-Y. Wang, *Dalton Trans.* **2018**, *47*, 5298-5303; (d) D. Andirova, C. F. Cogswell, Y. Lei, S. Choi, *Microporous Mesoporous Mater.* **2016**, *219*, 276-305; (e) X. Liu, H. Lin, Z. Xiao, W. Fan, A. Huang, R. Wang, L. Zhang, D. Sun, *Dalton Trans.* **2016**, *45*, 3743-3749; (f) H. H. Wang, W. J. Shi, L. Hou, G. P. Li, Z. Zhu, Y. Y. Wang, *Chem. Eur. J.* **2015**, *21*, 16525-16531; (g) D.-M. Chen, J.-Y. Tian, C.-S. Liu, *Inorg. Chem.* **2016**, *55*, 8892-8897; (h) D. K. Maity, K. Otake, S. Ghosh, H. Kitagawa, D. Ghoshal, *Inorg. Chem.* **2017**, *56*, 1581-1590; (i) S. Chand, S. M. Elahi, A. Pal, M. C. Das, *Dalton Trans.* **2017**, *46*, 9901-9911; (j) J. A. Gould, J. Bacsa, H. Park, J. B. Claridge, A. M. Fogg, V. Ramanathan, J. E. Warren, M. J. Rosseinsky, *Cryst. Growth & Des.* **2010**, *10*, 2977-2982.

21. J.-x. Ma, J. Guo, H. Wang, B. Li, T. Yang, B. Chen, *Inorg. Chem.* **2017**, *56*, 7145-7150.

22. S. Mukhopadhyay, P. B. Chatterjee, D. Mandal, G. Mostafa, A. Caneschi, J. van Slageren, T. J. Weakley, M. Chaudhury, *Inorg. Chem.* **2004**, *43*, 3413-3420.

23. (a) A. L. Spek, *Acta Crystallogr. Sect. C: Struct. Chem.* **2015**, *71*, 9-18; (b) A. L. Spek, *J. Appl. Crystallogr.* **2003**, *36*, 7-13.; (c) C.-Y. Sun, X.-L. Wang, X. Zhang, C. Qin, P. Li, Z.-M. Su, D.-X. Zhu, G.-G. Shan, K.-Z. Shao, H. Wu, *Nat. Commun.* **2013**, *4*, 1-8.

24. (a) D. Saha, Z. Bao, F. Jia, S. Deng, *Environ. Sci. Technol.* **2010**, *44*, 1820-1826; (b) Z. Zhao, Z. Li, Y. Lin, *Ind. Eng. Chem. Res.* **2009**, *48*, 10015-10020.

25. S. J. Datta, C. Khumnoon, Z. H. Lee, W. K. Moon, S. Docao, T. H. Nguyen, I. C. Hwang, D. Moon, P. Oleynikov, O. Terasaki, *Science* **2015**, *350*, 302-306.

2B.A. Appendix:

2B.A.1. X-ray Crystallographic structure determination:

Solvent composition of IISERP-MOF24 using SQUEEZE and analytical data Asymmetric unit present in IISERP-MOF24 is $Ce_{0.5}Na_{0.5}(BPDC)_{0.5}(IMDA)_{0.5}$

Formula unit present in IISERP-MOF24 is $Ce_3Na_3(BPDC)_3(IMDA)_3$.

So, Formula unit is just six times of the asymmetric unit.

Again, Z for IISERP-MOF24 is 3.

So, 3 units of $Ce_3Na_3(BPDC)_3(IMDA)_3$ and $(6 \times 3) = 18$ units of $Ce_{0.5}Na_{0.5}(BPDC)_{0.5}(IMDA)_{0.5}$ are present in unit Cell.

Again, squeeze results suggest that 507 electrons are present from solvent molecules in the unit cell. So, per asymmetric unit $507 /(6 \times 3) = 28.6$ electrons are present & Per formula unit $507/3 = 169$ electrons are present.

2B.A.1.1. Number of Solvent molecules determination:

CHN analysis:

No. of DMF	No. of water	Electron counts	CHN analysis
2	9	$(2 \times 40) + (9 \times 10) = 170$	Calc: C = 37.7, H = 3.74, N = 3.66 Obsd. 37.79, H = 3.64, N =5.35

So, actually from CHN analysis it is understandable that 2 DMF and 9 water molecules present in the formula unit, $Ce_3Na_3(C_{14}H_8O_4)_3(C_4H_5NO_4)_3.(C_3H_7NO)_2(H_2O)_9$ or $Ce_3Na_3(BDC)_3(IMDA)_3.(DMF)_2(H_2O)_9$.

TGA analysis:

(For TGA plot see figure 2B.A3) Molecular mass of formula unit without solvent $Ce_3Na_3(BPDC)_3(IMDA)_3$ is 1603.2 g mol^{-1}.

Now, molecular mass of formula unit with solvent $Ce_3Na_3(BPDC)_3(IMDA)_3(DMF)_2(H_2O)_9$ is $1603.2 + (9 \times 18) + (2 \times 40) = 1911.533$.

% mass of DMF = $(160/1911) \times 100 = 8.4$

% mass of water = $(162/1911) \times 100 = 8.5$

Total calculated % mass loss = (8.4 + 8.5) = 16.9

Note that there are solvent losses at low temperatures from the surface adsorbed methanol molecules used during the washing of the sample. This most likely is the origin of the discrepancy in the calculated and the observed CHN values.

Table 2B.A1. Crystal structure information for the solvated and squeezed structure of IISERP-MOF24 obtained from SCXRD and PLATON analysis.

Crystal Parameters	Non-squeezed IISERP-MOF24	Squeezed IISERP-MOF24
Chemical formula	$Ce_3Na_3(BDC)_3(IMDA)_3 \cdot (DMF)_2(H_2O)_9$	$Ce_3Na_3(BDC)_3(IMDA)_3$
Formula weight	1911.5	1603.19
Crystal system	Trigonal	Trigonal
Space group	R32	R32
Unit-cell parameter	a(Å) =12.8523(4), b(Å) =12.8523(4), c(Å) =45.7558(17), $\alpha = \beta = 90°$, $\gamma = 120°$, V(Å) = 6545.43(4)	a(Å) =12.8523(4), b(Å) =12.8523(4), c(Å) =45.7558(17), $\alpha = \beta = 90°$, $\gamma = 120°$, V(Å) = 6545.43(4)
Crystal color	Colorless prismatic crystal	Colorless prismatic crystal
Temperature	100(2)	100(2)
No. of formula units in unit cell (Z)	3	3
Density (g cm^{-1})	1.27	1.22
Abs. Coeff. (mm^{-1})	12.578	12.522
F(000)	2436.0	2430.0
Flack	0.007 (5)	-0.087(7)
Reflection Data		
No. of reflections meas.	17802	5365
No. of uniq. reflections	2862	2862
No. of obs. reflections	2834	2821
λ (Å)	1.54178	1.54178
R_{merge}	0.041	0.027
Av. I/sig(l)	31.35	24.88
θ_{max}	72.3	72.3
θ_{min}	4.4	4.4
Refinement Data		
R_{all}	0.036	0.028
R_{obs}	0.036	0.027
$wR_{2(all)}$	0.120	0.080
$wR_{2(obs)}$	0.120	0.120
Ext. Coeff.	0.0002	0.0003
Goodness-of-fit (GOOF)	1.193	1.132
Largest diff. peak and hole: Delta-rho (eÅ^3)$_{max}$	1.276	1.044
Largest diff. peak and hole: Delta-rho (eÅ^3)$_{min}$	-0.906	-0.623

2B.A.1.2. The structure of IISERP-MOF24:
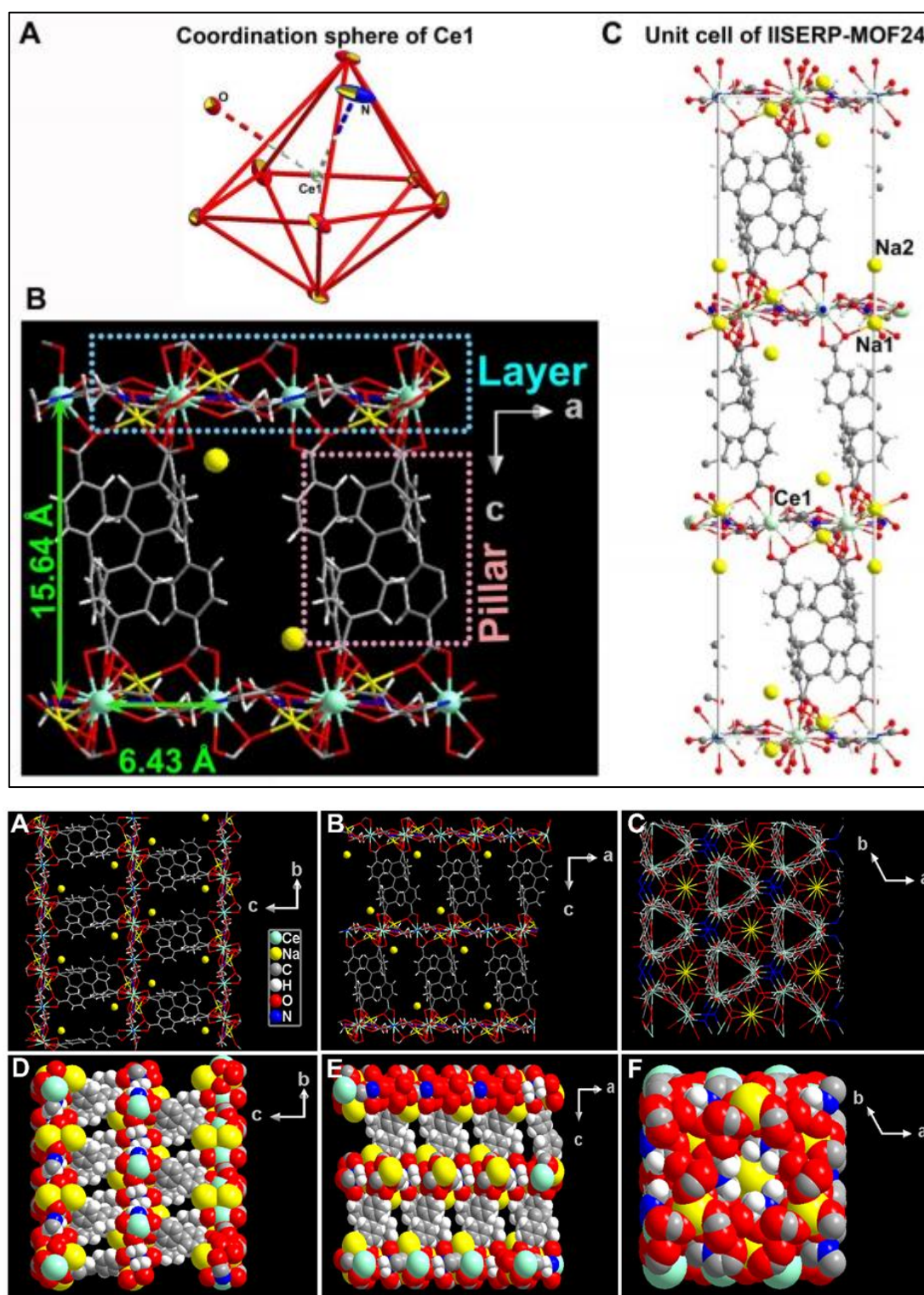
Figure 2B.A1. Top: (A) Shows the coordination sphere of Cerium ions, which adopts a bicapped pentagonal bipyramidal geometry. (B) The 3D layered-pillared topology of IISERP-MOF24. (C) The unit cell of IISERP-MOF24 showing selected atomic labels. The thermal ellipsoids are plotted at 50% probability. Bottom: (A) View along a-axis, (B) View along b-axis (a layered pillared structure), (C) View along c- axis, (D) Space-fill model along a-axis (without pore DMF and water molecules), (E) Space-fill model along b- axis and (F) Space fill model along c- axis.

2B.A.2. Analytical characterizations:
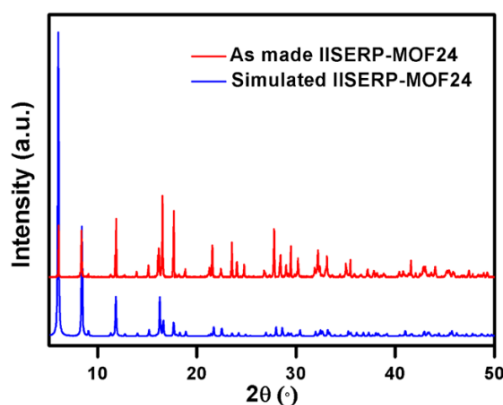
Figure 2B.A2. Comparison between the powder X-ray diffraction patterns of simulated from the single crystal data and the experimentally obtained one.
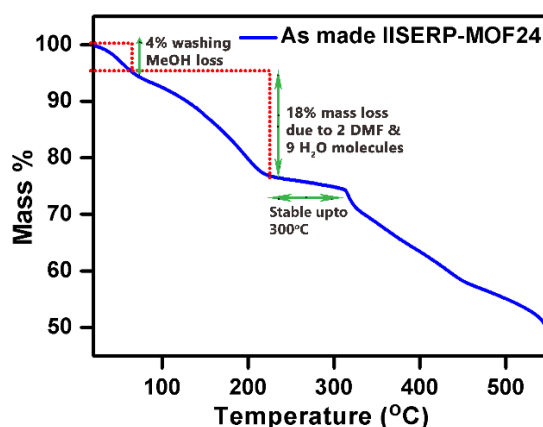
Figure 2B.A3. TGA carried out on the as made IISERP-MOF24. A two-step weight loss is observed from room temperature to 220 °C. The first mass loss up to 100 °C is due to the evaporation of pore water molecules, while the second mass loss observed from 100 °C to 220 °C is due to the loss of DMF molecules trapped inside the pore (total mass loss calc.: 23.9%; obsd: 24%). The mass loss has been calculated using the formula $Ce_3Na_3(BDC)_3(IMDA)_3 \cdot (DMF)_2(H_2O)_9$ (M. mass. 1603.2 g mol^{-1}).
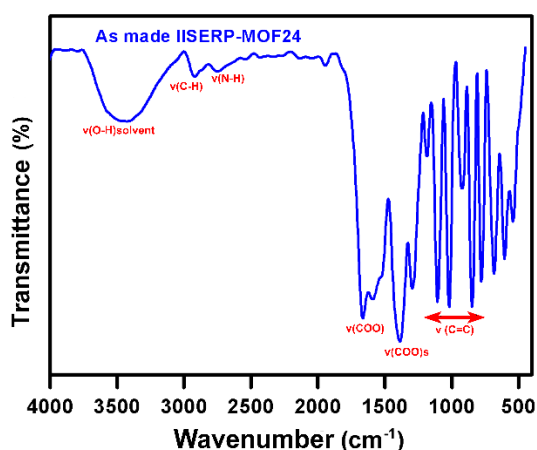
Figure 2B.A4. Infrared spectra (IR) of IISERP-MOF24 showing the various stretching and bending modes present. Selected peaks: IR (KBr pellet, cm^{-1}): ν(O-H) solvent: 3455s; ν(C-H): 2924; ν(N-H): 2749; ν(COO): 1662s and 1593vs, ν(COO)s 1396s, 1300 vs; ν(C=C): 1190 to 780. (*Source: Infrared and Raman Spectra of Inorganic and Coordination Compounds, Part B, Applications in Coordination, Organometallic, and Bioinorganic Chemistry, 6th Edition, Kazuo Nakamoto*).
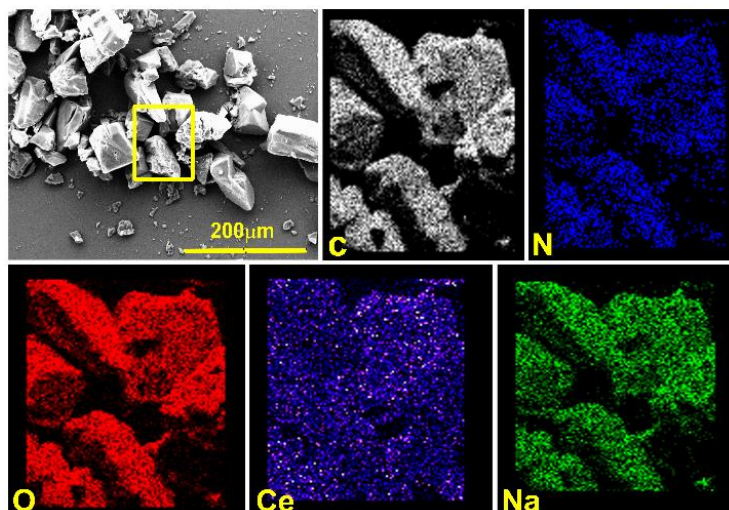
Figure 2B.A5. Elemental mapping using Energy-dispersive X-ray analysis (EDXA) technique shows homogeneous distributions of both the Ce and Na in IISERP-MOF24.

Calculation of Ce:Na from SEM-EDX analysis:

From the composition determined from SCXRD analysis (Ce$_3$Na$_3$(BPDC)$_3$(IMDA)$_3$•(DMF)$_2$(H$_2$O)$_9$), a ratio Ce:Na of 1.00 is expected. EDXA was performed on five different regions of the sample. The results are presented below.

SEM-EDX & elemental analysis of IISERP-MOF24:

Region-1	Element	Atomic %	Ce to Na ratio
	Na	1.63	0.78
	Ce	1.27	
Region-2	Na	1.49	0.93
	Ce	1.28	
Region-3	Na	1.09	0.86
	Ce	1.01	
Region-4	Na	1.45	0.73
	Ce	1.63	
Region-5	Na	1.41	1.13
	Ce	1.02	
Ce to Na ratio calculated from the chemical formula obtained from single crystal X-ray diffraction data analysis technique			1.00
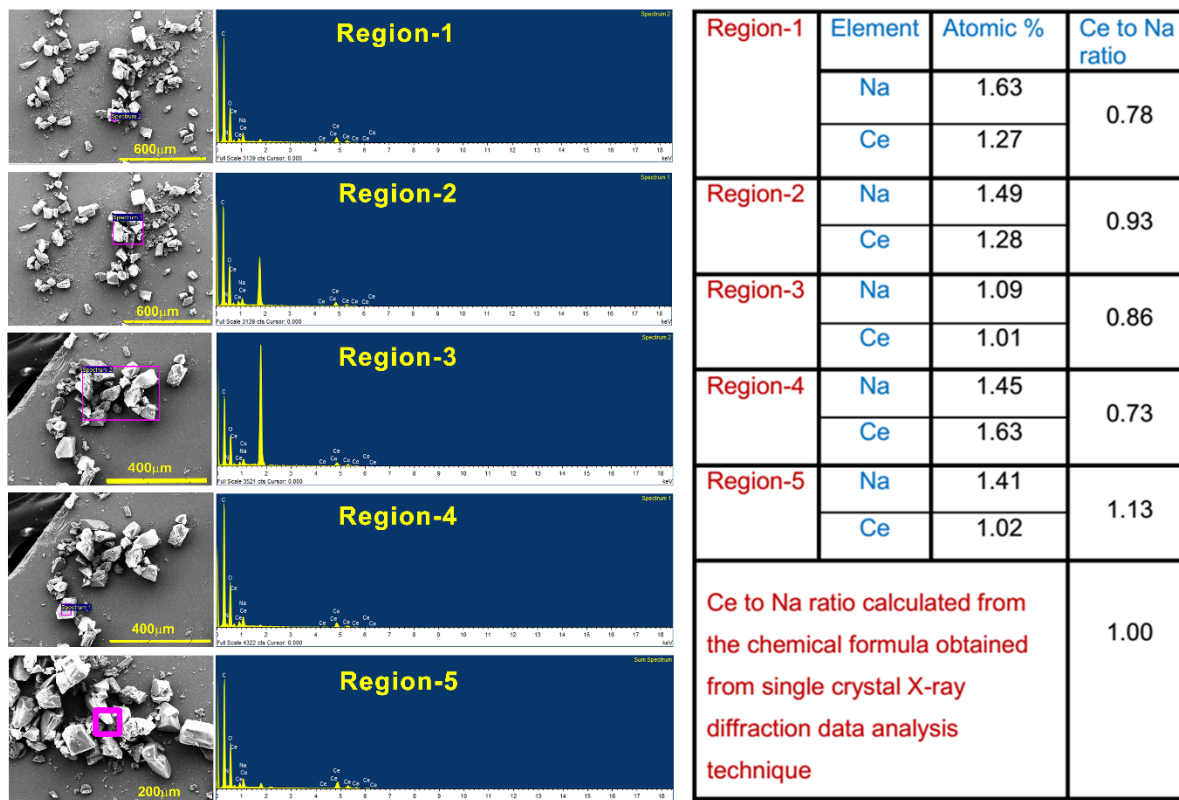
Figure 2B.A6. Comparison of the Ce to Na ratio of IISERP-MOF24 from SEM-EDX analysis with that obtained from single crystal X-ray analysis data.

Table 2B.A2. EDAX elemental analysis data.

Element	C		N		O		Na		Ce	
Region	Weight %	Atomic %	Weight %	Atomic %	Weight %	Atomic %	Weight %	Atomic %	Weight %	Atomic %
Region-1	51.92	64.92	3.78	4.06	29.97	28.13	2.49	1.63	11.84	1.27
Region-2	46.91	59.40	5.12	5.56	33.94	32.27	2.24	1.49	11.78	1.28
Region-3	47.55	58.75	6.65	7.04	34.62	32.11	1.69	1.09	9.50	1.01
Region-4	49.01	63.34	3.55	3.93	30.56	29.65	2.14	1.45	14.74	1.63
Region-5	49.40	60.87	6.36	6.73	32.40	29.97	2.20	1.41	9.65	1.02

2B.A.3. Adsorption Analysis:

BET surface area: 771.5241 ± 2.0173 m²/g
Slope: 0.126447 ± 0.000331 g/mmol
Y-intercept: 0.000003 ± 0.000001 g/mmol
Correlation coefficient: 0.9999487
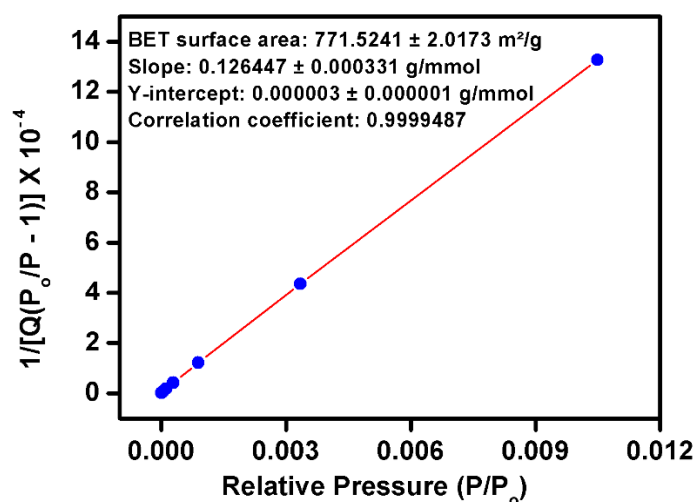
Figure 2B.A7. BET fit for the IISERP-MOF24 from the 77 K N_2 isotherm data.

Langmuir surface area: 851.0570 ± 0.1466 m²/g
Slope: 0.11463 ± 0.00002 g/mmol
Y-intercept: 0.32 ± 0.01 mmHg·g/mmol
Correlation coefficient: 1.000000
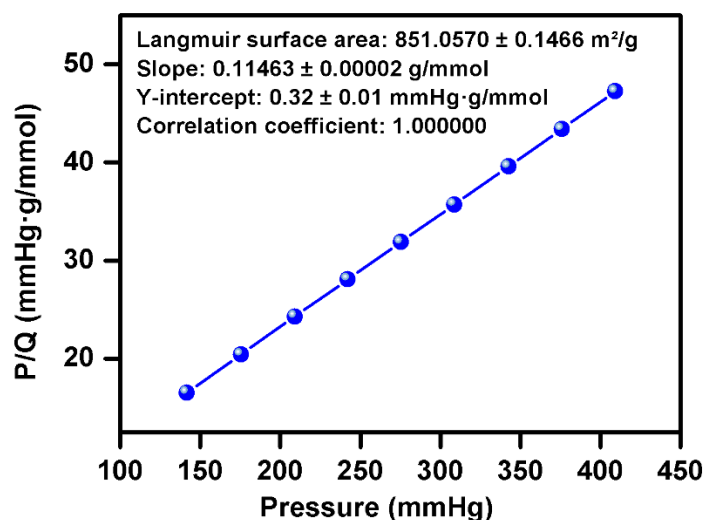
Figure 2B.A8. Langmuir fit for the IISERP-MOF24 from the 77 K N_2 isotherm data.
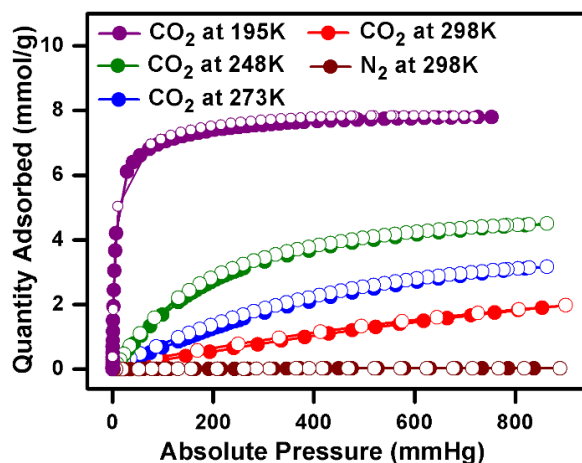
Figure 2B.A9. CO_2 isotherms collected at 195, 248, 273 and 298 K along with N_2 isotherms collected at 298 K.

Remark: At 298 K, there is no uptake of N_2; whereas there is significant uptake of CO_2. So, IISERP-MOF24 selectively physisorps CO_2 over N_2.
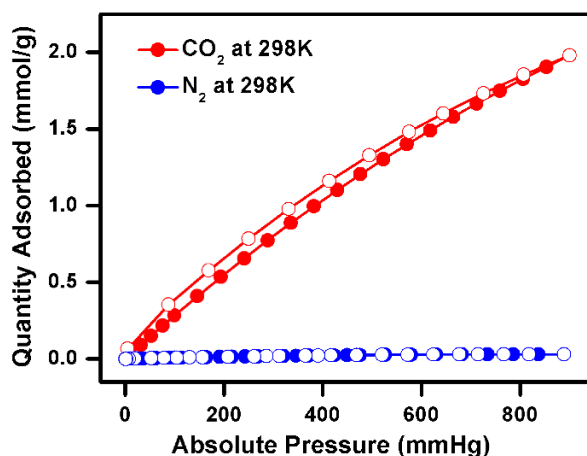
Figure 2B.A10. CO_2 and N_2 adsorption isotherms at 298 K showing the selectivity of IISERP-MOF24 towards CO_2 at 298 K and 1 bar.
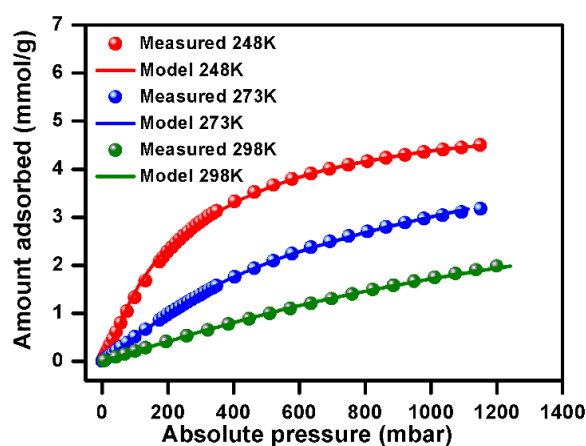
Figure 2B.A11. Comparison of experimental isotherms to the ones obtained from Virial modelling carried out using CO_2 isotherms collected at 248, 273, and 298 K.
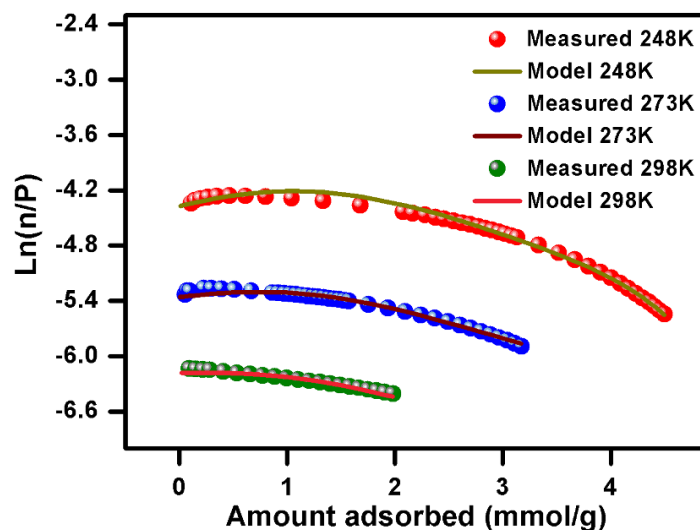
Figure 2B.A12. Virial fits for the CO_2 isotherms collected at 248, 273, and 298 K.

Virial analysis:

The CO_2 adsorption data were collected from 0-1 bar at 298, 273 and 248 K. For virial fitting the 248, 273 and 298 K isotherms were taken and fitted by the virial equation (1).

$$ln(P) = ln(Va)+(A0+A1*Va +A2*Va^2 …+ A6*Va^6)/T+(B0+B1*Va).......... (1)$$

Where, P is the pressure during the experiment, Va is amount of gas adsorbed, T is temperature, and A0, A1, A2…, A4 and B0, B1 are temperature independent empirical parameters.

Table 2B.A.3. Summary of the fitted Virial parameters for IISERP-MOF24.

IISERP-MOF26	
Parameters	**Numeric values**
A0	-2674.227686
A1	-379.4005948
A2	68.13796624
A3	3.61670552
A4	2.581397795
A5	-1.118482926
A6	0.161750942
B0	15.15554664
B1	0.3484236
B2	1.248964199
B3	0.01295927
B4	-0.008084079

IAST fitting parameters for IISERP-MOF24 (CO$_2$/N$_2$):

At 273 K, Gas A =CO$_2$, Gas B = N$_2$

Table 2B.A.4. Fitted IAST parameters for CO$_2$/N$_2$ (15CO$_2$:85N$_2$) selectivity at 273 K for IISERP-MOF24.

Gas Mixture		Intrinsic Selectivity	
YA =	0.15		
YB =	0.85		
Gas A Constants		**Gas B Constants**	
qA1 =	4.993007085	qA1 =	0.06135295
qA2 =	0	qA2 =	0
kA1 =	0.000624444	kA1 =	0.00024766
kA2 =	0	kA2 =	0
na1 =	1.127025588	na1 =	1.37724099
na2 =	0	na2 =	0
HA1 =	0	HB1 =	0
HA2 =	0	HB2 =	0

At 273 K, Gas A =CO$_2$, Gas B = N$_2$

Table 2B.A.5. Fitted IAST parameters for CO$_2$/N$_2$ (15CO$_2$:85N$_2$) selectivity at 298 K for IISERP-MOF24.

Gas Mixture		Intrinsic Selectivity	
YA =	0.15		
YB =	0.85		
Gas A Constants		**Gas B Constants**	
qA1 =	6.458188067	qA1 =	0.03890991
qA2 =	0	qA2 =	0
kA1 =	0.00027967	kA1 =	0.00033726
kA2 =	0	kA2 =	0
na1 =	1.03926659	na1 =	1.31047808
na2 =	0	na2 =	0
HA1 =	0.001806162	HB1 =	1.3123E-05
HA2 =	0	HB2 =	0

With increase of the temperature, thermal energy of the gas molecules increases and the difference in binding energies of CO$_2$ and N$_2$, which are reasonably constant with respect to temperature, becomes less significant, and the selectivity gradually decreases. That is why selectivity at 298 K is less than 273 K. Again, there is a difference of CO$_2$/N$_2$ selectivities at low pressures between two different temperatures (273 K & 298 K) because at low pressure region at 273 K first selectivity decreases and then increases at high pressure region whereas at 298 K the selectivity increases from starting onwards. This is probably due to temperature effect on the framework. Since, BPDC units act as a pillaring agent its two phenyl rings can flip around the C-C single bond under the partial pressure of CO$_2$ at room temperature to bring a gate pass for CO$_2$ entrance from starting onwards while at 273 K the flipping of phenyl rings is restricted due to low energy input which creates

obstacle for CO_2 entrance at low pressure region. At high pressure region at 273 K the CO_2 partial pressure is high enough to bring gate pass for CO_2 entrance and that is why selectivity increases gradually. The selectivity increases in both the cases as there is various types of interactions such as CO_2-framework, $CO_2...Na^+$ and $CO_2...CO_2$ interactions.

2B.A.4. Stability studies:
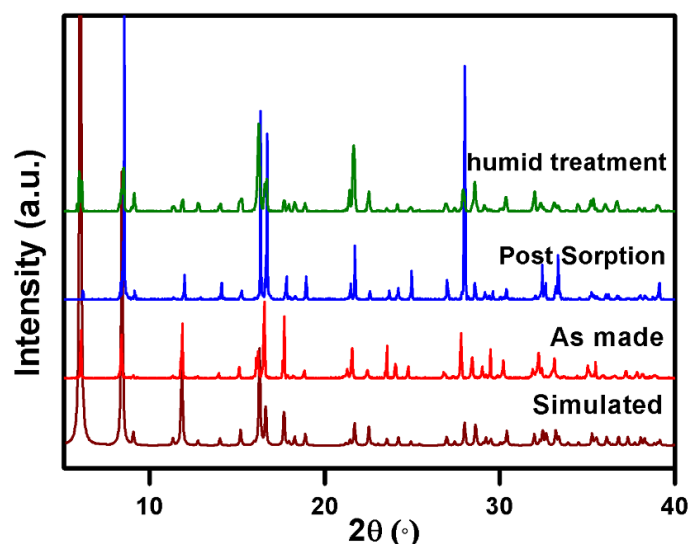
Figure 2B.A13. PXRD comparisons indicating the complete retention of crystallinity by IISERP-MOF24 following repeated heating and cooling during multiple gas adsorption runs followed by exposure to open atmosphere. For the humid treatment, the sample was exposed to a humid stream of N_2 (75%RH) for about 12hrs.

IISERP-MOF24 has excellent shelf-life - complete retention of porosity even after 6 months on the shelf.
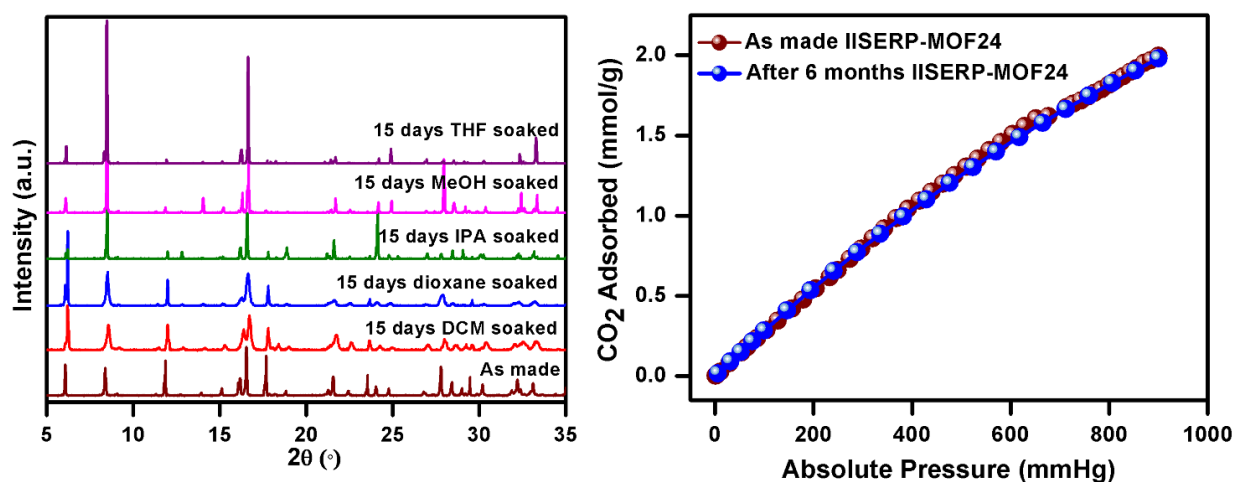
Figure 2B.A14. Stability studies: left: PXRDs showing the exceptional solvent stability of IISERP-MOF24, Right: IISERP-MOF24 retains complete porosity even after 6 months keeping on shelf.

The complete retention of crystallinity was also observed in the microscopic crystal images of IISERP-MOF24 for pre- & post- sorption treated samples.
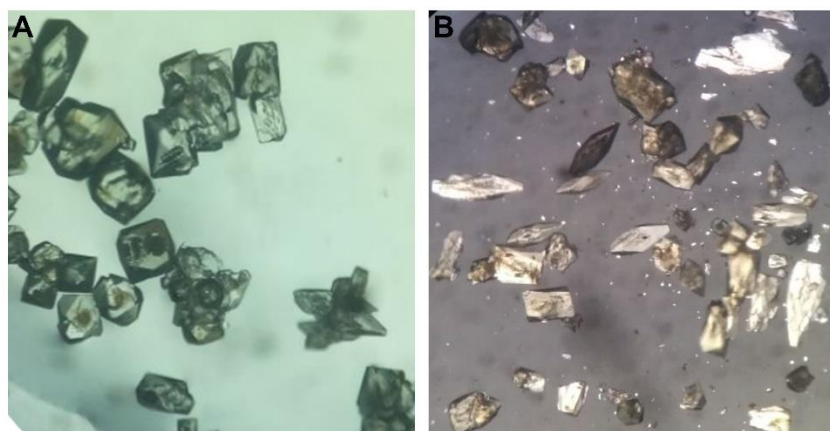
Figure 2B.A15. Optical microscopic images showing comparisons between the state of (A) pre-sorption and (B) post-sorption sample of IISERP-MOF24.
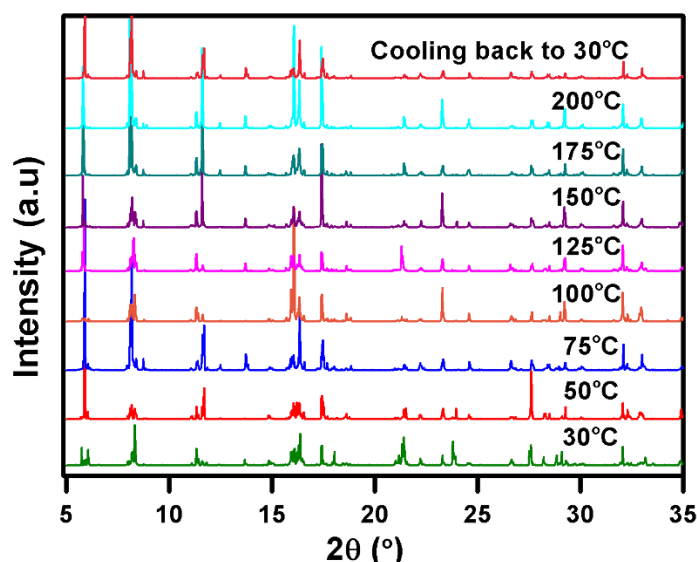
Figure 2B.A16. Variable temperature PXRD for displaying complete retention of crystallinity to temperatures as high as 200 ºC.

2B.A.5. Simulation Studies:

All the simulations have been carried out using Material Studio program V.6.0 (Accelrys). The adsorption isotherms were simulated using the Grand Canonical Monte Carlo routine embedded in the Materials Studio V6 software. For this, considering that CO_2 is a small probe with no torsional degree of freedom, a Metropolis algorithm was employed. Universal force field was used. The isotherm simulations were carried out over three times and the error bars were calculated. The simulated isotherm matched well with the experimental one (Figure 2B.A17). From this GCMC simulated structure, the most probable densities of CO_2 were found to be well distributed in the entire pore space. For the binding site location, the framework was frozen and the CO_2 molecules were allowed to find the again using the GCMC routine. An automated temperature control and

Universal force field were used with about 1000000 steps per cycle. Applying rotational and translation freedom did not make much of a change in the positions or the orientations in the minimized structure. Energy distribution, density and energy field were all optimized. The CO_2 positions were obtained from the lowest energy configuration have been shown in Figure 2B.4.
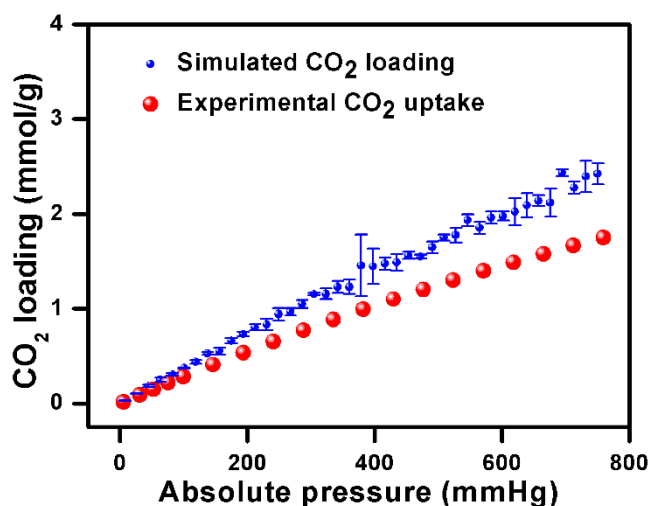
Figure 2B.A17. Experimental and simulated CO_2 adsorption isotherms of IISERP-MOF24 at 298 K (0 to 1 bar). The isotherms were simulated using the Grand Canonical Monte Carlo methods embedded in the Materials Studio V6.

2B.A.9. References:

2B.A1. G. Kemmer, S. Keller, *Nat. Protoc.* **2010**, *5*, 267-281.

2B.A2. E. Richter, W. Schuetz, A. L. Myers, *Chem. Eng. Sci.* **1989**, *44*, 1609-1616.

2B.A3. A. L. Myers, J. M. Prausnitz, *AIChE J.* **1965**, *11*, 121-127.

2B.A4. (a) K. Malek and M.-O. Coppens, *J. Chem. Phys.* **2003**, *119*, 2801;

(b) Adsorption analysis and equilibria kinetics, D. D. Do, Imperial College Press, Ed. **2008**.

Chapter 3

Water-stable Adenine-based MOFs with Polar Pores for Selective CO₂ Capture
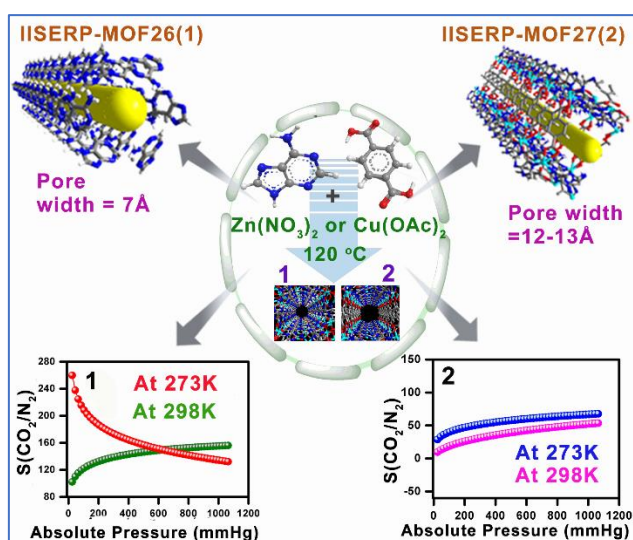
3.1 Introduction:

A rapid surge in urbanization and industrialization poses severe environmental threats. Mitigation of anthropogenic CO_2 emissions would help in minimizing the threat.[1] A recent report of NASA shows that this greenhouse issue is a global threat.[2] Developing novel physi-sorbents with high CO_2 selectivity and good chemical stability can contribute substantially to capture the CO_2 using energy-efficient pressure swing systems. Hence, there is sustained research interest in designing materials with advantageous capture characteristics and in gaining a better understanding of their properties. There are few technical methods already identified for the large-scale separation of the major greenhouse gas CO_2, which include biogas upgrading,[3] trace CO_2 removal utilizing confined space,[4] flue-gas separation,[5] and direct air capture.[6] But, Solid sorbents, due to their controlled adsorption behaviors with low energy input, fast kinetics, selectivity, and ease of regeneration attract much more interest, especially in the field of selective gas adsorption technology.[6] In this context porous polymer,[7] covalent-organic polymers,[8] porous cages,[9] and porous coordination polymer (PCP) or metal-organic framework (MOF)[10] along with traditional sorbents such as porous carbon, zeolites, and mesoporous silica are being studied for gas separations.[11] But MOF promises most of the desired physical and chemical parameters of a solid sorbent for efficient and cost-effective separation of greenhouse gases.[12] Designed incorporation of CO_2-loving functional groups in MOF makes them very attractive.[13,14] In contrast to many zeolites, some MOFs show superior stability under humid environments and can have better selectivity for CO_2 than even the industrially-used CO_2 capturing zeolites[15,16] Inspired by the efficiency of liquid amines to capture CO_2[17] inclusion of amines in MOFs with retaining their inherent advantage as a solid sorbent (easy-handling, ready recylcability, lowered energy penalty) has been an effective strategy for gaining high CO_2 selectivities. Amine functionality is either grafted on the ligand backbone, or a dangling amine is anchored to the exposed metal site[17] or they are encaged as neutral or charged guests within the framework pores.[10b,18] Among these, using amine functionality containing ligand to prepare MOF is very versatile and easy. For example, the use of amiotriazole or adenine or amino terephthalate has been prominent.[17e] Again, if pore width of the MOF falls in the ultra-micro pore region that will be an added advantage.[17f] For example, the basicity and the small length of the PyC: 4-Pyridine carboxylate or isonicotinate was well exploited in the construction of ultra-microporous MOF with exceptionally high CO_2 selectivities and sorption-energetics.[19] In-dependently,[20] Rosi and co-workers showed that adeninate MOFs could have high CO_2 capacity, with a high heat of adsorption for CO_2 (33.1 kJ mol^{-1}). The Lewis basic N-sites of amino and pyrimidine groups played a key role in gaining CO_2 selectivity. Li and co-workers reported an Zn-adeninate MOF, $Zn_3(A)(BTC)_2(H_2O)\cdot(CH_3)_2NH_2\cdot xDMF\cdot yH_2O$ (where, BTC=benzene1,3,5-tricarboxyl, A=adenine, DMF=N,N-dimethylformamide)[21] in which nitrogens are positioned uniformly along the pore. But, they did not show any gas capture or separation ability of the Zn-adeninate MOF. As adenine is N-rich, nontoxic, easily-available, and inexpensive having it as a co-ligand in the framework of MOF will be highly advantageous. Designing microporous/ultra-microporous frameworks from adenine thus becomes an effective approach to CO_2-selective MOFs.
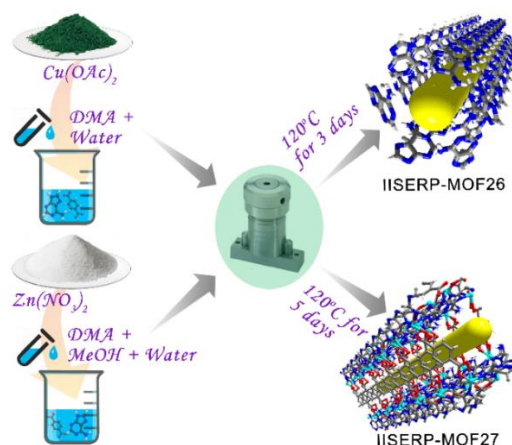
Scheme 3.1. Reaction Scheme for the synthesis of IISERP-MOF26 and IISERPMOF27.

Herein, we outline the synthesis, structural analysis, and gas capture properties of the new adenine MOFs, namely IISERPMOF26 (**1**) and IISERP-MOF27 (**2**) (Scheme 3.1). The **1** showedmoderate CO_2 uptake (2.7 mmol g^{-1}) with minimal zero-loading HOA (21 kJ mol^{-1}) for the facile regeneration of adsorbed CO_2 and high CO_2/N_2 (160 at 298 K using $15CO_2$:$85N_2$) and CO_2/CH_4 (14 at 298 K using $55CO_2$:$50CH_4$) selectivity at room temperature. But, **2** showed comparatively less uptake (2.2 mmol g^{-1}) at 298 K and 1 bar pressure with respect to CuMOF but gives still impressive CO_2/N_2 (73 using $15CO_2$:$85N_2$) and CO_2/CH_4 (13 using $50CO_2$:$50N_2$) selectivity at room temperature.

3.2. Materials and Methods:

3.2.1. Synthesis of IISERP-MOF26 (([DMA$^+$][Cu$_2$O(Ad)(BDC)]•(H$_2$O)$_2$(DMA), 1):

1 was synthesized via solvothermal method using mixed ligand approach. In a typical synthetic procedure Cu(OAc)$_2$.H$_2$O (40.00 mg, 0.2 mmol), adenine (Had; 27.00 mg, 0.2 mmol), and terepthalic acid aka 1,4-benzene di-carboxylic acid (H$_2$BDC; 16.66 mg, 0.1 mmol) were taken successively in a conical flask and then 2 ml N,N'-di-methyl acetamide (DMA) and 2 ml H$_2$O was added. The final reaction mixture was sonicated for few minutes to completely dissolve the ligand and metal salt. Then sonicated solution was transferred to the 23 ml Teflon liner-autoclave and kept it in a 120 °C oven for 120 hrs. On slow cooling to RT over 12 hrs green brick shaped smaller crystals, suitable for X-ray diffraction were obtained and collected by filtration and washing with fresh DMA and methanol. Finally, it was dried in 80 °C hot air oven (yield, 75 %).

3.2.2. Gram scale synthesis of IISERP-MOF26:

In a typical synthetic procedure Cu(OAc)$_2$.H$_2$O (800.00 mg, 4 mmol), adenine (Had; 540.00 mg, 4 mmol), and terepthalic acid (H$_2$BDC; 333.2 mg, 2 mmol) were taken successively in a conical flask and then 40 ml DMA and 40 ml H$_2$O were added. The final reaction mixture was sonicated for few minutes. Then sonicated solution was transferred to the 23 ml Teflon liner- autoclave and kept it in a 120 °C programmable oven for 120 hrs. On slow cooling to RT over 12 hrs green brick shaped smaller crystals were obtained and

collected by filtration and washing with fresh DMA and methanol. Finally, it was dried in 80 °C hot air oven (yield: 1.2 g, 75 %).

3.2.3. Synthesis of IISERP-MOF27 ((DMA$^+$)$_{1/2}$[Zn$_4$O(Ad)$_3$(BDC)$_2$•(H$_2$O)$_2$(DMF)$_{1/2}$, 2):

2 was synthesized via solvothermal method using mixed ligand approach. Zn(NO$_3$)$_2$.6H$_2$O (60.00 mg, 0.2 mmol), adenine (Had; 27.00 mg, 0.2 mmol), and terepthalic acid aka 1,4-benzene di-carboxylic acid (H$_2$BDC; 16.66 mg, 0.1 mmol) were taken successively in a 23 ml Teflon liner autoclave and then 2.5 ml DMF, 2.5 ml H$_2$O, and methanol 1.5 ml were added. Then, the autoclave was kept in 120 °C oven for 72 hrs. On slow cooling to RT colorless rod shaped crystals, suitable for X-ray diffraction were obtained and collected by filtration and washing with fresh DMF and methanol. Finally, it was dried in 80 °C oven (yield, 80 %).

3.2.4. Analytical Characterisations:

All reagents and solvents were purchased from a commercial source and used without further purification.

Single Crystal X-ray diffraction and Structures determinations:

Single-crystal X-ray diffraction was done on a Bruker SMART APEX four-circle diffractometer equipped with a CMOS photon 100 detector and Micro focus(IμS) using Cu-Kα radiation. The crystal of 1 and 2 were mounted on nylon Cryo loops using Paratone-N oil. Data were collected at 100 (2) K. Total data were integrated using Bruker SAINT Software and using SADABS it was corrected for absorption. The structure was solved using Intrinsic Phasing routine and was refined using the SHELXTL 6.3.1 (2004) software suite. All the non-hydrogen atoms were located from iterative examination of difference F-maps following which the structure was refined using least-squares method. Hydrogen atoms were fixed geometrically in a riding model. CCDC 1943233 and 1943234 contain the supplementary crystallographic data for this paper.

Powder X-ray Diffraction:

Powder XRDs were done using a Rigaku Miniflex-600 instrument and processed using PDXL software. The Variable temperature powder X-ray diffraction (VT-PXRD) was carried out on a full fledge Bruker instrument using the in-built furnace and in air.

Thermogravimetric Analysis:

Thermogravimetry analysis (TGA) of as made MOF was performed on NETSZCH TGA-DSC instrument. The routine TGAs were done under N$_2$ gas flow (20 ml min^{-1}) (purge + protective) and samples were heated in the temperature range of 25 to 550 °C with a heating rate of 5 °K min^{-1}

Infrared (IR) spectroscopy:

The infrared (IR) spectrum was recorded on a Nicolet FT-170SX instrument using KBr discs in the 400−4000 cm^{-1} region.

Scanning Electron Microscopy:

Field Emission Scanning Electron Microscopic (FESEM) study was done using the Ultra Plus Field Emission Scanning Electron Microscope with integral charge compensator and embedded EsB and AsB detectors.

3.2.5 Adsorption Analysis

All the gas adsorption analysis were carried out using ~100 mg of IISERP-MOF26 (**1**) and IISERP-MOF27 (**2**). The sample was directly activated by evacuation at 150 ºC for 24 hrs (10^{-6} mbar) till an outgassing rate was ≤ 2 µbar min^{-1} was achieved. Then the activated MOF was transferred to the analysis port of Micromeritics ASAP 2020HD or 3-FLEX instrument for the gas sorption analysis. Gas analyses were carried out with ultrahigh purity gases ($\geq$4.8 grade).

Langmuir Fits:

In all cases the isotherms were fit to the Single-Site Langmuir (SSL) equation. The isotherms were fit by solving the Langmuir isotherm equation using the solver function in Microsoft Excel following a similar protocol to Keller *et al.* [3.A1] Utilizing this routine circumvents some of the problems associated with favouring either high- or low-pressure regions when linearizing the following Langmuir equation and offers a balanced approach.

Single-Site Langmuir (SSL): $\quad \boldsymbol{q_i = q_m \dfrac{k_i}{1+k_i P} P}$

Dual-Site Langmuir (DSL): $\quad \boldsymbol{q_i = q_{m,1} \dfrac{K_1}{1+K_1 P} P + q_{m,2} \dfrac{K_2}{1+K_2 P} P}$

Ideal Adsorbed Solution Theory (IAST):

IAST calculations were undertaken as described by Prausnitz et al [3.A3]. The selectivity equation involved in calculation is provided below.

Selectivity: $\quad \boldsymbol{S_{1,2} = \dfrac{q_1/q_2}{p_1/p_2}}$

CO$_2$ cycling Experiment Procedure:

Isotherm cycling experiments were done using ASAP 2020HD instrument associated with Iso-Cycling software. About 100 mg of samples were loaded in the sample cell and activated until the outgassing rate was ≤ 2 µbar min^{-1}. The iso-cycling program was created with 15 cycles, each cycle having 14 to 15 data points (equilibration time 100 sec) in between 0.015 bar to 1.2 bar. After each cycle, the material was maintained under vacuum for 10 mins before continuing the subsequent cycles.

3.3. Results and Discussions:

Single-crystal diffraction reveals that **1**, synthesized solvothermally by reacting terephthalic acid adenine with $Cu(OAc)_2.H_2O$. **1** crystallizes in a trigonal system in the R-3 space group (Table 3.A2). The framework of **1** is constructed from one unique BDC^{2-} and one adeninate^{1-} ligand. There are two crystallographically unique Cu^{2+} centers (Cu1 and Cu2) are present in the asymmetric unit (Figure 3.1A). The framework is made up of tetrameric Cu_4 clusters formed by the carboxylate and adeninate units. Three such
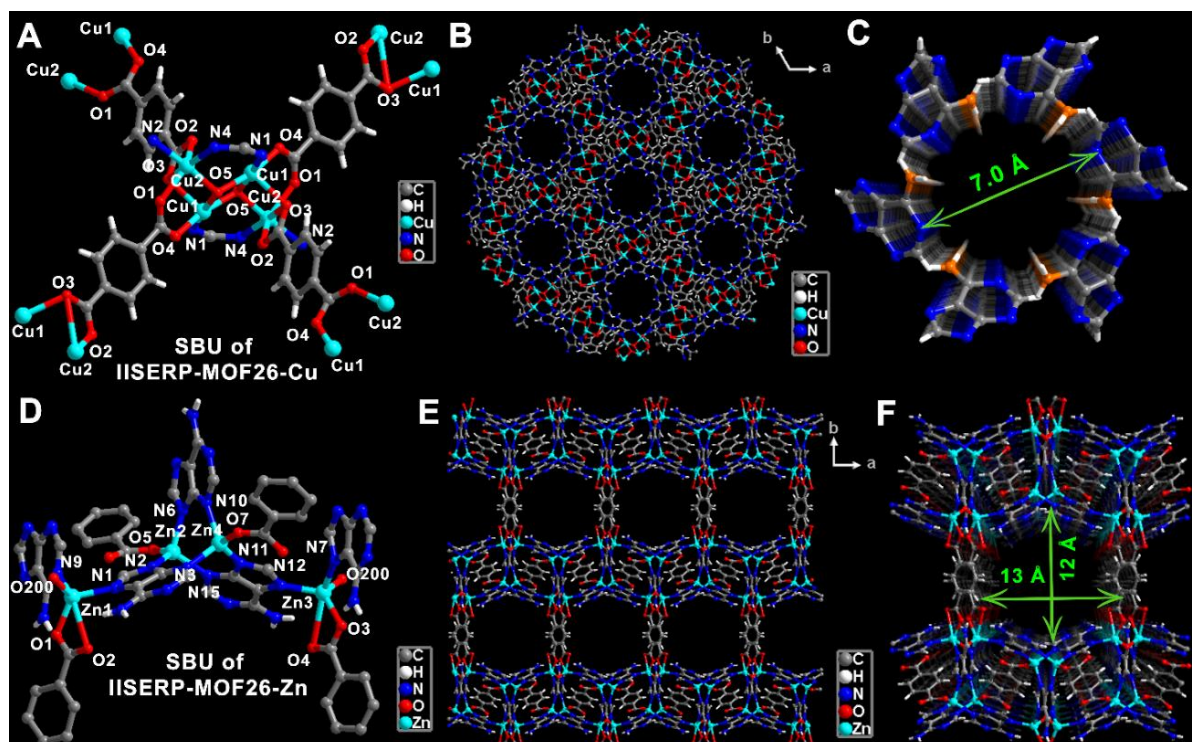
Figure 3.1. (A) Secondary building unit in the crystal structure of IISERP-MOF26. (B) One directional micro-pore present along c-axis in the crystal structure. (C) Pore dimension of IISERP-MOF26. Graphic shows pyrimidine-N (blue) and amine-N (orange) are pointed towards the pore. (D) Secondary building unit in the crystal structure of IISERP-MOF27. Hydrogens are removed for clarity (E) One directional micro-pore present along c-axis in the crystal structure of IISERPMOF27. (F) The pore structure of IISERP-MOF27.

Cu_4 clusters are positioned in a trigonal lattice giving rise to an anionic framework of the formula $[Cu_2O(Ad)(BDC)]^-$ (Figure 3.1A). The charge of the framework is balanced by monoprotonated dimethylacetamide cation (DMA^+) hosted in the pores which gives rise to a molecular formula of $[DMA^+][Cu_2O(Ad)(BDC)]\cdot(H_2O)_2(DMA)$. The connectivity between the trigonally arranged Cu_4 clusters yield uniform circular 1D channels. The free-amine group of the adenine beautifully decorate the entire walls of the channel. The microporous channels running along the c-axis are lined with the six amino and six pyrimidine groups (7.0 a, not factoring the Vander Waal radii, Figures 3.1B, 3.1C and 3.A1) making them rich in Lewis basic character, best suited for interacting specifically with CO_2. Undesirably, the channels get occupied by the charge- balancing DMA cations. The Zn-MOF, **2**, crystallizes in the monoclinic Cc space group. It has a layered-pillared structure where the Zn centers, adeninates, and the terephthalate units are

connected to generate an inorganic layer, which gets pillared by the out-of-plane BDC^{2-} units (Figure 3.1D and Figure 3.A2). In the crystal structure, there are four unique Zn^{2+} ions. Two tetrahedrally coordinated Zn(2) centers bridged by three μ-2 bridging adeninates to form symmetrical dimers. And these are linked to Zn(1) and Zn(3) centers which adopt a distorted trigonal-bipyramidal geometry giving rise to a molecular formula of (DMA^{+})$_{1/2}$[Zn$_4$O(Ad)$_3$(BDC)$_2$·(H$_2$O)$_2$(DMF)$_{1/2}$. The 3D structure contains 1D channels along the c-axis with dimensions of ~1.3 nm (not factoring Vander Waal radii, Figure 3.1E, and 3.1F).
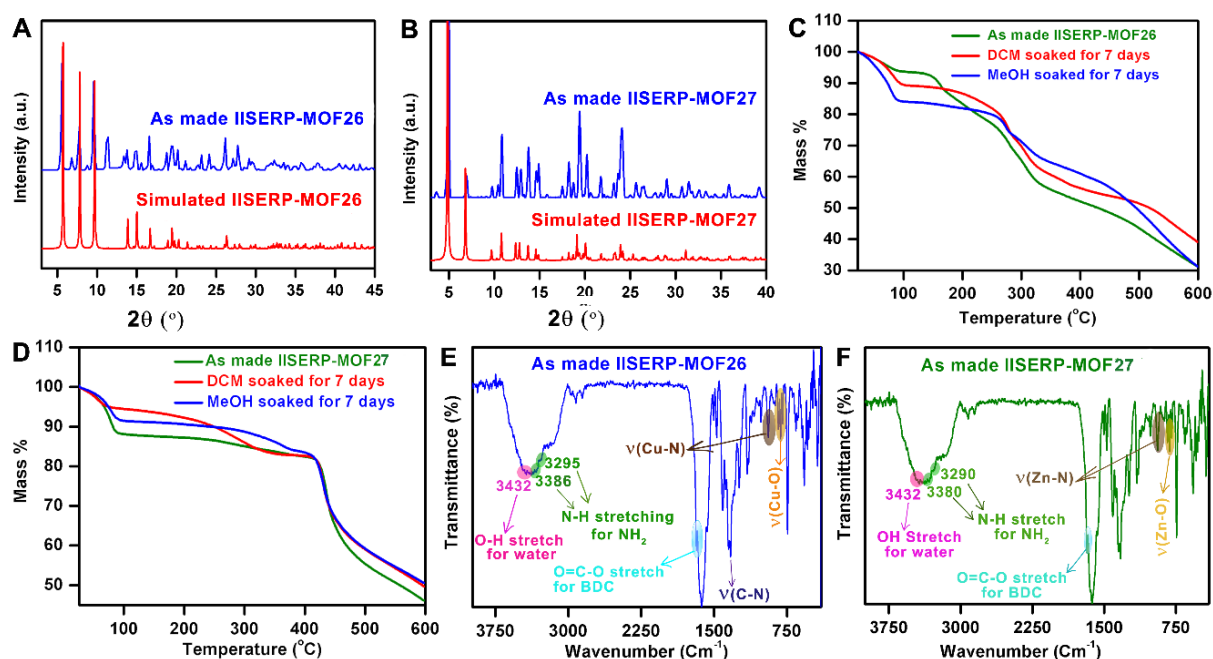
Figure 3.2. Comparative PXRD profile of as made with that simulated obtained from single crystal X-ray diffraction for the (A) IISERP-MOF26 and (B) IISERPMOF27 respectively. (C) TGA profile of as made and different low-boiling solvent soaked IISERP-MOF26 is showing stability up to 270 °C. (D) TGA profile of as made and different low-boiling solvent soaked IISERP-MOF27 is showing stability up to 400 °C. Infrared spectra are showing characteristic selective peaks due to free -NH$_2$, Cu-O, Cu-N functionalities, and O-H of water of (E) IISERP-MOF26 and (F) IISERP-MOF27 referenced to KBr, respectively.

The phase purity of both the MOFs was confirmed from the powder X-ray diffraction (XRD) analysis (Figures 3.2A and 3.2B). In both cases, they form as tiny brick shaped crystals, but upon careful examination, it could be seen that they were built-up from aggregation of several tiny platelets. This results in crystal twinning. Due to this PXRDs does have noticeable preferred orientation causing some of the peaks to have unusually large intensities. Importantly, all these peaks could be indexed and assigned to specific hkl markers (Figure 3.A3). PLATON analysis of **1** and **2** suggested a solvent-accessible void volume of 47.0 and 33 % respectively (see appendix). For, **1** and **2**, the electron counts obtained from the SQUEEZE routine[22] were assigned to two water+one DMA molecules and two water+half DMF molecules, respectively. This matched well with guest composition estimated from the TG analysis. Both MOFs have good thermal stability (up to 200 °C) as evidenced by TGA (Figures 3.2 C-D, Figures 3.A4-5). Infrared spectra (IR) for both MOFs gave characteristic peaks due to the carboxylates, Cu-N, Cu-O, N-H (free amine) and C-H stretching and bending

vibrations (Figure 3.2E–F and Figure 3.A6). Elemental mapping using energy dispersive X-ray analysis (EDXA) for both the samples showed a homogenous distribution of all the elements present across the entire sample (Figures 3.3-3.6).
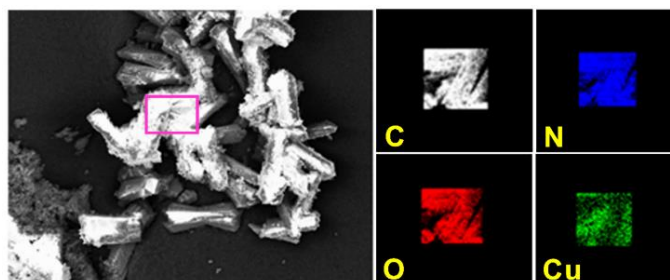
Figure 3.3. Elemental mapping using Energy-dispersive X-ray analysis (EDXA) technique shows homogeneous distributions of the elements present in IISERP-MOF26.
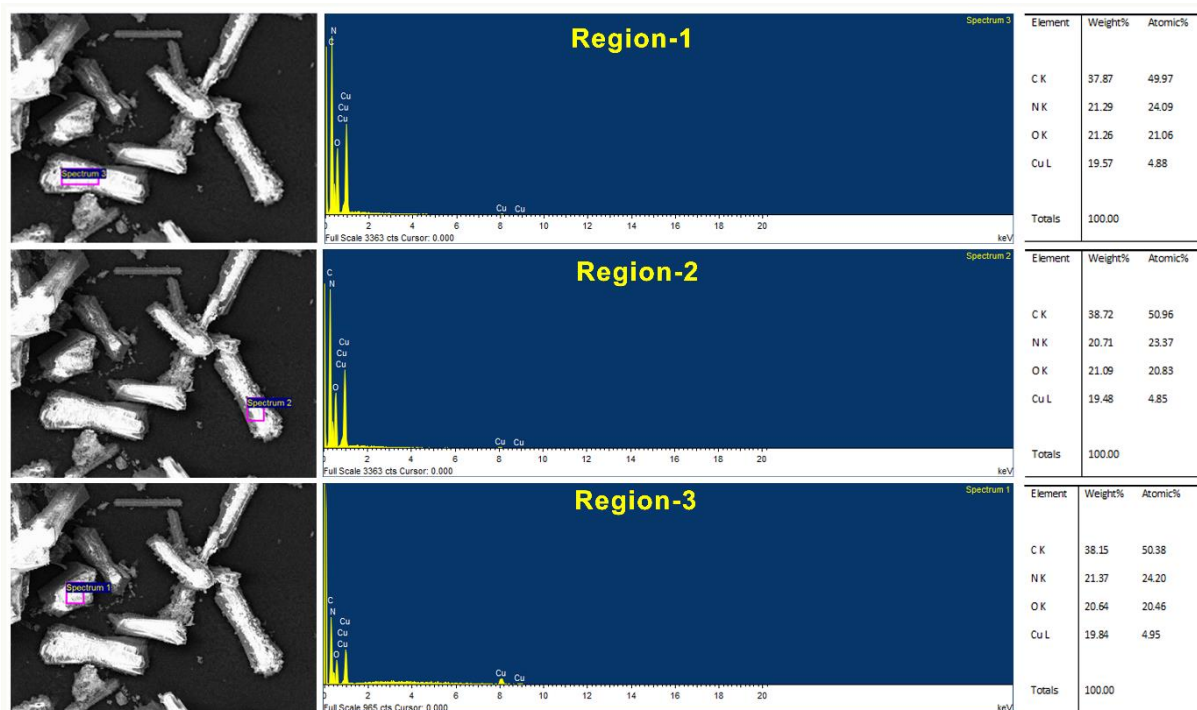
Figure 3.4. Comparison of the different regions in terms of element percentage ratio of IISERP-MOF26 from SEM-EDX analysis.
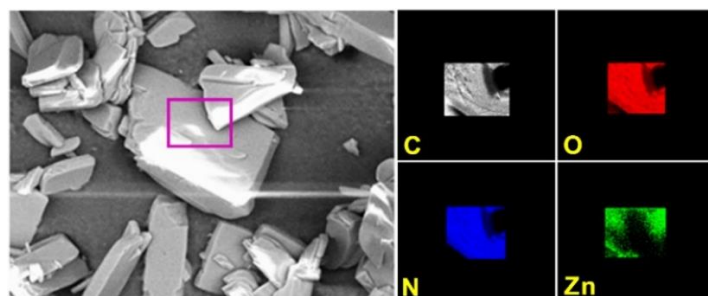
Figure 3.5. Elemental mapping using Energy-dispersive X-ray analysis (EDXA) technique shows homogeneous distributions of the elements present in IISERP-MOF27.

Element	Weight%	Atomic%
C K	46.25	54.49
N K	24.06	24.31
O K	22.12	19.56
Zn L	7.57	1.64
Totals	100.00	
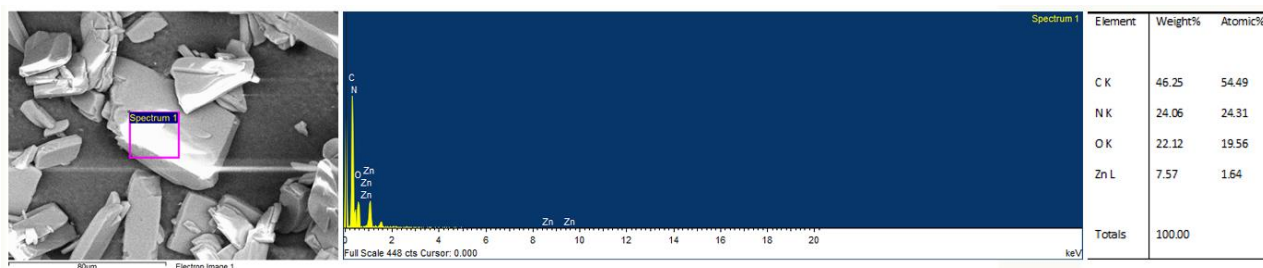
Figure 3.6. The element percentage ratio of IISERP-MOF27 from SEM-EDX analysis.

The permanent porosity of **1** and **2** were confirmed by CO_2 sorption measurements at 273 K. **1** showed ~4 mmol g^{-1} uptake of CO_2, as expected for a microporous MOF (Figure 3.7A). Brunauer-Emmett-Teller (BET) and Langmuir surface areas were calculated as 210.6 and 481.1 $m^2 g^{-1}$, respectively (Figure 3.A7-8). Both MOFs did not adsorb any N_2 at 77 K. An NLDFT fit (slit pore, carbon, 273 K CO_2) to the adsorption branch of the 273 K CO_2 isotherm yielded one major pore size (6.2 Å, not factoring the Vander Waal radii); Figure 3.8). This agreed well with the dimensions of the micro pores present in the crystal structure (Figure 3.1C). Inside the pore of **1**, there are dimethyl ammonium cation (Me_2N^+) to counter balance the charge of the anionic framework and these cations occupy the pore and it might result in an overall a truly ultra-microporous MOF. The ultra-micro pore, permanent porosity, potentially polarizing basic amino and pyrimidine group in **1** galvanized us to find out the CO_2 adsorption characteristics of this material. CO_2 adsorption isotherms were collected at 248, 273, and 298 K up to 1 bar (Figure 3.7A). All gas adsorption isotherms were completely reversible without any appreciable hysteresis. The CO_2 uptakes of **1** at 298, 273,
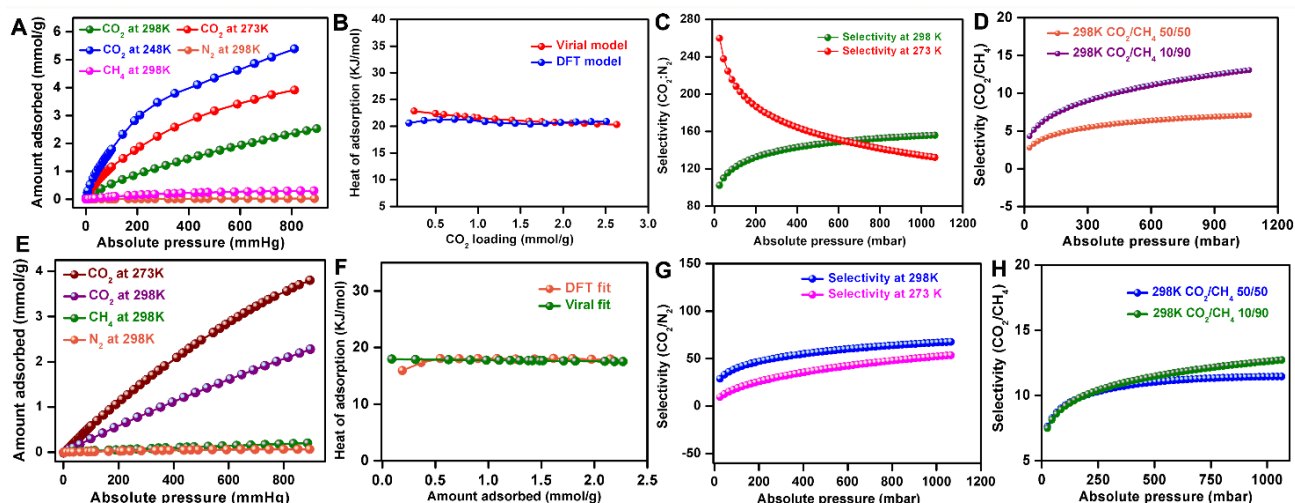
Figure 3.7. CO_2 isotherms at 248, 273, and 298 K for the (A) IISERP-MOF26 and (E) IISERP-MOF27 respectively. HOA for CO_2 adsorption on (B) IISERP-MOF26 and for (F) IISERP-MOF27 respectively. CO_2/N_2 selectivity of (C) IISERP-MOF26 and (G) IISERP-MOF27 calculated at 298 and 273 K (composition: $15CO_2 : 85N_2$) using the IAST method and without considering competitive binding. CO_2/CH_4 selectivity of (D) IISERP-MOF26 and of (H) IISERP-MOF27 calculated at 298 K (composition: $50CO_2:50CH_4$ and $10CO_2:90CH_4$) using the IAST method and without considering competitive binding.
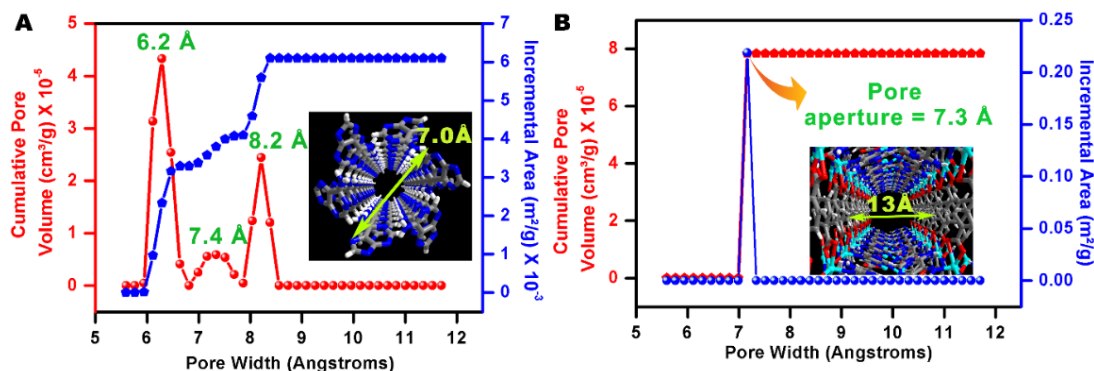
Figure 3.8. The graphical figure shows the pore size distribution of (A) IISERP-MOF26 (**1**) and (B) IISERP-MOF27 (**2**) (DFT pore-size) from CO_2 isotherm at 273 K. Inset shows pore size from single crystal x-ray diffraction study along c-axis. Pore aperture calculated from the gas adsorption agrees well with the pore width deduced from the single crystal X-ray diffraction data analysis.

and 248 K were 2.7, 4.3, and 5.2 mmol g^{-1}, respectively (Figure 3.7A). Similarly, the CO_2 uptake of **2** at 298 and 273 K were 2.2 and 3.8 mmol g^{-1}, respectively (Figure 3.7E). To establish the interaction strength between CO_2 and the framework, we calculated the HOA using the virial method, employing CO_2 isotherms collected at 248, 273, and 298 K. The zero loading HOA was found to be 22 kJ mol^{-1} and did not show any significant variation across the entire loading (Figure 3.7B). But this is quite counter-intuitive as the presence of potentially polarizing basic amino and pyrimidine ring along the pore walls would be expected to provide strong interactions with CO_2 giving rise to significantly high HOA. Notably, the observed weak interactions favour an easy and smooth diffusion of CO_2. One plausible explanation is that there are too many electrostatic and dispersive centers balancing each other and they may not be able to polarize the incoming CO_2 strong enough,[23] which would mean most of the adsorption is due to pore- confinement effect. Both **1** and **2** show no N_2 or CH_4 uptake at 298 K (Figures 3.7A and 3.7E). This motivated us to deduce the CO_2/N_2 and CO_2/CH_4 selectivity for both the **1** and **2** at 273 K and 298 K using the IAST model with a typical composition of $15CO_2:85N_2$ and $50CO_2:50CH_4$ which are a composition of the flue gas and natural gas, respectively. The CO_2/N_2 selectivities for **1** were calculated to be 160 and 145 at 273 and 298 K (Figure 3.7C). It showed a
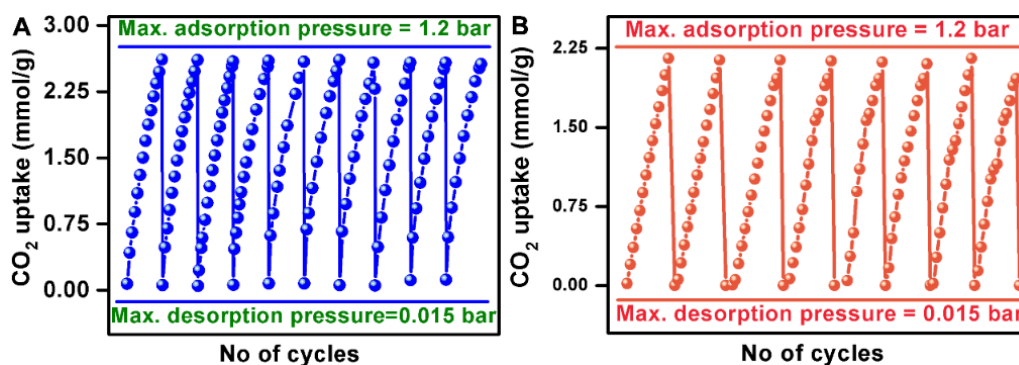
Figure 3.9. CO_2 adsorption cycles at 25 °C for (A) IISERP-MOF26 and (B) IISERP-MOF27. Note the uptakes remains nearly the same in all cycles.

CO_2/CH_4 selectivity of 15 at 298 K (Figure 3.7D). Similarly, **2** shows CO_2/N_2 selectivities of 55 and 75 at 273 and 298 K, respectively, and a CO_2/CH_4 selectivity of 12 at 298 K (Figures 3.7G and 3.7H). Importantly, the CO_2 uptakes for both the MOFs remained unaltered over several pressure-swing cycles as confirmed from the CO_2-isocycling experiment (Figure 3.9).

3.4. Batch studies:

In our experience, with MOFs, it is quite a bit difficult to obtain the same capacity across the multiple syntheses and also the uptake capacities could fall with repeated adsorption cycles. IISERP-MOF26 and IISERP-MOF27 showed excellent synthetic homogeneity across batches and also good repeatability of its CO_2 uptake as evidenced by their sorption isotherms, PXRDs, TGAs, and IR (Figures 3.10 and 3.11). It was also evidenced from the adsorption studies and cycling studies from CO_2 on/off cycling experiment (Figure 3.9). PXRD studies indicate the complete retention of crystallinity after multiple times adsorption experiment of CO_2 and N_2 followed by leaving in the open atmosphere for a few months. In general, it is very demanding to retain such high degree of crystallinity in many of the large-pore MOFs.

3.A.7.1. IISERP-MOF26:
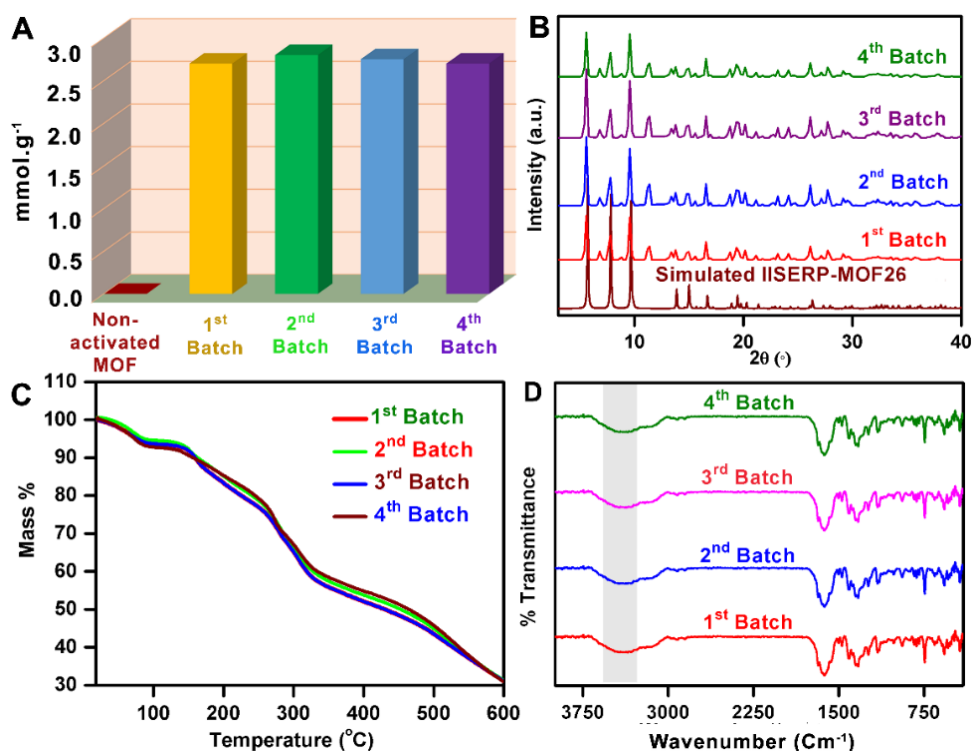
Figure 3.10. (A) Bar plot for the CO_2 uptake for one gram of IISERP-MOF26 (**1**) of different batch samples prepared in several times. (B) PXRDs for different batch samples of IISERP-MOF26 (**1**) showing similar crystanility and structure. (C) TGAs of IISERP-MOF26 (**1**) for different batches show that in all the cases MOF has similar thermal stability as well as similar mass loss due to removal of solvent from the pore. (D) Infrared spectra of the MOF for different batches show same functionality present in the framework across the multiple time synthesis.

3.A.7.2. IISERP-MOF27:
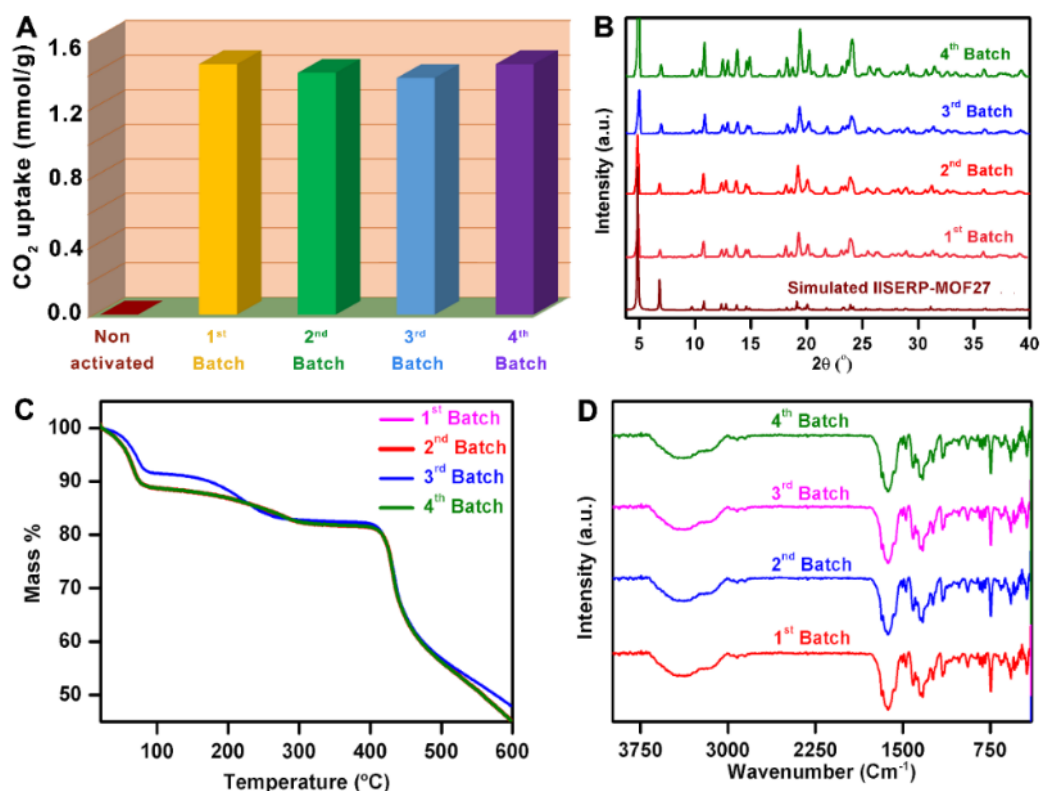
Figure 3.11. (A) Bar plot for the CO_2 uptake for one gram of IISERP-MOF27 (**2**) of different batch samples prepared in several times. (B) PXRDs for different batch samples of IISERP-MOF27 (**2**) showing similar crystanility and structure. (C) TGAs of IISERP-MOF27 (**2**) for different batches show that in all the cases MOF has similar thermal stability as well as similar mass loss due to removal of solvent from the pore. (D) Infrared spectra of the MOF for different batches show same functionality present in the framework across the multiple times' synthesis.

3.5. Stability studies:

      PXRD studies indicate the complete retention of crystallinity of both the MOFs even after multiple cycles of gas adsorption and desorption (Figure 3.12). To establish humidity stability of MOFs, Both MOFs were exposed to a humid stream of N_2 (75 % RH) for about 12 h. PXRD patterns of the steam-treated samples confirmed the complete retention of crystallinity (Figure 3.12). To establish hydrolytic stability of MOFs, the samples were soaked in water for a day, and PXRD measurements of this water-soaked MOFs confirmed complete retention of crystallinity (Figure 3.13). Furthermore, they exhibit good solvent stability, as confirmed by the PXRD patterns of the solvent-treated samples (Figure 3.13). Notably, both the MOFs have good CO_2 uptakes even after 6 months in the shelf (Figure 3.14). Notably, the morphology and texture of the crystals remained intact even after various solvents treatment and repeated adsorption-desorption cycles (Figures 3.15 and 3.16).
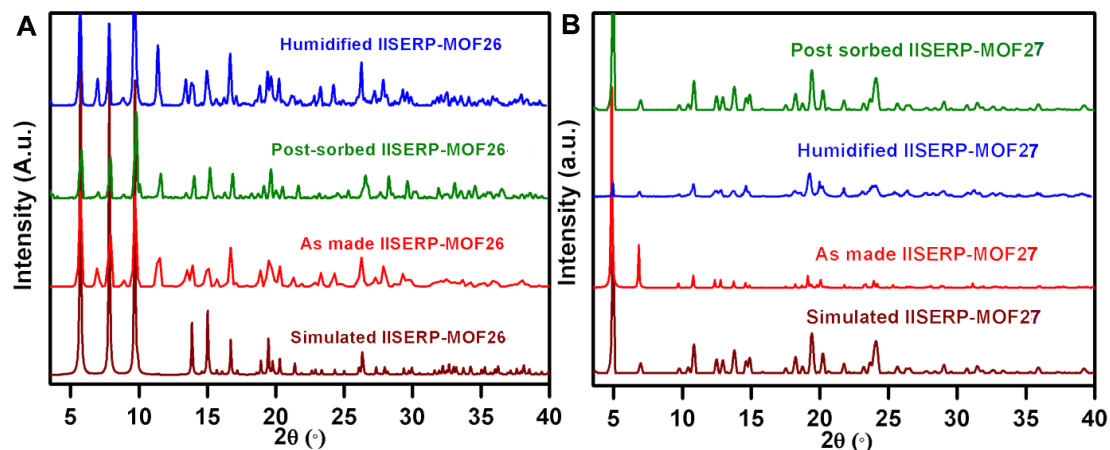
Figure 3.12. PXRD comparisons indicating the complete retention of crystallinity by (A) IISERP-MOF26 (**1**) and (B) IISERP-MOF27 (**2**) following repeated heating and cooling during multiple gas adsorption runs followed by exposure to open atmosphere. For the humid treatment, the sample was exposed to a humid stream of N_2 (75 % RH) for about 12 hrs.
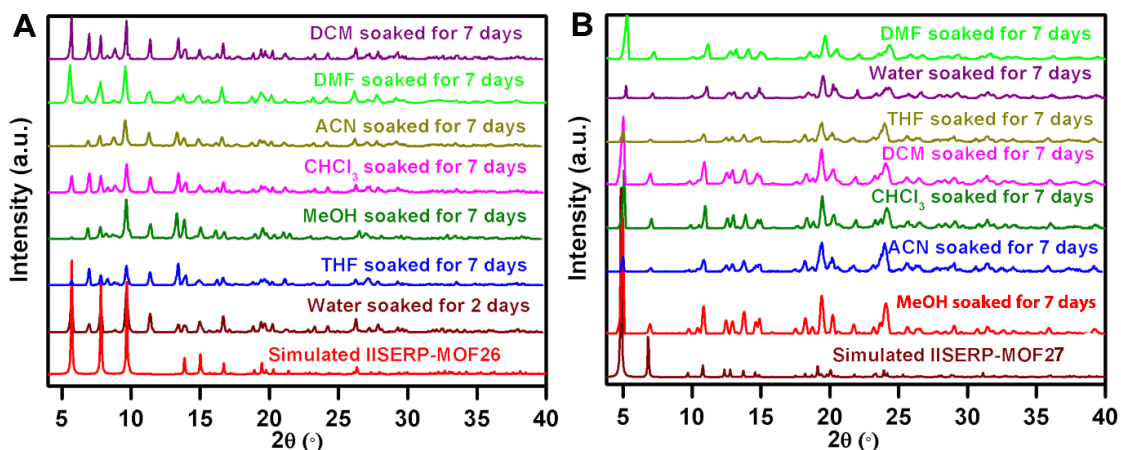
Figure 3.13. Stability studies: left: PXRDs showing the exceptional solvent stability of IISERP-MOF26 (**1**), Right: PXRDs showing the exceptional solvent stability of IISERP-MOF27 (**2**).
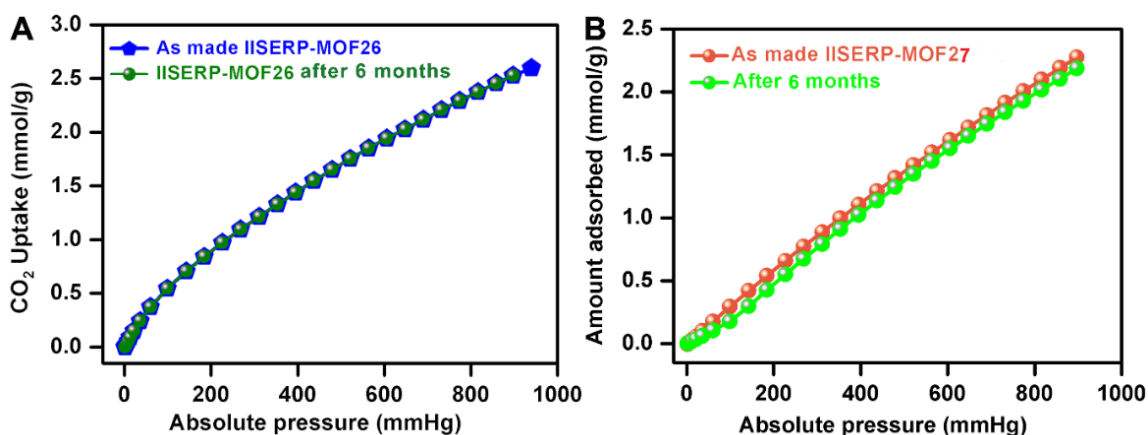
Figure 3.14. Stability studies: left: IISERP-MOF26(**1**) retains complete porosity even after 6 months keeping on shelf, Right: IISERP-MOF27(**2**) retains complete porosity even after 6 months keeping on the shelf.
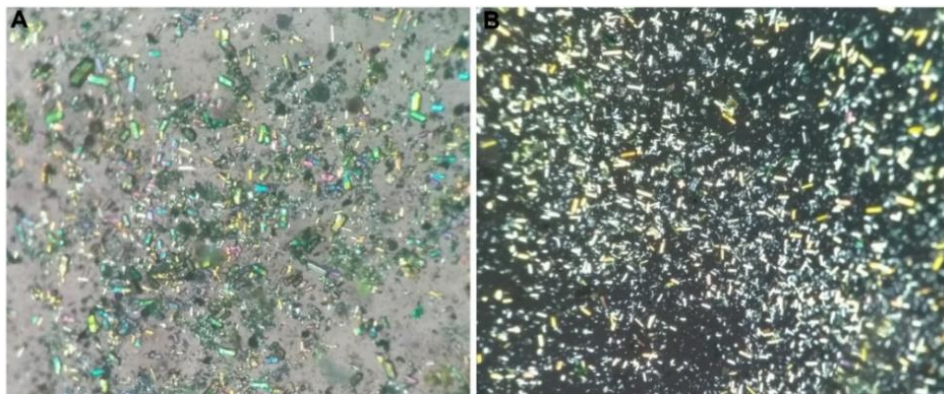
Figure 3.15. Optical microscopic images showing comparisons between the state of (A) pre-sorption and (B) post-sorption sample of IISERP-MOF26 (**1**).
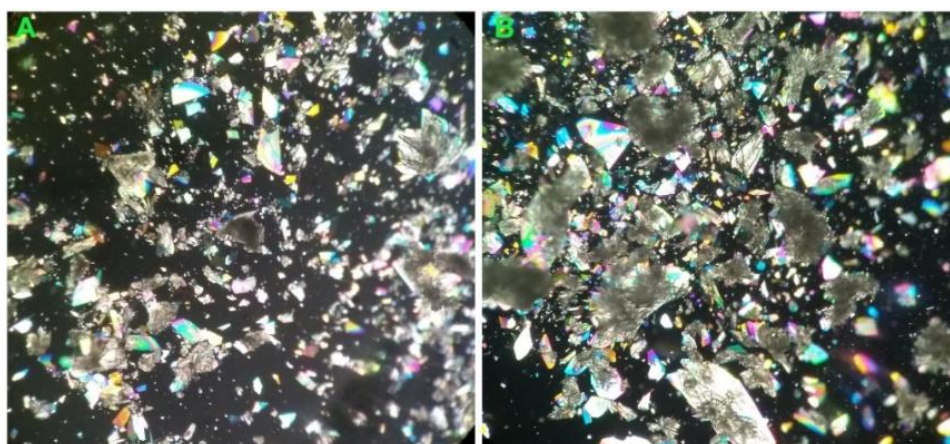
Figure 3.16. Optical microscopic images showing comparisons between the state of (A) pre-sorption and (B) post-sorption sample of IISERP-MOF27 (**2**).

3.6. Comparison of of 1 and 2 with other amine containing porous solid sorbents:

Here, we have been listed a few other works of literature reported nitrogen containing MOFs along with this work describing their CO_2 capacity, heat of adsorption (HOA), CO_2/N_2 and CO_2/CH_4 selectivities (Table 3.1). $Zn_2(Atz)_2Ox$ oxalate has good CO_2 uptake (3.2 mmol g^{-1} at 303 K) but it has very high zero-loading HOA (55 kJ mol^{-1}) suggesting a stronger CO_2-framework interaction. Despite having high HOA it showed moderate CO_2-selectivity (85 at 303 K and 1 bar). MAF-66 showed significant amount of CO_2 uptake (4.42 mmol g^{-1}), optimal HOA (26 kJ mol^{-1}), and high CO_2/N_2 selectivity (185, see Table 3.1) Although ethylenediamine-functionalized en-CuBTTri (open-metal sites of desolvated pristine CuBTTri are occupied by N-donor ethylenediamine) showed a relatively higher CO_2 uptake (0.366 mmol g^{-1}) than desolvated pristine CuBTTri (0.277 mmol g^{-1}), at 298 K and pressures and 0.1 bar, en-CuBTTri showed less uptake (1.27 mmol g^{-1}) compare to pristine CuBTTri (3.24 mmol g^{-1}) at pressure more than 0.1 bar. Due to the stronger affinity of Lewis basic amine groups for CO_2 en-CuBTTri adsorbs comparatively less amount of CO_2 at lower partial pressure and pore filling by CO_2 at higher partial pressure. The overall uptake of CuBTTri is greater than en-CuBTTri and this could be explained by the surface area drop from 1770 m^2 g^{-1} (CuBTTri) to

$345 \text{ m}^2 \text{ g}^{-1}$ (en-CuBTTri). But**,** en-CuBTTri exhibits a higher HOA (90 kJ mol^{-1}) for CO_2 compare to pristine CuBTTri (21 kJ mol^{-1}). This high HOA value directly suggests en-CuBTTri adsorbs CO_2 via chemisorption. To date, this high HOA value is the highest reported value for an azolate-based metal−organic framework used for the post-combustion CO_2 capture. However, due to the low uptake of en-CuBTTri at lower partial pressure, CO_2 selectivity is less compared to other reported MOFs. Due to same chemisorption, and high surface area N, N'-dimethylethylenediamine (mmen) functionalized CuBTTri (mmen-CuBTTri) also showed very high CO_2 uptake (3.86 mmol g^{-1}), selectivity as well as a high HOA (75 kJ mol^{-1}). Despitehaving high zero-loading HOA, it possesses the reversible CO_2 sorption characteristics and CO_2 could be easily regenerated from the framework at 333 K. Thus, mmen-CuBTTri offered 27 min cycling time with no loss in CO_2-uptake over 72 cycles of adsorption/desorption branches. The amino-MIL-101 showed very good uptake (3.48 mmol g^{-1}) but exhibited very high HOA (60 kJ mol^{-1}) and very less CO_2-selectivity (20, see Table 3.1). CAU-1 showed impressive CO_2 uptake (3.9 kJ mol^{-1}) and good CO_2-selectivity (101 at 273 K and 1 bar, see Table 3.1) but HOA value for it is still high (48 kJ mol^{-1}). Notably, $[Co^{II}Co^{III}(OH)Cl_2(bbta)]$ showed volumetric CO_2 uptake of 4.1 mmol cm^{-3} from the simulated flue gas-mixture (pressure range = 0.10–0.15 bar at 313 K) even at relative humidity as high as 82 % and after sorption CO_2 was regenerated by purging N_2 at 358 K. The zero-loading HOA for $[Co^{II}Co^{III}(OH)Cl_2(bbta)]$ was calculated to be 110 suggesting its very high affinity towards CO_2. This is the MOF based solid-sorbent that exhibited the best CO_2 capture ability reported till today. Now, these MOFs having very high HOA, could be useful for CO_2 activation or CO_2 fixation to a valuable organic compounds and intermediates. In comparison, it was found that IISERP-MOF26 and 27 are as good as other reported MOFs. IISERP-MOF26 and 27 are superior compared to some zeolitic imidazolate MOFs in term of either capacity or selectivities for CO_2 over N_2 and CH_4. Presence of numerous pyrimidine and free amine nitrogen atoms along the pore/channel of both the MOFs are responsible for this superior uptake and selectivity in comparison to the Bio-MOF series and other amine-based MOFs. Again, low heat of adsorption (HOA) of both the IISERP-MOFs enables the facile regeneration of CO_2 from adsorbed materials. Some MOFs shows better CO_2 selectivity upon introduction of amine to the open metal site in post synthetic modification method. But, every time getting the same amount of loading of amine into the MOF and hence same amount of CO_2 uptake, selectivity and HOA across the multiple loading can be a difficult task. But, IISERP-MOF26 and 27 by default offers CO_2 polarisable amine groups decorated in the pore wall, micro-pore which provides decent uptakes, low HOAs, high selectivities which make these MOFs very good recyclable candidates for selective CO_2 capture.

Table 3.1. A comparison of CO_2 adsorption capacity, the heat of adsorption, selectivity of CO_2 over N_2 and CH_4 of **1** and **2** with other reported amine containing, triazole and imidazole-based porous adsorbents.

MOFs	CO_2 capacity (mmol g^{-1}) at 298 K and 1 bar	HOA (kJ mol^{-1}) (loading, cm^3 g^{-1})	CO_2/N_2 (15/85) Selectivity at 298 K and 1 bar	CO_2/CH_4 (50/50) Selectivity at 298 K and 1 bar	Ref.
Triazolyl moiety based metal-organic frameworks					
$Zn_2(Atz)_2Ox$ (synthesis solvents: H_2O (2) (Atz: 3-amino-1,2,4-triazole; Ox: oxalate)	~3.2 mmol g^{-1} at 303 K and 1 bar	~55 (zero loading)	~85 at 303 K and 1 bar	N/A	24
$Zn_2(Ox)(Atz)_2$	4.35 (273 K and 1.2 bar)	~40.8 (zero loading)	N/A	N/A	25
ZnDATzF	No uptake available	N/A	N/A	N/A	26
ZnATzF	No uptake available	N/A	N/A	N/A	27
MAF-66	4.42	26	185	N/A	28a
[Co^{II}Co^{III}(OH)Cl$_2$(BBTA)] (H$_2$BBTA = 1H,5H-benzo(1,2-d:4,5-d0)bistriazole)	Volumetric capacity = 9.1 at 298 K and 1 bar	110 (zero loading)	262	N/A	28b
Adenine based metal-organic frameworks					
Bio-MOF-11: Co$_2$(Ad)$_2$(CH$_3$CO$_2$)$_2$	4.68	33.1 (2.18)	43	N/A	29
Bio-MOF-12: (Co$_2$(Ad)$_2$(CH$_3$CH$_2$CO$_2$)$_2$	3.17	38.4 (2.91)	52	N/A	29
Bio-MOF-13: Co$_2$(Ad)$_2$(C$_3$H$_7$CO$_2$)$_2$	2.0	40.5 (3.01)	40	N/A	29
Bio-MOF-14: Co$_2$(Ad)$_2$(C$_4$H$_9$CO$_2$)$_2$	1.38	N/A	N/A	N/A	29
Other types of nitrogen containing metal-organic frameworks:					
[Cu(INAIP)]	~2.12	35.36 (zero loading)	N/A	N/A	30
Amino-MIL-53	3.48	60 (zero loading)	20	N/A	31
CAU-1 Al$_4$(OH)$_2$(OCH$_3$)$_4$(H$_2$N–BDC)$_3$	3.9	48 (zero loading)	101 (at 273 K and 1 bar)	N/A	32

BDC = 1,4-benzene dicarboxylate					
NH_2-MIL-101(Cr)	1.9	~52 (zero loading)	8–16	3-5	33
en-CuBTTri	1.27	~90	25	N/A	34
mmen-CuBTTri	3.86	~96	327	N/A	35
CPF-13	3.62	~28.2	31 (at 273 K and 1 bar)	5 (at 273 K and 1 bar)	36
PEI-MIL-101-125	~4.8	N/A	770	N/A	37
UIO-66-NH_2	3.02	28	32.4	N/A	38
NH_2-MIL-125(Ti)	~6 (273K and 1 bar)	N/A	N/A	N/A	39
IRMOF-74-III-CH_3NH_2	3.2	N/A	N/A	N/A	40
ZJU-8: $[Cu_2(L)(H_2O)_2] \cdot (DMF)_6 \cdot (H_2O)$ (H_4L=2'-amino-[1,1':4,1'-terphenyl]-3,3'',5,5''-tetracarboxylic acid)	4.24	21.9 (zero loading)	12.27 (298 K) 43.6 (273 K)	7.38	41
$\{[Cd(Py_2TTz)(2-NH_2-BDC)] \cdot (DMF) \cdot 0.5(H_2O)\}_n.$	1.56 (273 K and 1 bar)	19.7 (zero loading)	N/A	N/A	42
Imidazole based metal-organic frameworks					
Zn-ZIF-8	0.70	N/A	N/A	N/A	43
$Co_{25}Zn_{75}$-ZIF-8	0.77	N/A	N/A	N/A	43
$Co_{50}Zn_{50}$-ZIF-8	0.87	N/A	N/A	N/A	43
$Co_{75}Zn_{25}$-ZIF-8	0.90	N/A	N/A	N/A	43
$Co_{90}Zn_{10}$-ZIF-8	0.81	N/A	N/A	N/A	43
Co-ZIF-8	0.85	N/A	N/A	N/A	43
Flower shaped ZIF-L	1.15	N/A	N/A	N/A	44
ZIF-95	0.88		18	4.3	45
ZIF-100	1.45 (at 273 K and 1 bar)		25	5.9	45
ZIF-78	2.3		50.1	10.6	45
ZIF-81	1.71		23.8	5.7	45
ZIF-79	1.5		23.2	5.4	45
ZIF-69	1.82		19.9	5.1	45
ZIF-68	1.7		18.7	5.0	45

ZIF-82	2.36		35.3	9.6	45
ZIF-70	2.46		17.3	5.2	45
IISERP-MOF26	2.7	23	160	15	This work
IISERP-MOF27	2.2	18	75	12	This work

3.7. Conclusion:

In conclusion, **1** and **2** are two adenine-based MOFs showing selective CO_2 capture properties; their low heat of adsorption for CO_2 enables smooth adsorption-desorption with favorable cycling stability. The mild HOA (18–22 kJ mol^{-1}) for CO_2 in these amine-rich channels is counter-intuitive but can be explained based on the presence of multiple electrostatic and dispersive centers engaged in balancing/cancelling each other making the pore environment less polarizing towards the incoming CO_2 molecules.[23] The presence of appreciable CO_2 uptake despite the micropores being partly blocked by counter-balancing cations is noteworthy. In terms of several important CO_2 capture and separation performance criteria, this material outperforms other amine-functionalized MOFs and imidazole-based frameworks. Collectively, these results point toward the value of utilizing of adenine as a building block for constructing a library of MOFs for selective CO_2 capture applications.

3.8. References

1. https://www.weforum.org/agenda/2019/04/middle-east-front-lines-climate-change-mena/.https://ourworldindata.org/co2-and-other-greenhouse-gas-emissions

2. https://climate.nasa.gov/news/2876/new-studies-increase-confidencein-nasas-measure-of-earths-temperature/.

3. K. Zhou, S. Chaemchuen, F. Verpoort, *Renewable and sustainable energy reviews* **2017**, *79*, 1414-1441.

4. Q. Ke, T. Sun, X. Wei, Y. Guo, S. Wang, *ChemSusChem* **2017**, *10*, 4207-4214.

5. a) J. Mustafa, M. Farhan, M. Hussain, *J. Membra. Sci. Technol.* **2016**, 6, 153; b) D. Aaron, C. Tsouris, *Sep. Sci. Technol.* **2005**, *40*, 321-348.

6. a) M. Ranjan, H. J. Herzog, *Energy Procedia* **2011**, *4*, 2869-2876; b) M. Mazzotti, R. Baciocchi, M. J. Desmond, R. H. Socolow, *Climatic change* **2013**, *118*, 119-135; c)https://www.aps.org/policy/reports/assessments/upload/dac2011.pdf; d)https://www.ipcc.ch/pdf/special reports/srccs/srccs_wholereport.pdf.

7. a) S. Nandi, J. Rother, D. Chakraborty, R. Maity, U. Werner-Zwanziger, R. Vaidhyanathan, *J. Mater. Chem. A* **2017**, *5*, 8431-8439; b) S. Nandi, U. Werner-Zwanziger, R. Vaidhyanathan, *J. Mater. Chem. A*

2015, *3*, 21116-21122; c) S. Sung, M. P. Suh, *J. Mater. Chem. A* **2014**, *2*, 13245-13249; d) L. H. Xie, M. P. Suh, *Chem. Eur. J.* **2013**, *19*, 11590-11597.

8. Y. Zeng, R. Zou, Y. Zhao, *Adv. Mater.* **2016**, *28*, 2855-2873.

9. a) W. Wu, Z. Tian, S. Wang, C. Peng, H. Liu, S. Dai, D.-e. Jiang, *Ind. Eng. Chem. Res.* **2017**, *56*, 4502-4507; b) J. R. Holst, A. Trewin, A. I. Cooper, *Nature Chem.* **2010**, *2*, 915-920; c) Z. Wang, H. Ma, T. L. Zhai, G. Cheng, Q. Xu, J. M. Liu, J. Yang, Q. M. Zhang, Q. P. Zhang, Y. S. Zheng, *Adv. Sci.* **2018**, *5*, 1800141; d) T. Hasell, J. A. Armstrong, K. E. Jelfs, F. H. Tay, K. M. Thomas, S. G. Kazarian, A. I. Cooper, *Chem. Commun.* **2013**, *49*, 9410-9412.

10. a) D. Britt, H. Furukawa, B. Wang, T. G. Glover, O. M. Yaghi, *Proc. Natl. Acad. Sci.* **2009**, *106*, 20637-20640; b) R. Maity, D. Chakraborty, S. Nandi, K. Rinku, R. Vaidhyanathan, *CrystEngComm* **2018**, *20*, 6088-6093; c) S. Nandi, R. Maity, D. Chakraborty, H. Ballav, R. Vaidhyanathan, *Inorg. Chem.* **2018**, *57*, 5267-5272.

11. a) A. Sayari, Y. Belmabkhout, R. Serna-Guerrero, *Chem. Eng. J.* **2011**, *171*, 760-774; b) J. C. Hicks, J. H. Drese, D. J. Fauth, M. L. Gray, G. Qi, C. W. Jones, *J. Am. Chem. Soc.* **2008**, *130*, 2902-2903; c) A. Thomas, *Angew. Chem.* **2010**, *122*, 8506-8523; d) R. V. Siriwardane, M.-S. Shen, E. P. Fisher, J. A. Poston, *Energy & Fuels* **2001**, *15*, 279-284.

12. a) J. C. Tan, T. D. Bennett, A. K. Cheetham, *Proc. Natl. Acad. Sci.* **2010**, *107*, 9938-9943; b) A. J. Howarth, Y. Liu, P. Li, Z. Li, T. C. Wang, J. T. Hupp, O. K. Farha, *Nat. Rev. Mater.* **2016**, *1*, 1-15.

13. a) P. Nugent, Y. Belmabkhout, S. D. Burd, A. J. Cairns, R. Luebke, K. Forrest, T. Pham, S. Ma, B. Space, L. Wojtas, *Nature* **2013**, *495*, 80-84; bV. Sharma, D. De, R. Saha, R. Das, P. K. Chattaraj, P. K. Bharadwaj, *Chem. Commun.* **2017**, *53*, 13371-13374; c) D. Wu, Q. Xu, D. Liu, C. Zhong, *J. Phys. Chem. C* **2010**, *114*, 16611-16617; d) D.-S. Zhang, Z. Chang, Y.-F. Li, Z.-Y. Jiang, Z.-H. Xuan, Y.-H. Zhang, J.-R. Li, Q. Chen, T.-L. Hu, X.-H. Bu, *Sci. Rep.* **2013**, *3*, 3312; e) H. Jasuja, Y.-g. Huang, K. S. Walton, *Langmuir* **2012**, *28*, 16874-16880; f) N. Lv, T. Guo, B. Liu, C. Wang, V. Singh, X. Xu, X. Li, D. Chen, R. Gref, J. Zhang, *Pharm. Res.* **2017**, *34*, 269-278; g) T. Wu, L. Shen, M. Luebbers, C. Hu, Q. Chen, Z. Ni, R. I. Masel, *Chem. Commun.* **2010**, *46*, 6120-6122; h) R. Feng, Y.-Y. Jia, Z.-Y. Li, Z. Chang, X.-H. Bu, *Chem. Sci.* **2018**, *9*, 950-955.

14. a) E. J. Carrington, I. J. Vitórica-Yrezábal, L. Brammer, *Acta Crystallographica Section B: Structural Science, Crystal Engineering and Materials* **2014**, *70*, 404-422; b) P. G. Boyd, T. K. Woo, *CrystEngComm* **2016**, *18*, 3777-3792; c) S. P. Collins, T. D. Daff, S. S. Piotrkowski, T. K. Woo, *Sci. Adv.* **2016**, *2*, e1600954; d) H. Wu, J. M. Simmons, G. Srinivas, W. Zhou, T. Yildirim, *J. Phys. Chem. Lett.* **2010**, *1*, 1946-1951; e) Y. Jiao, Z. Li, Y. Ma, G. Zhou, S. Wang, G. Lu, *AIP Adv.* **2017**, *7*, 085009; f) Z. Lu, H. G. W. Godfrey, I. da Silva, Y. Cheng, M. Savage, F. Tuna, E. J. L. McInnes, S. J. Teat, K. J. Gagnon, M. D. Frogley, P. Manuel, S. Rudic´, A. J. Ramirez-Cuesta, T. L. Easun, S. Yang, M. Schrçder, *Nat. Commun.* **2017**, *8*, 1-10.

15. a) Lourdes F. Vega, Daniel Bahamon, Society of Petroleum Engineers, Abu Dhabi International Petroleum Exhibition & Conference, 7 –10 November, Abu Dhabi, UAE, https://doi.org/10.2118/183480-MS, 2016; b) J. Caro, *Procedia Engineering 44 (2012)* **2012**, *44*, 1-2; c) D. Saha, Z. Bao, F. Jia, S. Deng, *Environ. Sci. Technol.* **2010**, *44*, 1820-1826; d) R. Krishna, J. M. van Baten, *Sep. Purif. Technol.* **2012**, *87*, 120-126.

16. a) X. Kong, E. Scott, W. Ding, J. A. Mason, J. R. Long, J. A. Reimer, *J. Am. Chem. Soc.* **2012**, *134*, 14341-14344; b) J. Park, H. Kim, S. S. Han, Y. Jung, *J. Phys. Chem. Lett.* **2012**, *3*, 826-829; c) J. Qian, Q. Li, L. Liang, T.-T. Li, Y. Hu, S. Huang, *Dalton Trans.* **2017**, *46*, 14102-14106.

17. a) S. Kazemi, V. Safarifard, *Nanochem. Res.* **2018**, *3*, 62-78; b) A. Demessence, D. M. D'Alessandro, M. L. Foo, J. R. Long, *J. Am. Chem. Soc.* **2009**, *131*, 8784-8786; c) T. M. McDonald, D. M. D'Alessandro, R. Krishna, J. R. Long, *Chem. Sci.* **2011**, *2*, 2022-2028; d) S. Couck, J. F. Denayer, G. V. Baron, T. Rémy, J. Gascon, F. Kapteijn, *J. Am. Chem. Soc.* **2009**, *131*, 6326-6327; e) R. Vaidhyanathan, S. S. Iremonger, G. K. Shimizu, P. G. Boyd, S. Alavi, T. K. Woo, *Science* **2010**, *330*, 650-653; f) S. Shalini, S. Nandi, A. Justin, R. Maity, R. Vaidhyanathan, *Chem. Commun.* **2018**, *54*, 13472-13490.

18. a) I. Kochetygov, S. Bulut, M. Asgari, W. L. Queen, *Dalton Trans.* **2018**, *47*, 10527-10535; b) J. An, N. L. Rosi, *J. Am. Chem. Soc.* **2010**, *132*, 5578-5579; c) J. Yu, L.-H. Xie, J.-R. Li, Y. Ma, J. M. Seminario, P. B. Balbuena, *Chem. Rev.* **2017**, *117*, 9674-9754; d) K. M. Gupta, Y. Chen, Z. Hu, J. Jiang, *Phys. Chem. Chem. Phys.* **2012**, *14*, 5785-5794; e) K. M. Gupta, *Fluid Phase Equilib.* **2016**, *415*, 34-41; f) C. Wang, H. Luo, H. Li, X. Zhu, B. Yu, S. Dai, *Chem. Eur. J.* **2012**, *18*, 2153-2160.

19. a) S. Nandi, P. De Luna, T. D. Daff, J. Rother, M. Liu, W. Buchanan, A. I. Hawari, T. K. Woo, R. Vaidhyanathan, *Sci. Adv.* **2015**, *1*, e1500421; b) S. Nandi, S. Collins, D. Chakraborty, D. Banerjee, P. K. Thallapally, T. K. Woo, R. Vaidhyanathan, *J. Am. Chem. Soc.* **2017**, *139*, 1734-1737.

20. J. An, S. J. Geib, N. L. Rosi, *J. Am. Chem. Soc.* **2010**, *132*, 38-39.

21. H. Cai, M. Li, X. R. Lin, W. Chen, G. H. Chen, X. C. Huang, D. Li, *Angew. Chem.* **2015**, *127*, 10600-10605.

22. a) A. L. Spek, *Acta Crystallogr. Sect. C: Struct. Chem.* **2015**, *71*, 9-18; b) A. Spek, *J. Appl. Crystallogr.* **2003**, *36*, 7-13; c) C.-Y. Sun, X.-L. Wang, X. Zhang, C. Qin, P. Li, Z.-M. Su, D.-X. Zhu, G.-G. Shan, K.-Z. Shao, H. Wu, *Nat. Commun.* **2013**, *4*, 1-8.

23. R. Vaidhyanathan, S. S. Iremonger, G. K. Shimizu, P. G. Boyd, S. Alavi, T. K. Woo, *Angew. Chem.* **2012**, *124*, 1862-1865.

24. A. Banerjee, S. Nandi, P. Nasa, R. Vaidhyanathan, *Chem. Commun.* **2016**, *52*, 1851-1854.

25. R. Vaidhyanathan, S. S. Iremonger, K. W. Dawson, G. K. Shimizu, *Chem. Commun.* **2009**, 5230-5232.

26. A. M. Goforth, C.-Y. Su, R. Hipp, R. B. Macquart, M. D. Smith, H.-C. zur Loye, *J. Solid State Chem.* **2005**, *178*, 2511-2518.

27. C.-Y. Su, A. M. Goforth, M. D. Smith, P. Pellechia, H.-C. zur Loye, *J. Am. Chem. Soc.* **2004**, *126*, 3576-3586.

28. R.-B. Lin, D. Chen, Y.-Y. Lin, J.-P. Zhang, X.-M. Chen, *Inorg. Chem.* **2012**, *51*, 9950-9955.

29. T. Li, D.-L. Chen, J. E. Sullivan, M. T. Kozlowski, J. K. Johnson, N. L. Rosi, *Chem. Sci.* **2013**, *4*, 1746-1755.

30. M.-S. Chen, M. Chen, S. Takamizawa, T.-a. Okamura, J. Fan, W.-Y. Sun, *Chem. Commun.* **2011**, *47*, 3787-3789.

31. J. Kim, W. Y. Kim, W.-S. Ahn, *Fuel* **2012**, *102*, 574-579.

32. X. Si, C. Jiao, F. Li, J. Zhang, S. Wang, S. Liu, Z. Li, L. Sun, F. Xu, Z. Gabelica, *Energy Environ. Sci.* **2011**, *4*, 4522-4527.

33. Y. Lin, C. Kong, L. Chen, *Rsc Adv.* **2012**, *2*, 6417-6419.

34. A. Demessence, D. M. D'Alessandro, M. L. Foo, J. R. Long, *J. Am. Chem. Soc.* **2009**, *131*, 8784-8786.

35. T. M. McDonald, D. M. D'Alessandro, R. Krishna, J. R. Long, *Chem. Sci.* **2011**, *2*, 2022-2028.

36. Q.-G. Zhai, Q. Lin, T. Wu, L. Wang, S.-T. Zheng, X. Bu, P. Feng, *Chem. Mater.* **2012**, *24*, 2624-2626.

37. Y. Lin, Q. Yan, C. Kong, L. Chen, *Sci. Rep.* **2013**, *3*, 1859.

38. Q. Huang, J. Ding, X. Huang, X. Wei, W. Wang, *Energy Procedia* **2017**, *105*, 4395-4401.

39. Y. Fu, D. Sun, Y. Chen, R. Huang, Z. Ding, X. Fu, Z. Li, *Angew. Chem. Int. Ed.* **2012**, *51*, 3364-3367.

40. A. M. Fracaroli, H. Furukawa, M. Suzuki, M. Dodd, S. Okajima, F. Gándara, J. A. Reimer, O. M. Yaghi, *J. Am. Chem. Soc.* **2014**, *136*, 8863-8866.

41. J. Cai, H. Wang, H. Wang, X. Duan, Z. Wang, Y. Cui, Y. Yang, B. Chen, G. Qian, *Rsc Adv.* **2015**, *5*, 77417-77422.

42. Z.-W. Zhai, S.-H. Yang, Y.-R. Lv, C.-X. Du, L.-K. Li, S.-Q. Zang, *Dalton Trans.* **2019**, *48*, 4007-4014.

43. G. Kaur, R. K. Rai, D. Tyagi, X. Yao, P.-Z. Li, X.-C. Yang, Y. Zhao, Q. Xu, S. K. Singh, *J. Mater. Chem. A* **2016**, *4*, 14932-14938.

44. S. Wang, B. Zang, Y. Chang, H. Chen, *CrystEngComm* **2019**, *21*, 6536-6544.

45. A. Phan, C. J. Doonan, F. J. Uribe-Romo, C. B. Knobler, M. O'keeffe, O. M. Yaghi, *Acc Chem Res.* **2010**, *43*, 58-67.

3.A. Appendix:

3.A.1. X-ray Crystallographic structure determination:
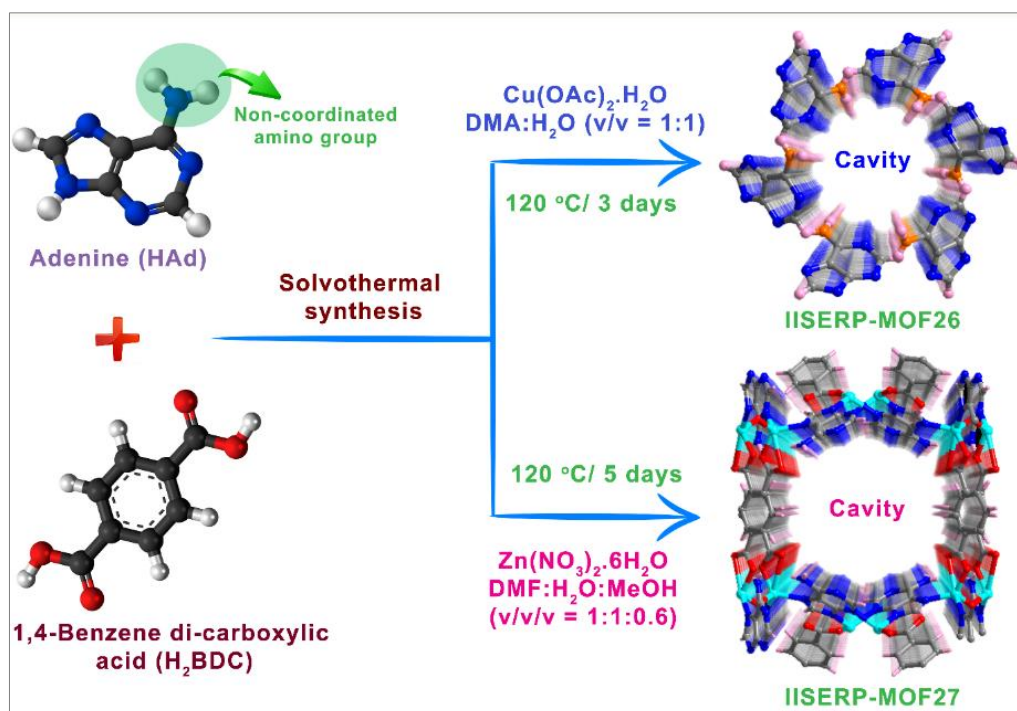
Scheme 3A1. Schematic representation for the synthesis of IISERP-MOF26 (**1**) and IISERP-MOF27 (**2**).

3.A.1.1. The structure of IISERP-MOF26 (1):

Solvent composition of IISERP-MOF26 (1) using SQUEEZE and analytical data:

The solvent molecules (DMF and H_2O) in the pores of as-made IISERP-MOF26 crystals are disordered and their numbers to the X-ray diffraction patterns were estimated by using PLATON/SQUEEZE analysis methods.

a. *PLATON analysis:*

Total Potential Solvent Accessible Void Vol including charge balancing di-methyl ammonium cations (SOLV-Map Value) = 4848.00 $Å^3$

Unit cell volume, V = 10,309.0 $Å^3$

Now, Void volume = (4848/10,309) x 100 = ~ 47 % of the IISERP-MOF26

Now, IISERP-MOF26 (**1**) has an anionic framework with Dimethyl ammonium cation (DMA$^+$) per asymmetric unit. So, asymmetric unit or formula unit present in the crystal structure of the IISERP-MOF26 is (DMA$^+$)$_x$[Cu$_2$O(Ad)(BDC)]•(H$_2$O)$_y$(DMA)$_z$, where, x = any integer represents no of DMA$^+$ (NH$_2$Me$_2$), y = any integer represents no of water molecules, and z = any integer represents no of DMA molecules. Z for IISERP-MOF26 is 18. Hence the unit cell formula is *(DMA$^+$)$_{18x}$[Cu$_{36}$O$_{18}$(Ad)$_{18}$(BDC)$_{18}$]•(H$_2$O)$_{18y}$(DMA)$_{18z}$.*

From squeeze result, electrons found in solvent Accessible Void = 1632. So, squeeze results suggest that 1632 electrons are present from solvent molecules in the unit cell. So, per asymmetric unit 1678/18 = 93.3 electrons are present and per formula unit also 90.6 electrons are present. Considering 27 e's for DMA$^+$ cation, 48 for DMA and 10 for water, the best possible solvents combination and their electrons counts are given in table 3.A.1.

Table 3.A.1. The number of Solvent molecules determination from PLATON analysis for IISERP-MOF26 (**1**).

Cation and solvents combination	No of electrons from DMA	No of electrons from H$_2$O	No of electrons from DMA$^+$	Total electron counts
DMA + 2 H$_2$O + DMA$^+$	48	2 x 10 = 20	27	95

So, from *PLATON* analysis x = 2 and y = 1.

Therefore, according to the *PLATON* analysis formula of asymetric unit or formula unit is:

(NH$_2$Me$_2$)[Cu$_2$O(C$_5$H$_4$N$_5$)(C$_8$H$_4$O$_4$)]•(H$_2$O)$_2$(C$_4$H$_9$NO)$_1$ or [(DMA$^+$)$_2$][Cu$_2$O(Ad)(BDC)]•(H$_2$O)$_2$(DMA)$_1$

And the unit cell formula is [(NH$_2$Me$_2$)]$_{18}$[Cu$_{36}$O$_{18}$(C$_5$H$_4$N$_5$)$_{18}$(C$_8$H$_4$O$_4$)$_{18}$]•(H$_2$O)$_{36}$(C$_4$H$_9$NO)$_{18}$ or (DMA$^+$)$_{18}$[Cu$_{36}$O$_{18}$(Ad)$_{18}$(BDC)$_{18}$]•(H$_2$O)$_{36}$(DMA)$_{18}$

b. TGA analysis:

The molecular mass of formula unit, (DMA$^+$)[Cu$_2$O(Ad)(BDC)]•(H$_2$O)$_2$(DMA) = 610.32 g mol^{-1}.

Now mass loss due to solvents and DMA$^+$ cation is 160.1 g mol^{-1}.

So, according to PLATON analysis mass loss is (160.1/610.32) x 100 = ~26.2 % is expexted.

- Now, expected mass loss due to water = (36/610.32) x 100 = 5.9 %,
- expected mass loss due to DMA solvent = (87/610.32) x 100 = 14.2 % and
- expected mass loss due to DMA$^+$ = (46.1/610.32) x 100 = 7.6 %

Now, from TGA,
- mass loss due to water = 6.1 %
- mass loss due to DMA solvent = 14.5 % and
- mass loss due to DMA$^+$ = 9.4 %

So, total mass loss due to solvents is (6.1 + 14.5 + 9.4) % = 30 % which approximately matching with the value obtaine from *PLATON-SQUEEZE* analysis.

Therefore, TGA analysis also supports the molecular formula of the formula unit or asymetric unit and unit cell obtained from the *PLATON* analysis.

Table 3.A.2. Crystal structure information for the Non-squeezed and squeezed structure of IISERP-MOF26 (**1**) obtained from SCXRD and *PLATON* analysis.

Parameters	Non-squeezed IISERP-MOF26 (1)	Squeezed IISERP-MOF26
Chemical formula	$(DMA^+)[Cu_2O(Ad)(BDC)]\bullet(H_2O)_2$ (DMA)	$(DMA^+)[Cu_2O(Ad)(BDC)]$
Formula weight	610.32 g mol^{-1}	441.32 g mol^{-1}
Crystal system	Trigonal	Trigonal
Space group	R-3	R-3
Unit-cell parameter	a = 30.9216(13), b = 30.9216(13), c=12.4440(6), α= β= 90°, γ=120°	a = 30.9216(13), b = 30.9216(13), c=12.4440(6), α= 90°, β= 90°, γ=120°
Crystal colour and shape	Greenish brick shaped	Greenish brick shaped
Temperature	100 K	100 K
Z	18	18
Density (g cm^{-1})	1.53	1.28
Abs. Coeff. (mm^{-1})	2.680	2.533
F(000)	4806.0	3942.0
Reflection Data		
No. of reflections meas.	65813.00	65813.00
No. of uniq. reflections	4,537.00	4537.00
No. of obs. reflections	3163.00	3163.00
λ (Å)	1.54178	1.54178
R_{merge}	0.121	0.121
Av. I/sig(l)	15.02	15.02
θ_{max}	72.8	72.8
θ_{min}	2.9	2.9
Refinement Data		
R_{all}	0.118	0.092
R_{obs}	0.081	0.061
$wR_2(all)$	0.250	0.173
$wR_2(obs)$	0.225	0.161
Ext. Coeff.	0.0002	-
Goodness-of-fit (GOOF)	1.061	1.131
Largest diff. peak and hole: Delta-rho (eÅ^{-3})$_{max}$	2.499	1.054
Largest diff. peak and hole: Delta-rho (eÅ^{-3})$_{min}$	-0.604	-0.582

*Note. PLATON analysis suggests the presence of a substantial amount of solvent accessible voids in the structure of IISERPMOF26. The solvents could not be modelled satisfactorily. From the *SQUEEZE* analysis was carried out to determine the number of DMA$^+$ cation, DMA solvent and H$_2$O molecules. From squeezed electron counts and with the aid of feasible analytical method like TG analysis the solvent content was estimated. It was found that 1 DMA$^+$ cation, 1 DMA solvent and 2 water molecules present in each formula unit of IISERP-MOF26 ($(DMA^+)[Cu_2O(Ad)(BDC)]$). So, actual formula of IISERP-MOF26 is $(DMA^+)[Cu_2O(Ad)(BDC)]\bullet(H_2O)_2(DMA)$.
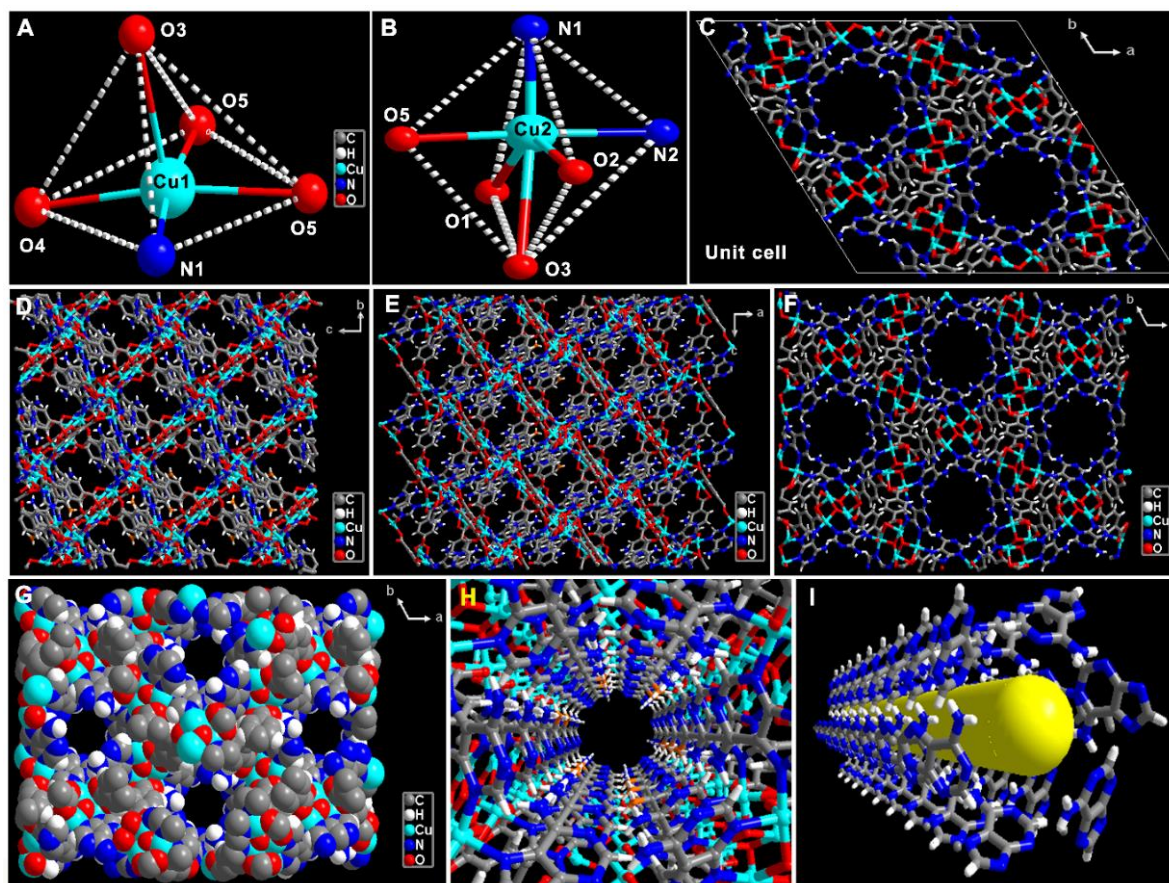
Figure 3.A1. (A) Shows the coordination sphere of Cu1, which adopts a distorted square pyramidal geometry, showing selected atomic labels. The thermal ellipsoids are plotted at 50% probability. (B) Shows the coordination sphere of Cu2, which adopts a distorted octahedral geometry. (C) The unit cell present in the crystal structure of IISERP-MOF26. Crystallographic view along (D) a-axis, (E) b-axis, (F) c-axis. (H) Perspective view of the pore along C-axis. (I) The 3D channel topology of IISERP-MOF26 along crystallographic c-axis. Note that the channel is surrounded by the N sites of both amino and pyrimidine groups, give rise to a Lewis basic-polar channel, suitable for hosting Lewis acidic guest species.

3.A.1.2. The structure of IISERP-MOF27 (2):

Solvent composition of IISERP-MOF27 (2) using SQUEEZE and analytical data:

a. *PLATON analysis:*

Total Potential Solvent Accessible Void Vol (SOLV-Map Value) = 1626.00 Å^3

Unit cell volume, V = 4812.0 Å^3

Void volume = ~ 33.75 % of the IISERP-MOF27.

Formula unit present in IISERP-MOF27 is $[Zn_4O(Ad)_3(BDC)_2]$.

Again, Z for IISERP-MOF27 is 4. Hence the unit cell formula is $[Zn_{16}O_4(Ad)_{12}(BDC)_8]$.

Again, squeeze results suggest that 200 electrons are present from solvent molecules in the unit cell. So, per formula unit 200/4 = 50 electrons are present. Considering 40 e-'s for DMF and 10 for water and 27 electron from the dimethyl ammonium cations (DMA$^+$ or Me$_2$NH$_2^+$) the best possible solvent combination and their electron counts are given in table 3.A.3.

Table 3.A.3. Number of Solvent molecules determination from PLATON analysis for IISERP-MOF27 (**2**).

Solvent combination	No of electrons from DMF	No of electrons from H_2O	No of electrons from DMA^+	Total electron counts
½ DMF + 2H_2O + ½ DMA^+	40 X ½ = 20	2 x 10 = 20	27 x ½ = 13.5	53.5

Table 3.A.4. Crystal structure information for the Non-squeezed and squeezed structure of IISERP-MOF27 (**2**) obtained from SCXRD and *PLATON* analysis.

Parameters	Non-squeezed IISERP-MOF27(2)	Squeezed IISERP-MOF27(2)
Chemical formula	$(DMA^+)_{1/2}[Zn_4O(Ad)_3(BDC)_2 \cdot (H_2O)_2(DMF)_{1/2}$	$(DMA^+)_{1/2}[Zn_4O(Ad)_3(BDC)_2$
Formula weight	1103.60 g mol^{-1}	1008.10 g mol^{-1}
Crystal system	Monoclinic	Monoclinic
Space group	Cc	Cc
Unit-cell parameter	a =14.4056(7), b = 36.3878(19), c =9.5535(5), α=90º, β= 106.1º, γ=90º	a =14.4056(7), b = 36.3878(19), c =9.5535(5), α=90º, β= 106.7º, γ=90º
Crystal colour and shape	Colorless-plate shape	Colorless plate shape
Temperature	100 K	100 K
Z	4	4
Density (g cm^{-1})	2.24	2.24
Abs. Coeff. (mm^{-1})	8.551	8.551
F(000)	3120.0	3120.0
Reflection Data		
No. of reflections meas.	11059.00	11059.00
No. of uniq. reflections	6152.00	6152.00
No. of obs. reflections	5516.00	5516.00
λ (Å)	1.54178	1.54178
R_{merge}	0.043	0.043
Av. I/sig(l)	17.24	17.24
θ_{max}	68.7	68.7
θ_{min}	3.4	3.4
Refinement Data		
R_{all}	0.068	0.092
R_{obs}	0.061	0.061
$wR_2(all)$	0.184	0.173
$wR_2(obs)$	0.178	0.161
Goodness-of-fit (GOOF)	1.060	1.131
Largest diff. peak and hole: Delta-rho (eÅ^{-3})$_{max}$	1.844	1.054
Largest diff. peak and hole: Delta-rho (eÅ^{-3})$_{min}$	-0.455	-0.582

*Note. PLATON analysis suggests the presence of a substantial amount of solvent accessible voids in the structure of IISERPMOF27. The solvents could not be modelled satisfactorily. From the *SQUEEZE* analysis

was carried out to determine the number of DMA$^+$ cation, DMF solvent and H$_2$O molecules. From squeezed electron counts and with the aid of feasible analytical method like TG analysis the solvent content was estimated. It was found that ½ DMA$^+$ cation, ½ DMF solvent and 2 water molecules present in each formula unit of IISERP-MOF27. So, actual formula of IISERP-MOF27 is (DMA$^+$)$_{1/2}$[Zn$_4$O(Ad)$_3$(BDC)$_2$]•(H$_2$O)$_2$(DMF)$_{1/2}$.
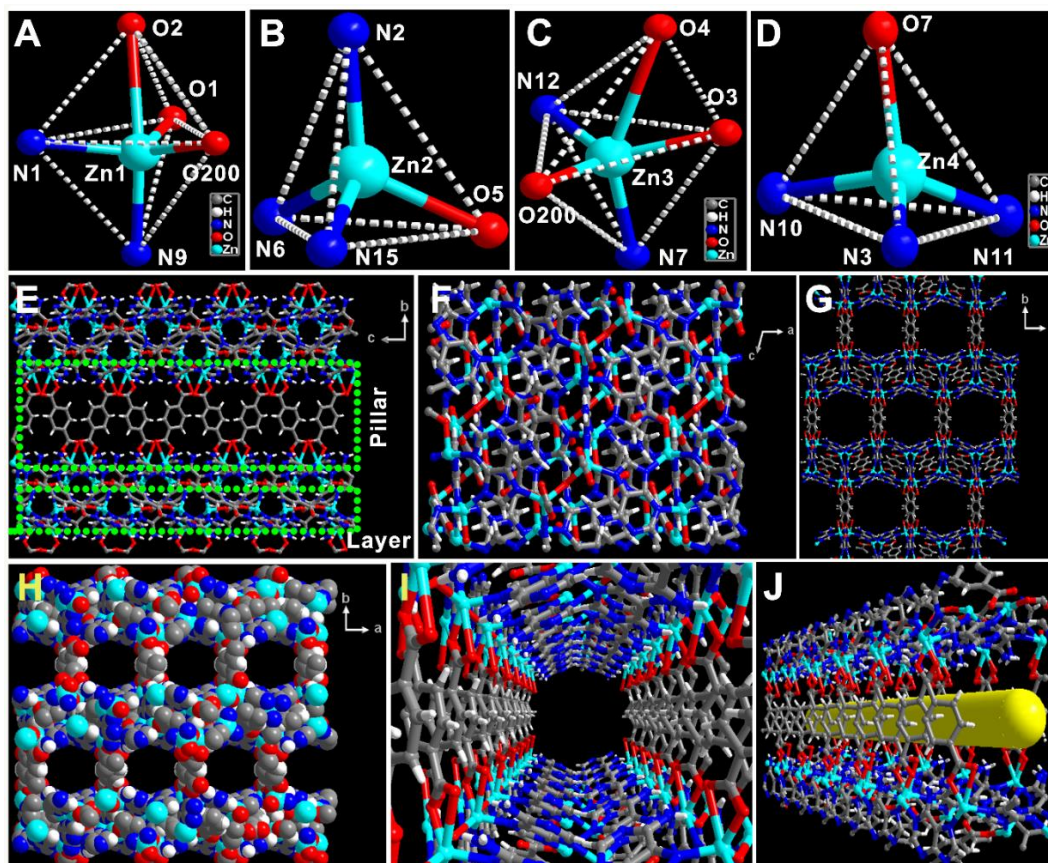
Figure 3.A2. (A), (B), (C), (D) Show the coordination sphere of Zn1, Zn2, Zn3 and Zn4 with selected atomic labels. The thermal ellipsoids are plotted at 50% probability. Zn1 and Zn3 adopt a distorted trigonal bi-pyramidal geometry whereas Zn2 and Zn4 are in distorted tetrahedral environment. Crystallographic view along (E) a-axis, (F) b-axis, (G) c-axis. (H) Space-fill model, and (I) Perspective view of the pore along C-axis. (J) The 3D channel topology of IISERP-MOF27 (**2**) along crystallographic c-axis. Note that the channel is surrounded by the N sites of both amino and pyrimidine groups, give rise to a Lewis basic-polar channel.

(b) TGA analysis:

The molecular mass of formula unit, (DMA$^+$)$_{1/2}$[Zn$_4$O(Ad)$_3$(BDC)$_2$]•(H$_2$O)$_2$(DMF)$_{1/2}$ = 1103.60 g mol^{-1}

Now mass loss due to solvents is 72.50 g mol^{-1}

So, according to PLATON analysis mass loss is (72.50/1103.60) x 100 = ~6.6 % is expexted.

- Now, expected mass loss due to water = (36/1103.60) x 100 = 3.26 %,
- expected mass loss due to DMF solvent = (36.5/1103.60) x 100 = 3.31 % and

Now, from TGA,

- mass loss due to water = 3.1 %
- mass loss due to DMA solvent = 3.5 % and

So, total mass loss due to solvents is (3.1 + 3.5) % = 6.6 % which approximately matching with the value obtaine from *PLATON-SQUEEZE* analysis.

Therefore, TGA analysis also supports the molecular formula of the formula unit or asymetric unit and unit cell obtained from the *PLATON* analysis.

3.A.2. Powder X-ray diffraction analysis:
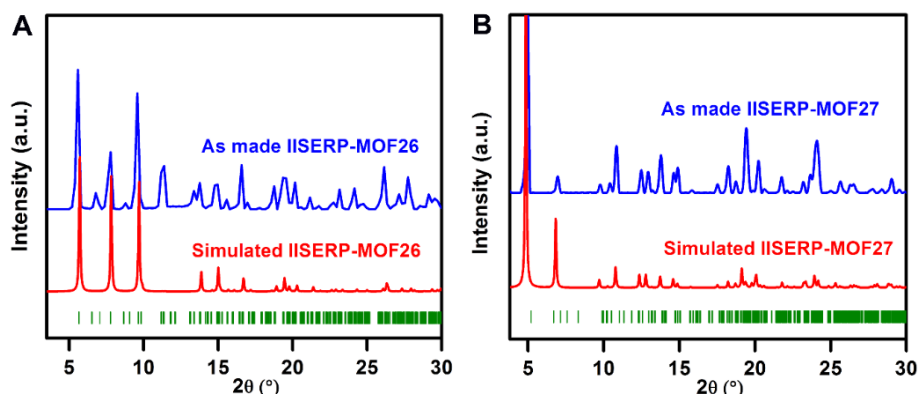
Figure 3.A3. A comparative PXRD plots of (A) IISERP-MOF26(**1**) and (B) IISERP-MOF27(**2**) showing the bulk purity. The exact positions of all peaks are shown with green markers in both **1** and **2** in solvated phases.

3.A.3. Thermogravimetric analysis (TGA):

IISERP-MOF26 (1): There is a two-step gradual mass loss up to 260 ºC due to loss of solvent molecules trapped in the pore of IISERP-MOF26. Initial 6.4 % mass loss is due to the evaporation of pore water molecules whereas the latter 16.2 % mass loss is due to evaporation of comparatively high boiling DMF molecules. Overall, 22.4 % mass loss happened for IISERP-MOF26 which was agreed well with the mass loss (19 %) of solvent calculated from the *PLATON*-SQUEEZE result.
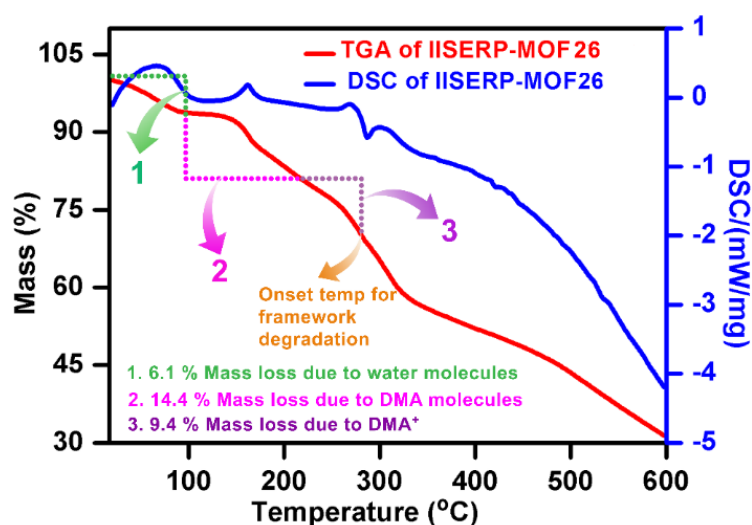
Figure 3.A4. TGA of as made IISERP-MOF26 (**1**) shows thermal stability and onset temperature for degradation of the framework upon removal of the DMA$^+$ cations from the framework.

IISERP-MOF27 (2): Similarly, a total of 6.0 % mass loss happened for IISERP-MOF27 (**2**) which was matched well with the solvent composition calculated from the *PLATON*-SQUEEZE result (6.6 %). And that is why may be the CO_2 uptake for the IISERP-MOF27 is low.
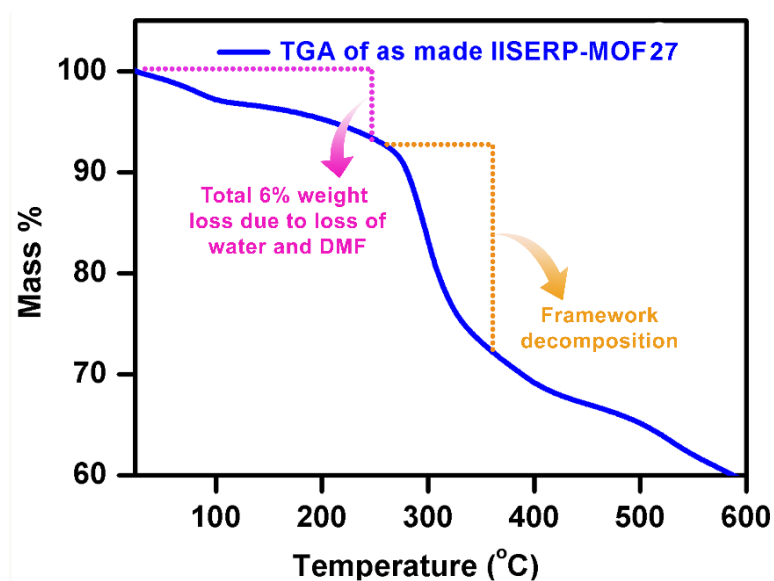
Figure 3.A5. TGA of as made IISERP-MOF27 shows thermal stability and temperature for degradation of the framework.

3.A.4. IR analysis:
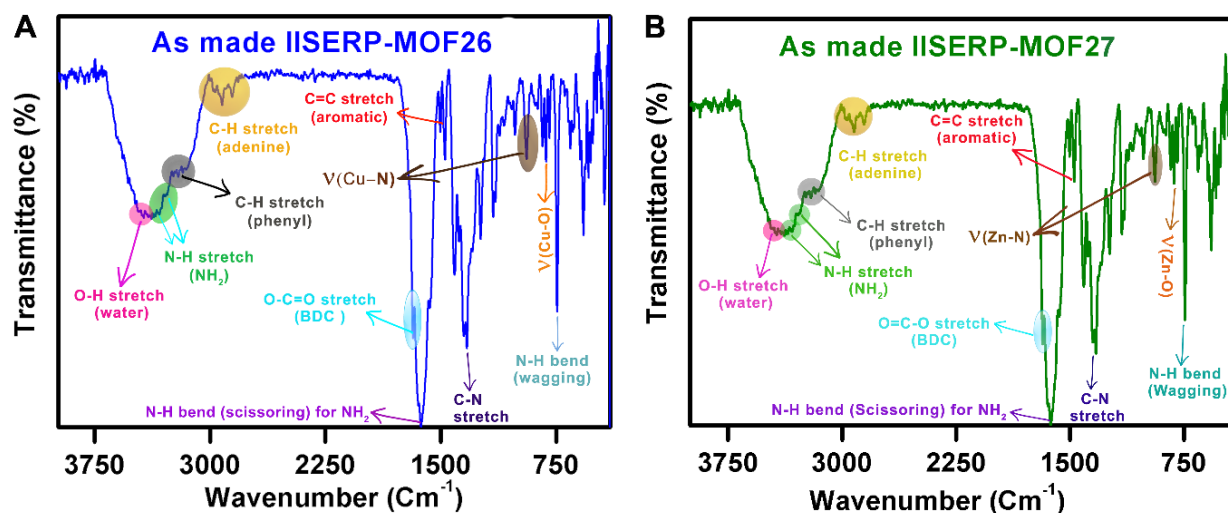
Figure 3.A6. Infrared-red (IR) spectra of IISERP-MOF26 (A) and IISERP-MOF27 (B) referenced to KBr.

3.A.5. Adsorption analysis:
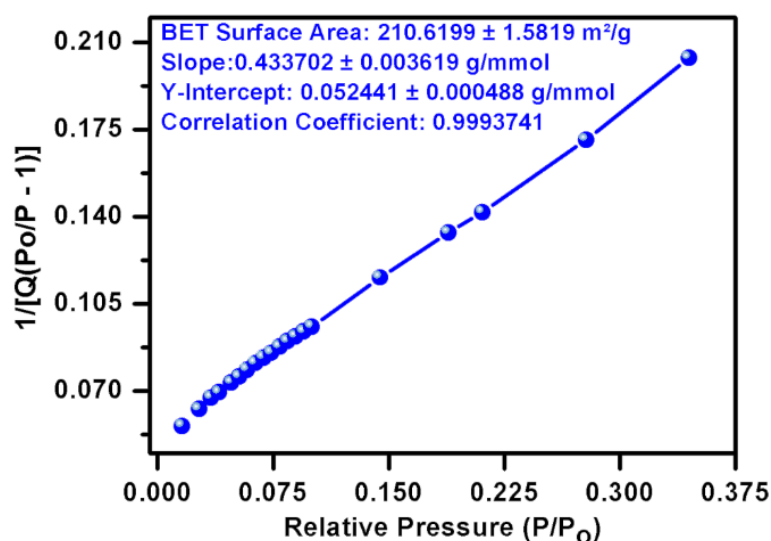
Figure 3.A7. BET fit for the IISERP-MOF26 from the 273 K CO_2 isotherm data.
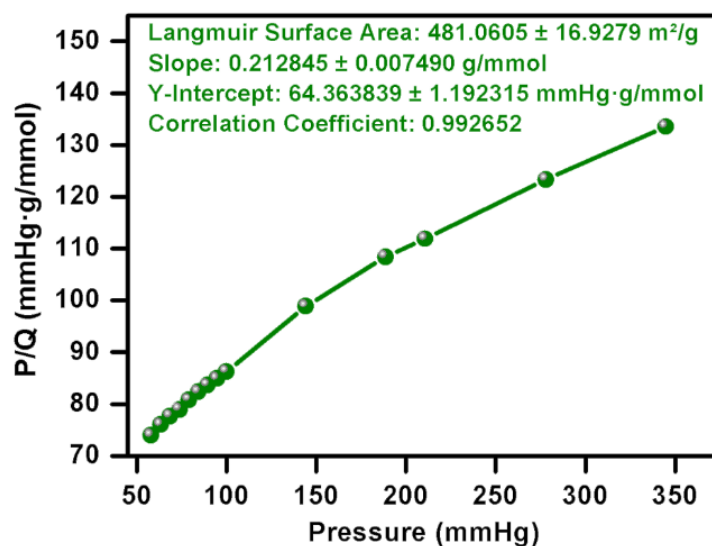
Figure 3.A8. Langmuir fit for the IISERP-MOF26 from the 273 K CO_2 isotherm data.

Virial analysis:

The CO_2 adsorption data were collected from 0-1 bar at 298, 273 and 248 K. For virial fitting the 248, 273 and 298 K isotherms were taken and fitted by the virial equation (1).

$$ln(P) = ln(Va)+(A0+A1*Va +A2*Va^2 \ldots+ A6*Va^6)/T+(B0+B1*Va)\ldots\ldots (1)$$

Where, P is the pressure during the experiment, Va is amount of gas adsorbed, T is temperature, and A0, A1, A2…, A4 and B0, B1 are temperature independent empirical parameters.

Table 3.A.5. Summary of the fitted Virial parameters for IISERP-MOF26 and IISERP-MOF27.

IISERP-MOF26		IISERP-MOF27	
Parameters	**Numeric values**	**Parameters**	**Numeric values**
A0	-3021.007647	A0	-2160.410101
A1	28.62222918	A1	24.01283961
A2	44.99830255	A2	0
A3	-39.15845217	A3	0
A4	11.59761075	A4	0
A5	-1.271978201	A5	0
A6	0.038731417	A6	0
B0	15.40480588	B0	13.32848494
B1	0.3484236	B1	0
B2	-0.04094761	B2	0
B3	9.0388E-06	B3	0
B4	-7.72639E-06	B4	0
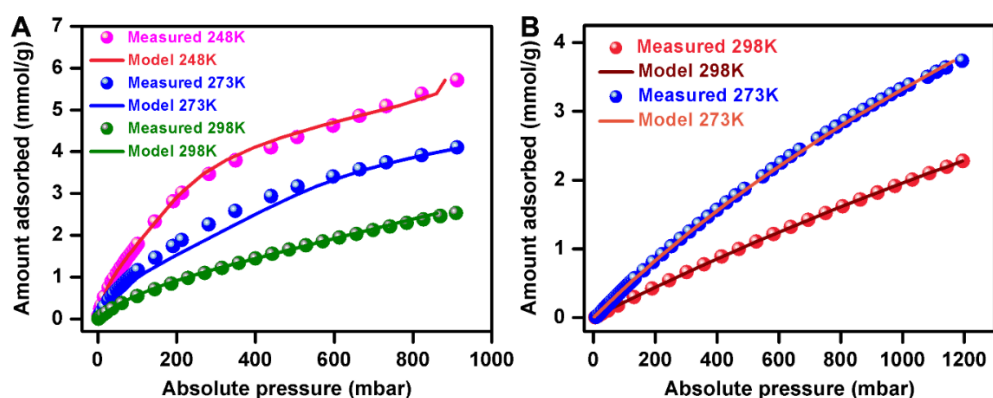
Figure 3.A9. Comparison of experimental isotherms to the ones obtained from Virial modelling carried out using CO_2 isotherms collected at 248, 273, and 298 K (A: IISERP-MOF26, B: IISERP-MOF27).
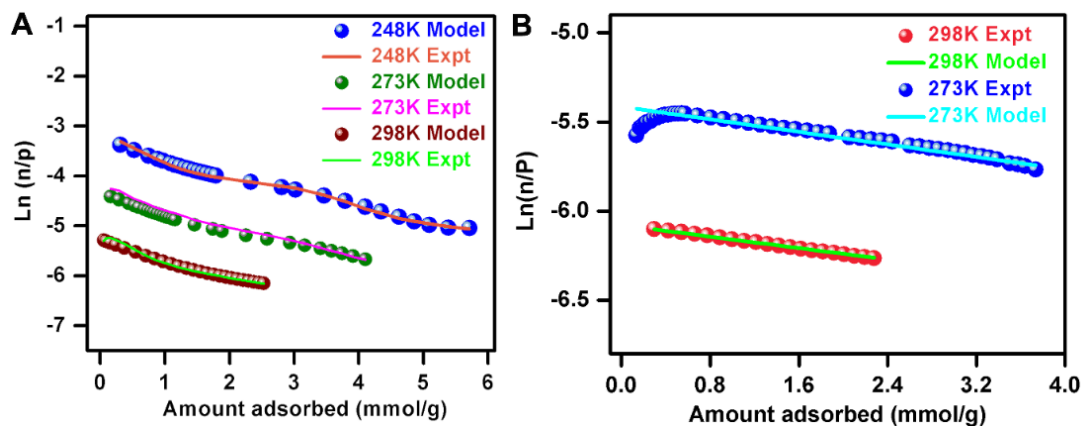
Figure 3.A10. Virial fits for the CO_2 isotherms of (A) IISERP-MOF26 (B) IISERP-MOF27 collected at 248, 273, and 298 K.

IAST selectivities:

CO$_2$/N$_2$ selectivity was calculated for IISERP-MOF26 (**1**) and IISERP-MOF27 (**2**) using the experimental single component CO$_2$ and N$_2$ isotherms and ideal adsorbed solution theory (IAST) with a nominal composition of 15CO$_2$:85N$_2$. At 1 bar total pressure, and 298 K and 273 K, conditions of relevance to post combustion CO$_2$ capture, IISERP-MOF26 have an exceptional CO$_2$/N$_2$ selectivity of 67 and 105 which is remarkable. This unusually high selectivity is due to ultra-low nitrogen uptake for the MOF at that temperature.

IAST fitting parameters for IISERP-MOF26 and IISERP-MOF27 (CO$_2$/N$_2$):

At 298 K
Gas A = CO$_2$ and Gas B = N$_2$

Table 3.A.6. Fitted IAST parameters for CO$_2$/N$_2$ (15CO$_2$:85N$_2$ composition) selectivity at 298 K for **2**.

Gas Mixture		Intrinsic Selectivity	
YA =	0.15	α_1 =	55.557541
YB =	0.85	α_2 =	--------
Gas A Constants		**Gas B Constants**	
qA1 =	7.730371468	qA1 =	3.58431484
qA2 =	0	qA2 =	0
kA1 =	0.000954888	kA1 =	3.7068E-05
kA2 =	0	kA2 =	0
na1 =	0.880472334	na1 =	0.74846139
na2 =	0	na2 =	0
HA1 =	0.007381641	HB1 =	0.00013286
HA2 =	0	HB2 =	0

At 273 K
Gas A = CO$_2$, and Gas B = N$_2$

Table 3.A.7. Fitted IAST parameters for CO$_2$/N$_2$ (15CO$_2$:85N$_2$ composition) selectivity at 273 K for (**1**).

Gas Mixture		Intrinsic Selectivity	
YA =	0.15	α_1 =	0
YB =	0.85	α_2 =	-------
Gas A Constants		**Gas B Constants**	
qA1 =	8.273226386	qA1 =	2.32517931
qA2 =	0	qA2 =	0
kA1 =	0.002881064	kA1 =	3.4193E-05
kA2 =	0	kA2 =	0
na1 =	0.828092453	na1 =	0.9700404
na2 =	0	na2 =	0
HA1 =	0	HB1 =	7.9505E-05
HA2 =	0	HB2 =	0
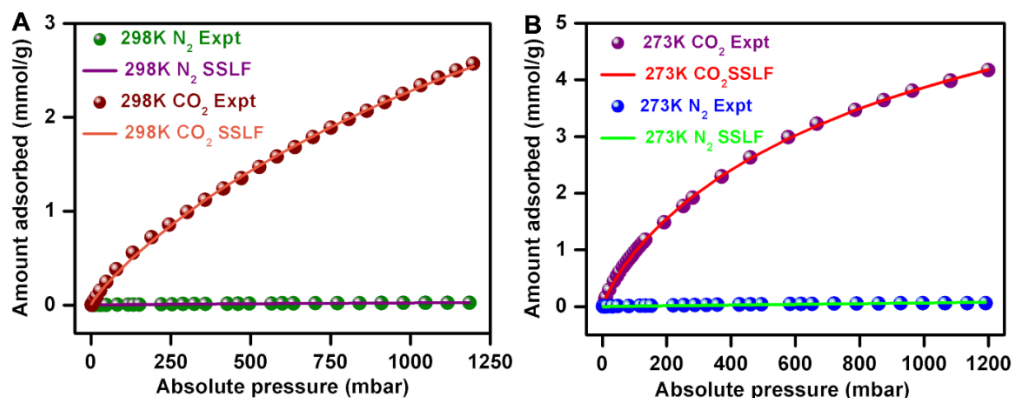
Figure 3.A11. IAST fits for CO_2 and N_2 at different temperatures, 298 K and 273 K for IISERP-MOF26 (**1**). (A: 298 K; B: 273 K).

IAST fitting parameters for IISERP-MOF27 (CO_2/N_2):

At 298 K
Gas A = CO_2 Gas B = N_2

Table 3.A.8. Fitted IAST parameters for CO_2/N_2 ($15CO_2$:$85N_2$ composition) selectivity at 298 K for IISERP-MOF27 (**2**).

Gas Mixture		Intrinsic Selectivity	
YA =	0.15	α_1 =	133.68769
YB =	0.85	α_2 =	-------
Gas A Constants		**Gas B Constants**	
qA1 =	2.012883888	qA1 =	8.27322472
qA2 =	0	qA2 =	0
kA1 =	0.00697733	kA1 =	1.2698E-05
kA2 =	0	kA2 =	0
na1 =	0.751999957	na1 =	0.82803895
na2 =	0	na2 =	0
HA1 =	0.014044555	HB1 =	0.00010505
HA2 =	0	HB2 =	0

IAST fitting parameters for IISERP-MOF27 (CO_2/N_2):

At 273 K
Gas A = CO_2
Gas B = N_2

Table 3.A.9. Fitted IAST parameters for CO_2/N_2 ($15CO_2$:$85N_2$ composition) selectivity at 273 K for **2**.

Gas Mixture		Intrinsic Selectivity	
YA =	0.15	α_1 =	10.787201
YB =	0.85	α_2 =	-------
Gas A Constants		**Gas B Constants**	
qA1 =	4.536774612	qA1 =	8.27324109
qA2 =	0	qA2 =	0
kA1 =	0.000519344	kA1 =	2.6401E-05

kA2 =	0	kA2 =	0
na1 =	1.035176686	na1 =	0.8280619
na2 =	0	na2 =	0
HA1 =	0.002356148	HB1 =	0.00021842
HA2 =	0	HB2 =	0
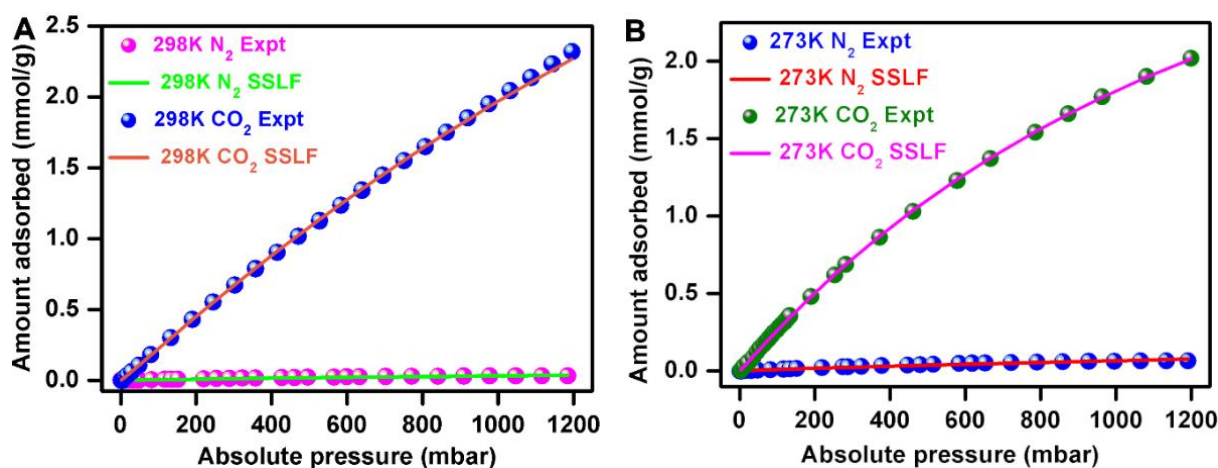
Figure 3.A12. IAST fits for CO_2 and N_2 at different temperatures, 298 K and 273 K for IISERP-MOF27 (**2**) (A: 298 K; B: 273 K).

The explanation for different types of graph in CO_2/N_2 selectivity plot of both IISERP-MOF26 (1) and IISERP-MOF27 (2):

This opposite anomaly might be explained by the positional orientation changing of dimethyl ammonium cations ($(CH_3)_2NH_2^+$, DMA^+). And this is because there are DMA^+ in the pore of IISERP-MOF26 which are under the interaction with the framework to counter balance the negative charge of the framework. While up taking of CO_2 molecules into the pore at 298 K the DMA^+ rearranges their positional orientation under the increasing pressure which creates additional room for CO_2 molecules to occupy and results in increased CO_2/N_2 selectivity and upon desorption again the cation takes its original position. But, at 273 K, the available thermal energy might not be sufficient to reorganise the DMA^+ cations. So, with increase of pressure due to the filling up of the CO_2 molecules, the amount of the bare pore surface will decrease for next CO_2 adsorption which will decrease quantity of CO_2 molecules to be adsorbed for next CO_2 adsorption and hence decrease the overall selectivity. The number of DMA^+ cations per formula unit is more in IISERP-MOF26 as compare to IISERP-MOF27. Furthermore, the pore window is a little bit less in the IISERP-MOF26 relative to IISERP-MOF27. And both the facts might be affecting the reorganisation of DMA^+ cations inside the pore. The fewer number of DMA^+ cations and little bit bigger pore window in the IISERP-MOF27 might be helping to reorganise the DMA^+ cations even at 273 K. That is why at both 273 and 298 K CO_2/N_2 selectivity increases with increase of gas pressure.
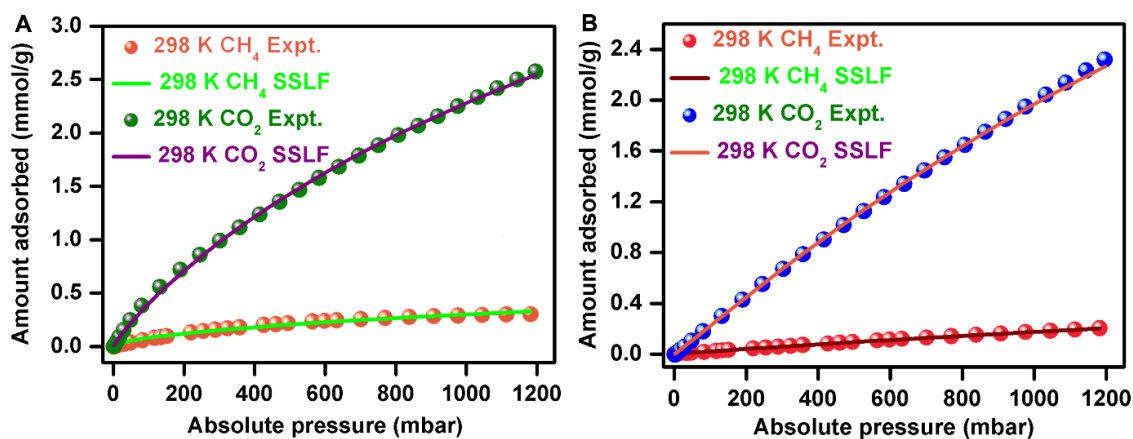
Figure 3.A13. IAST fits for CO_2 and CH_4 at different temperatures, 298 K for (A) IISERP-MOF26 (**1**) and (B) IISERP-MOF27 (**2**).

3.A.6. References:

A1 G. Kemmer, S. Keller, *Nat. Protoc.* **2010**, *5*, 267.

A2. E. Richter, S. Wilfried, A. L. Myers, *Chem. Eng. Sci.* **1989**, *44*, 1609-1616.

A3. A. L. Myers, J. M. Prausnitz, *AlChE J.* **1965**, *11*, 121-127.

Chapter 4

Presence of Multiple CO$_2$ Interactions in a humidity stable Adeninate MOF for Selective CO$_2$ capture
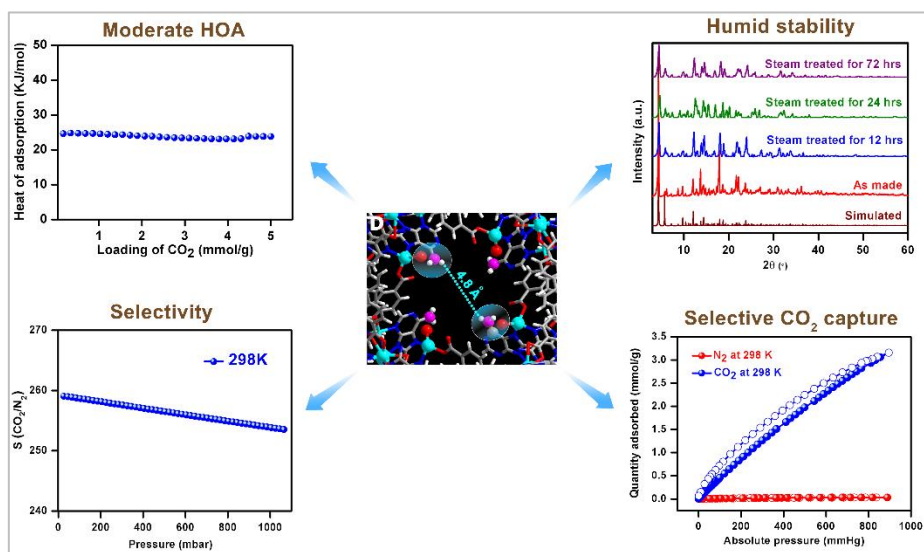
4.1 Introduction:

CO$_2$ capture has attracted immense attention in the last few decades due to the continually warming earth. In this scenario, capturing CO$_2$ with energy-efficient methods is a priority.[1] Of the many practiced methods, adsorption-based CO$_2$ separation process employing porous materials like microporous carbons zeolites, and metal-organic frameworks (MOFs) has shown big promise.[2-4] The overall efficiency of such a process relies sizeably on the sorbent's CO$_2$-capacity and CO$_2$-selectivity. Several approaches and strategies have been proposed to enhance the CO$_2$ interactions with the MOF, for example, the incorporation of Lewis basic sites in the ligand structure,[5] creating open metal sites (OMS)[5g,6] and insertion of the charged guest inside the pore of an ionic framework.[7] Compared to these adsorption sites, much less is known about the use of free/terminal hydroxyl groups. Very recently, the potential of hydroxyl groups to form strong interaction with CO$_2$ through hydrogen bonding was revealed. In these cases, the hydroxyls are terminally coordinated to the metal or they remain as a free guest in the pore. Both have shown considerable interactions with CO$_2$ (OH•••OCO = 1.863(1) Å).[8] Importantly, the cooperativity from the adjacent phenyl rings has been key. Similarly, in Zn$_2$Atz$_2$Ox (**1**), the oxalates have cooperatively assisted the strong interaction between the CO$_2$ and the lone-pairs of the amine group.[9] If all these interactions are simultaneously present in the pore-wall of MOF, the uptake will be reasonably high. Here, according the Aproach-2 (one of the strategies of this thesis), our choice is of N-rich adenine as an azolate ligand that acts as important building block for the formation of steam/humidity stable framework. In another side, it offers its free pyrimidine-N and amine groups to generate highly CO$_2$ polarising pores.

In this Chapter we have designed and synthesized a novel adenine-based MOF, Zn$_4$(Ad)$_3$(BPDC)$_2$(H$_2$O)$_2$•(OH), namely IISERP-MOF23 which possess a relatively superior CO$_2$ adsorption environment by having a non-coordinated carboxylic oxygen atom, amine and bare-metal lined pores. The MOF has a cationic framework with water molecules bound to the open Zn-metal centre and charge balancing free hydroxyl ions in the pore. In IISERP-MOF23, the amine groups lining the pore is positioned next to a pyridyl nitrogen (from adenine) and the open Zinc site (after activation). Due to the combined effect of all these CO$_2$-loving sites, IISERP-MOF23 exhibited a room-temperature CO$_2$ uptake of ~3.3 mmol g^{-1} at 1 bar.

4.2. Materials and Methods:

4.2.1. Synthesis of IISERP-MOF23 (Zn$_4$(Ad)$_3$(BPDC)$_2$(H$_2$O)$_2$•OH):

A mixture of Zn(NO$_3$)$_3$·6H$_2$O (95.0 mg, 0.32 mmol), isonicotinic acid (69.0 mg, 0.8 mmol), 4,4'-biphenyl dicarboxylic acid (H$_2$BPDC) (65 mg, 0.27 mmol) and adenine were dissolved by sonication into a combined solvents of N,N'- dimethyl formamide (DMF), methanol and H$_2$O (6.5 ml; v/v/v= 2.5:2.5:1.5) in a Pyrex vial (8 mL). The vial was heated in a programmable oven at 120 °C for 3 days. Colourless rod-shaped crystals were isolated by filtration and washed a few times with DMF to afford the MOF in 75 % yield based

on metal salt (Scheme 4.1). The expt. PXRD profile of the as made MOF agrees well with the simulated pattern obtained from the single-crystal X-ray data, suggesting that IISERP-MOF23 is a pure phase material.
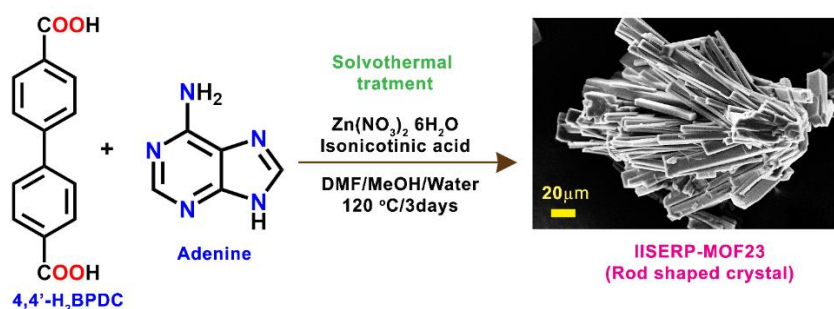
Scheme 4.1. Scheme for the synthesis of IISERP-MOF23.

4.2.2. Analytical Characterisations:

All chemicals were procured from a commercial source (Sigma Aldrich). All routine characterizations including Single Crystal X-ray Diffraction (SCXRD), PXRD, TGA, IR, microscopy and adsorption data were collected using the same conditions and equipment as reported in the Chapter 2 of this thesis. Any specific modification to the measurement conditions has been mentioned in the results and discussion section of this chapter.

Langmuir Fits: In all cases the isotherms were fit to the Single-Site Langmuir (SSL) equation. The isotherms were fit by solving the Langmuir isotherm equation using the Microsoft Excel based solver function following a similar method to Keller *et al.*[10] Utilizing this routine circumvents some of the problems associated with favouring either high- or low-pressure regions when linearizing the Langmuir equation[11] and offers a balanced approach.

Single-Site Langmuir (SSL): $\qquad q_i = q_m \dfrac{k_i}{1 + k_i P} P$

Dual-Site Langmuir (DSL): $\qquad q_i = q_{m,1} \dfrac{K_1}{1 + K_1 P} P + q_{m,2} \dfrac{K_2}{1 + K_2 P} P$

Ideal Adsorbed Solution Theory (IAST): IAST calculations were undertaken as described by Prausnitz et al[12]. The selectivity equation involved in calculation is provided below.

Selectivity: $\qquad S_{1,2} = \dfrac{q_1/q_2}{p_1/p_2}$

TGA Cycling Experiment: For the TGA on-off cycling experiments, no protective gas was used, and the gas flows were systematically switched between CO_2 and N_2 on the purge lines. The methanol/DCM exchanged IISERP-MOF23 was loaded on to the alumina pans and evacuated for 16 hours prior to start the runs. TGA and DSC calibration and corrections runs were done just prior to carrying out the cycling experiments. This seemed to be critical to obtain error-less data from these cycling experiments. Without these systematic sample preparations and instrumentations, the collected data were evaluated to be overestimated.

4.3. Results and Discussions:

In the asymmetric unit of IISERP-MOF23, there are four unique Zn^{2+} centers. Also, there are two unique bpdc ligands and three adeninates. The basic building unit consists of a dimeric Zn_2 cluster, formed by three adeninates which bind in a chelating fashion with the Zn(1) and Zn(2) (Figure 4.1A). Both Zn(1) and Zn(2) are tetrahedral ZnN_3O units. Now the apical site of the Zn(1) is coordinated by a terminal oxygen, while the Zn(2) by a carboxylate oxygen of a BPDC. This terminal oxygen on Zn(1) is assigned as water based on the Zn(1)-O distance (2.235(3) Å, *Remark: Too long for a Zn-hydroxyl bond*). Of the three adenine units constituting this dimeric cluster, one of them bind to two different Zn(3) centers through the N-centers exo to the Zn_2 dimer, while the other two adeninates bind to two different Zn(4) centers (Figure 1a). Both Zn(3) and Zn(4) adopt a tetrahedral coordination with coordinations from both adenine and bpdc units. Zn(4) just like Zn(1) has a terminally coordinated water (Zn(4)-O = 2.22(1)A). Notably, the Zn_2 dimers are discrete (Figure 4.A1). Meanwhile, the Zn(3) and Zn(4) centers are linked into a complex 1-D chain that propagates along the C-axis (Figure 4.1). When viewed down the C-axis, they can be seen as interesting four connecting units with BPDC and adeninate units placed towards the periphery (Figure 4.1B). These are the units that
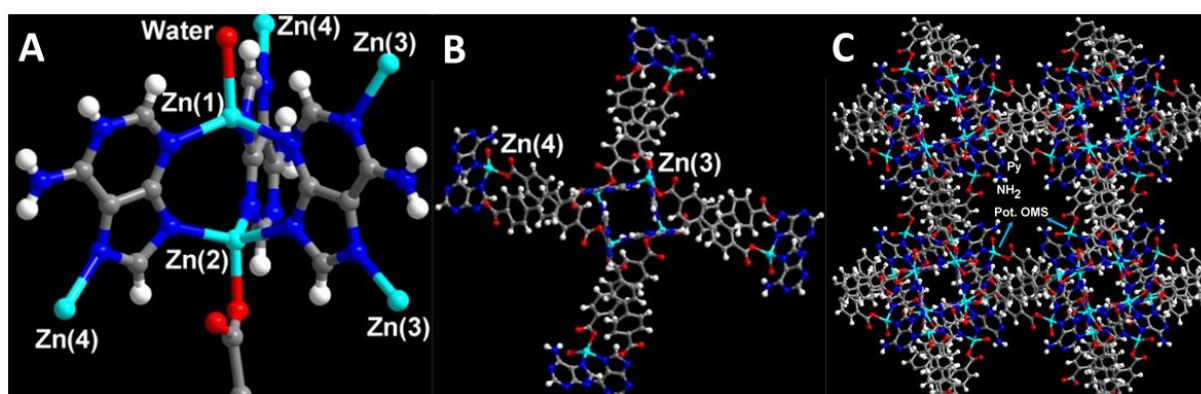
Figure 4.1. (A) The Zn-adenine-carboxylate cluster in IISERP-MOF23. (B) A view of the 1-D chain running down the c-axis with BPDC and adeninate units placed towards the periphery making it a four-connecting unit (Figure 1b). (C) The 3-D framework of IISERP-MOF23 showing the 1-D channels along the C-direction decorated with CO_2 binding moieties- amine, pyridyl and potential bare-metal site. The free OH moieties in the pore could not be located, but its presence is corroborated from modelling and analytical methods.

connect the dimeric SBU formed by the Zn(1) and Zn(2) centers into a cationic 3D-framework of $[Zn_4(Ad)_3(BPDC)_2(H_2O)_2]^{1+}$ with 1-D channels running along C-axis (Figure 4.1C). There are a plenty of disordered guest molecules in the pores of this cationic framework, which we believe is a combination of water and free, charge-balancing hydroxyls, giving an overall formula, $Zn_4(Ad)_3(BPDC)_2(H_2O)_2•(OH)$. Upon activation, the bound water molecules could leave the zinc centres (Figure 4.1A and Figure 4.A1F). Given the uniform cylindrical pores of ~4.0 Å diameter (Figure 4.1C), in either case, there should be substantial gas accessible spaces (PLATON solvent accessible void = ~40 %). Importantly, in the activated structure, the pore is functionalized simultaneously with the amine, pyridyl, open Zn and hydroxyl sites (Figure 4.1C).

The bulk phase purity of the as made MOF was verified by powder X-ray diffraction (XRD) (Figure 4.2A). The DMF molecules in the as-synthesized MOF could be exchanged with DCM/MeOH without any crystallinity loss as confirmed from the intact PXRD profile (Figure 4.A2). Thermogravimetric analysis displays a 24 % mass loss due to a two-step solvent loss (30° to 280 °C) and the MOF is thermally stable up to 370 °C (Figure 4.2B). The first mass loss up to 100 °C is due to the evaporation of surface trapped moisture and washing methanol, while the second loss observed from 100-350 °C is due to the loss of the guest DMF and water molecules present in the pore of IISERP-MOF23. Thus, different solvents treated MOF samples could be activated at 180 °C (Figure 4.A4). Infrared spectra (IR) for IISERP-MOF23 gave the characteristic peaks for the ligand-carboxylates, Cu-O, Cu-N, C-H and N-H (free amine) stretching and bending vibrations (Figure 4.2C). SEM-imaging shows rod shape crystals of as made IISERP-MOF23. Elemental mapping using energy dispersive X-ray analysis (EDXA) for IISERP-MOF23 showed a homogenous distribution of different elements present in the entire MOF sample (Figures 4.3-4.4).
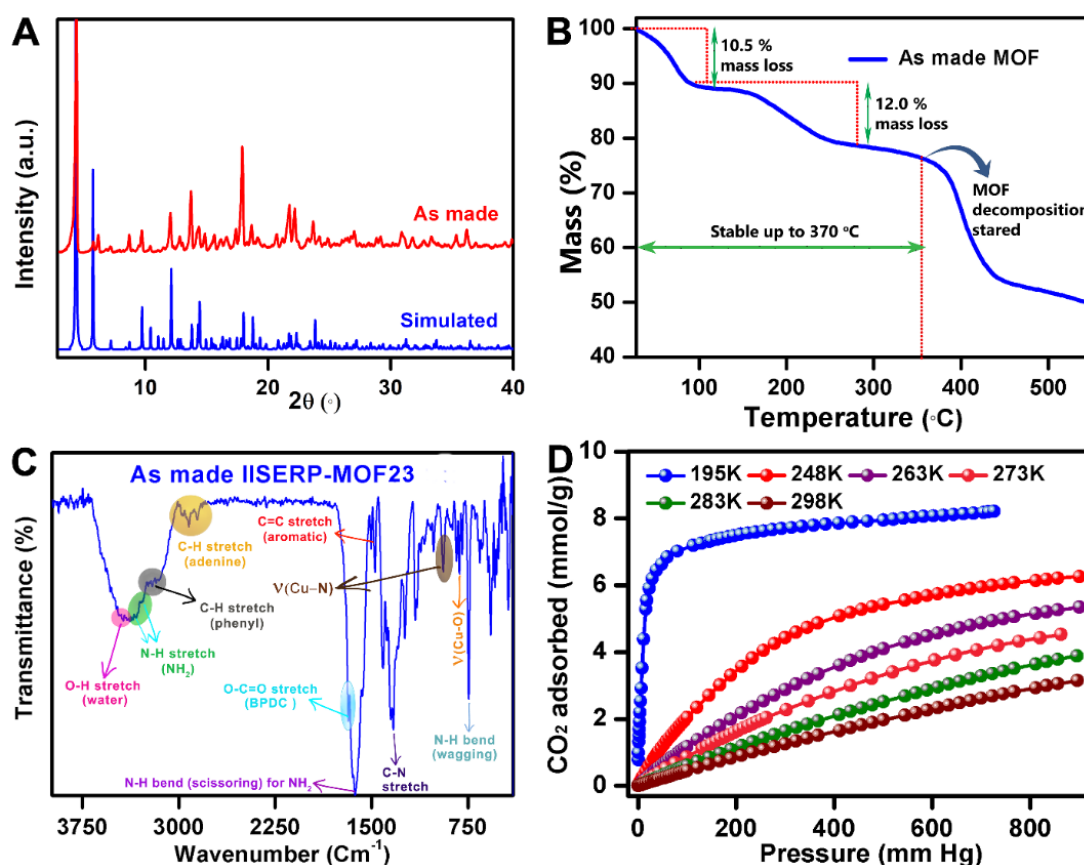
Figure 4.2. (A) PXRD profile of as synthesized IISERP-MOF23 with that simulated pattern found from single crystal X-ray diffraction. (B) TGA plot of the as-made IISERP-MOF23 carried out from 25 to 550 °C under N_2. A two-step mass loss is observed from room temperature to 300 °C. First mass loss (10.5 %) below 100 °C is due to the surface adsorbed moisture and low boiling washing methanol. So, second mass loss due to pore solvents was calculated to be 13.5 % and corresponding observed value was 12.0 % in TGA. The mass loss has been calculated using the formula $Zn_4(Ad)_3(BPDC)_2(H_2O)_6(DMF)\cdot(OH)$. (Mol. mass. 1193.4 g/mol). (C) IR spectra are showing characteristic selective peaks for the free $-NH_2$, Cu-N, Cu-O, functionalities, and O-H of water of IISERP-MOF23 referenced to KBr. (D) CO_2 isotherms at different temperature for the IISERP-MOF23.
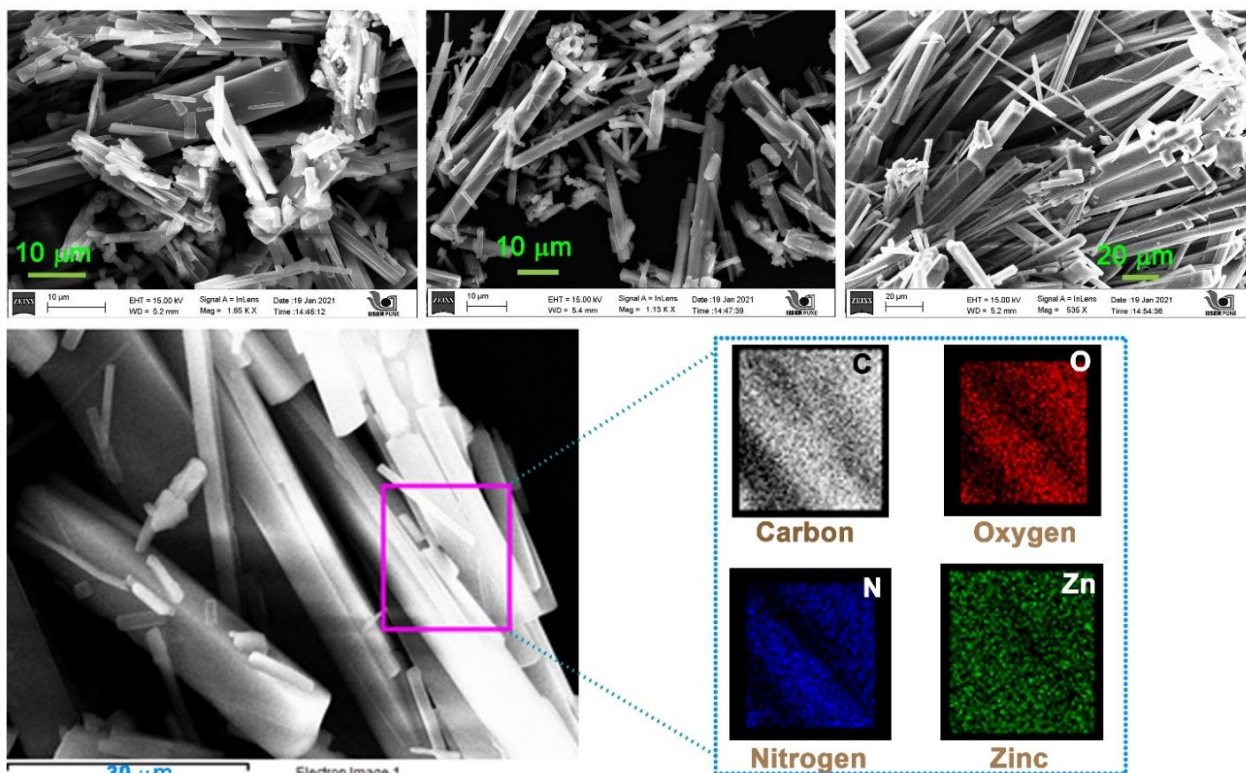
Figure 4.3. Above: Three images show the rod shape morphology of the IISERP-MOF23. Bottom: Images show the elemental mapping using Energy-dispersive X-ray analysis (EDXA) technique that shows homogeneous distributions of the different elements in the selected area (pink line) present in the IISERP-MOF23.

Element	Weight %	Atomic %
C K	46.09	59.35
N K	22.06	24.36
O K	11.99	11.59
Zn L	19.86	4.70
Totals	100.00	
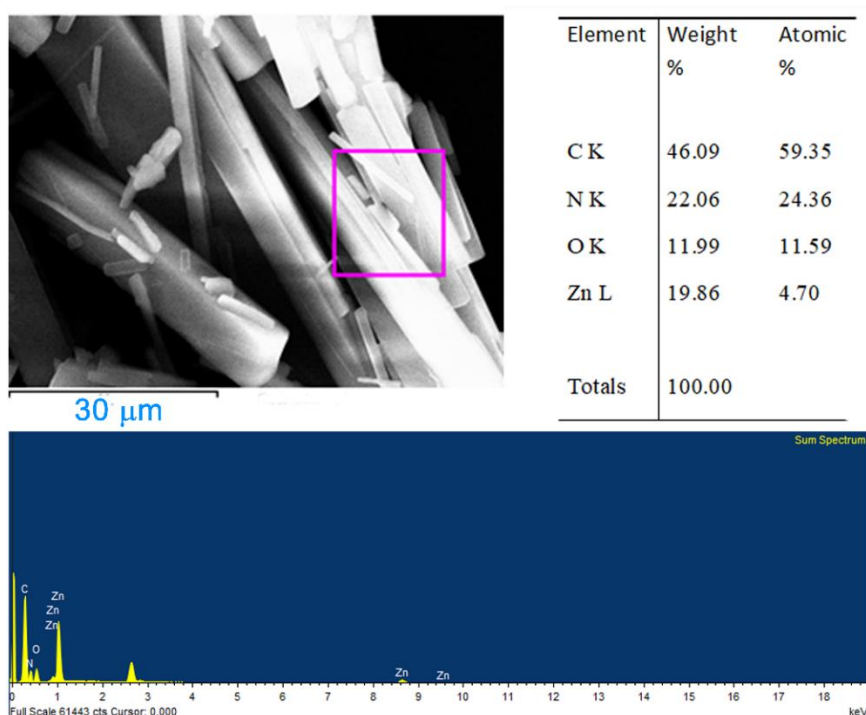
Figure 4.4. SEM-elemental analysis of IISERP-MOF23 using the Energy-dispersive X-ray analysis (EDXA) analysis.

The IISERP-MOF23 exhibits permanent porosity towards N_2 (77K) (Figure 4.A4) and CO_2 (195K) (Figure 4.2D) yielding a type-I isotherm characteristic of ultra-microporous MOF. A BET-surface area of 360 m^2 g^{-1} was obtained from 273 K CO_2 adsorption (Figures 4.2D, 4.A5 and 4.A6) isotherm, which is good for a MOF of small pore size. The pore width obtained from a NLDFT fit of N_2 77 K sorption isotherm yeilded one major pore size of 5.7 Å (Figure 4.5). This pore size matches reasonably with the pore width deduced from the X-ray crystallography structural data analysis. Interestingly, the 195 K CO_2 uptake is 8.2 mmol g^{-1} which is almost double that of the saturation uptake observed for N_2 (cf. 77 K N_2 isotherm, Figure 4.A4) at 77 K. A room temperature CO_2 uptake of 3.3 mmol g^{-1} (Figure 4.2D) and the negligible N_2 uptake (Figure 4.6) under the same conditions means that the MOF could be a potential CO_2 separation sorbent. Considering the richness of CO_2-interacting functional groups and binding sites in the pore wall, strong CO_2-framework interactions reflecting in the sharp uptake at low P/P_0 was expected. In fact, the original design of the MOF was aimed not only at capturing the CO_2 but to activate them through these strong binding sites embedded within the confinement of the small ultra-micropores. Surprisingly, it was not the case; the virial model showed that the zero-loading HOA was only about 22 kJ mol^{-1} (Figure 4.7) and this remained constant through out the CO_2 loading, which can be explained by the fact that we have a uniformly functionalized tunnel-like pores in the framework. However, such a moderate HOA from this highly Lewis-base and Lewis-acid site functionalized pore flouts the presence of periodically positioned attractively interacting groups all along the wall. A plausible explanation for this can be pursued from the single crystal structure of the MOF. There are many very closely spaced electron-rich CO_2-binding amines decorating the pore wall. With such an arrangement, say the δ-ve amine group (lone-pair) could attract the δ+ve carbon pole of quadrupolar CO_2, however, undesirably, the proximally positioned adjacent amine could be repelling the δ-ve oxygen pole of the same CO_2. This weakens the overall framework-CO_2 interactions leading to a moderate HOA. This hypotheis requires intense modeling to gain a foot and we will seek some computational collaboration do substantiate this.
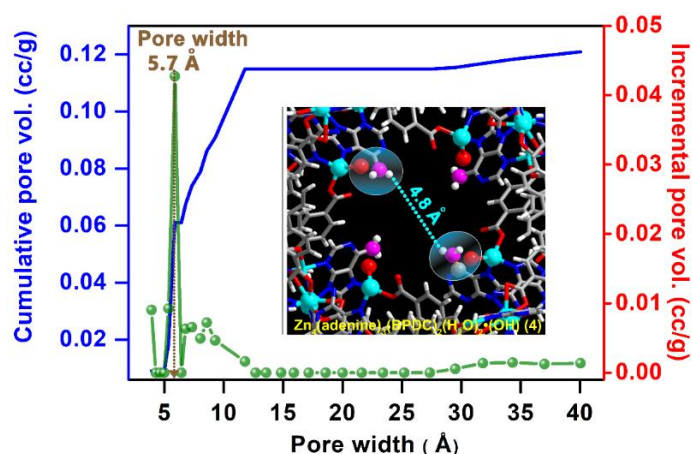
Figure 4.5. The figure shows the pore size distribution of IISERP-MOF23 (DFT pore-size) from 77 K N_2 sorption isotherm. Inset of the figure shows pore width determined from X-ray crystallographic structure along the c-direction. Cavity width calculated from the 77 K N_2-sorption approximately matched with the crystallographically obtained pore size.

IISER-MOF23 showed no uptake for N_2 at 298 K (Figure 4.6). This inspired us to calculate the IAST CO_2/N_2 selectivity for IISERP-MOF23 at 273 K and 298 K with a composition of $15CO_2:85N_2$ which are a composition of the flue gas, respectively. The CO_2/N_2 selectivities for the MOF was calculated to be 259-253 and 216-157 at 298 and 273 K (Figures 4.8) respectively. Importantly, IISERP-MOF23 has very smooth adsorption-desorption characteristics as evidenced from the TGA on-off cycling experiments, the results of that can be understood from Figure 4.9. In the TGA-cycling process, the CO_2 uptake is recycled up to ~4.5 % by mass at 35 °C. This ease of CO_2 removal is attributed to the optimal CO_2-framework interactions (HOA = 22 to 23 kJ mol^{-1}, optimal for a pressure swing)[13] for facile regeneration of CO_2 from the framework.
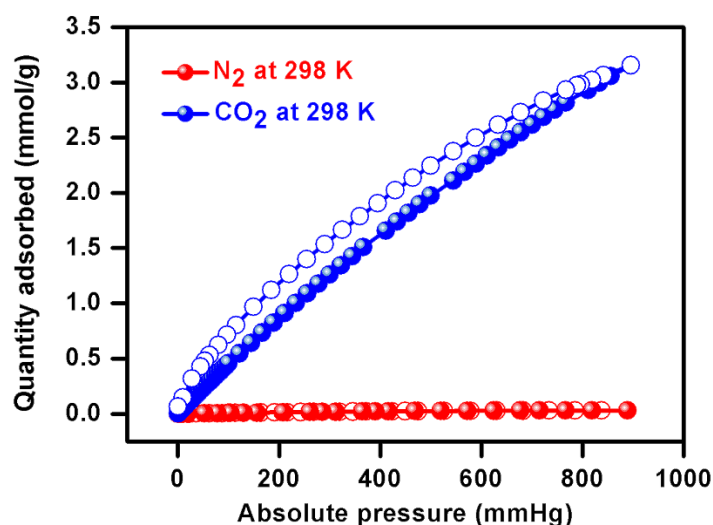
Figure 4.6. N_2 and CO_2 sorption/desorption isotherms at 298 K showing the selectivity of IISERP-MOF23 towards CO_2 at 298 K.
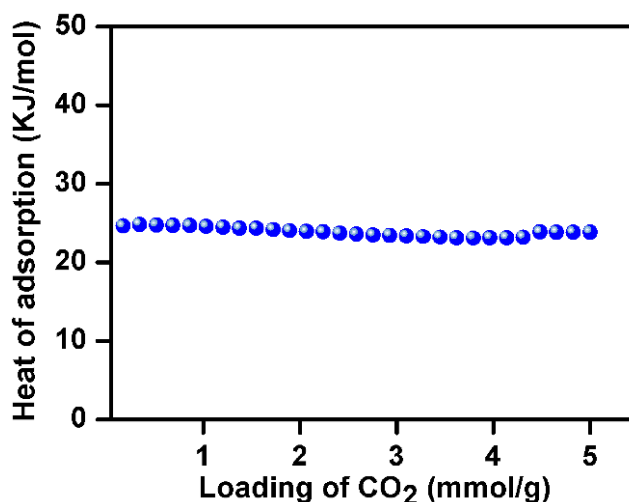
Figure 4.7. Heat of adsorption for CO_2 in IISERP-MOF23.
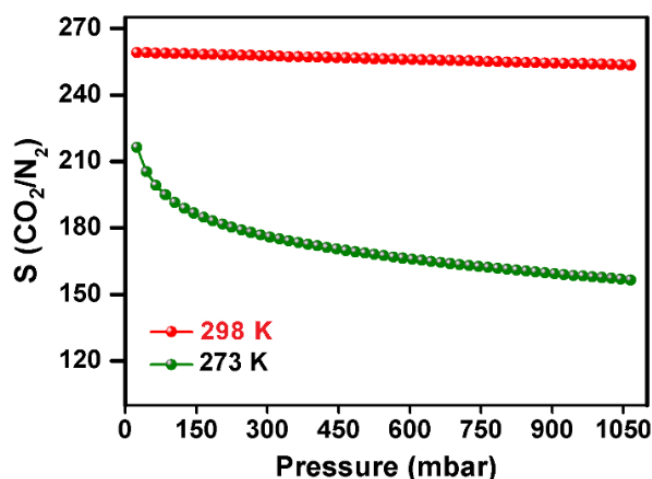
Figure 4.8. CO_2/N_2 selectivity obtained using IAST at 298 K and 273 K, respectively with a nominal composition of $15CO_2:85N_2$.
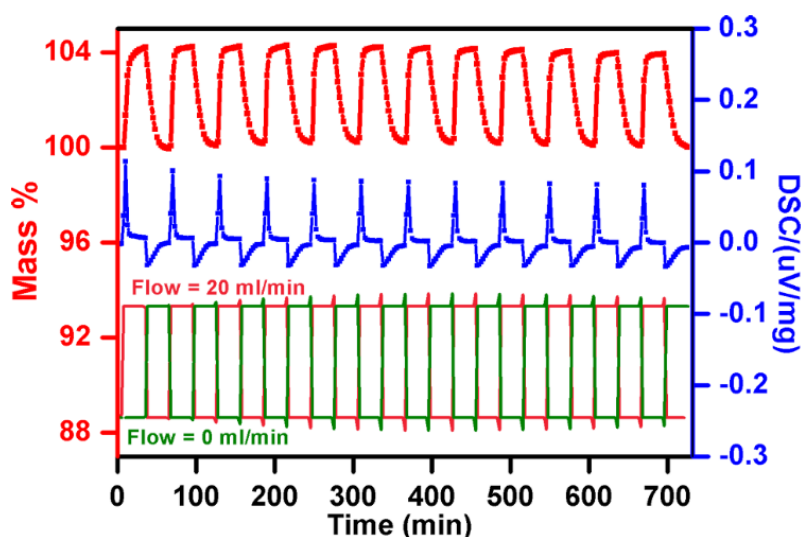
Figure 4.9. TGA cycling data on IISERP-MOF23 was carried out at 298 K.

4.4. Stability studies:

Importantly, IISERP-MOF23 have good CO_2 uptake capacity even after 6 months of keeping on the shelf (Figure 4.10), and crystallinity also remained intact after various solvents exchange/soaking and repeated adsorption-desorption cycles (Figure 4.11). For confirming the moisture stability of IISERP-MOF23, it was subjected to a flow of humid N_2 (75 % RH) for various time intervals (12-72 hours), and every time PXRD was recorded for the humidity treated MOF. The MOF exhibits excellent humidity/hydrolytic stability as evidenced from the intact PXRD profiles (Figure 4.12). This is owing to the nearly double-wall thick organic framework generated by the unique arrangement of the tetrameric Zn_4 clusters coordinations in the framework (Figure 4.1).
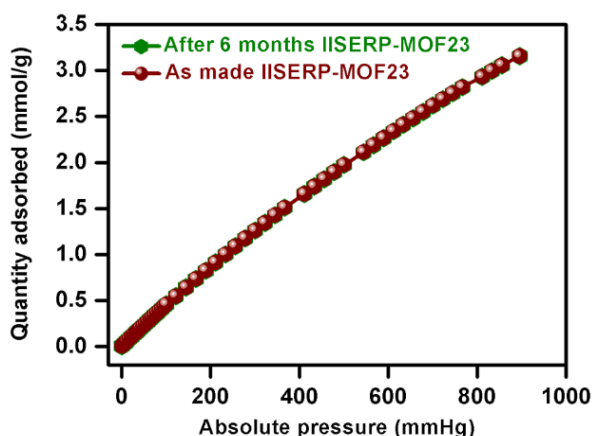
Figure 4.10. Stability studies: IISERP-MOF23 retains complete porosity even after 6 months keeping on shelf.
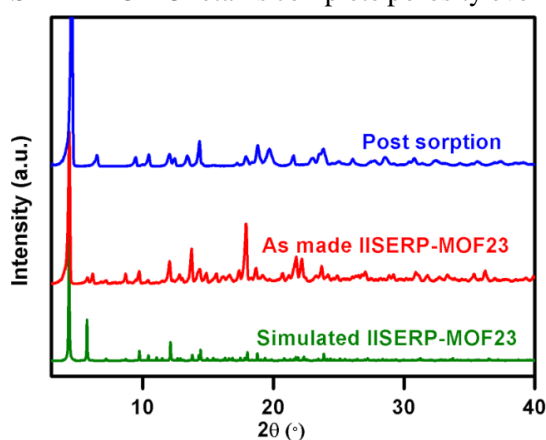
Figure 4.11. A comparative PXRD plot between the as-synthesized sample of IISERP-MOF23 and the sample obtained after all the gas adsorption measurements. This shows that the IISERP-MOF23 can retain its crystanility after the gas adsorption measurements. Note: The apparent appearance of some extra-peaks in the experimental PXRD of the as-made sample compared to the simulated pattern is entirely due to mismatched relative intensities, in fact, every peak in the experimental peak could be addressed to a marker position (of expected peak) in the simulated PXRD. This change in relative intensities is most likely due to the variation in the degree of solvation or some preferred orientation. Multiple batches yielded similar experimental PXRDs.
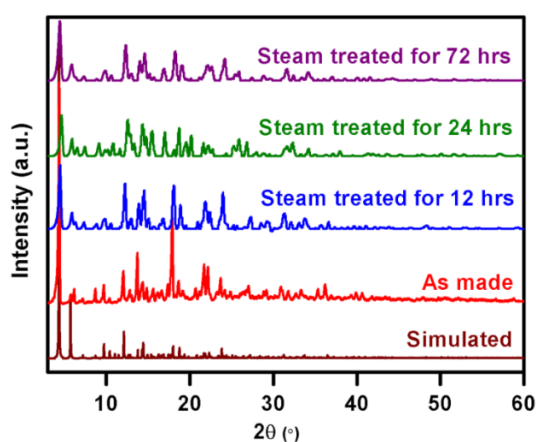
Figure 4.12. PXRD comparisons indicating the complete retention of crystallinity by IISERP-MOF23 after exposure to the humid environment, the sample was exposed to a flow of moist N_2 (with 75 % RH) for about 12, 24, and 72 hrs.

4.5. Comparison with other electron-rich functional group-containing MOFs:

Here, for comparative study we have chosen a list of reported aminotriazole, diaminotiazole, and adenine-based MOFs along with the IISERP-MOF23 (Table 4.1). The adenine-based $Zn_4(Ad)_3(BPDC)_2(H_2O)_2 \cdot (OH)$ (IISERP-MOF23), poses a relatively superior CO_2 interactive environment by having a free hydroxyl group within the amine and bare-metal lined pores. Notably, the amine-lined 1-D pores in this MOF closely resemble the 1-D channels in the Zur Loye's Zn-trizolate-fluoride MOFs in both size and shape. The major structural difference is in the pore environment; in IISERP-MOF23, the amine groups lining the pore is positioned next to pyridyl nitrogen (from adenine) and the open Zinc site and has a free hydroxyl ion in the pore, while in Zur Loye's MOF, the amine groups adjacent to a μ^2-briding fluoride group. In contrast to the latter, which does not exhibit any tendency to adsorb CO_2 at room temperature, IISERP-MOF23 shows a ~3.3 mmol g^{-1} of CO_2 uptake at 25 °C and 1 bar Among other reported adenine-based MOFs containing free amine groups, bio-MOF-1 loaded with diamino guanidinium cations and the guest-free bio-MOF-11 showed high CO_2 uptakes (5.13 mol g^{-1} and 4.68 mmol g^{-1}, respectively, at 273 K). The uptake by the guanidinium loaded framework is impressive but getting same CO_2 uptake for the amine-cation loaded MOFs (obtained via post synthetic loading) across the multiple batches is bit of a difficult job. Interestingly, the guest-free bio-MOF-11 has relatively high HOA (33.1 kJ mol^{-1}) compared to the diamino guanidinium cations containing bio-MOF-1 (24.2 kJ mol^{-1}). Notably, the bio-MOF-13 showed the highest HOA (40.5 kJ mol^{-1}) among all the adenine based-MOFs. Unfortunately, all the bio-MOFs exhibit a poor CO_2/N_2 selectivities as evidenced by their IAST evaluations. In this context, IISERP-MOF23 possess a moderate HOA (zero loading HOA = 22 kJ mol^{-1}) over entire loading of CO_2. Importantly, all the bio-MOFs have good water-stability due to having metal-adeninate linkages in their frameworks, which is a concept borrowed in the construction of the IISERP-MOF23. During CO_2 adsorption on IISERP-MOF23, CO_2 molecules are influenced by the attraction force of the mentioned binding sites as well as by the repulsion force of adjacent electron-rich free amine in the closely positioned in the MOF backbone (pore-width = 4.8 Å). Hence HOA (22 kJ mol^{-1}) was found to be moderate for IISERP-MOF23. It has also good CO_2/N_2-selectivity (253, using $15CO_2$: $85N_2$ composition) at 298 K and 1 bar pressure. However, all the structural advantages and very good performance taking into account, the adenine containing IISERP-MOF23 can play a superior role in CO_2 capture and separation process. Importantly, the IISERP-MOF23 displays exceptional shelf-life, moisture and steam stability which most probably arises from the thickly-walled organic framework provided by the uniquely positioned Zn_4 clusters.

Table 4.1. The comparison of IISERP-MOF23 with other functional MOFs in terms of performance.

MOFs	Surface area in m^2 g^{-1} (pore size in Å)	CO$_2$ Uptake (mmol g^{-1})	HOA (kJ mol^{-1})	*IAST* Selectivity at 298 K and 1 bar	Reference
ZnDATzF	-	-	-	-	*J. Solid State Chem.* **2005**, *178*, 2511.
ZnATzF	-	-	-	-	*J. Am. Chem. Soc.* **2004**, *126*, 3576.
Zinc-Adeninate Macrocycle: Zn$_6$(Ad)$_6$(Py)$_6$(DMC)$_6$•10.5DMF Ad = adenine, Py = pyridine, DMC = dimethyl carbamate	Pore size = 5 × 20 Å	~3.6 at 273 K	~21	-	*J. Am. Chem. Soc.* **2009**, *131, 24*, 8401–8403.
bio-MOF-1: [(Zn$_8$O(Ad)$_4$(BPDC)$_6$]•2(DMA$^+$) Ad = adeninate, BPDC = 1,4-biphenyldicarboxylate, DMA$^+$ = dimethylammonium cation	1630	3.93 at 273 K	24.2	-	*Chem. Commun.* **2013**, *49*, 11385--11387.
GND@bio-MOF-1 GND$^+$ = guanidinium cations	1640	4.82 at 273 K	28.8	-	*Chem. Commun.* **2013**, *49*, 11385--11387.
AmGND@bio-MOF-1 AmGND$^+$ = aminoguanidinium cations	1600	4.87 at 273 K	28.3	-	*Chem. Commun.* **2013**, *49*, 11385--11387.
DiAmGND@bio-MOF-1 DiAmGND$^+$ = diamino guanidinium cations	1500	5.13 at 1 bar and 273 K	24.2	-	*Chem. Commun.* **2013**, *49*, 11385--11387.
Bio-MOF-11: Co$_2$(Ad)$_2$(CH$_3$CO$_2$)$_2$	1148	4.68	33.1 (loading = 2.18 cm^3 g^{-1})	CO$_2$/N$_2$ (15/85) Selectivity = 43	*Chem. Sci.* **2013**, *4*, 1746–1755.
Bio-MOF-12: (Co$_2$(Ad)$_2$(CH$_3$CH$_2$CO$_2$)$_2$	1008	3.17	38.4 (loading =2.91 cm^3 g^{-1})	CO$_2$/N$_2$ (15/85) Selectivity = 52	*Chem. Sci.* **2013**, *4*, 1746–1755.

Bio-MOF-13: $Co_2(Ad)_2(C_3H_7CO_2)_2$	412	2.0	40.5 (loading =3.01 $cm^3 g^{-1}$)	CO_2/N_2 (15/85) Selectivity = 40	*Chem. Sci.* **2013**, *4*, 1746–1755.
Bio-MOF-14: $Co_2(Ad)_2(C_4H_9CO_2)_2$	17	1.38	N/A	-	*Chem. Sci.* **2013**, *4*, 1746–1755.
AD-MOF-1: $[Co_2(HAd)_2(Ad)_2(BA)]•DMF•$ $2H_2O$ HAd = adenine and BA = butanedioic acid	318.5490 (~6.5)	2.33 at 1 bar and 298 K	-	-	*Angew. Chem. Int. Ed.* **2019**, *58*, 5226 – 5231.
ADMOF-2: $[Co_2(HAd)_2(Ad)_2(IA)_2]•DMF$ IA = isobutyric acid	355.5497 (~6.5)	1.86 at 1 bar and 298 K	-	-	*Angew. Chem. Int. Ed.* **2019**, *58*, 5226 – 5231.
$Ni_3(PZDC)_2(HAd)_2(H_2O)_4$ $(H_2O)_{1.5}$ H_3PZDC = 3,5-pyrazole dicarboxylic acid and HAd = adenine	124.4	2.46 at 1 bar and 298 K	22.4	-	*Chem. Commun.* **2011**, *47*, 3389–3391.
$[DMA^+][Zn_4(ABTC)_2(Ad)H_2O)]$ $•4DMF$ ABTC = 3,3′,5,5′-azobenzene-tetracarboxylic acid DMA^+ = dimethyl ammonium cation	305	1.23 at 1 bar and 298 K	28.4	CO_2/CH_4 (50/50) Selectivity = 15.8	*Inorg. Chem. Commun.* **2016**, *69*, 20–23.
IISERP-MOF23 $Zn_4(Ad)_3(BPDC)_2)•(OH)$ $(H_2O)_6(DMF)$ Ad = adenine and BPDC = 4,4′-biphenyl dicarboxylate	360	3.3 at 1 bar and 298 K (CO_2/N_2 selectivity = 255 at 1 bar and 298 K.)	22	CO_2/N_2 (15/85) Selectivity = 253	*Manuscript under preparation*

4.6. Conclusion:

In summary, using the Approach-2 we have successfully designed and preared Zn-adeninate MOF that has not only steam/humidity stability but also high uptake and selectivity and moderate HOA. IISERP-MOF23 has highly functionalised pore decorated with many binding sites such as free -NH$_2$ and pyrimidine-N, OMS, and extra-framework hydroxyl ions. The binding sites and moderate HOA make CO$_2$ capture technique easy using this regenerable steam-stable MOF. Overall the study showed the low cost CO$_2$ capture ability of adeninate MOF that may open up new possibilities for economical large-scale CO$_2$ capture.

4.7. References:

1. (a) D. Singh, E. Croiset, P. L. Douglas, M. A. Douglas, *Energy Convers. Manage.* **2003**, *44*, 3073-3091; b) CO$_2$ Emissions from Fuel Combustion Highlights (2015 Edition) © OECD/IEA, 2015; c) CO$_2$ Capture from Existing Coal-Fired Power Plants (US DOE): South Park Township, 2007; d) L.-C. Lin, A. H. Berger, R. L. Martin, J. Kim, J. A. Swisher, K. Jariwala, C. H. Rycroft, A. S. Bhown, M. W. Deem, M. Haranczyk, *Nat. Mater.* **2012**, *11*, 633-641; e) T. C. Merkel, H. Lin, X. Wei, R. Baker, *J. Membr. Sci.* **2010**, *359*, 126-139; f) http://www.globalcarbonproject.org/ carbonbudget/ 17 /highlights.htm.

2. a) D. M. D'Alessandro, B. Smit, J. R. Long, *Angew. Chem. Int. Ed.* **2010**, *49*, 6058-6082; b) D. Ko, R. Siriwardane, L. T. Biegler, *Ind. Eng. Chem. Res.* **2003**, *42*, 339-348.

3. a) P. M. Bhatt, Y. Belmabkhout, A. Cadiau, K. Adil, O. Shekhah, A. Shkurenko, L. J. Barbour, M. Eddaoudi, *J. Am. Chem. Soc.* **2016**, *138*, 9301-9307; b) P.-Q. Liao, X.-W. Chen, S.-Y. Liu, X.-Y. Li, Y.-T. Xu, M. Tang, Z. Rui, H. Ji, J.-P. Zhang, X.-M. Chen, *Chem. Sci.* **2016**, *7*, 6528-6533; (c) H.-C. Zhou, J. R. Long, O. M. Yaghi, *Chem. Rev*. **2012**, *112*, 673-674; d) Y.-S. Bae, O. K. Farha, J. T. Hupp, R. Q. Snurr, *J. Mater. Chem.* **2009**, *19*, 2131-2134; e) Z. Zhang, Z.-Z. Yao, S. Xiang, B. Chen, *Energy Environ. Sci.* **2014**, *7*, 2868-2899; f) R. Vaidhyanathan, S. S. Iremonger, G. K. Shimizu, P. G. Boyd, S. Alavi, T. K. Woo, *Science* **2010**, *330*, 650-653; g) J. An, S. J. Geib, N. L. Rosi, *J. Am. Chem. Soc.* **2010**, *132*, 38-39; h) A. L. Dzubak, L.-C. Lin, J. Kim, J. A. Swisher, R. Poloni, S. N. Maximoff, B. Smit, L. Gagliardi, *Nature Chem.* **2012**, *4*, 810-816; i) A. Kumar, D. G. Madden, M. Lusi, K. J. Chen, E. A. Daniels, T. Curtin, J. J. Perry IV, M. J. Zaworotko, *Angew. Chem. Int. Ed.* **2015**, *54*, 14372-14377.

4. a) JJ.-R. Li, Y. Ma, M. C. McCarthy, J. Sculley, J. Yu, H.-K. Jeong, P. B. Balbuena, H.-C. Zhou, *Coord. Chem. Rev.* **2011**, *255*, 1791-1823; (b) N. T. Nguyen, H. Furukawa, F. Gándara, H. T. Nguyen, K. E. Cordova, O. M. Yaghi, *Angew. Chem.* **2014**, *126*, 10821-10824; (c) A. M. Fracaroli, H. Furukawa, M. Suzuki, M. Dodd, S. Okajima, F. Gándara, J. A. Reimer, O. M. Yaghi, *J. Am. Chem. Soc.* **2014**, *136*, 8863-8866; (d) H.-C. Zhou, S. Kitagawa, *Chem. Soc. Rev.* **2014**, *43*, 5415-5418; (e) S. Xiang, Y. He, Z. Zhang, H. Wu, W. Zhou, R. Krishna, B. Chen, *Nat. Commun.* **2012**, *3*, 1-9; (f) O. Benson, I. da Silva, S. P. Argent, R. Cabot, M. Savage, H. G. W. Godfrey, Y. Yan, S. F. Parker, P. Manuel, M. J. Lennox, T. Mitra, T. L. Easun, W. Lewis, A. J. Blake, E. Besley, S. Yang, M. Schröder, *J. Am. Chem. Soc.* **2016**, *138*, 14828-

14831; g) Q. Yang, S. Vaesen, F. Ragon, A. D. Wiersum, D. Wu, A. Lago, T. Devic, C. Martineau, F. Taulelle, P. L. Llewellyn, *Angew. Chem. Int. Ed.* **2013**, *52*, 10316-10320.

5.   a) Y. Kim, S. Huh, *CrystEngComm* **2016**, *18*, 3524-3550; b) C. Song, J. Hu, Y. Ling, Y. Feng, D.-L. Chen, Y. He, *Dalton Trans.* **2015**, *44*, 14823-14829; c) H.-M. Wen, H. Wang, B. Li, Y. Cui, H. Wang, G. Qian, B. Chen, *Inorg. Chem.* **2016**, *55*, 7214-7218; d) X.-Y. Li, L.-N. Ma, Y. Liu, L. Hou, Y.-Y. Wang, Z. Zhu, *ACS Appl. Mater. Interfaces* **2018**, *10*, 10965-10973; e) J. W. Maina, C. Pozo-Gonzalo, L. Kong, J. Schütz, M. Hill, L. F. Dumée, *Mater. Horiz.* **2017**, *4*, 345-361; f) R. Vaidhyanathan, S. S. Iremonger, G. K. Shimizu, P. G. Boyd, S. Alavi, T. K. Woo, *Science* **2010**, *330*, 650-653; g) S. Nandi, R. Maity, D. Chakraborty, H. Ballav, R. Vaidhyanathan, *Inorg. Chem.* **2018**, *57*, 5267-5272.

6.   a) X. Kong, E. Scott, W. Ding, J. A. Mason, J. R. Long, J. A. Reimer, *J. Am. Chem. Soc.* **2012**, *134*, 14341-14344; b) S. Wongsakulphasatch, W. Kiatkittipong, J. Saupsor, J. Chaiwiseshphol, P. Piroonlerkgul, V. Parasuk, S. Assabumrungrat, *Greenhouse Gas Sci Technol.* **2017**, *7*, 383-394; c) C. X. Chen, S. P. Zheng, Z. W. Wei, C. C. Cao, H. P. Wang, D. Wang, J. J. Jiang, D. Fenske, C. Y. Su, *Chem. Eur. J.* **2017**, *23*, 4060-4064; d) J. Qian, Q. Li, L. Liang, T.-T. Li, Y. Hu, S. Huang, *Dalton Trans.* **2017**, *46*, 14102-14106.

7.   aB. Liu, R. Zhang, C.-Y. Pan, H.-L. Jiang, *Inorg. Chem.* **2017**, *56*, 4263-4266; b) Y. Noori, K. Akhbari, *Rsc Adv.* **2017**, *7*, 1782-1808; c) Y. Cao, Y. Zhao, F. Song, Q. Zhong, *Journal of energy chemistry* **2014**, *23*, 468-474, d) Y. Ban, Z. Li, Y. Li, Y. Peng, H. Jin, W. Jiao, A. Guo, P. Wang, Q. Yang, C. Zhong, *Angew. Chem. Int. Ed.* **2015**, *54*, 15483-15487; e) Y.-S. Bae, B. G. Hauser, O. K. Farha, J. T. Hupp, R. Q. Snurr, *Microporous Mesoporous Mater.* **2011**, *141*, 231-235.

8.   P.-Q. Liao, H. Chen, D.-D. Zhou, S.-Y. Liu, C.-T. He, Z. Rui, H. Ji, J.-P. Zhang, X.-M. Chen, *Energy Environ. Sci.* **2015**, *8*, 1011-1016.

9.   R. Vaidhyanathan, S. S. Iremonger, G. K. Shimizu, P. G. Boyd, S. Alavi, T. K. Woo, *Science* **2010**, *330*, 650-653.

10. G. Kemmer, S. Keller, *Nat. Protoc.* **2010**, *5*, 267-281.

11. E. Richter, S. Wilfried, A. L. Myers, *Chem. Eng. Sci.* **1989**, *44*, 1609-1616.

12. A. L. Myers, J. M. Prausnitz, *AlChE J.* **1965**, *11*, 121-127.

13. J. M. Simmons, H. Wu, W. Zhou, T. Yildirim, *EnergyEnviron. Sci.* **2011**, *4*, 2177-2185.

4.A. Appendix:

4.A.1. X-ray Crystallographic structure determination:

Solvent composition of IISERP-MOF23 (1) using SQUEEZE and analytical data:

The solvent molecules (DMF and H_2O) in the pores of as-made IISERP-MOF23 crystals are disordered and their numbers to the X-ray diffraction patterns were estimated by using PLATON/SQUEEZE analysis methods.

a. *PLATON analysis:*

Total Potential Solvent Accessible Void Vol including charge balancing di-methyl ammonium cations (SOLV-Map Value) = 2742.00 $Å^3$

Unit cell volume, V = 27419.0 $Å^3$

Now, Void volume = (2742/27419) x 100 = 10.0 % of the IISERP-MOF23

Now, IISERP-MOF23 (**1**) has a cationic framework with hydroxyl anions (OH^-) per asymmetric unit. So, asymmetric unit or formula unit present in the crystal structure of the IISERP-MOF23 is $Zn_4(Ad)_3(BPDC)_2(H_2O)_2(OH)•(H_2O)_x(DMF)_y$, where, x = any integer represents no of water molecules and y = any integer represents no of DMA molecules.

Z for IISERP-MOF23 is 16.

Hence the unit cell formula is $Zn_{64}(Ad)_{48}(BPDC)_{32}(H_2O)_{32}(OH)_{16}•(H_2O)_{16x}(DMF)_{16y}$.

From squeeze result, electrons found in solvent Accessible Void = 1632. So, squeeze results suggest that 1632 electrons are present from solvent molecules in the unit cell.

So, per asymmetric unit 1215/16 = 76 = ~80 electrons are present and per formula unit also 76 electrons are present.

Considering 40 electrons for DMF and 10 for water, the best possible solvents combination and their electrons counts are given in table 3.A.1.

Table 4.A1. The number of Solvent molecules determination from PLATON analysis for IISERP-MOF23.

Cation and solvents combination	No of electrons from DMF	No of electrons from H_2O	Total electron counts
1 DMF + 4 H_2O	40	4 x 10 = 40	80

So, from *PLATON* analysis x = 4 and y = 1. Therefore, according to the *PLATON* analysis formula of asymetric unit or formula unit is:

$Zn_4(Ad)_3(BPDC)_2(H_2O)_2(OH)•(H_2O)_4(DMF)$ or $Zn_4(C_5H_4N_5)_3(C_{14}H_8O_4)_2(H_2O)_2(OH)•(H_2O)_4(C_3H_7NO)$.

And unit cell formula is $Zn_{64}(Ad)_{48}(BPDC)_{32}(H_2O)_{32}(OH)_{16}•(H_2O)_{64}(DMF)_{16}$ or

$Zn_{64}(C_5H_4N_5)_{48}(C_{14}H_8O_4)_{32}(H_2O)_{32}(OH)_{16} \bullet (H_2O)_{64}(C_3H_7NO)16$.
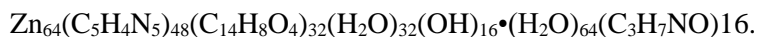
b. TGA analysis:

The molecular mass of formula unit, $Zn_4(C_5H_4N_5)_3(C_{14}H_8O_4)_2(H_2O)_2(OH) \bullet (H_2O)_4(C_3H_7NO) = 1338.4$ g mol^{-1}. Now mass loss due to solvents and DMA^+ cation is $(1338.4-1157.4) =$ g mol^{-1}. So, according to PLATON analysis mass loss is $(181/610.32)$ x $100 = \sim13.5$ % is expexted.

- Now, expected mass loss due to water = $(108/1338.4)$ x $100 = 8.0$ %,
- expected mass loss due to DMA solvent = $(73/1338.4)$ x $100 = 5.5$ % and

Now, from TGA,

- mass loss due to water and DMF solvent = 12.0 %

So, from TGA total mass loss due to solvents is 12.0 % which approximately matching with the value obtaine from *PLATON-SQUEEZE* analysis (13.5 %). Therefore, TGA analysis also supports the molecular formula of the formula unit or asymetric unit and unit cell obtained from the *PLATON* analysis.

Table 4.A2. Crystal structure information for the Non-squeezed and squeezed structure of IISERP-MOF23 obtained from SCXRD and *PLATON* analysis.

Parameters	Non-squeezed IISERP-MOF23	Squeezed IISERP-MOF23
Chemical formula	$Zn_4(Ad)_3(BPDC)_2(H_2O)_2(OH) \bullet (H_2O)_x(DMF)_y$	$Zn_4(Ad)_3(BPDC)_2(H_2O)_2(OH)$
Formula weight	1193.4 g mol^{-1}	441.32 g mol^{-1}
Crystal system	Tetragonal	Tetragonal
Space group	I41/a	I41/a
Unit-cell parameter	a = 40.5830 (22), b = 40.5830(22), c=16.6479(12), α= 90°, β= 90°, γ=90°, V = 27418.82 (29)	a = 40.5830 (22), b = 40.5830(22), c=16.6479(12), α= 90°, β= 90°, γ=90° V = 27418.82 (29)
Crystal colour and shape	Colorless rod shape	Colorless rod shape
Temperature	100 K	100 K
(Z)	16	16
Density (g cm^{-1})	1.13	1.16
Abs. Coeff. (mm^{-1})	2.028	2.041
F(000)	9360.0	9600.0
Reflection Data		
No. of reflections meas.	42281.0	42281.0
No. of uniq. reflections	9484.0	9484.0

No. of obs. reflections	6567.0	6567.0
λ (Å)	1.54178	1.54178
R_{merge}	0.071	0.071
Av. I/sig(l)	12.14	12.14
θ_{max}	65.3	72.8
θ_{min}	2.2	2.9
Refinement Data		
R_{all}	0.159	0.134
R_{obs}	0.119	0.1011
wR_2(all)	0.361	0.321
wR_2(obs)	0.334	0.294
Ext. Coeff.	0.0002	-
Goodness-of-fit (GOOF)	1.373	1.230
Largest diff. peak and hole: Delta-rho (eÅ^{-3})$_{max}$	7.043	6.248
Largest diff. peak and hole: Delta-rho (eÅ^{-3})$_{min}$	-1.570	-1.198

*Note. PLATON analysis suggests the presence of a substantial amount of solvent accessible voids in the structure of IISERPMOF23 ($Zn_4(Ad)_3(BPDC)_2(H_2O)_2(OH)\bullet(H_2O)_x(DMF)_y$). The solvents could not be modelled satisfactorily. From the *SQUEEZE* analysis was carried out to determine the number of DMF solvent and H_2O molecules. From squeezed electron counts and with the aid of feasible analytical method like TG analysis the solvent content was estimated. It was found that 1 DMF solvent and 4 water molecules present in each formula unit of IISERP-MOF23 ($Zn_4(Ad)_3(BPDC)_2(H_2O)_2(OH)\bullet(H_2O)_4(DMF)$). So, actual formula of IISERP-MOF23 is $Zn_4(Ad)_3(BPDC)_2(H_2O)_6(DMF)\bullet(OH)$.
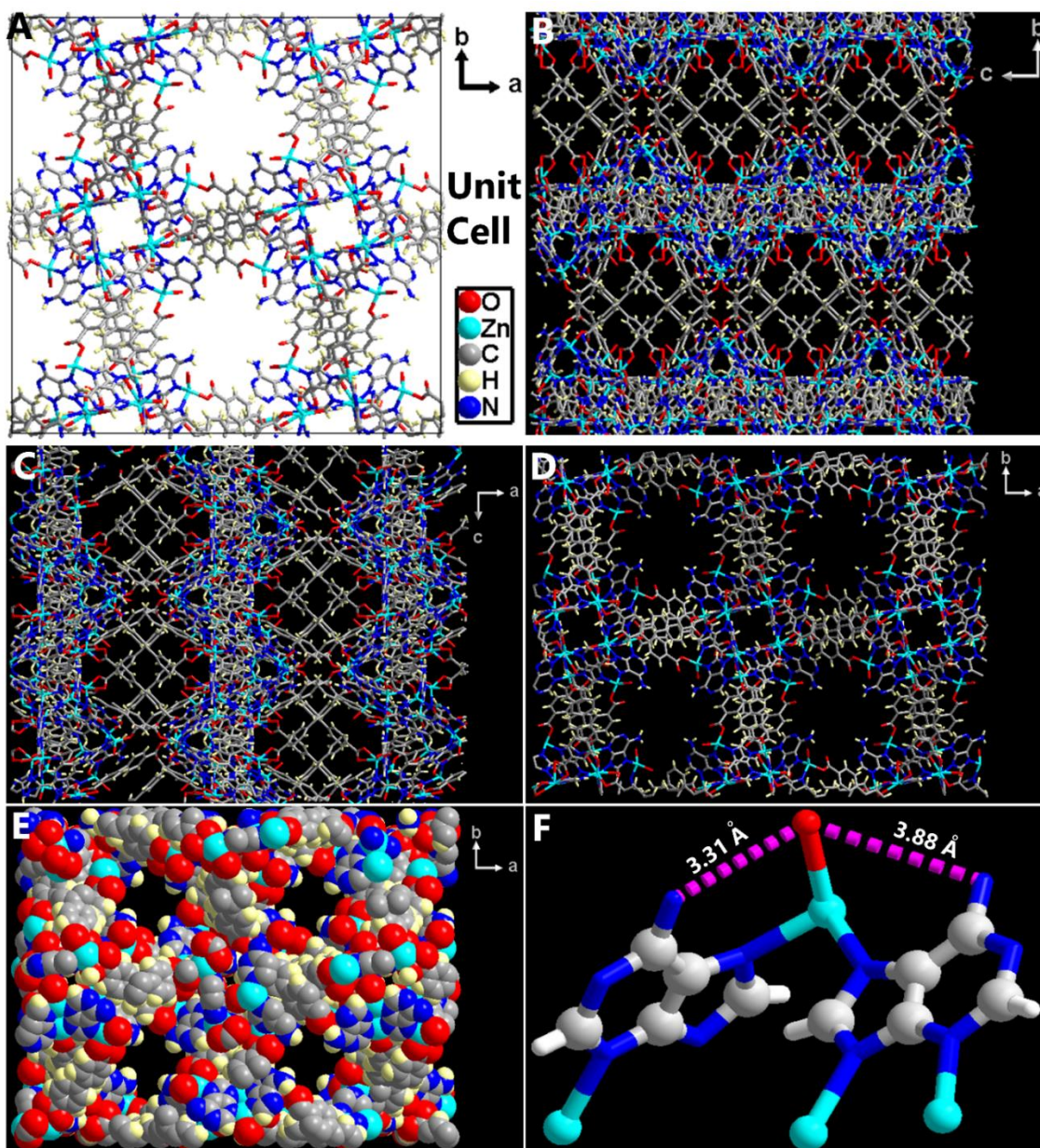
Figure 4.A1. (A) The unit cell of IISERP-MOF23. (B) View along a-axis, (C) View along b-axis, (D) View along c- axis, (E) Space-fill model along c- axis (without pore solvent molecules), and (F) Potential CO_2 adsorption sites in the MOF: Free amines and bare-metal site at Zn, if the coordinated water molecule (shown in red) is removed.

4.A.2. Analytical characterizations:

The phase purity of the MOF was confirmed by powder X-ray diffraction (XRD). It was found from the TG analysis that MOF has 24 % mass loss due to removal of solvent molecules from the pore. Thermal stability of MOF was examined using the TG analysis carried out from room temperature to 550 °C. There is a two-step gradual weight loss up to 250 °C due to water and DMF respectively. These high boiling solvents could be exchanged with DCM/MeOH and the MOF was stable up to 350 °C. After exchanging these high boiling solvents with DCM/MeOH no obvious change was found in the PXRD of MOF.
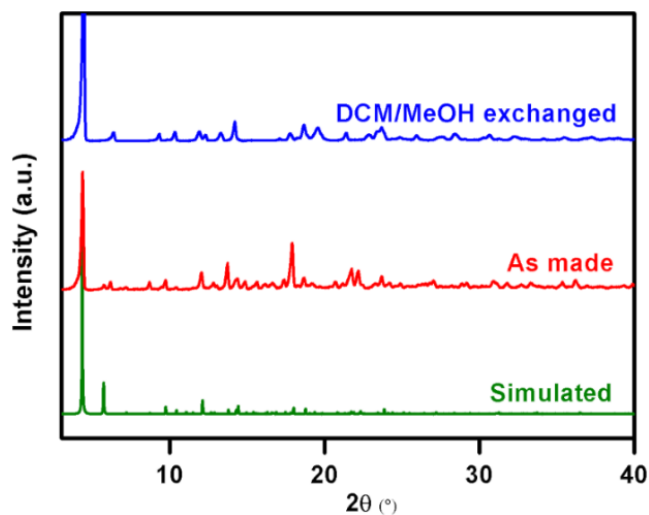
Figure 4.A2: Comparative powder X-ray diffraction patterns: simulated vs. experimental ones, after exchange with low boiling solvents and after activation.
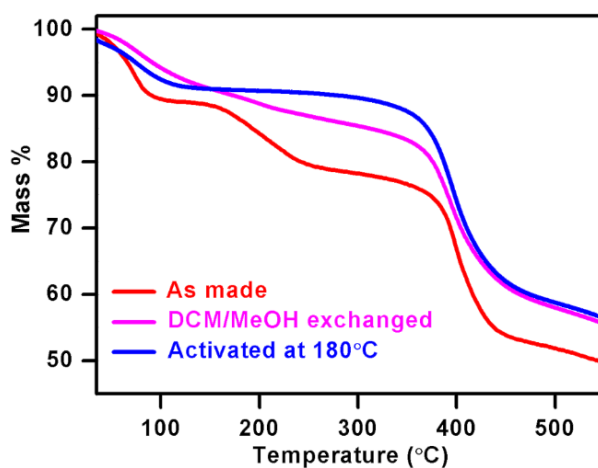
Figure 4.A3. Comparative TGA plots of IISERP-MOF23.

4.A.3. Adsorption Studies
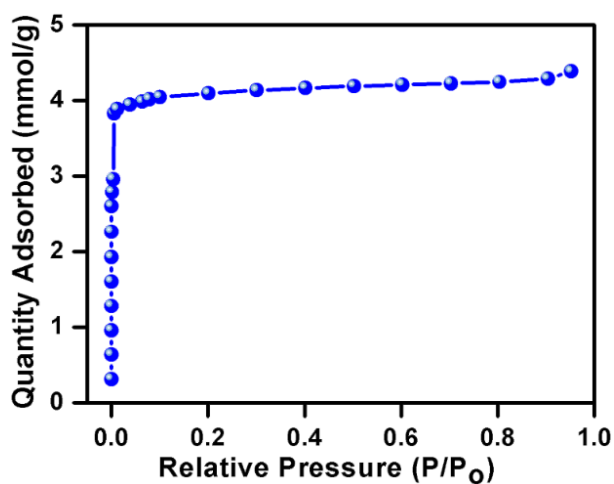
Figure 4.A4: N_2 adsorption isotherm of IISERP-MOF23 measured at 77 K.
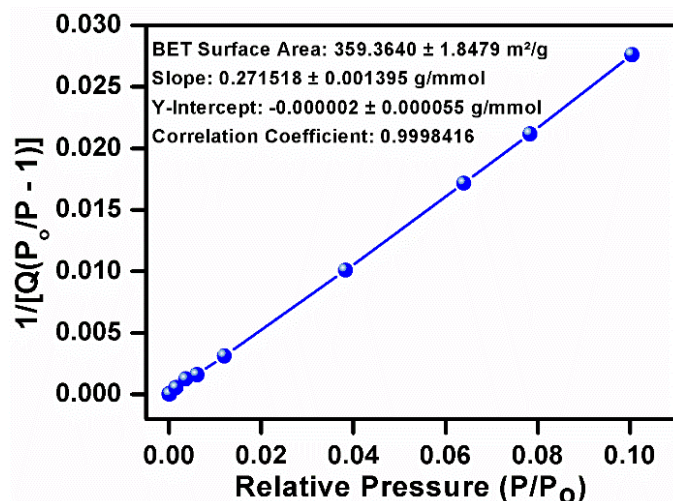
Figure 4.A5. BET fit for the IISERP-MOF23 from the 273 K CO_2 isotherm data.
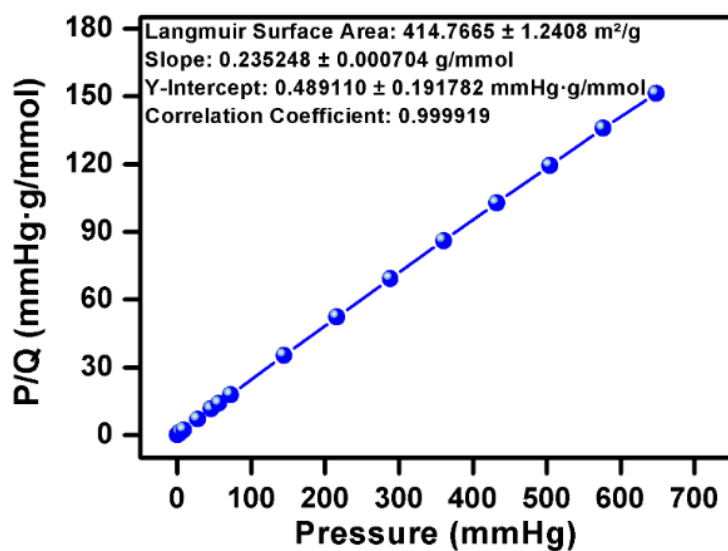
Figure 4.A6. Langmuir fit for the IISERP-MOF23 from the 273 K CO_2 isotherm data.
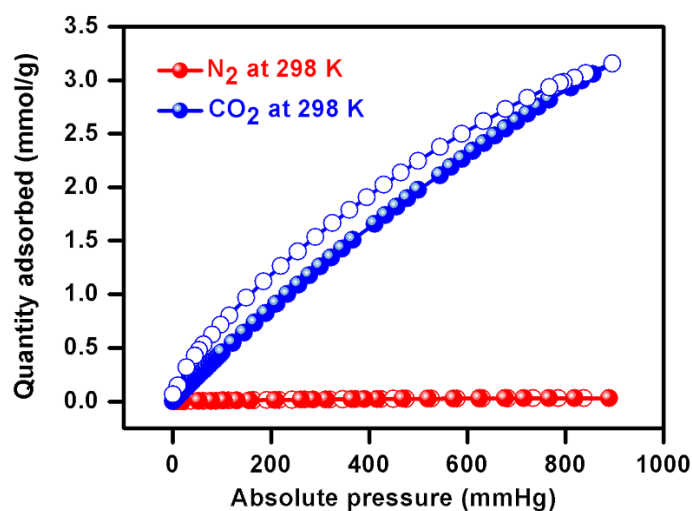
Figure 4.A7. CO_2 and N_2 adsorption isotherms at 298 K showing the selectivity of IISERP-MOF23 towards CO_2 at 298 K.
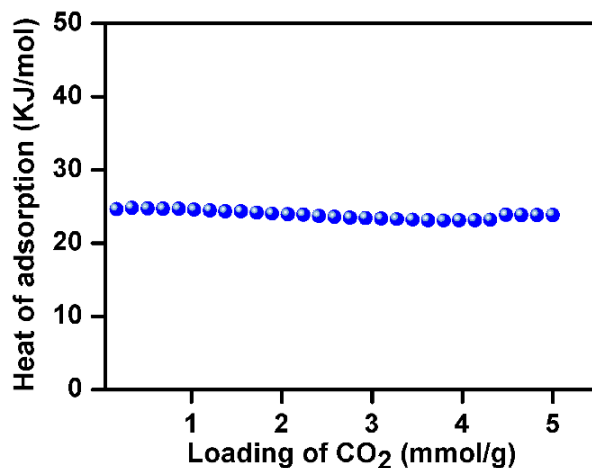
Figure 4.A8. Heat of adsorption for CO_2 in IISERP-MOF23.
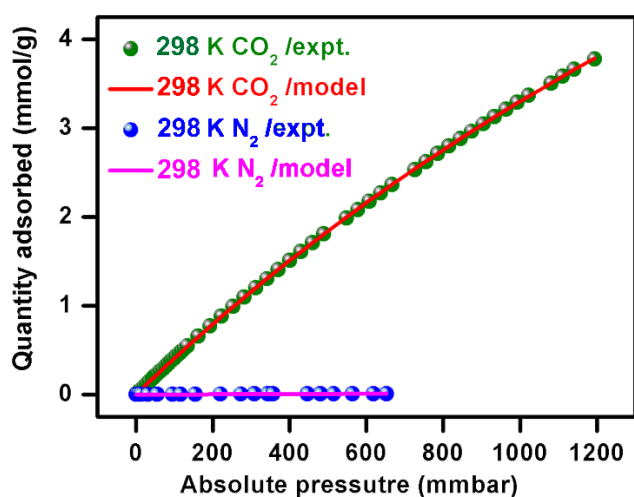
Figure 4.A9. IAST fitting of 298 K CO_2 and N_2 isotherms.

IAST selectivities:

CO_2/N_2 selectivity was calculated for IISERP-MOF23 using the experimental single component CO_2 and N_2 isotherms and ideal adsorbed solution theory (IAST) with a nominal composition of $15CO_2$:$85N_2$. At 1 bar total pressure, and 303 K, conditions of relevance to post-combustion CO_2 capture, it has an exceptional CO_2/N_2 selectivity of 258 which is descent for separation of mixture of CO_2 and N_2. This unusually high selectivity is due to ultra-low nitrogen uptake for the MOF at that temperature.

IAST fitting parameters for IISERP-MOF23 (CO_2/N_2):

At 298 K
Gas A = CO_2 and
Gas B = N_2

Table 4.A3. Fitted IAST parameters for CO_2/N_2 selectivity at 298 K for IISERP-MOF23.

Gas Mixture		Intrinsic Selectivity	
YA =	0.15	α_1 =	259.250413
YB =	0.85	α_2 =	0
Gas A Constants		**Gas B Constants**	
qA1 =	15.8267794	qA1 =	0.90637225
qA2 =	0	qA2 =	1.0068E-07
kA1 =	0.000263263	kA1 =	1.7732E-05
kA2 =	0	kA2 =	0.83908359
na1 =	1	na1 =	1.00000001
na2 =	0	na2 =	1
HA1 =	0.004166599	HB1 =	1.6072E-05
HA2 =	0	HB2 =	8.4476E-08

At 273 K
Gas A = CO_2 and
Gas B = N_2

Table 4.A4. Fitted IAST parameters for CO_2/N_2 selectivity at 273 K for IISERP-MOF23.

Gas Mixture		Intrinsic Selectivity	
YA =	0.15	α_1 =	259.250413
YB =	0.85	α_2 =	0
Gas A Constants		**Gas B Constants**	
qA1 =	5.671523397	qA1 =	1.47695365
qA2 =	6.135896585	qA2 =	8.9309E-08
kA1 =	0.000725884	kA1 =	2.3708E-05
kA2 =	0.000724282	kA2 =	0.93776436
na1 =	0.784739867	na1 =	1
na2 =	1.000141316	na2 =	1.00028412
HA1 =	0.004116867	HB1 =	3.5016E-05
HA2 =	0.004444121	HB2 =	8.3751E-08

Chapter 5

Summary and Future Perspective

5.1. Comparative study of the MOFs:

The thesis presents a systematic designing and evolution of MOFs as deliverables for selective CO_2 capture applications. In particular, the MOFs in the thesis, possess both humid/water stability and a variety of CO_2 binding sites for selective CO_2 capture. Results show that in IISERP-MOF24 CO_2 adsorption is guided by the confinement effect and its interaction with the extra-framework cation (Na^+) interactions. Hence, CO_2 uptake and selectivity are less, whereas due to a minimal number of interaction sites in micropores, it has optimal HOA (zero-loading HOA = 22 kJ mol^{-1}). Then, three different adeninate MOFs (Figure 5.1) and their gas capture abilities are discussed in Chapter-3 and Chapter-4. The IISER-MOF23 has a pore width of 4.8 Å, whereas there is a pore width of 7.0 Å and ~13 Å in IISER-MOF26 and IISERP-MOF27, respectively. Hence, the order of pore width is IISERP-MOF23 > IISERP-MOF26 > IISERP-MOF27. Now, the number of different types of binding sites are listed in table 5.1. So, considering different types and number of interactions and pore-size, the order of CO_2-framework interaction strength is IISERP-MOF23 > IISERP-MOF26 > IISERP-MOF27. Due to the presence of high-number density of CO_2 binding sites, the IISERP-MOF23 has the highest uptake and better selectivity compared to IISERP-MOF26 and IISERP-MOF27.
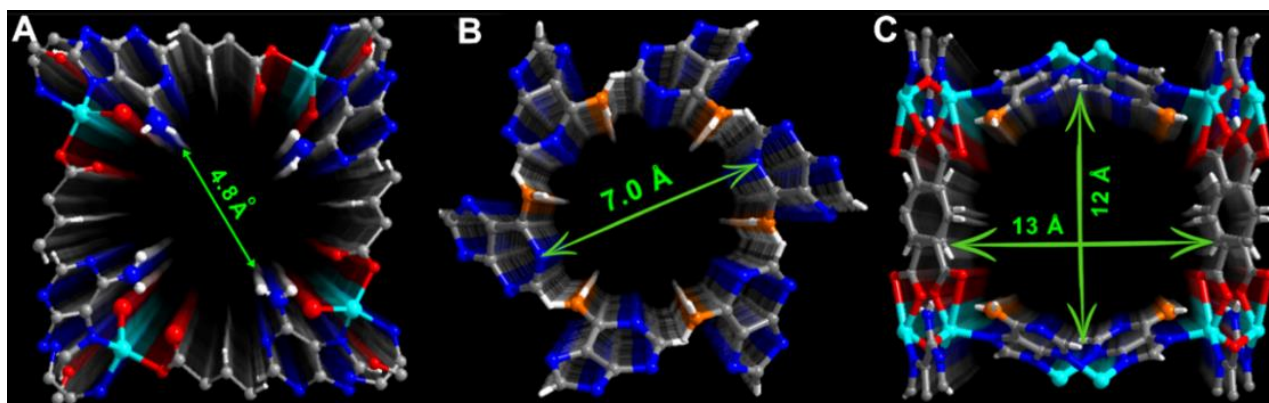
Figure 5.1. Unidirectional micro-pores present along the c-axis in the crystal structure of MOFs. (A) Pore dimension of IISERP-MOF26. (B) Pore dimension of IISERP-MOF26. The graphic shows pyrimidine-N (blue) and amine-N (orange) are pointed towards the pore. (C) The pore structure of IISERP-MOF27.

Table 5.1. The number of various CO_2-framework interaction sites present in the pore surface of MOFs.

Materials	Number of Free pyrimidine nitrogen	Number of Free amine (-NH$_2$) group	Number of free carboxylic O atoms	Number of Open metal site (OMS)	Total interaction sites
IISERP-MO23	4	4	4	4	16
IISERP-MOF26	6	6	-	-	12
IISERP-MOF27	4	4	-	-	8

As the number of interactions and pore size decreases from IISERP-MOF23 to IISERP-MOF27, the HOA value also decreases from IISERP-MOF23 to IISERP-MOF27 due to heavy confinement effect and strong interactions. So, the order of HOA is IISERP-MOF23> IISERP-MOF26> IISERP-MOF27. However, HOAs for all the MOFs presented in this thesis are moderate (18-22 kJ mol^{-1}) compared to other highly functionalized MOFs listed in Table 5.2. This is because the high density of CO_2 binding sites (Lewis basic pyrimidine N and free -NH_2 groups) inside the ultra-microporous MOF results in an attractive-repulsive pore environment. A plausible explanation for the moderate HOA despite richly functionalized pores can be pursued from the single crystal structure of the MOF. There are many very closely spaced electron-rich CO_2-binding amines decorating the pore wall. With such an arrangement, say the δ-ve amine group (lone-pair) could attract the δ+ve carbon pole of quadrupolar CO_2, however, undesirably, the proximally positioned adjacent amine could be repelling the δ-ve oxygen pole of the same CO_2. This weakens the overall interactions between the framework and the CO_2 leading to a moderate HOA. This hypothesis requires intense modeling to gain a foot and we will seek some computational collaboration do substantiate this. (Figure 5.2). But in MOFs with larger pore sizes, the CO_2 interacting functional groups are far spaced and this prevents too many repulsive interactions. Independently, presence of aliphatic amine in the MOF backbone also interacts very strongly (as liquid amine solution does for the chemi-sorption)
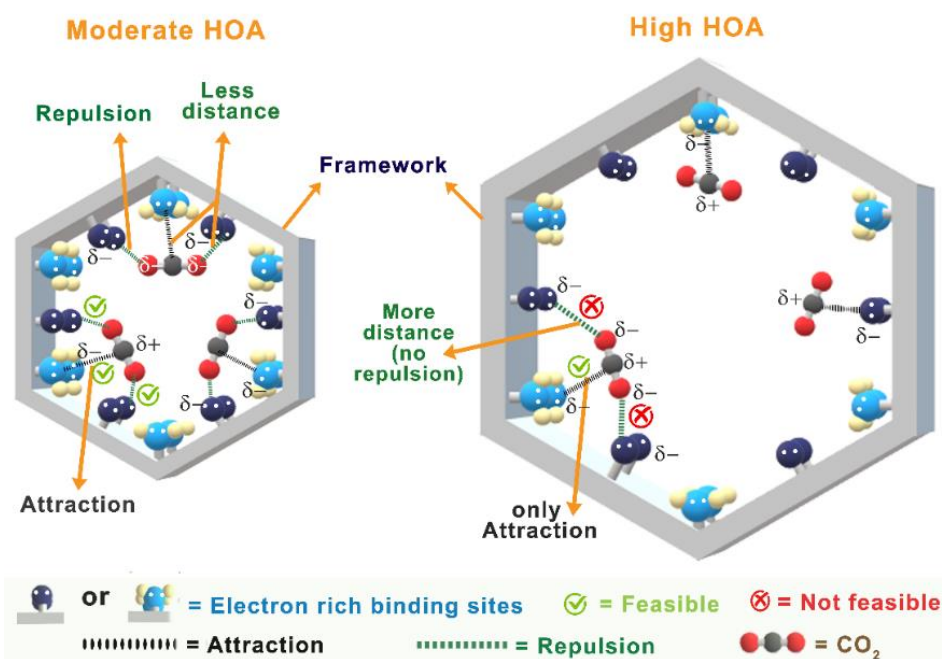
Figure 5.2. The schematic diagram showed the role of pore size on the heat of adsorption.

that not only increases the uptake but also the regeneration energy of CO_2 from the framework. This is might be due to the more availability of nitrogen-lone pair of aliphatic amines for interacting with the CO_2 molecules. Comparably, lone pair of aromatic-amine is less available due to its conjugation with aromatic ring and hence provides truly physisorptive interactions. Thus, aromatic amine such as adenine has better prospect to offer

moderate HOA. Due to the same electronic reason IISERP-MOF23-27, dmpn-Mg_2(dobpdc) and UiO-66-NH_2 has comparatively less HOA value than UiO-66-EA (*see* Table 5.2).

Table 5.2. A comparative table shows the surface areas and HOAs for various MOFs.

MOFs	Surface area ($m^2 g^{-1}$)	HOA ($kJ mol^{-1}$)	Reference
UTSA-16	6,000	~33	*Nat. Com.* **2012**, *3*, 954.
[$Co^{II}Co^{III}(OH)Cl_2(BBTA)$] ($H_2BBTA$ = 1H,5H-benzo(1,2-d:4,5-d0)bistriazole)	1,167	130 - 140	*Energy Environ. Sci.* **2015**, *8*, 1011-1016.
Mg-MOF-74 (Prepared by sonochemical method)	1640	42	*Energy Environ. Sci.* **2012**, *5*, 6465-6473.
[$V^{III}_2(OH)_2(L)$](MFM-300(VIII) LH_4=biphenyl-3,3′,5,5′-tetracarboxylic acid)	1,892	27.5–28	*Nat. Commun.* **2017**, *8*, 14212.
[$Al_2(OH)_2(L)$]($H_2O)_6$ (NOT-300-solvate; L = biphenyl-3,3′,5,5′ tetracarboxylate)	1,370	27–30	*Nat. Chem.* **2012**, *4*, 887.
CuTDPAT	1938	42.2	*Angew. Chem. Int. Ed.* **2012**, *51*, 1412-1415.
DMPN-Mg_2(DOBPDC) $DOBPDC^{4−}$ = 4,4′-dioxidobiphenyl-3,3′-dicarboxylate and DMPN = 2,2-dimethyl-1,3-diaminopropane	5770 (before grafting of diamine)	70	*J. Am. Chem. Soc.* **2018**, *140*, 18016−18031.
UiO-66-NH_2	1112	28	*Chem. Commun.* 2018, **54**, 13472-13490.
UiO-66-EA	567	66	*Chem. Commun.* 2018, **54**, 13472-13490.
Zr-FMA (MOF-801-P)	990	29	*Chem. Commun.* 2018, **54**, 13472-13490; *J. Am. Chem. Soc.* **2014**, *136, 4369-4381.*
IISERP-MOF23	360	22	*Manuscript under preparation*
IISERP-MOF24	771	22	*CrystEngComm, 2018, 20, 6088–6093.*
IISERP-MOF26	210.6	22	*Chem. Asian J.* **2019,** *14,* 3736 – 3741.
IISERP-MOF27	481.1	18	*Chem. Asian J.* **2019,** *14,* 3736 – 3741.
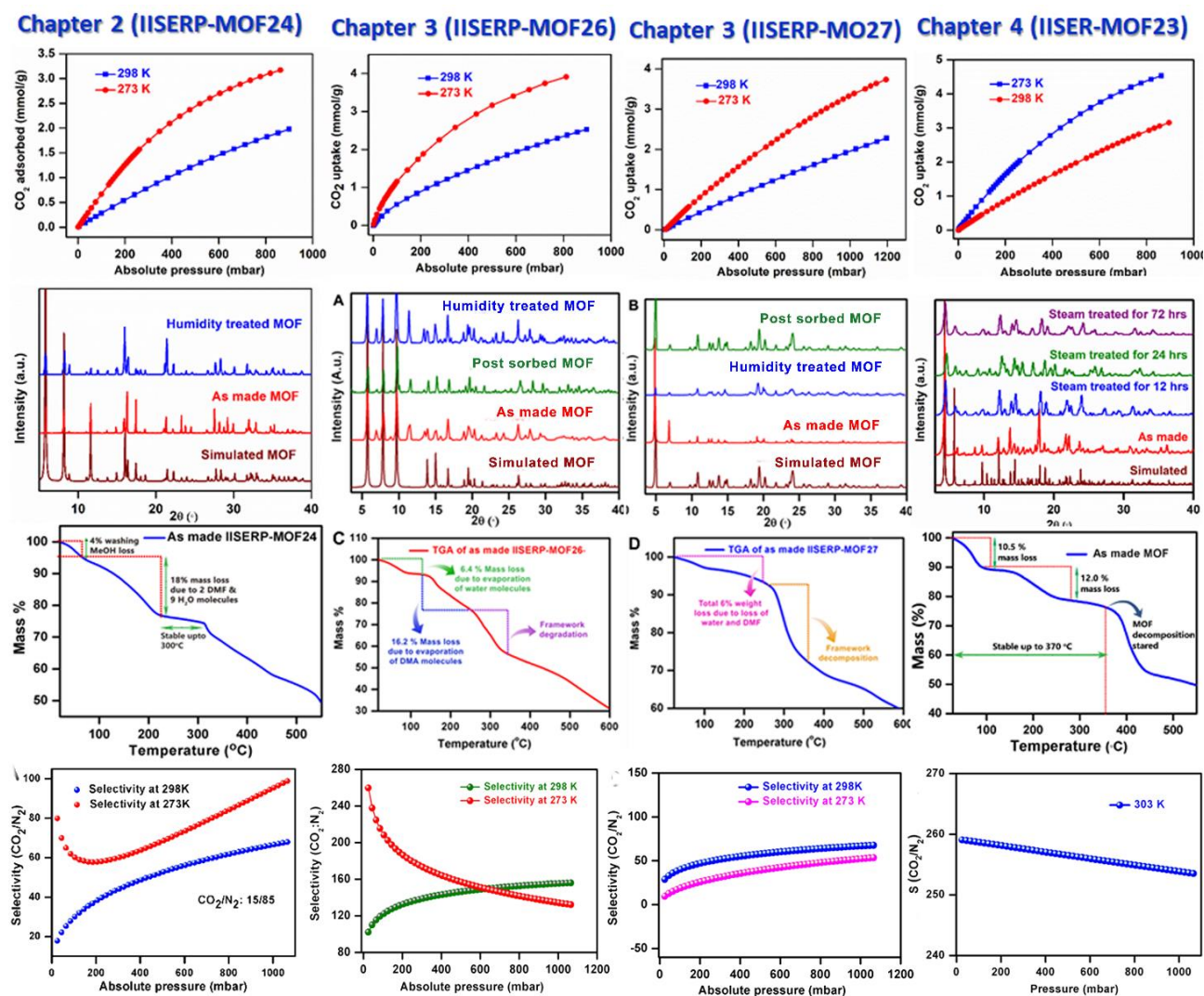
Figure 5.3. Schematic shows good uptake, stability (thermal and humidity stability), and sorption selectivity for CO_2 for all the MOFs included in the thesis.

Overall, following the two strategies, a range of water stable MOFs were synthesized for selective CO_2 capture, introducing moderate to good uptake, optimal HOAs, and high CO_2 selectivities (Figure 5.3). The comparison between the MOFs displays that IISERP-MOF23 has the most promising scope to be used in PSA processes of CCS. In conclusion, the CO_2 binding sites in the confined spaces and their strength of CO_2-binding are the most responsible factors for the cost-efficient separation at low pressure in PSA technology under CCS.

5.2. Summary and Future Perspective:

MOFs are new generation materials and show strong potential in physisorption based CO_2 capture and separation from flue gas. Due to having M-L bonds, most of the MOFs lose their crystallinity and durability in the presence of moisture. This thesis has brought ideas for building water/moisture stable frameworks, simultaneously increasing the number of CO_2-interacting sites in the pore for getting moderate to good uptakes. In the first part, high charged metal ions (hard metals) were combined with O-donor ligands (hard ligand) to generate humidity stable Lanthanide-MOFs (Ce-MOFs, and IISERP-MOF24). In the second part or approach, lower charged metal ions (soft metals) have been combined with azolate (adeninate) ligands, to form few water-stable adeninate-frameworks (IISERP-MOF23, IISERP-MOF26, and IISERP-MOF27). However, adeninate, as a smart linker, increases the water-stability of MOFs on one side and generates ultra-microporosity in the MOF providing good molecular sieving property of CO_2 over other gasses. Moreover, being a short linker with aromatic amine and nitrogen-rich centres, responsible for producing optimum HOA for facile regeneration of CO_2 from the framework-making capture process cost-efficient. So, the reported all MOFs (IISERP-MOF23, IISERP-MOF24, IISERP-MOF26, and IISERP-MOF27) have moderate to good uptake, excellent selectivities, and optimal HOAs. Therefore, adeninate frameworks with polar and ultra-micro pores and open-metal sites are suitable sorbents for CO_2 capture in a humid environment (Figure 5.4).
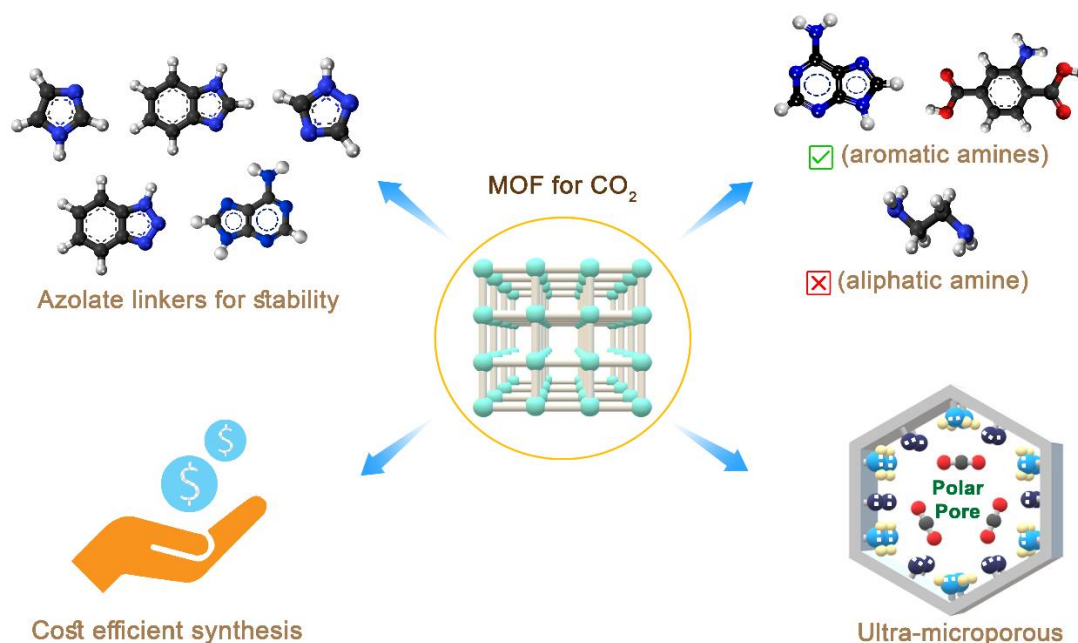
Figure 5.4. The coveted characteristics of MOFs expected to have for the size selective separation of CO_2 from flue gas mixture.

Rights and Permissions

Copyright Clearance Center Marketplace™

Order Confirmation

Thank you, your order has been placed. An email confirmation has been sent to you. Your order license details and printable licenses will be available within 24 hours. Please access Manage Account for final order details.

This is not an invoice. Please go to manage account to access your order history and invoices.

CUSTOMER INFORMATION

Payment by invoice: You can cancel your order until the invoice is generated by contacting customer service.

Billing Address

Mr. Rahul Maity
New Hostel2, IISER Pune, Pashan, Pune
Dr. Homi Bhabha Road
Near NCL Innovation Park
Pune, Maharashtra 411008
India

+91 7001322540
rahul.maity@students.iiserpune.ac.in

Customer Location

Mr. Rahul Maity
New Hostel2, IISER Pune, Pashan, Pune
Dr. Homi Bhabha Road
Near NCL Innovation Park
Pune, Maharashtra 411008
India

PO Number (optional)

N/A

Payment options

Invoice

PENDING ORDER CONFIRMATION

Confirmation Number: Pending

Order Date: 25-Jan-2021

1. Chemical science   0.00 USD

Order license ID	Pending	**Publisher**	Royal Society of Chemistry
ISSN	2041-6539		
Type of Use	Republish in a thesis/dissertation	**Portion**	Chart/graph/table/figure

LICENSED CONTENT

Publication Title	Chemical science	**Country**	United Kingdom of Great Britain and Northern Ireland
Author/Editor	Royal Society of Chemistry (Great Britain)		
Date	01/01/2010	**Rightsholder**	Royal Society of Chemistry
Language	English	**Publication Type**	e-Journal
		URL	http://www.rsc.org/Publishing/Journals/SC/Index.asp

REQUEST DETAILS

Portion Type	Chart/graph/table/figure	**Distribution**	Worldwide
Number of charts / graphs / tables / figures requested	1	**Translation**	Original language of publication
Format (select all that apply)	Print, Electronic	**Copies for the disabled?**	Yes
		Minor editing privileges?	Yes
Who will republish the content?	Academic institution	**Incidental promotional use?**	Yes
Duration of Use	Life of current edition	**Currency**	USD
Lifetime Unit Quantity	Up to 999		
Rights Requested	Main product		

NEW WORK DETAILS

Title	Crafting pore architecture of water-stable microporous MOFs for selective CO2 capture	**Institution name**	IISER Pune
		Expected presentation date	2021-03-01
Instructor name	Rahul Maity		

ADDITIONAL DETAILS

Order reference number	N/A	**The requesting person / organization to appear on the license**	Rahul Maity

REUSE CONTENT DETAILS

Title, description or numeric reference of the portion(s)	Figure 2	**Title of the article/chapter the portion is from**	Systematic modulation and enhancement of CO2 : N2 selectivity and water stability in an isoreticular series of bio-MOF-11 analogues
Editor of portion(s)	N/A		
Volume of serial or monograph	NA		
		Author of portion(s)	Royal Society of Chemistry (Great Britain)
Page or page range of portion	1749		
		Issue, if republishing an article from a serial	N/A

Publication date of portion	2010-01-01

Total Items: 1

Total Due: 0.00 USD

Accepted: All Publisher and CCC Terms and Conditions

Copyright Clearance Center Marketplace™

Order Confirmation

Thank you, your order has been placed. An email confirmation has been sent to you. Your order license details and printable licenses will be available within 24 hours. Please access Manage Account for final order details.

This is not an invoice. Please go to manage account to access your order history and invoices.

CUSTOMER INFORMATION

Payment by invoice: You can cancel your order until the invoice is generated by contacting customer service.

Billing Address

Mr. Rahul Maity
New Hostel2, IISER Pune, Pashan, Pune
Dr. Homi Bhabha Road
Near NCL Innovation Park
Pune, Maharashtra 411008
India

+91 7001322540
rahul.maity@students.iiserpune.ac.in

Customer Location

Mr. Rahul Maity
New Hostel2, IISER Pune, Pashan, Pune
Dr. Homi Bhabha Road
Near NCL Innovation Park
Pune, Maharashtra 411008
India

PO Number (optional)

N/A

Payment options

Invoice

PENDING ORDER CONFIRMATION

Confirmation Number: Pending

Order Date: 25-Jan-2021

1. Dalton transactions   0.00 USD

Order license ID	Pending	**Publisher**	ROYAL SOCIETY OF CHEMISTRY
ISSN	1477-9234		
Type of Use	Republish in a thesis/dissertation	**Portion**	Chart/graph/table/figure

LICENSED CONTENT

Publication Title	Dalton transactions	**Country**	United Kingdom of Great Britain and Northern Ireland
Author/Editor	Royal Society of Chemistry (Great Britain)	**Rightsholder**	Royal Society of Chemistry
Date	01/01/2003		
Language	English	**Publication Type**	e-Journal

REQUEST DETAILS

Portion Type	Chart/graph/table/figure	**Distribution**	Worldwide
Number of charts / graphs / tables / figures requested	5	**Translation**	Original language of publication
		Copies for the disabled?	Yes
Format (select all that apply)	Print, Electronic	**Minor editing privileges?**	Yes
Who will republish the content?	Academic institution	**Incidental promotional use?**	No
Duration of Use	Life of current edition	**Currency**	USD
Lifetime Unit Quantity	Up to 999		
Rights Requested	Main product		

NEW WORK DETAILS

Title	Crafting pore architecture of water-stable microporous MOFs for selective CO2 capture	**Institution name**	IISER Pune
		Expected presentation date	2021-03-01
Instructor name	Rahul Miaty		

ADDITIONAL DETAILS

Order reference number	N/A	**The requesting person / organization to appear on the license**	Rahul Miaty

REUSE CONTENT DETAILS

Title, description or numeric reference of the portion(s)	Figure 1, Figure 3, Figure 4, Figure 6, Figure 8B	**Title of the article/chapter the portion is from**	Humidity-induced CO2 capture enhancement in Mg-CUK-1
Editor of portion(s)	N/A	**Author of portion(s)**	Royal Society of Chemistry (Great Britain)
Volume of serial or monograph	N/A	**Issue, if republishing an article from a serial**	N/A
Page or page range of portion	15828,15830, 15831, 15832	**Publication date of portion**	2003-01-01

Total Items: 1

Total Due: 0.00 USD

Accepted: All Publisher and CCC Terms and Conditions

RightsLink®

Highly Efficient Synthesis of a Moisture-Stable Nitrogen-Abundant Metal–Organic Framework (MOF) for Large-Scale CO2 Capture

ACS Publications
Most Trusted. Most Cited. Most Read.

Author: Chao Chen, Qingbin Jiang, Huifang Xu, et al

Publication: Industrial & Engineering Chemistry Research

Publisher: American Chemical Society

Date: Jan 1, 2019

Copyright © 2019, American Chemical Society

JOHN WILEY AND SONS LICENSE
TERMS AND CONDITIONS

Jan 25, 2021

This Agreement between Mr. Rahul Maity ("You") and John Wiley and Sons ("John Wiley and Sons") consists of your license details and the terms and conditions provided by John Wiley and Sons and Copyright Clearance Center.

License Number	4995951065850
License date	Jan 25, 2021
Licensed Content Publisher	John Wiley and Sons
Licensed Content Publication	Angewandte Chemie
Licensed Content Title	Low-Energy Selective Capture of Carbon Dioxide by a Pre-designed Elastic Single-Molecule Trap
Licensed Content Author	Hong-Cai Zhou, Perla B. Balbuena, Gregory J. Halder, et al
Licensed Content Date	Sep 3, 2012
Licensed Content Volume	124
Licensed Content Issue	39
Licensed Content Pages	5

Type of use	Dissertation/Thesis
Requestor type	University/Academic
Format	Print and electronic
Portion	Figure/table
Number of figures/tables	5
Will you be translating?	No
Title	Crafting pore architecture of water-stable microporous MOFs for selective CO2 capture
Institution name	IISER Pune, India
Expected presentation date	Jan 2021
Portions	Figure 1, Figure 2, Figure 3, Figure 4a, and Figure S11
Requestor Location	Mr. Rahul Maity New Hostel2, IISER Pune, Pashan, Pune Dr. Homi Bhabha Road Near NCL Innovation Park Pune, Maharashtra 411008 India Attn: Indian Institute of Science Education and Research (IISER) Pune
Publisher Tax ID	EU826007151
Total	0.00 USD

Terms and Conditions

TERMS AND CONDITIONS

This copyrighted material is owned by or exclusively licensed to John Wiley & Sons, Inc. or one of its group companies (each a"Wiley Company") or handled on behalf of a society with which a Wiley Company has exclusive publishing rights in relation to a particular work (collectively "WILEY"). By clicking "accept" in connection with completing this licensing transaction, you agree that the following terms and conditions apply to this transaction (along with the billing and payment terms and conditions established by the Copyright Clearance Center Inc., ("CCC's Billing and Payment terms and conditions"), at the time that you opened your RightsLink account (these are available at any time at http://myaccount.copyright.com).

Terms and Conditions

- The materials you have requested permission to reproduce or reuse (the "Wiley Materials") are protected by copyright.

- You are hereby granted a personal, non-exclusive, non-sub licensable (on a stand-alone basis), non-transferable, worldwide, limited license to reproduce the Wiley Materials for the purpose specified in the licensing process. This license, **and any CONTENT (PDF or image file) purchased as part of your order,** is for a one-time use only and limited to any maximum distribution number specified in the license. The first instance of republication or reuse granted by this license must be completed within two years of the date of the grant of this license (although copies prepared before the end date may be distributed thereafter). The Wiley Materials shall not be used in any other manner or for any other purpose, beyond what is granted in the license. Permission is granted subject to an appropriate acknowledgement given to the author, title of the material/book/journal and the publisher. You shall also duplicate the copyright notice that appears in the Wiley publication in your use of the Wiley Material. Permission is also granted on the understanding that nowhere in the text is a previously published source acknowledged for all or part of this Wiley Material. Any third party content is expressly excluded from this permission.

- With respect to the Wiley Materials, all rights are reserved. Except as expressly granted by the terms of the license, no part of the Wiley Materials may be copied, modified, adapted (except for minor reformatting required by the new Publication), translated, reproduced, transferred or distributed, in any form or by any means, and no derivative works may be made based on the Wiley Materials without the prior permission of the respective copyright owner.**For STM Signatory Publishers clearing permission under the terms of the STM Permissions Guidelines only, the terms of the license are extended to include subsequent editions and for editions in other languages, provided such editions are for the work as a whole in situ and does not involve the separate exploitation of the permitted figures or extracts,** You may not alter, remove or suppress in any manner any copyright, trademark or other notices displayed by the Wiley Materials. You may not license, rent, sell, loan, lease, pledge, offer as security, transfer or assign the Wiley Materials on a stand-alone basis, or any of the rights granted to you hereunder to any other person.

- The Wiley Materials and all of the intellectual property rights therein shall at all times remain the exclusive property of John Wiley & Sons Inc, the Wiley Companies, or their respective licensors, and your interest therein is only that of having possession of and the right to reproduce the Wiley Materials pursuant to Section 2 herein during the continuance of this Agreement. You agree that you own no right, title or interest in or to the Wiley Materials or any of the intellectual property rights therein. You shall have no rights hereunder other than the license as provided for above in Section 2. No right,

license or interest to any trademark, trade name, service mark or other branding ("Marks") of WILEY or its licensors is granted hereunder, and you agree that you shall not assert any such right, license or interest with respect thereto

- NEITHER WILEY NOR ITS LICENSORS MAKES ANY WARRANTY OR REPRESENTATION OF ANY KIND TO YOU OR ANY THIRD PARTY, EXPRESS, IMPLIED OR STATUTORY, WITH RESPECT TO THE MATERIALS OR THE ACCURACY OF ANY INFORMATION CONTAINED IN THE MATERIALS, INCLUDING, WITHOUT LIMITATION, ANY IMPLIED WARRANTY OF MERCHANTABILITY, ACCURACY, SATISFACTORY QUALITY, FITNESS FOR A PARTICULAR PURPOSE, USABILITY, INTEGRATION OR NON-INFRINGEMENT AND ALL SUCH WARRANTIES ARE HEREBY EXCLUDED BY WILEY AND ITS LICENSORS AND WAIVED BY YOU.

- WILEY shall have the right to terminate this Agreement immediately upon breach of this Agreement by you.

- You shall indemnify, defend and hold harmless WILEY, its Licensors and their respective directors, officers, agents and employees, from and against any actual or threatened claims, demands, causes of action or proceedings arising from any breach of this Agreement by you.

- IN NO EVENT SHALL WILEY OR ITS LICENSORS BE LIABLE TO YOU OR ANY OTHER PARTY OR ANY OTHER PERSON OR ENTITY FOR ANY SPECIAL, CONSEQUENTIAL, INCIDENTAL, INDIRECT, EXEMPLARY OR PUNITIVE DAMAGES, HOWEVER CAUSED, ARISING OUT OF OR IN CONNECTION WITH THE DOWNLOADING, PROVISIONING, VIEWING OR USE OF THE MATERIALS REGARDLESS OF THE FORM OF ACTION, WHETHER FOR BREACH OF CONTRACT, BREACH OF WARRANTY, TORT, NEGLIGENCE, INFRINGEMENT OR OTHERWISE (INCLUDING, WITHOUT LIMITATION, DAMAGES BASED ON LOSS OF PROFITS, DATA, FILES, USE, BUSINESS OPPORTUNITY OR CLAIMS OF THIRD PARTIES), AND WHETHER OR NOT THE PARTY HAS BEEN ADVISED OF THE POSSIBILITY OF SUCH DAMAGES. THIS LIMITATION SHALL APPLY NOTWITHSTANDING ANY FAILURE OF ESSENTIAL PURPOSE OF ANY LIMITED REMEDY PROVIDED HEREIN.

- Should any provision of this Agreement be held by a court of competent jurisdiction to be illegal, invalid, or unenforceable, that provision shall be deemed amended to achieve as nearly as possible the same economic effect as the original provision, and the legality, validity and enforceability of the remaining provisions of this Agreement shall not be affected or impaired thereby.

- The failure of either party to enforce any term or condition of this Agreement shall not constitute a waiver of either party's right to enforce each and every term and condition of this Agreement. No breach under this agreement shall be deemed waived or excused by either party unless such waiver or consent is in writing signed by the party granting such waiver or consent. The waiver by or consent of a party to a breach of any provision of this Agreement shall not operate or be construed as a waiver of or consent to any other or subsequent breach by such other party.

- This Agreement may not be assigned (including by operation of law or otherwise) by you without WILEY's prior written consent.

- Any fee required for this permission shall be non-refundable after thirty (30) days from receipt by the CCC.

- These terms and conditions together with CCC's Billing and Payment terms and conditions (which are incorporated herein) form the entire agreement between you and WILEY concerning this licensing transaction and (in the absence of fraud) supersedes all prior agreements and representations of the parties, oral or written. This Agreement may not be amended except in writing signed by both parties. This Agreement shall be binding upon and inure to the benefit of the parties' successors, legal representatives, and authorized assigns.

- In the event of any conflict between your obligations established by these terms and conditions and those established by CCC's Billing and Payment terms and conditions, these terms and conditions shall prevail.

- WILEY expressly reserves all rights not specifically granted in the combination of (i) the license details provided by you and accepted in the course of this licensing transaction, (ii) these terms and conditions and (iii) CCC's Billing and Payment terms and conditions.

- This Agreement will be void if the Type of Use, Format, Circulation, or Requestor Type was misrepresented during the licensing process.

- This Agreement shall be governed by and construed in accordance with the laws of the State of New York, USA, without regards to such state's conflict of law rules. Any legal action, suit or proceeding arising out of or relating to these Terms and Conditions or the breach thereof shall be instituted in a court of competent jurisdiction in New York County in the State of New York in the United States of America and each party hereby consents and submits to the personal jurisdiction of such court, waives any objection to venue in such court and consents to service of process by registered or certified mail, return receipt requested, at the last known address of such party.

WILEY OPEN ACCESS TERMS AND CONDITIONS

Wiley Publishes Open Access Articles in fully Open Access Journals and in Subscription journals offering Online Open. Although most of the fully Open Access journals publish open access articles under the terms of the Creative Commons Attribution (CC BY) License only, the subscription journals and a few of the Open Access Journals offer a choice of Creative Commons Licenses. The license type is clearly identified on the article.

The Creative Commons Attribution License

The Creative Commons Attribution License (CC-BY) allows users to copy, distribute and transmit an article, adapt the article and make commercial use of the article. The CC-BY license permits commercial and non-

Creative Commons Attribution Non-Commercial License

The Creative Commons Attribution Non-Commercial (CC-BY-NC)License permits use, distribution and reproduction in any medium, provided the original work is properly cited and is not used for commercial purposes.(see below)

Creative Commons Attribution-Non-Commercial-NoDerivs License

The Creative Commons Attribution Non-Commercial-NoDerivs License (CC-BY-NC-ND) permits use, distribution and reproduction in any medium, provided the original work is properly cited, is not used for commercial purposes and no modifications or adaptations are made. (see below)

Use by commercial "for-profit" organizations

Use of Wiley Open Access articles for commercial, promotional, or marketing purposes requires further explicit permission from Wiley and will be subject to a fee.

Further details can be found on Wiley Online Library
http://olabout.wiley.com/WileyCDA/Section/id-410895.html

Other Terms and Conditions:

v1.10 Last updated September 2015

Questions? customercare@copyright.com or +1-855-239-3415 (toll free in the US) or +1-978-646-2777.

Copyright Clearance Center **Marketplace**™

Order Confirmation

Thank you, your order has been placed. An email confirmation has been sent to you. Your order license details and printable licenses will be available within 24 hours. Please access Manage Account for final order details.

This is not an invoice. Please go to manage account to access your order history and invoices.

CUSTOMER INFORMATION

Payment by invoice: You can cancel your order until the invoice is generated by contacting customer service.

📇 Billing Address

Mr. Rahul Maity
New Hostel2, IISER Pune, Pashan, Pune
Dr. Homi Bhabha Road
Near NCL Innovation Park
Pune, Maharashtra 411008
India

+91 7001322540
rahul.maity@students.iiserpune.ac.in

📍 Customer Location

Mr. Rahul Maity
New Hostel2, IISER Pune, Pashan, Pune
Dr. Homi Bhabha Road
Near NCL Innovation Park
Pune, Maharashtra 411008
India

📄 PO Number (optional)

N/A

💳 Payment options

Invoice

PENDING ORDER CONFIRMATION

Confirmation Number: Pending

Order Date: 25-Jan-2021

1. Nanoscale   0.00 USD

Order license ID	Pending	**Publisher**	RSC Pub
ISSN	2040-3372	**Portion**	Chart/graph/table/figure
Type of Use	Republish in a thesis/dissertation		

LICENSED CONTENT

Publication Title	Nanoscale	**Country**	United Kingdom of Great Britain and Northern Ireland
Author/Editor	National Center for Nanoscience and Technology., Royal Society of Chemistry (Great Britain)	**Rightsholder**	Royal Society of Chemistry
		Publication Type	e-Journal
Date	01/01/2009	**URL**	http://www.rsc.org/Publishing/Journals/NR/index.asp
Language	English		

REQUEST DETAILS

Portion Type	Chart/graph/table/figure	**Distribution**	Worldwide
Number of charts / graphs / tables / figures requested	5	**Translation**	Original language of publication
		Copies for the disabled?	Yes
Format (select all that apply)	Print, Electronic	**Minor editing privileges?**	Yes
Who will republish the content?	Academic institution	**Incidental promotional use?**	No
Duration of Use	Life of current edition	**Currency**	USD
Lifetime Unit Quantity	Up to 999		
Rights Requested	Main product		

NEW WORK DETAILS

Title	Crafting pore architecture of water-stable microporous MOFs for selective CO2 capture	**Institution name**	IISER Pune
		Expected presentation date	2021-03-01
Instructor name	Rahul Maity		

ADDITIONAL DETAILS

Order reference number	N/A	**The requesting person / organization to appear on the license**	Rahul Maity

REUSE CONTENT DETAILS

Title, description or numeric reference of the portion(s)	Figure 1, Figure 5,	**Title of the article/chapter the portion is from**	Imparting surface hydrophobicity to metal–organic frameworks using a facile solution-immersion process to enhance water stability for CO2 capture
Editor of portion(s)	N/A		
Volume of serial or monograph	N/A		
Page or page range of portion	2005, 2007		

Author of portion(s)	National Center for Nanoscience and Technology.; Royal Society of Chemistry (Great Britain)
Issue, if republishing an article from a serial	N/A
Publication date of portion	2021-03-01

Total Items: 1

Total Due: 0.00 USD

Accepted: All Publisher and CCC Terms and Conditions

Copyright
Clearance
Center

Marketplace™

Order Confirmation

Thank you, your order has been placed. An email confirmation has been sent to you. Your order license details and printable licenses will be available within 24 hours. Please access Manage Account for final order details.

This is not an invoice. Please go to manage account to access your order history and invoices.

CUSTOMER INFORMATION

Payment by invoice: You can cancel your order until the invoice is generated by contacting customer service.

🧾 Billing Address

Mr. Rahul Maity
New Hostel2, IISER Pune, Pashan, Pune
Dr. Homi Bhabha Road
Near NCL Innovation Park
Pune, Maharashtra 411008
India

+91 7001322540
rahul.maity@students.iiserpune.ac.in

📄 PO Number (optional)

N/A

📍 Customer Location

Mr. Rahul Maity
New Hostel2, IISER Pune, Pashan, Pune
Dr. Homi Bhabha Road
Near NCL Innovation Park
Pune, Maharashtra 411008
India

💳 Payment options

Invoice

PENDING ORDER CONFIRMATION

Confirmation Number: Pending

Order Date: 25-Jan-2021

1. Chemical communications

0.00 USD

Order license ID	Pending		
ISSN	1364-548X	**Publisher**	ROYAL SOCIETY OF CHEMISTRY
Type of Use	Republish in a thesis/dissertation	**Portion**	Chart/graph/table/figure

LICENSED CONTENT

Publication Title	Chemical communications	**Country**	United Kingdom of Great Britain and Northern Ireland
Author/Editor	Royal Society of Chemistry (Great Britain)	**Rightsholder**	Royal Society of Chemistry
Date	01/01/1996	**Publication Type**	e-Journal
Language	English		

REQUEST DETAILS

Portion Type	Chart/graph/table/figure	**Distribution**	Worldwide
Number of charts / graphs / tables / figures requested	3	**Translation**	Original language of publication
Format (select all that apply)	Print, Electronic	**Copies for the disabled?**	Yes
Who will republish the content?	Academic institution	**Minor editing privileges?**	Yes
		Incidental promotional use?	No
Duration of Use	Life of current edition	**Currency**	USD
Lifetime Unit Quantity	Up to 999		
Rights Requested	Main product		

NEW WORK DETAILS

Title	Crafting pore architecture of water-stable microporous MOFs for selective CO2 capture	**Institution name**	IISER Pune
		Expected presentation date	2021-03-01
Instructor name	Rahul Maity		

ADDITIONAL DETAILS

Order reference number	N/A	**The requesting person / organization to appear on the license**	Rahul Miaty

REUSE CONTENT DETAILS

Title, description or numeric reference of the portion(s)	Figure 1 and Figure 2	**Title of the article/chapter the portion is from**	A new approach towards tetrahedral imidazolate frameworks for high and selective CO2 uptake
Editor of portion(s)	N/A		
Volume of serial or monograph	N/A	**Author of portion(s)**	Royal Society of Chemistry (Great Britain)
Page or page range of portion	5829, 5830	**Issue, if republishing an article from a serial**	N/A
		Publication date of portion	1996-01-01

Total Items: 1   **Total Due: 0.00 USD**

Accepted: All Publisher and CCC Terms and Conditions

![Copyright Clearance Center] **Marketplace**™

Order Confirmation

Thank you, your order has been placed. An email confirmation has been sent to you. Your order license details and printable licenses will be available within 24 hours. Please access Manage Account for final order details.

This is not an invoice. Please go to manage account to access your order history and invoices.

CUSTOMER INFORMATION

Payment by invoice: You can cancel your order until the invoice is generated by contacting customer service.

📠 Billing Address

Mr. Rahul Maity
New Hostel2, IISER Pune, Pashan, Pune
Dr. Homi Bhabha Road
Near NCL Innovation Park
Pune, Maharashtra 411008
India

+91 7001322540
rahul.maity@students.iiserpune.ac.in

📍 Customer Location

Mr. Rahul Maity
New Hostel2, IISER Pune, Pashan, Pune
Dr. Homi Bhabha Road
Near NCL Innovation Park
Pune, Maharashtra 411008
India

📄 PO Number (optional)

N/A

💳 Payment options

Invoice

PENDING ORDER CONFIRMATION

Confirmation Number:　Pending

Order Date:　25-Jan-2021

1. Journal of materials chemistry　　　　0.00 USD

Order license ID	Pending	**Publisher**	ROYAL SOCIETY OF CHEMISTRY,
ISSN	1364-5501		
Type of Use	Republish in a thesis/dissertation	**Portion**	Chart/graph/table/figure

LICENSED CONTENT

Publication Title	Journal of materials chemistry	**Country**	United Kingdom of Great Britain and Northern Ireland
Author/Editor	Royal Society of Chemistry (Great Britain)	**Rightsholder**	Royal Society of Chemistry
Date	01/01/1991	**Publication Type**	e-Journal
Language	English	**URL**	http://firstsearch.oclc.org

REQUEST DETAILS

Portion Type	Chart/graph/table/figure	**Distribution**	Worldwide
Number of charts / graphs / tables / figures requested	2	**Translation**	Original language of publication
		Copies for the disabled?	Yes
Format (select all that apply)	Print, Electronic	**Minor editing privileges?**	Yes
Who will republish the content?	Academic institution	**Incidental promotional use?**	No
Duration of Use	Life of current edition	**Currency**	USD
Lifetime Unit Quantity	Up to 999		
Rights Requested	Main product		

NEW WORK DETAILS

Title	Crafting pore architecture of water-stable microporous MOFs for selective CO2 capture	**Institution name**	IISER Pune
		Expected presentation date	2021-03-01
Instructor name	Rahul Maity		

ADDITIONAL DETAILS

Order reference number	N/A	**The requesting person / organization to appear on the license**	Rahul Maity

REUSE CONTENT DETAILS

Title, description or numeric reference of the portion(s)	Figure 1 and Figure 3	**Title of the article/chapter the portion is from**	Guest selectivity of a porous tetrahedral imidazolate framework material during self-assembly
Editor of portion(s)	N/A		
Volume of serial or monograph	N/a	**Author of portion(s)**	Royal Society of Chemistry (Great Britain)
Page or page range of portion	19734, 19736	**Issue, if republishing an article from a serial**	N/A

Publication date of portion	1991-01-01

Total Items: 1

Total Due: 0.00 USD

Accepted: All Publisher and CCC Terms and Conditions

Water Stable Metal–Organic Framework Evolutionally Formed from a Flexible Multidentate Ligand with Acylamide Groups for Selective CO2 Adsorption

Author: Zhiyong Lu, Hang Xing, Ran Sun, et al

Publication: Crystal Growth and Design

Publisher: American Chemical Society

Date: Mar 1, 2012

Copyright © 2012, American Chemical Society

PERMISSION/LICENSE IS GRANTED FOR YOUR ORDER AT NO CHARGE

This type of permission/license, instead of the standard Terms & Conditions, is sent to you because no fee is being charged for your order. Please note the following:

- Permission is granted for your request in both print and electronic formats, and translations.
- If figures and/or tables were requested, they may be adapted or used in part.
- Please print this page for your records and send a copy of it to your publisher/graduate school.
- Appropriate credit for the requested material should be given as follows: "Reprinted (adapted) with permission from (COMPLETE REFERENCE CITATION). Copyright (YEAR) American Chemical Society." Insert appropriate information in place of the capitalized words.
- One-time permission is granted only for the use specified in your request. No additional uses are granted (such as derivative works or other editions). For any other uses, please submit a new request.
If credit is given to another source for the material you requested, permission must be obtained from that source.

BACK   CLOSE WINDOW

Copyright Clearance Center

Marketplace™

Order Confirmation

Thank you, your order has been placed. An email confirmation has been sent to you. Your order license details and printable licenses will be available within 24 hours. Please access Manage Account for final order details.

This is not an invoice. Please go to manage account to access your order history and invoices.

CUSTOMER INFORMATION

Payment by invoice: You can cancel your order until the invoice is generated by contacting customer service.

Billing Address

Mr. Rahul Maity
New Hostel2, IISER Pune, Pashan, Pune
Dr. Homi Bhabha Road
Near NCL Innovation Park
Pune, Maharashtra 411008
India

+91 7001322540
rahul.maity@students.iiserpune.ac.in

Customer Location

Mr. Rahul Maity
New Hostel2, IISER Pune, Pashan, Pune
Dr. Homi Bhabha Road
Near NCL Innovation Park
Pune, Maharashtra 411008
India

PO Number (optional)

N/A

Payment options

Invoice

PENDING ORDER CONFIRMATION

Confirmation Number: Pending

Order Date: 25-Jan-2021

1. Dalton transactions

0.00 USD

Order license ID	Pending	**Publisher**	ROYAL SOCIETY OF CHEMISTRY
ISSN	1477-9234		
Type of Use	Republish in a thesis/dissertation	**Portion**	Chart/graph/table/figure

LICENSED CONTENT

Publication Title	Dalton transactions	**Country**	United Kingdom of Great Britain and Northern Ireland
Author/Editor	Royal Society of Chemistry (Great Britain)		
Date	01/01/2003	**Rightsholder**	Royal Society of Chemistry
Language	English	**Publication Type**	e-Journal

REQUEST DETAILS

Portion Type	Chart/graph/table/figure	**Distribution**	Worldwide
Number of charts / graphs / tables / figures requested	3	**Translation**	Original language of publication
Format (select all that apply)	Print, Electronic	**Copies for the disabled?**	Yes
		Minor editing privileges?	Yes
Who will republish the content?	Academic institution	**Incidental promotional use?**	No
Duration of Use	Life of current edition	**Currency**	USD
Lifetime Unit Quantity	Up to 999		
Rights Requested	Main product		

NEW WORK DETAILS

Title	Crafting pore architecture of water-stable microporous MOFs for selective CO2 capture	**Institution name**	IISER Pune
		Expected presentation date	2021-03-01
Instructor name	Rahul Miaty		

ADDITIONAL DETAILS

Order reference number	N/A	**The requesting person / organization to appear on the license**	Rahul Miaty

REUSE CONTENT DETAILS

Title, description or numeric reference of the portion(s)	Figure 1, Figure 3, Figure 4	**Title of the article/chapter the portion is from**	A robust and water-stable two-fold interpenetrated metal–organic framework containing both rigid tetrapodal carboxylate and rigid bifunctional nitrogen linkers exhibiting selective CO2 capture
Editor of portion(s)	N/A		
Volume of serial or monograph	N/A		
Page or page range of portion	417, 418, 419		
		Author of portion(s)	Royal Society of Chemistry (Great Britain)

Issue, if republishing an article from a serial	N/A
Publication date of portion	2003-01-01

Total Items: 1

Total Due: 0.00 USD

Accepted: All Publisher and CCC Terms and Conditions

Copyright Clearance Center

RightsLink®

ACS Publications
Most Trusted. Most Cited. Most Read.

A Water-Stable Twofold Interpenetrating Microporous MOF for Selective CO2 Adsorption and Separation

Author: Arun Pal, Santanu Chand, Madhab C. Das

Publication: Inorganic Chemistry

Publisher: American Chemical Society

Date: Nov 1, 2017

Copyright © 2017, American Chemical Society

PERMISSION/LICENSE IS GRANTED FOR YOUR ORDER AT NO CHARGE

This type of permission/license, instead of the standard Terms & Conditions, is sent to you because no fee is being charged for your order. Please note the following:

- Permission is granted for your request in both print and electronic formats, and translations.
- If figures and/or tables were requested, they may be adapted or used in part.
- Please print this page for your records and send a copy of it to your publisher/graduate school.
- Appropriate credit for the requested material should be given as follows: "Reprinted (adapted) with permission from (COMPLETE REFERENCE CITATION). Copyright (YEAR) American Chemical Society." Insert appropriate information in place of the capitalized words.
- One-time permission is granted only for the use specified in your request. No additional uses are granted (such as derivative works or other editions). For any other uses, please submit a new request.
If credit is given to another source for the material you requested, permission must be obtained from that source.

BACK   CLOSE WINDOW

THE AMERICAN ASSOCIATION FOR THE ADVANCEMENT OF SCIENCE LICENSE
TERMS AND CONDITIONS

Jan 25, 2021

This Agreement between Mr. Rahul Maity ("You") and The American Association for the
Advancement of Science ("The American Association for the Advancement of Science")
consists of your license details and the terms and conditions provided by The American
Association for the Advancement of Science and Copyright Clearance Center.

License Number	4995970813296
License date	Jan 25, 2021
Licensed Content Publisher	The American Association for the Advancement of Science
Licensed Content Publication	Science
Licensed Content Title	Direct Observation and Quantification of CO_2 Binding Within an Amine-Functionalized Nanoporous Solid
Licensed Content Author	Ramanathan Vaidhyanathan,Simon S. Iremonger,George K. H. Shimizu,Peter G. Boyd,Saman Alavi,Tom K. Woo
Licensed Content Date	Oct 29, 2010
Licensed Content Volume	330
Licensed Content Issue	6004
Volume number	330

Issue number	6004
Type of Use	Thesis / Dissertation
Requestor type	Scientist/individual at a research institution
Format	Print and electronic
Portion	Figure
Number of figures/tables	2
Title	Crafting pore architecture of water-stable microporous MOFs for selective CO2 capture
Institution name	IISER Pune, India
Expected presentation date	Jan 2021
Portions	Figure 1 and Figure 2
Requestor Location	Mr. Rahul Maity New Hostel2, IISER Pune, Pashan, Pune Dr. Homi Bhabha Road Near NCL Innovation Park Pune, Maharashtra 411008 India Attn: Indian Institute of Science Education and Research (IISER) Pune
Total	0.00 USD

Terms and Conditions

American Association for the Advancement of Science TERMS AND CONDITIONS

Regarding your request, we are pleased to grant you non-exclusive, non-transferable permission, to republish the AAAS material identified above in your work identified above, subject to the terms and conditions herein. We must be contacted for permission for any uses other than those specifically identified in your request above.

The following credit line must be printed along with the AAAS material: "From [Full Reference Citation]. Reprinted with permission from AAAS."

All required credit lines and notices must be visible any time a user accesses any part of the AAAS material and must appear on any printed copies and authorized user might make.

This permission does not apply to figures / photos / artwork or any other content or materials included in your work that are credited to non-AAAS sources. If the requested material is sourced to or references non-AAAS sources, you must obtain authorization from that source as well before using that material. You agree to hold harmless and indemnify AAAS against any claims arising from your use of any content in your work that is credited to non-AAAS sources.

If the AAAS material covered by this permission was published in Science during the years 1974 - 1994, you must also obtain permission from the author, who may grant or withhold permission, and who may or may not charge a fee if permission is granted. See original article for author's address. This condition does not apply to news articles.

The AAAS material may not be modified or altered except that figures and tables may be modified with permission from the author. Author permission for any such changes must be secured prior to your use.

Whenever possible, we ask that electronic uses of the AAAS material permitted herein include a hyperlink to the original work on AAAS's website (hyperlink may be embedded in the reference citation).

AAAS material reproduced in your work identified herein must not account for more than 30% of the total contents of that work.

AAAS must publish the full paper prior to use of any text.

AAAS material must not imply any endorsement by the American Association for the Advancement of Science.

This permission is not valid for the use of the AAAS and/or Science logos.

AAAS makes no representations or warranties as to the accuracy of any information contained in the AAAS material covered by this permission, including any warranties of

merchantability or fitness for a particular purpose.

If permission fees for this use are waived, please note that AAAS reserves the right to charge for reproduction of this material in the future.

Permission is not valid unless payment is received within sixty (60) days of the issuance of this permission. If payment is not received within this time period then all rights granted herein shall be revoked and this permission will be considered null and void.

In the event of breach of any of the terms and conditions herein or any of CCC's Billing and Payment terms and conditions, all rights granted herein shall be revoked and this permission will be considered null and void.

AAAS reserves the right to terminate this permission and all rights granted herein at its discretion, for any purpose, at any time. In the event that AAAS elects to terminate this permission, you will have no further right to publish, publicly perform, publicly display, distribute or otherwise use any matter in which the AAAS content had been included, and all

fees paid hereunder shall be fully refunded to you. Notification of termination will be sent to the contact information as supplied by you during the request process and termination shall be immediate upon sending the notice. Neither AAAS nor CCC shall be liable for any costs, expenses, or damages you may incur as a result of the termination of this permission, beyond the refund noted above.

This Permission may not be amended except by written document signed by both parties.

The terms above are applicable to all permissions granted for the use of AAAS material. Below you will find additional conditions that apply to your particular type of use.

FOR A THESIS OR DISSERTATION

If you are using figure(s)/table(s), permission is granted for use in print and electronic versions of your dissertation or thesis. A full text article may be used in print versions only of a dissertation or thesis.

Permission covers the distribution of your dissertation or thesis on demand by ProQuest / UMI, provided the AAAS material covered by this permission remains in situ.

If you are an Original Author on the AAAS article being reproduced, please refer to your License to Publish for rules on reproducing your paper in a dissertation or thesis.

FOR JOURNALS:

Permission covers both print and electronic versions of your journal article, however the AAAS material may not be used in any manner other than within the context of your article.

FOR BOOKS/TEXTBOOKS:

If this license is to reuse figures/tables, then permission is granted for non-exclusive world rights in all languages in both print and electronic formats (electronic formats are defined below).

If this license is to reuse a text excerpt or a full text article, then permission is granted for non-exclusive world rights in English only. You have the option of securing either print or electronic rights or both, but electronic rights are not automatically granted and do garner additional fees. Permission for translations of text excerpts or full text articles into other languages must be obtained separately.

Licenses granted for use of AAAS material in electronic format books/textbooks are valid only in cases where the electronic version is equivalent to or substitutes for the print version of the book/textbook. The AAAS material reproduced as permitted herein must remain in situ and must not be exploited separately (for example, if permission covers the use of a full text article, the article may not be offered for access or for purchase as a stand-alone unit), except in the case of permitted textbook companions as noted below.

You must include the following notice in any electronic versions, either adjacent to the reprinted AAAS material or in the terms and conditions for use of your electronic products: "Readers may view, browse, and/or download material for temporary copying purposes only, provided these uses are for noncommercial personal purposes. Except as provided by law, this material may not be further reproduced, distributed, transmitted, modified, adapted, performed, displayed, published, or sold in whole or in part, without prior written permission from the publisher."

If your book is an academic textbook, permission covers the following companions to your textbook, provided such companions are distributed only in conjunction with your textbook at no additional cost to the user:

- Password-protected website
- Instructor's image CD/DVD and/or PowerPoint resource
- Student CD/DVD

All companions must contain instructions to users that the AAAS material may be used for non-commercial, classroom purposes only. Any other uses require the prior written permission from AAAS.

If your license is for the use of AAAS Figures/Tables, then the electronic rights granted herein permit use of the Licensed Material in any Custom Databases that you distribute the electronic versions of your textbook through, so long as the Licensed Material remains within the context of a chapter of the title identified in your request and cannot be downloaded by a user as an independent image file.

Rights also extend to copies/files of your Work (as described above) that you are required to provide for use by the visually and/or print disabled in compliance with state and federal laws.

This permission only covers a single edition of your work as identified in your request.

FOR NEWSLETTERS:
Permission covers print and/or electronic versions, provided the AAAS material reproduced as permitted herein remains in situ and is not exploited separately (for example, if permission covers the use of a full text article, the article may not be offered for access or for purchase as a stand-alone unit)

FOR ANNUAL REPORTS:
Permission covers print and electronic versions provided the AAAS material reproduced as permitted herein remains in situ and is not exploited separately (for example, if permission covers the use of a full text article, the article may not be offered for access or for purchase as a stand-alone unit)

FOR PROMOTIONAL/MARKETING USES:
Permission covers the use of AAAS material in promotional or marketing pieces such as information packets, media kits, product slide kits, brochures, or flyers limited to a single print run. The AAAS Material may not be used in any manner which implies endorsement or promotion by the American Association for the Advancement of Science (AAAS) or Science of any product or service. AAAS does not permit the reproduction of its name, logo or text on promotional literature.

If permission to use a full text article is permitted, The Science article covered by this permission must not be altered in any way. No additional printing may be set onto an article copy other than the copyright credit line required above. Any alterations must be approved in advance and in writing by AAAS. This includes, but is not limited to, the placement of sponsorship identifiers, trademarks, logos, rubber stamping or self-adhesive stickers onto the article copies.

Additionally, article copies must be a freestanding part of any information package (i.e. media kit) into which they are inserted. They may not be physically attached to anything, such as an advertising insert, or have anything attached to them, such as a sample product. Article copies must be easily removable from any kits or informational packages in which they are used. The only exception is that article copies may be inserted into three-ring binders.

FOR CORPORATE INTERNAL USE:
The AAAS material covered by this permission may not be altered in any way. No additional printing may be set onto an article copy other than the required credit line. Any alterations must be approved in advance and in writing by AAAS. This includes, but is not limited to the placement of sponsorship identifiers, trademarks, logos, rubber stamping or self-adhesive stickers onto article copies.

If you are making article copies, copies are restricted to the number indicated in your request and must be distributed only to internal employees for internal use.

If you are using AAAS Material in Presentation Slides, the required credit line must be visible on the slide where the AAAS material will be reprinted

If you are using AAAS Material on a CD, DVD, Flash Drive, or the World Wide Web, you must include the following notice in any electronic versions, either adjacent to the reprinted AAAS material or in the terms and conditions for use of your electronic products: "Readers may view, browse, and/or download material for temporary copying purposes only, provided these uses are for noncommercial personal purposes. Except as provided by law, this material may not be further reproduced, distributed, transmitted, modified, adapted, performed, displayed, published, or sold in whole or in part, without prior written permission from the publisher." Access to any such CD, DVD, Flash Drive or Web page must be restricted to your organization's employees only.

FOR CME COURSE and SCIENTIFIC SOCIETY MEETINGS:
Permission is restricted to the particular Course, Seminar, Conference, or Meeting indicated in your request. If this license covers a text excerpt or a Full Text Article, access to the reprinted AAAS material must be restricted to attendees of your event only (if you have been granted electronic rights for use of a full text article on your website, your website must be password protected, or access restricted so that only attendees can access the content on your site).

If you are using AAAS Material on a CD, DVD, Flash Drive, or the World Wide Web, you must include the following notice in any electronic versions, either adjacent to the reprinted AAAS material or in the terms and conditions for use of your electronic products: "Readers may view, browse, and/or download material for temporary copying purposes only, provided these uses are for noncommercial personal purposes. Except as provided by law, this material may not be further reproduced, distributed, transmitted, modified, adapted, performed, displayed, published, or sold in whole or in part, without prior written permission from the publisher."

FOR POLICY REPORTS:
These rights are granted only to non-profit organizations and/or government agencies. Permission covers print and electronic versions of a report, provided the required credit line appears in both versions and provided the AAAS material reproduced as permitted herein remains in situ and is not exploited separately.

FOR CLASSROOM PHOTOCOPIES:
Permission covers distribution in print copy format only. Article copies must be freestanding and not part of a course pack. They may not be physically attached to anything or have anything attached to them.

FOR COURSEPACKS OR COURSE WEBSITES:
These rights cover use of the AAAS material in one class at one institution. Permission is valid only for a single semester after which the AAAS material must be removed from the Electronic Course website, unless new permission is obtained for an additional semester. If

the material is to be distributed online, access must be restricted to students and instructors enrolled in that particular course by some means of password or access control.

FOR WEBSITES:
You must include the following notice in any electronic versions, either adjacent to the reprinted AAAS material or in the terms and conditions for use of your electronic products: "Readers may view, browse, and/or download material for temporary copying purposes only, provided these uses are for noncommercial personal purposes. Except as provided by law, this material may not be further reproduced, distributed, transmitted, modified, adapted, performed, displayed, published, or sold in whole or in part, without prior written permission from the publisher."

Permissions for the use of Full Text articles on third party websites are granted on a case by case basis and only in cases where access to the AAAS Material is restricted by some means of password or access control. Alternately, an E-Print may be purchased through our reprints department (brocheleau@rockwaterinc.com).

REGARDING FULL TEXT ARTICLE USE ON THE WORLD WIDE WEB IF YOU ARE AN 'ORIGINAL AUTHOR' OF A SCIENCE PAPER

If you chose "Original Author" as the Requestor Type, you are warranting that you are one of authors listed on the License Agreement as a "Licensed content author" or that you are acting on that author's behalf to use the Licensed content in a new work that one of the authors listed on the License Agreement as a "Licensed content author" has written.

Original Authors may post the 'Accepted Version' of their full text article on their personal or on their University website and not on any other website. The 'Accepted Version' is the version of the paper accepted for publication by AAAS including changes resulting from peer review but prior to AAAS's copy editing and production (in other words not the AAAS published version).

FOR MOVIES / FILM / TELEVISION:
Permission is granted to use, record, film, photograph, and/or tape the AAAS material in connection with your program/film and in any medium your program/film may be shown or heard, including but not limited to broadcast and cable television, radio, print, world wide web, and videocassette.

The required credit line should run in the program/film's end credits.

FOR MUSEUM EXHIBITIONS:
Permission is granted to use the AAAS material as part of a single exhibition for the duration of that exhibit. Permission for use of the material in promotional materials for the exhibit must be cleared separately with AAAS (please contact us at permissions@aaas.org).

FOR TRANSLATIONS:
Translation rights apply only to the language identified in your request summary above.

The following disclaimer must appear with your translation, on the first page of the article, after the credit line: "This translation is not an official translation by AAAS staff, nor is it endorsed by AAAS as accurate. In crucial matters, please refer to the official English-language version originally published by AAAS."

FOR USE ON A COVER:
Permission is granted to use the AAAS material on the cover of a journal issue, newsletter

issue, book, textbook, or annual report in print and electronic formats provided the AAAS material reproduced as permitted herein remains in situ and is not exploited separately

By using the AAAS Material identified in your request, you agree to abide by all the terms and conditions herein.

Questions about these terms can be directed to the AAAS Permissions department permissions@aaas.org.

Other Terms and Conditions:

v 2

Questions? customercare@copyright.com or +1-855-239-3415 (toll free in the US) or +1-978-646-2777.

JOHN WILEY AND SONS LICENSE
TERMS AND CONDITIONS

Jan 13, 2021

This Agreement between Mr. Rahul Maity ("You") and John Wiley and Sons ("John Wiley and Sons") consists of your license details and the terms and conditions provided by John Wiley and Sons and Copyright Clearance Center.

License Number	4986990113865
License date	Jan 13, 2021
Licensed Content Publisher	John Wiley and Sons
Licensed Content Publication	Chemistry - An Asian Journal
Licensed Content Title	Water-stable Adenine-based MOFs with Polar Pores for Selective CO2 Capture
Licensed Content Author	Ramanathan Vaidhyanathan, Debanjan Chakraborty, Ankit Kumar Yadav, et al
Licensed Content Date	Sep 16, 2019
Licensed Content Volume	14
Licensed Content Issue	20
Licensed Content Pages	6
Type of use	Dissertation/Thesis

Requestor type	Author of this Wiley article
Format	Print and electronic
Portion	Full article
Will you be translating?	No
Title	Crafting pore architecture of water-stable microporous MOFs for selective CO2 capture
Institution name	IISER Pune, India
Expected presentation date	Jan 2021
Order reference number	no
Requestor Location	Mr. Rahul Maity New Hostel2, IISER Pune, Pashan, Pune Dr. Homi Bhabha Road Near NCL Innovation Park Pune, Maharashtra 411008 India Attn: Indian Institute of Science Education and Research (IISER) Pune
Publisher Tax ID	EU826007151
Total	0.00 USD

Terms and Conditions

TERMS AND CONDITIONS

transaction, you agree that the following terms and conditions apply to this transaction (along with the billing and payment terms and conditions established by the Copyright Clearance Center Inc., ("CCC's Billing and Payment terms and conditions"), at the time that you opened your RightsLink account (these are available at any time at http://myaccount.copyright.com).

Terms and Conditions

- The materials you have requested permission to reproduce or reuse (the "Wiley Materials") are protected by copyright.

- You are hereby granted a personal, non-exclusive, non-sub licensable (on a stand-alone basis), non-transferable, worldwide, limited license to reproduce the Wiley Materials for the purpose specified in the licensing process. This license, **and any CONTENT (PDF or image file) purchased as part of your order,** is for a one-time use only and limited to any maximum distribution number specified in the license. The first instance of republication or reuse granted by this license must be completed within two years of the date of the grant of this license (although copies prepared before the end date may be distributed thereafter). The Wiley Materials shall not be used in any other manner or for any other purpose, beyond what is granted in the license. Permission is granted subject to an appropriate acknowledgement given to the author, title of the material/book/journal and the publisher. You shall also duplicate the copyright notice that appears in the Wiley publication in your use of the Wiley Material. Permission is also granted on the understanding that nowhere in the text is a previously published source acknowledged for all or part of this Wiley Material. Any third party content is expressly excluded from this permission.

- With respect to the Wiley Materials, all rights are reserved. Except as expressly granted by the terms of the license, no part of the Wiley Materials may be copied, modified, adapted (except for minor reformatting required by the new Publication), translated, reproduced, transferred or distributed, in any form or by any means, and no derivative works may be made based on the Wiley Materials without the prior permission of the respective copyright owner.**For STM Signatory Publishers clearing permission under the terms of the STM Permissions Guidelines only, the terms of the license are extended to include subsequent editions and for editions in other languages, provided such editions are for the work as a whole in situ and does not involve the separate exploitation of the permitted figures or extracts,** You may not alter, remove or suppress in any manner any copyright, trademark or other notices displayed by the Wiley Materials. You may not license, rent, sell, loan, lease, pledge, offer as security, transfer or assign the Wiley Materials on a stand-alone basis, or any of the rights granted to you hereunder to any other person.

- The Wiley Materials and all of the intellectual property rights therein shall at all times remain the exclusive property of John Wiley & Sons Inc, the Wiley Companies, or their respective licensors, and your interest therein is only that of having possession of and the right to reproduce the Wiley Materials pursuant to Section 2 herein during the continuance of this Agreement. You agree that you own no right, title or interest in or to the Wiley Materials or any of the intellectual property rights therein. You shall have no rights hereunder other than the license as provided for above in Section 2. No right, license or interest to any trademark, trade name, service mark or other branding ("Marks") of WILEY or its licensors is granted hereunder, and you agree that you shall not assert any such right, license or interest with respect thereto

- NEITHER WILEY NOR ITS LICENSORS MAKES ANY WARRANTY OR REPRESENTATION OF ANY KIND TO YOU OR ANY THIRD PARTY, EXPRESS, IMPLIED OR STATUTORY, WITH RESPECT TO THE MATERIALS OR THE ACCURACY OF ANY INFORMATION CONTAINED IN THE MATERIALS, INCLUDING, WITHOUT LIMITATION, ANY IMPLIED WARRANTY OF MERCHANTABILITY, ACCURACY, SATISFACTORY QUALITY, FITNESS FOR A PARTICULAR PURPOSE, USABILITY, INTEGRATION OR NON-INFRINGEMENT AND ALL SUCH WARRANTIES ARE HEREBY EXCLUDED BY WILEY AND ITS LICENSORS AND WAIVED BY YOU.

- WILEY shall have the right to terminate this Agreement immediately upon breach of this Agreement by you.

- You shall indemnify, defend and hold harmless WILEY, its Licensors and their respective directors, officers, agents and employees, from and against any actual or threatened claims, demands, causes of action or proceedings arising from any breach of this Agreement by you.

- IN NO EVENT SHALL WILEY OR ITS LICENSORS BE LIABLE TO YOU OR ANY OTHER PARTY OR ANY OTHER PERSON OR ENTITY FOR ANY SPECIAL, CONSEQUENTIAL, INCIDENTAL, INDIRECT, EXEMPLARY OR PUNITIVE DAMAGES, HOWEVER CAUSED, ARISING OUT OF OR IN CONNECTION WITH THE DOWNLOADING, PROVISIONING, VIEWING OR USE OF THE MATERIALS REGARDLESS OF THE FORM OF ACTION, WHETHER FOR BREACH OF CONTRACT, BREACH OF WARRANTY, TORT, NEGLIGENCE, INFRINGEMENT OR OTHERWISE (INCLUDING, WITHOUT LIMITATION, DAMAGES BASED ON LOSS OF PROFITS, DATA, FILES, USE, BUSINESS OPPORTUNITY OR CLAIMS OF THIRD PARTIES), AND WHETHER OR NOT THE PARTY HAS BEEN ADVISED OF THE POSSIBILITY OF SUCH DAMAGES. THIS LIMITATION SHALL APPLY NOTWITHSTANDING ANY FAILURE OF ESSENTIAL PURPOSE OF ANY LIMITED REMEDY PROVIDED HEREIN.

- Should any provision of this Agreement be held by a court of competent jurisdiction to be illegal, invalid, or unenforceable, that provision shall be deemed amended to achieve as nearly as possible the same economic effect as the original provision, and the legality, validity and enforceability of the remaining provisions of this Agreement shall not be affected or impaired thereby.

- The failure of either party to enforce any term or condition of this Agreement shall not constitute a waiver of either party's right to enforce each and every term and condition of this Agreement. No breach under this agreement shall be deemed waived or excused by either party unless such waiver or consent is in writing signed by the party granting such waiver or consent. The waiver by or consent of a party to a breach of any provision of this Agreement shall not operate or be construed as a waiver of or consent to any other or subsequent breach by such other party.

- This Agreement may not be assigned (including by operation of law or otherwise) by you without WILEY's prior written consent.

- Any fee required for this permission shall be non-refundable after thirty (30) days from receipt by the CCC.

- These terms and conditions together with CCC's Billing and Payment terms and conditions (which are incorporated herein) form the entire agreement between you and WILEY concerning this licensing transaction and (in the absence of fraud) supersedes all prior agreements and representations of the parties, oral or written. This Agreement may not be amended except in writing signed by both parties. This Agreement shall be binding upon and inure to the benefit of the parties' successors, legal representatives, and authorized assigns.

- In the event of any conflict between your obligations established by these terms and conditions and those established by CCC's Billing and Payment terms and conditions, these terms and conditions shall prevail.

- WILEY expressly reserves all rights not specifically granted in the combination of (i) the license details provided by you and accepted in the course of this licensing transaction, (ii) these terms and conditions and (iii) CCC's Billing and Payment terms and conditions.

- This Agreement will be void if the Type of Use, Format, Circulation, or Requestor Type was misrepresented during the licensing process.

- This Agreement shall be governed by and construed in accordance with the laws of the State of New York, USA, without regards to such state's conflict of law rules. Any legal action, suit or proceeding arising out of or relating to these Terms and Conditions or the breach thereof shall be instituted in a court of competent jurisdiction in New York County in the State of New York in the United States of America and each party hereby consents and submits to the personal jurisdiction of such court, waives any objection to venue in such court and consents to service of process by registered or certified mail, return receipt requested, at the last known address of such party.

WILEY OPEN ACCESS TERMS AND CONDITIONS

Wiley Publishes Open Access Articles in fully Open Access Journals and in Subscription journals offering Online Open. Although most of the fully Open Access journals publish open access articles under the terms of the Creative Commons Attribution (CC BY) License only, the subscription journals and a few of the Open Access Journals offer a choice of Creative Commons Licenses. The license type is clearly identified on the article.

The Creative Commons Attribution License

The [Creative Commons Attribution License (CC-BY)](#) allows users to copy, distribute and transmit an article, adapt the article and make commercial use of the article. The CC-BY license permits commercial and non-

Creative Commons Attribution Non-Commercial License

The [Creative Commons Attribution Non-Commercial (CC-BY-NC)License](#) permits use, distribution and reproduction in any medium, provided the original work is properly cited and is not used for commercial purposes.(see below)

Creative Commons Attribution-Non-Commercial-NoDerivs License

The [Creative Commons Attribution Non-Commercial-NoDerivs License](#) (CC-BY-NC-ND) permits use, distribution and reproduction in any medium, provided the original work is

properly cited, is not used for commercial purposes and no modifications or adaptations are made. (see below)

Use by commercial "for-profit" organizations

Use of Wiley Open Access articles for commercial, promotional, or marketing purposes requires further explicit permission from Wiley and will be subject to a fee.

Further details can be found on Wiley Online Library http://olabout.wiley.com/WileyCDA/Section/id-410895.html

Other Terms and Conditions:

v1.10 Last updated September 2015

Questions? customercare@copyright.com or +1-855-239-3415 (toll free in the US) or +1-978-646-2777.